

Springer Theses

Recognizing Outstanding Ph.D. Research

Xiaoshi Wang

A Novel Heme-Thiolate
Peroxygenase *AaeAPO*
and Its Implications
for C–H Activation
Chemistry

 Springer

Springer Theses

Recognizing Outstanding Ph.D. Research

Aims and Scope

The series “Springer Theses” brings together a selection of the very best Ph.D. theses from around the world and across the physical sciences. Nominated and endorsed by two recognized specialists, each published volume has been selected for its scientific excellence and the high impact of its contents for the pertinent field of research. For greater accessibility to non-specialists, the published versions include an extended introduction, as well as a foreword by the student’s supervisor explaining the special relevance of the work for the field. As a whole, the series will provide a valuable resource both for newcomers to the research fields described, and for other scientists seeking detailed background information on special questions. Finally, it provides an accredited documentation of the valuable contributions made by today’s younger generation of scientists.

Theses are accepted into the series by invited nomination only and must fulfill all of the following criteria

- They must be written in good English.
- The topic should fall within the confines of Chemistry, Physics, Earth Sciences, Engineering and related interdisciplinary fields such as Materials, Nanoscience, Chemical Engineering, Complex Systems and Biophysics.
- The work reported in the thesis must represent a significant scientific advance.
- If the thesis includes previously published material, permission to reproduce this must be gained from the respective copyright holder.
- They must have been examined and passed during the 12 months prior to nomination.
- Each thesis should include a foreword by the supervisor outlining the significance of its content.
- The theses should have a clearly defined structure including an introduction accessible to scientists not expert in that particular field.

More information about this series at <http://www.springer.com/series/8790>

Xiaoshi Wang

A Novel Heme-Thiolate Peroxygenase *AaeAPO* and Its Implications for C–H Activation Chemistry

Doctoral Thesis accepted by
Princeton University, USA

 Springer

Author
Dr. Xiaoshi Wang
Philadelphia, PA
USA

Supervisor
Prof. Mohammad R. Seyedsayamdost
Princeton University
Princeton
USA

ISSN 2190-5053

Springer Theses

ISBN 978-3-319-03235-1

DOI 10.1007/978-3-319-03236-8

ISSN 2190-5061 (electronic)

ISBN 978-3-319-03236-8 (eBook)

Library of Congress Control Number: 2015949451

Springer Cham Heidelberg New York Dordrecht London

© Springer International Publishing Switzerland 2016

This work is subject to copyright. All rights are reserved by the Publisher, whether the whole or part of the material is concerned, specifically the rights of translation, reprinting, reuse of illustrations, recitation, broadcasting, reproduction on microfilms or in any other physical way, and transmission or information storage and retrieval, electronic adaptation, computer software, or by similar or dissimilar methodology now known or hereafter developed.

The use of general descriptive names, registered names, trademarks, service marks, etc. in this publication does not imply, even in the absence of a specific statement, that such names are exempt from the relevant protective laws and regulations and therefore free for general use.

The publisher, the authors and the editors are safe to assume that the advice and information in this book are believed to be true and accurate at the date of publication. Neither the publisher nor the authors or the editors give a warranty, express or implied, with respect to the material contained herein or for any errors or omissions that may have been made.

Printed on acid-free paper

Springer International Publishing AG Switzerland is part of Springer Science+Business Media
(www.springer.com)

Parts of this thesis have been published in the following journal articles:

X. Wang, R. Ullrich, M. Hofrichter, J. T. Groves, The heme-thiolate ferryl from aromatic peroxygenase is basic and reactive, *Proceedings of the National Academy of Sciences*, **2015**, 112 (12), 3686–3691

X. Wang, S. Peter, R. Ullrich, M. Hofrichter and J. T. Groves, Driving Force for Oxygen Atom Transfer by Heme-Thiolate Enzymes, *Angew. Chem. Int. Ed.*, **2013**, 52 (35), 9238–9241

X. Wang, S. Peter, M. Kinne, M. Hofrichter and J. T. Groves, Detection and Kinetic Characterization of a Highly Reactive Heme-Thiolate Peroxygenase Compound I, *J. Am. Chem. Soc.* **2012**, 134 (31), 12897–12900

S. Peter, M. Kinne, X. Wang, R. Ullrich, G. Kayser, J. T. Groves and M. Hofrichter, Selective Hydroxylation of Alkanes by an Extracellular Fungal Peroxygenase, *FEBS J.*, **2011**, 278, 3667–75.

Dedicated to my loving parents

Supervisor's Foreword

In Dr. Wang's thesis, she examined the mechanism of action of a new extracellular heme-thiolate P450 peroxygenase. P450 enzymes are versatile catalysts that carry out a number of important and difficult modifications. For decades, the application of this enzyme class in the industry has been a major goal; however, their instability and lack of solubility has precluded wide-spread industrial use. Dr. Wang's thesis focused on an extracellular P450 enzyme that does not have many of these limitations. In her thesis she demonstrates that the peroxygenase catalyzes a wide scope of reactions, in some cases very difficult transformations in molecules that are highly inert. Her detailed investigations provide a mechanistic framework for how the peroxygenase catalyzes this wide array of reactions. A major highlight of her thesis is the identification of key short-lived intermediates in the catalytic cycle of the peroxygenase, using rapid kinetic and spectroscopic methods, as well as elucidation of the thermodynamic properties of these high-energy intermediates. Heme-thiolate P450 enzymes have been studied for over 40 years, yet the thermodynamic information gathered on the peroxygenase by Dr. Wang is a major 'first'. Her work adds new insight into an important class of enzymes.

Princeton
August 2015

Prof. Mohammad R. Seyedsayamdost

Abstract

AaeAPO, a novel extracellular heme-thiolate peroxygenase, from the agaric fungus *Agrocybe aegerita* was recently discovered to catalyze the cytochrome P450-like monooxygenation of diverse organic compounds, using hydrogen peroxide as a cosubstrate. In this dissertation, the function and mechanism of alkane hydroxylation reactions catalyzed by *AaeAPO* are addressed.

In Chap. 1, current studies on the functions and mechanisms of heme-thiolate enzymes are reviewed. In Chap. 2, *AaeAPO* is found to catalyze various alkane hydroxylation reactions with high efficiency and selectivity. In Chap. 3, the hydroxylation event is probed with intramolecular kinetic hydrogen isotope effect substrates and radical clocks. Reasonable KIEs and the presence of radical rearranged alcohol products indicate the hydrogen atom abstraction step and the rebound mechanism. In Chap. 4, *AaeAPO* compound I (oxo-Fe^{IV} porphyrin radical cation) is detected and kinetically characterized by using the UV-vis, rapid-mixing stopped-flow spectroscopy. The kinetics of *AaeAPO*-I toward a panel of alkanes is directly measured and results in extraordinarily fast second-order rate constants. Both the shape and slope of Brønsted-Evans-Polanyi plot suggest that the reaction is entropically controlled with an early transition state for weaker C–H bonds. Additionally, in Chap. 5, the redox potentials of the couple *AaeAPO*-I/ferric *AaeAPO* are determined over a wide range of pHs, based on the reversible oxygen atom transfer between *AaeAPO*-I and halide ions. This analysis has allowed the highly reactive *AaeAPO*-I intermediate to be placed on an absolute energy scale for the first time. In Chap. 6, the rebound intermediate, *AaeAPO* compound II (Fe^{IV}-OH), is generated with a high yield by a one-electron direct reduction of *AaeAPO*-I, using nitroxides as the reducing reagents. *AaeAPO*-II is characterized to have a basic p*K*_a of 10. The protonated nature of *AaeAPO*-II at physiological conditions proves its role as the rebound intermediate. The kinetics of *AaeAPO*-II is also investigated and compared with those of *AaeAPO*-I. Finally, in Chap. 7, the *apo* gene is cloned into *E. coli* and over-expressed. The resulting recombinant *AaeAPO* has opened doors for many high potential applications, including industrial usage of *AaeAPO* as a biocatalyst, site-directed mutagenesis, protein engineering for better biocatalysts, and further mechanistic studies.

Acknowledgements

I would like to thank all the people who have been with me during my Ph.D. work. It is all of you that made my first six-years in the US a great experience in my life.

First, I would like to thank my advisor Prof. John T. Groves for his endless support and encouragement, training me to become a better scientist. His curiosity, vision and criticism helped move my research forward. He always gave me a lot of support and freedom to try different ideas, so that I learned many different techniques in various fields. He gave me many opportunities to attend conferences and exposure to the scientific community, allowing me to learn how to present my own work and at the same time learn from others. He is not only a research advisor but also a life mentor. He shared many experiences with me and encouraged me all the time. I learned so much from him. I really appreciate every moment being in his group and communicating with him.

I also would like to thank Prof. Michael Hecht agreeing to be the second reader and spending a lot of time proof-reading my dissertation. I also want to thank my other dissertation and general exam committee members, Prof. Thomas Muir, Prof. Mohammad R. Seyedsayamdost, Prof. Joshua Rabinowitz, and Prof. Roberto Car for enjoyable project discussions and giving me a lot of advice. I also learned a great deal from them by taking their courses. I also would like to thank them for allowing me to use many of their instruments.

I would like to thank my collaborators in Germany, Prof. Martin Hofrichter, Dr. Matthias Kinne, Dr. Sebastian Peter, Dr. René Ullrich, and Dr. Klaus Piontek on the *Aae*APO project, Prof. Katrin Scheibner and Dr. Glenn Groebe on the *Mro*APO project. I would like to thank them in initiating the collaboration, doing research work with me, discussing extensively, encouraging discoveries, and updating information. It was so nice to work with them in such an efficient way. Without their support, I could not have finished my current accomplishments. I also would like to thank Prof. Michael T. Green at PSU for EPR experiments and discussions and help on target testing analysis.

I would like to thank the very helpful facility managers in both Department of Chemistry and Molecular Biology to support my work. I would like to thank

Dr. John Eng for small molecule GC-MS, HPLC-MS, and EPR experiments, Dr. Istvan Pelczer and Dr. Carlos Pacheco for NMR experiments, Dr. David H. Perlman, Dr. Saw Kyin and Dr. Henry H. Shwe for protein mass spectrometry, and Dr. Joseph Goodhouse for confocal microscopy experiments.

It is also so enjoyable to work in Groves Lab with all the nice and talented labmates. I want to thank Prof. Minkui Luo, Dr. Kiat-Hwa Chan, Dr. Courtney McQueen, Patrick Kates, and Patrick Deifik for working and discussing together on the siderophore projects. I also would like to thank the biochemistry sub-group, especially Christin Monroe for proof-reading my dissertation, working together on fungus culture, protein expression and purification, Patrick Kates and Yang Lv for the help on recombinant protein production and purification. Also I would like to thank my other labmates including Dr. Alex Pavon, Dr. Dawn Wallace, Dr. Rodney Swartz, Dr. Erika Milczek, Dr. Dong Wang, Dr. Ning Jin, Dr. Dayi Deng, Dr. Jia Su, Dr. Julie Shilane, Dr. Basak Surmeli, Dr. Harriet Cooper, Dr. Seth Bell, Dr. Jyoti Tibrewala, Dr. Ryan Buzdygon, Dr. Thomas P. Umile, Dr. Christina Bergstrom, Kim Graves, Wei Liu, Xiongyi Huang, Nick Boaz, Irene Ojini, and undergraduate Philip Dershwitz for all the cooperation, help, and discussions together.

I also want to extend my thanks to many scientists from other labs including Boyuan Wang, Linjiao Zhou from the Muir lab and Dr. Barbara Dul from the Fiedler lab for the discussions on plasmid constructs and recombinant protein expression and purification. I also want to thank Dr. Carsten Milsmann from the Chirik lab, Dr. Miquel Vila-Perello and Dr. Galia Debelouchina from the Muir lab, Xun Sun and Dr. Ilona Rafalska-Metcalf from the Yang lab, Dr. Maria Korolev and Ann Mularz from the Hecht lab, and Mingxuan Wu from the Fiedler lab for help using many instruments.

I would like to give many thanks to the department graduate administrators, Sallie Dunner and Meghan Krause for their warm welcome when I first came to Princeton and great help on scheduling my final oral defense. They were able to answer all my questions regarding life at Princeton.

I want to thank my loving father Zhao Wang, grandfather Xuelun Wang, aunts, uncles, sisters, and brothers in China for their support all these years on my career choices and understanding on studying abroad. I want to thank my parents for raising me. I still remember vividly the moment I answered one of their questions, "What do you want to do in the future?" Here I am, "a scientist".

Last but not least, I would like to give deep thanks to my husband, Wenbo Li. He helped me all the time with great patience whenever I was in trouble. I want to thank him for spending a huge amount of time with me discussing research, analyzing data, fixing instruments, proof-reading manuscripts, and giving me so many suggestions on almost everything. He has always made life enjoyable and given me encouragement to accomplish my goals. Without him, I don't think I could have reached this point and been so happy. I also want to thank him for caring, appreciating me and loving me. I feel so lucky and thankful to have him with me in life. I Love you.

Thank you all.

Contents

1 Hydrocarbon Oxygenation by Heme-Thiolate Enzymes	1
1.1 Introduction.	2
1.1.1 Cytochrome P450S (CYPs).	2
1.1.2 Chloroperoxidase (CPO).	3
1.1.3 P450 _{SPα} and P450 _{BSβ}	5
1.1.4 Aromatic Peroxygenase (<i>Aae</i> APO).	5
1.2 Mechanistic Investigations of Intermediates in the Catalytic Cycle.	9
1.2.1 Compound 0.	11
1.2.2 Compound I.	12
1.2.3 Compound II.	12
1.2.4 Diagnostic Radical Clocks	13
1.2.5 Kinetic Isotope Effects	14
1.3 Application on the Design of New Biocatalysts with Protein Engineering.	15
1.4 Conclusions.	16
References	16
2 Efficient and Selective Alkane Hydroxylation Reactions Catalyzed by the Fungal Peroxygenase <i>Aae</i>APO	23
2.1 Introduction.	24
2.2 Results and Discussion	25
2.2.1 Hydroxylation of Alkanes with High Efficiency and Selectivity.	25
2.2.2 Hydroxylation at Benzyl Position with a High Degree of Stereoselectivity.	27
2.2.3 Hydroxylation of Neopentane and Ethane	29
2.2.4 Drug Metabolites	30
2.2.5 Flavin Cofactors and Glucose Oxidase Coenzymes.	33

2.3	Conclusions	37
2.4	Experimental	37
	References	38
3	Hydrocarbon Hydroxylations Catalyzed by <i>Aae</i>APO: Evidence of Radical Intermediates and Kinetic Isotope Effects	41
3.1	Introduction	42
3.2	Results and Discussion	43
3.2.1	Radical Clocks	43
3.2.2	Kinetic Isotope Effect (KIE)	47
3.3	Conclusions	53
3.4	Experimental	53
3.4.1	Synthesis of Substrates and Authentic Samples	54
	References	56
4	Detection and Kinetic Characterization of a Highly Reactive Heme-Thiolate Peroxygenase <i>Aae</i>APO Compound I	59
4.1	Results and Discussion	60
4.1.1	Kinetic Characterization of <i>Aae</i> APO Binding with Substrates	60
4.1.2	Detection and Generation of <i>Aae</i> APO-I	62
4.1.3	Kinetic Characterization of <i>Aae</i> APO-I Towards a Series of Alkanes	67
4.2	Conclusions	71
4.3	Experimental	71
	References	72
5	Driving Force for Oxygen Atom Transfer by Heme-Thiolate Enzymes	75
5.1	Results and Discussion	76
5.1.1	Kinetic Characterization of Compound I Generation by Hypohalous Acids	76
5.1.2	Kinetic Characterization of Compound I Reaction with Halide Ions	79
5.1.3	Determination the Redox Potential of Compound I and the Nernst Plots	82
5.1.4	Implication of Compound I Redox Properties on C–H Activation	84
5.2	Conclusions	86
5.3	Experimental	86
	References	87
6	Detection and Characterization of Heme-Thiolate Compound II from <i>Aae</i>APO Peroxygenase	91
6.1	Introduction	92
6.2	Results and Discussion	93

6.2.1	Direct Reductive Generation of <i>Aae</i> APO-II from <i>Aae</i> APO-I with Nitroxyl Radicals	93
6.2.2	Determination of the Ferryl-OH p <i>K</i> _a in <i>Aae</i> APO-II	95
6.2.3	Kinetic Characterization of <i>Aae</i> APO-II Towards Alkanes and Phenols	101
6.3	Conclusions.	108
6.4	Experimental	108
	References	109
7	Cloning and Expression of <i>Aae</i>APO from <i>Agroclybe aegerita</i> to <i>E. coli</i>, for Studies of Structure-Function Relationships by Site-Specific Mutagenesis	113
7.1	Results and Discussions	114
7.1.1	Purification of Wild Type <i>Aae</i> APO from <i>Agroclybe aegerita</i>	114
7.1.2	Construction Plasmids Containing <i>apo</i> Gene for the Over-Expression of <i>Aae</i> APO in <i>E. coli</i>	115
7.1.3	Comparison of Several Fungal Heme-Thiolate Enzymes	121
7.1.4	EPR Spectra of Resting Enzymes.	122
7.1.5	Alkane Hydroxylation Reactivity and Selectivity	124
7.1.6	Intermediate Generation and Stability	124
7.1.7	Site-Specific Mutagenesis for the Study of Structure-Function Relationships	125
7.2	Conclusions.	126
7.3	Experimental	126
	References	128

List of Figures

Figure 1.1	The active site structure of cytochrome P450cam (also called CYP101) from the gram-negative soil bacterium <i>Pseudomonas putida</i> (PDB 1DZ8) [22]. The <i>cyansphere</i> is water molecule. The <i>redspheres</i> are oxygen atoms.	3
Figure 1.2	The proposed mechanism of P450 compound I formation assisted by threonine, aspartic acid and the water network [23]	4
Figure 1.3	The active site structure of chloroperoxidase (also called CPO) from the fungus <i>Caldariomyces fumago</i> (PDB 2J5M) [29].	4
Figure 1.4	Proposed mechanism of CPO compound I formation assisted by glutamic acid and histidine in the active site [30]	5
Figure 1.5	The active site structure of P450 _{BSβ} from gram-positive <i>Bacillus subtilis</i> (PDB 1IZO) [35]	6
Figure 1.6	The proposed schematic representation of P450 _{BSβ} compound I formation mechanism	6
Figure 1.7	<i>Aae</i> APO UV-vis spectra under different conditions. <i>Black</i> trace is ferric <i>Aae</i> APO at pH 7.0. <i>Blue</i> trace is ferrous <i>Aae</i> APO reduced by Na ₂ S ₂ O ₄ at pH 7.0. <i>Red</i> trace is reduced <i>Aae</i> APO bound with CO (experimental in Chap. 7)	7
Figure 1.8	N-terminal sequence alignment of <i>Aae</i> APO with CPO. Identical residues are highlighted in <i>blue</i> . Chemically similar residues are colored in <i>light blue</i> . The access number of <i>Aae</i> APO protein sequence is B9W4V6	7

Figure 1.9	The preliminary active site structure of <i>Aae</i> APO from fungus <i>Agrocybe aegerita</i> [39]. <i>Aae</i> APO crystal structure is preliminary data from Dr. Klaus Piontek. Figures are reproduced with permission from Prof. Martin Hofrichter.	8
Figure 1.10	The proposed schematic representation of <i>Aae</i> APO compound I formation mechanism	8
Figure 1.11	The alignment of CPO structure (<i>green</i>) with <i>Aae</i> APO structure (<i>cyan</i>) [39]. <i>Left figure</i> is the alignment of two tertiary structures. <i>Right figure</i> is the alignment of active sites	9
Figure 1.12	A simplified phylogenetic tree of the heme/thiolate superfamily. Three characterized heme-thiolate proteins are in <i>bold</i> [36]	10
Figure 1.13	Catalytic cycle of heme-thiolate enzyme catalyzed hydroxylation reactions.	10
Figure 1.14	Thermodynamic relationships between intermediates in the catalytic cycle of heme-thiolate enzymes	13
Figure 2.1	GC/MS total ion chromatogram of alkane hydroxylation product mixtures catalyzed by <i>Aae</i> APO	27
Figure 2.2	<i>Left</i> GC trace of reaction mixture from the hydroxylation of ethylbenzene catalyzed by <i>Aae</i> APO. <i>Right</i> GC trace of diastereomeric (<i>S</i>)- <i>O</i> -acetylmandelyl esters of 1-phenylethanol mixtures	28
Figure 2.3	<i>Left</i> GC trace of product mixture after the reaction of neopentane with H ₂ O ₂ catalyzed by <i>Aae</i> APO. <i>Right</i> ¹ H NMR of product mixture and compare it with control. There are new peaks corresponding to neopentanol. The total turnover was about 30. The final concentration of ethanol was 13 μM calculated from an internal standard which was added before doing NMR	29
Figure 2.4	¹ H NMR of ethane oxidation catalyzed by <i>Aae</i> APO. New peaks are formed and corresponding to ethanol. The total turnover was about 10. The final concentration of ethanol was 6 μM calculated from an internal standard which was added when doing NMR	30
Figure 2.5	HPLC trace and ESI-MS of ticlopidine metabolites	31
Figure 2.6	Water suppressed ¹ H NMR of ibuprofen metabolites	32
Figure 2.7	GC trace of the imipramine metabolites	32
Figure 2.8	The product formation rates change catalyzed by <i>Aae</i> APO with different concentration of H ₂ O ₂	33
Figure 2.9	The UV-vis spectrum of TARF and LumiFIET at KP 50 mM pH 6. The red lines are oxidized forms and the black lines are reduced forms by excess DTT	34

Figure 2.10	Water suppressed ^1H NMR of ethylbenzoic acid hydroxylation products (94 % conversion)	36
Figure 2.11	Water suppressed ^1H NMR of cyclohexanecarboxylic acid hydroxylation product mixtures at pH 6, 7 or 8. The sharp two triplets at 3.78 and 3.95 ppm indicated that the hydroxylation happened on two axial sites	36
Figure 3.1	Mechanism for the cytochrome P450 reaction cycle and peroxide shunt pathway	42
Figure 3.2	Rearrangement pathways and products resulting from formation of a radical or a cation intermediate upon oxidation of norcarane	44
Figure 3.3	GC/MS total ion current chromatogram in the region of the alcohols produced from the hydroxylation of norcarane by <i>Aae</i> APO. In addition, traces of desaturation products and an epoxide were detected.	44
Figure 3.4	Compound I formation from H_2O_2 and NaClO_4	45
Figure 3.5	Rearrangement pathways and products resulting from the oxidation of bicycle[2.1.0]pentane.	45
Figure 3.6	GC/MS of the oxidation of bicycle[2.1.0]pentane by <i>Aae</i> APO.	46
Figure 3.7	Rearrangement pathways and products resulting from the oxidation of TMCP.	47
Figure 3.8	GC/MS of the oxidation of TMCP by <i>Aae</i> APO.	47
Figure 3.9	The simplest model of kinetic isotope effect	48
Figure 3.10	Preferential hydroxylation products of 2-hexanol- d_7 and 3-hexanol- d_7 in <i>n</i> -hexane-1,1,1,2,2,3,3- d_7 by <i>Aae</i> APO. Mass spectra of trimethylsilylether derivatives resulted the KIE of the reactions (experiments were performed by Sebastian Peter and data were from Ref. [11]).	49
Figure 3.11	Stereochemical courses of phenylethane-1- d_1 hydroxylation and the calculation of KIEs for <i>R</i> and <i>S</i> sites separately	52
Figure 3.12	The steric restriction in the active site of <i>Aae</i> APO.	52
Figure 4.1	<i>Left top view</i> , the crystal structure of <i>Aae</i> APO showing stacked phenylalanine residues above the heme binding pocket. <i>Right side view</i> , crystal structure of <i>Aae</i> APO showing the substrate entering channel which is surrounded by phenylalanine residues	61
Figure 4.2	Type I and type II changes of <i>Aae</i> APO UV-vis difference spectra upon substrate binding	61
Figure 4.3	a Absorbance changes of <i>Aae</i> APO at 433 nm upon binding with different concentration of <i>p</i> -ethylbenzoic acid at pH 5.0. b Plot the initial velocities of ethylbenzoic acid binding with substrate concentration	

	gave a second order rate constant of $2.6 \times 10^6 \text{ M}^{-1} \text{ s}^{-1}$. The final concentration of resting AaeAPO is 2 μM . A similar rate constant was obtained by fitting with single exponential decay and pseudo first order kinetics	62
Figure 4.4	UV-vis transients observed upon 1:1 mixing of 13 μM of ferric enzyme with 25 μM of <i>m</i> CPBA at pH 5.0, 4 $^\circ\text{C}$. Maximum yield of AaeAPO-I reached 70 % at 30 ms	63
Figure 4.5	Abstract spectra of SVD analysis on the stopped-flow data sets of AaeAPO reaction with 2 eq of <i>m</i> CPBA and CPO reaction with 2 eq of H_2O_2 , both at pH 5.0	63
Figure 4.6	Target testing of AaeAPO reaction with CPO-I	64
Figure 4.7	Absorbance traces at 417 nm upon mixing of ferric enzyme with 2 eq of <i>m</i> CPBA over a range of pHs.	65
Figure 4.8	a The Absorbance at 417 nm upon mixing ferric AaeAPO with different concentration of <i>m</i> CPBA at pH 6.0. b Single exponential decay of ferric enzyme as a function of <i>m</i> CPBA concentration. The second order rate constant of AaeAPO-I formation gave similar result if one uses initial velocity fitting	66
Figure 4.9	Water suppressed ^1H NMR of the reaction mixture of oxidation of <i>p</i> -ethylbenzoic acid by 0.22 μM of AaeAPO and H_2O_2 . Labeled resonances correspond to the product (<i>R</i>)-4-(1-hydroxyethyl) benzoic acid at 7.748 ppm (2H, dd), 7.330 ppm (2H, dd) and 1.368 ppm (3H, d). The benzylic proton resonance was obscured by the suppressed water peak	67
Figure 4.10	a UV-vis spectra obtained during the reaction of 10 μM AaeAPO-I with 16 μM <i>p</i> -ethylbenzoic acid at pH 5.0, 4 $^\circ\text{C}$. Inset: Observed first-order decay rates versus <i>p</i> -ethylbenzoic acid concentration. The apparent second-order rate constant, k_2 , was obtained from the slope. b Observed first-order decay rates versus con- centrations of THF or THF- d_8 . A KIE of 4.3 for THF and THF- d_8 was determined from the ratio of the slopes.	68
Figure 4.11	Plot of $\log k_2'$ versus substrate C-H BDE	70
Figure 4.12	Rate constants for the hydrogen abstraction by MnO_4^- , $\text{ROO}\cdot$, $\text{RO}\cdot$ and $\text{HO}\cdot$ versus the strength of the O-H bonds formed for toluene (<i>solid circles</i>) and <i>p</i> -ethyl- benzene (open diamonds [34, 35]). Plotting rate con- stants for hydrogen abstraction by AaeAPO-I with <i>p</i> - toluic acid and <i>p</i> -ethylbenzoic acid on the curves gives an $\text{Fe}^{\text{IV}}\text{O-H}$ bond strength of about 103 kcal/mol.	71

Figure 5.1	UV/vis spectra observed upon 1:1 mixing of 5 μM <i>AaeAPO</i> with 15 μM NaOBr at pH 5.0, 4 $^{\circ}\text{C}$. <i>Inset</i> Time courses of data obtained at 417 nm (ferric <i>AaeAPO</i>) and 361 nm (<i>AaeAPO</i> -I).	77
Figure 5.2	a UV-vis absorbance change at 417 nm upon <i>AaeAPO</i> mixing with different concentration of HOBr at pH 5.0 and 4 $^{\circ}\text{C}$, monitored by single wavelength stopped-flow instruments. b Initial velocity fitting of the absorbance changes versus time with the use of different concentration of HOBr.	78
Figure 5.3	Initial velocity of ferric <i>AaeAPO</i> oxidation as a function of [NaOX] for the reaction between 2 μM <i>AaeAPO</i> with NaOX, pH 3–7	78
Figure 5.4	UV/Vis spectral changes observed for the bromination of phenol red ($\lambda_{\text{max}} = 434$ nm to form bromophenol blue ($\lambda_{\text{max}} = 592$ nm) by 1 mM of H_2O_2 , 10 mM NaBr and 20 nM of <i>AaeAPO</i> at pH 5.0, RT	80
Figure 5.5	UV/Vis spectral changes observed for the bromination of phenol red ($\lambda_{\text{max}} = 434$ nm) to bromophenol blue ($\lambda_{\text{max}} = 592$ nm) by 1 mM of H_2O_2 , 10 mM NaBr and 20 nM of CPO at pH 5.0, RT	80
Figure 5.6	The decay of <i>AaeAPO</i> -I monitored at 417 nm upon its reaction with different concentration of Br^- at pH 6.0.	81
Figure 5.7	Pseudo-first order rate constants, k_{obs} , as a function of [NaX] for the reaction between <i>AaeAPO</i> -I with halide ions at different pHs.	81
Figure 5.8	Plots of $\log k_{\text{rev}}$ as a function of pH for oxo-transfer from <i>AaeAPO</i> -I and CPO-I to bromide ion	82
Figure 5.9	Calculated redox potentials $E'_{(\text{cpd-I}/\text{ferric})}$ as a function of pH for <i>AaeAPO</i> -I/ Fe^{III} (<i>open squares</i>) and CPO-I/ Fe^{III} (<i>closed circles</i>) at 4 $^{\circ}\text{C}$. Nernst equations for HRP-I/ Fe^{III} [32], HOBr/ Br^- and HOCl/ Cl^- are plotted in <i>gray</i> for comparison	83
Figure 5.10	Nernst plots for three different intermediate couples: ferric <i>AaeAPO</i> / <i>AaeAPO</i> -I, <i>AaeAPO</i> -I/ <i>AaeAPO</i> -II and ferric <i>AaeAPO</i> / <i>AaeAPO</i> -II. The <i>error bar</i> is the ± 2 from Eq. (5.5).	85
Figure 5.11	The stability (Pourbaix) diagram for <i>AaeAPO</i> high-valent iron intermediates	86
Figure 6.1	Cyclic voltammograms of 3-carboxyl PROXYL and 4-Carboxy TEMPO at pH 7.0 100 mM KP buffer at 4 $^{\circ}\text{C}$. E° is 593 mV for 3-carboxyl PROXYL and 572 mV for 4-carboxy TEMPO versus Ag/AgCl	94

Figure 6.2	UV-vis transients observed upon 1:1 mixing of 10 μM of ferric enzyme with 50 μM of <i>mCPBA</i> and 10 mM of 3-carboxy PROXYL (blanked) at pH 7.0, 4 $^{\circ}\text{C}$. The <i>insert</i> shows the formation and decay kinetics under these conditions.	94
Figure 6.3	<i>Left</i> 10 μM CPO mixed with a solution containing 20 μM of <i>mCPBA</i> and 0.5 mM of 3-carboxy PROXYL at pH 6.0. <i>Right</i> 4 μM CPO mixed with a solution containing 10 μM of <i>mCPBA</i> and 10 mM of 3-carboxy PROXYL at pH 6.0.	95
Figure 6.4	<i>Left</i> Far-UV CD spectra of wt CPO at different pHs. <i>Right</i> Far-UV CD spectra of wt <i>AaeAPO</i> at different pHs. CD spectra were the average of three parallel experiments and taken with a 1 mm pathway cuvette, 3.1 μM of CPO and 2.1 μM of <i>AaeAPO</i> at 4 $^{\circ}\text{C}$	96
Figure 6.5	UV-vis spectral change of 10 μM of ferric CPO in 10 mM pH 7 buffer upon mixing with a pH 9 200 mM strong buffered solution by stopped-flow single mixing experiments.	96
Figure 6.6	<i>Left</i> <i>AaeAPO</i> has no UV-vis spectral change at pH 12 after 150 s mixing. <i>Right</i> The heme of ferric resting <i>AaeAPO</i> begins to bleach away at pH 13. The spectral changes were obtained by mixing ferric enzyme in 10 mM NaP buffer at pH 7.0 with 200 mM strong buffered solution at pH 13 by using UV-vis stopped-flow spectroscopy	97
Figure 6.7	UV-vis spectra of <i>AaeAPO</i> -II at different pHs were obtained by using double mixing stopped-flow instrument. During the first mixing, <i>AaeAPO</i> -II was generated with its highest yield after 50 ms age time by mixing 45 μM ferric <i>AaeAPO</i> in 10 mM NaP buffer at pH 7.0 with 500 μM <i>mCPBA</i> and 10 mM PROXYL radical in 50 mM NaP buffer at pH 7.0. The second mixing was a pH jump experiment. <i>AaeAPO</i> -II spectra at various pHs were generated by mixing the low buffered <i>AaeAPO</i> -II with 200 mM strong buffered solution at different pHs. At pH 7, 8 and 12 NaP buffers were used. At pH 8 and 9, Tris buffers were used. At pH 9.5, 10, 10.5 and 11, $\text{NaHCO}_3/\text{Na}_2\text{CO}_3$ buffers were used.	98
Figure 6.8	pH titration curves for <i>AaeAPO</i> -II. pK_a of 10.0 was obtained for the hydroxyl group in <i>AaeAPO</i> -II by fitting the absorbance at 455 and 569 nm versus pHs	98

Figure 6.9	A linear correlation between $\log k_0$ and pH was obtained with a slope of -1 . The kinetics was obtained by fitting the absorbance at 441 nm during the decay of <i>AaeAPO-II</i>	99
Figure 6.10	The relationship of ferryl pKa and one electron redox potential of compound I according to Eq. 6.1	100
Figure 6.11	20 μM ferric <i>AaeAPO</i> mixed with a basic solution of 1 mM of peroxyxynitrite at pH 5.0	101
Figure 6.12	<i>Left</i> time traces of the disappearing of <i>AaeAPO-II</i> (2.5 μM) at 441 nm reacting with different concentration of ascorbate solutions at pH 7.0, 4 $^\circ\text{C}$. <i>Right</i> the plot of observed rate constants k_{obs} versus [ascorbate] resulted in a linear correlation and a second order rate constant was determined from the slope	102
Figure 6.13	<i>Left</i> time traces of the disappearing of <i>AaeAPO-II</i> (2.5 μM) at 441 nm reacting with different concentrations of xanthene at pH 7.0, 4 $^\circ\text{C}$. <i>Right</i> correlation between observed rate constant k_{obs} versus [xanthene]	103
Figure 6.14	Plot of $\log k_2'$ versus substrate C–H BDE for <i>AaeAPO-II</i> at pH 7.0 and <i>AaeAPO-I</i> at pH 5.0	103
Figure 6.15	Rate constants for the hydrogen abstraction by MnO_4^- , $\text{ROO}\cdot$, $\text{RO}\cdot$ and $\text{HO}\cdot$ versus the strength of the O–H bonds formed for toluene (<i>solid circles</i>) and <i>p</i> -ethylbenzene (<i>open diamonds</i>) [32, 44]. Plotting rate constants for hydrogen atom abstraction by <i>AaeAPO-I</i> and <i>AaeAPO-II</i> with <i>p</i> -toluic acid and <i>p</i> -ethylbenzoic acid on the curves gives an $\text{Fe}^{\text{IV}}\text{O-H}$ bond strength of about 103 kcal/mol and $\text{Fe}^{\text{III}}(\text{H}_2\text{O})$ O–H bond strength of about 92 kcal/mol	104
Figure 6.16	<i>Left</i> time traces of the disappearing of <i>AaeAPO-II</i> (2.5 μM) at 441 nm reacting with different concentrations of 4-CN phenol at pH 7.0, 4 $^\circ\text{C}$. <i>Right</i> observed rate constant k_{obs} at 441 nm versus [4-CN phenol] for its oxidation by <i>AaeAPO-II</i> at pH 7.0, 4 $^\circ\text{C}$	106
Figure 6.17	Plot of $\log k_2$ versus phenolic σ^+ for both <i>AaeAPO-I</i> ($R^2 = 0.6$) and <i>AaeAPO-II</i> ($R^2 = 0.93$) at pH 7.0.	106
Figure 6.18	Redox potential shift of phenols upon forming hydrogen bondings with surroundings.	107
Figure 7.1	The production of wild type <i>AaeAPO</i> over time in 1 L medium in a shaker. The activity was measured by determining the oxidation of veratryl alcohol into veratraldehyde with 1 mM of H_2O_2 at pH 7.0 and	

	calculated as unit which is the micromoles of product formed per minute or micromoles of substrate converted per minute	114
Figure 7.2	SDS-PAGE of purified <i>Aae</i> APO from each step: from <i>left to right</i> the lanes are the purified protein by collaborators at Germany, the thawed medium after ultrafiltration, the protein marker, the protein after the third size exclusive column, the protein after the second Q Sepharose column and the protein after the first SP Sepharose separation	115
Figure 7.3	IEF gel of purified <i>Aae</i> APO in left lane with two pI at about 4.4 and 4.9.	116
Figure 7.4	Mascot search result of the sequence match between purified <i>Aae</i> APO and <i>Aae</i> APO in database with an accession number of B9W4V6. The signal peptide is colored in <i>grey</i> . The matched peptides are shown in <i>red</i> (color online)	116
Figure 7.5	UV-vis spectra <i>Aae</i> APO under different conditions. <i>Black trace</i> is ferric <i>Aae</i> APO at pH 7.0. <i>Blue trace</i> is ferrous <i>Aae</i> APO reduced by Na ₂ S ₂ O ₄ at pH 7.0. <i>Red trace</i> is reduced <i>Aae</i> APO bound with CO (color online)	117
Figure 7.6	Primers used for RT-PCR and ligation. <i>Purple</i> is <i>Eco</i> RI. <i>Green</i> is <i>Bam</i> HI. <i>Red</i> is that start codon and the two <i>blue</i> codons are stop codons (color online).	117
Figure 7.7	The ligation of <i>apo</i> cDNA with double digested pUC19 vector. <i>Left</i> ligation experiment showed lots of colonies growing when inserts are provided but no colonies growing in the controls. <i>Middle</i> 2nd lane is <i>apo</i> cDNA, 3rd lane is empty pUC19 digested with <i>Eco</i> RI, 3rd lane is pUC19_ <i>apo</i> digested with <i>Eco</i> RI. <i>Right</i> a map showing <i>apo</i> gene is inserted into pUC19	118
Figure 7.8	The ligation of <i>apo</i> cDNA with double digested pCWori vector. <i>Left</i> ligation experiment showed lots of colonies growing when inserts are provided but no colonies in the controls. <i>Middle</i> 2nd lane is <i>apo</i> cDNA, 3rd lane is <i>Nde</i> I and <i>Xba</i> I double digested pCWori_CYP101, 3rd lane is pCWori_ <i>apo</i> digested with both <i>Acc65</i> I. <i>Right</i> a sequence map of the expression plasmid pCWori_ <i>apo</i>	118
Figure 7.9	<i>Left</i> the plasmid map of OmpA_ <i>apo</i> _pET21b. <i>Right</i> BL21 (DE3) cell pellets transformed with OmpA_ <i>apo</i> _pET21b and incubated at optimized conditions.	120

Figure 7.10	<i>Left</i> SDS-PAGE results of whole protein in cell lysis. <i>Right</i> Western blotting result of his-tag proteins in cell lysis. Lane 1 is 0.5 mM IPTG and 0.5 mM δ -ALA. Lane 2 is 0.5 mM IPTG. Lane 3 is 0.5 δ -ALA. Lane 4 is the control without adding any IPTG and δ -ALA.	120
Figure 7.11	Alignments the crystal structures of CPO (<i>green</i> , PDB 2J5M) with <i>Aae</i> APO (<i>cyan</i> , unpublished data) and crystal structures of P450cam (<i>purple</i> 1DZ4) with <i>Aae</i> APO (color online).	122
Figure 7.12	X-band EPR spectra of resting CPO and <i>Aae</i> APO	122
Figure 7.13	X-band EPR spectrum of resting <i>Mro</i> APO	123
Figure 7.14	<i>Left</i> GC/MS total ion trace in the region of the alcohols produced from the hydroxylation of norcarane by <i>Mro</i> APO. <i>Right</i> mass spectrum of the radical rearranged product cyclohex-2-en-1-ylmethanol.	124
Figure 7.15	<i>Left</i> the formation of <i>Mro</i> APO-I was detected by the fast-mixing stopped-flow spectroscopy at the optimized condition of 10 μ M <i>Mro</i> APO mixing with 1 mM PAC at pH 7.0 at 4 $^{\circ}$ C. <i>Right</i> similar and small amounts of <i>Mro</i> APO-I were detected with the use of stoichiometric amount of oxidants or using an excess amount of other oxidants including <i>m</i> CPBA and H_2O_2	125

List of Tables

Table 1.1	Radical clocks used in heme-enzyme studies	14
Table 2.1	Stability of peroxygenase <i>Aae</i> APO in different organic solvents.	25
Table 2.2	Product distributions (% total alcohols) and % <i>ee</i> of selected products	26
Table 2.3	Conversion of ethylbenzoic acid hydroxylation catalyzed by <i>Aae</i> APO and different flavins	37
Table 3.1	Hydroxylation products of methyl stepwise deuterated toluenes	50
Table 3.2	Derived isotope effects for <i>Aae</i> APO hydroxylation of deuterated toluenes	50
Table 3.3	Intramolecular KIE _(obs) on selective deuterated substrates for <i>Aae</i> APO and P450s	51
Table 4.1	The observed <i>Aae</i> APO compound I formation and spontaneous decay rate constants	65
Table 4.2	Summary of all substrates, equivalent C-H bonds, BDE, k_2 , k_2' and $\log k_2'$	69
Table 5.1	Data for oxygen atom transfer between halide ions and <i>Aae</i> APO-I at different pHs	78
Table 5.2	Kinetic and thermodynamic data, k_{for} , k_{rev} , K_{equi} and $E'_{(\text{cpd-I/ferri})}$, for oxygen atom transfer between halide ions and CPO-I at different pHs	79
Table 6.1	Summary of alkane substrates, equivalent C-H bonds, BDE, k_2 , k_2' and $\log k_2'$	102
Table 6.2	Summary of phenol substrates, sigma values, k_2 and $\log k_2$ for both <i>Aae</i> APO-I and <i>Aae</i> APO-II	105
Table 6.3	Previous data about phenol oxidation Hammett analysis, ρ values	107

Table 7.1	Primers used for pCWori and apo cDNA ligation	119
Table 7.2	Comparison of the proximal H-bonds to the cysteine sulfur in different heme-thiolate enzymes and g-values of ferric enzymes in EPR spectra	123

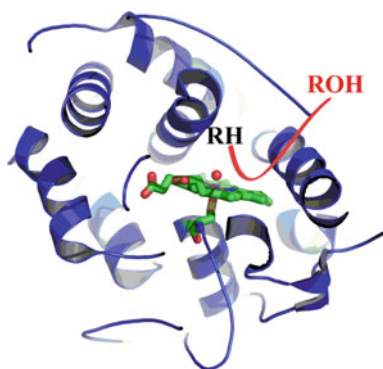
List of Schemes

Scheme 1.1	Alkane hydroxylation reactions catalyzed by CYPs	2
Scheme 1.2	Alkane hydroxylation reactions catalyzed by CPO	4
Scheme 2.1	Different types of reactions catalyzed by <i>Aae</i> APO	24
Scheme 2.2	Alkane hydroxylation catalyzed by <i>Aae</i> APO	26
Scheme 2.3	The determination of enantiomers	28
Scheme 2.4	Several examples of drug metabolites by <i>Aae</i> APO	31
Scheme 2.5	The couple of <i>Aae</i> APO and glucose oxidase catalytic cycles	34
Scheme 2.6	Ethylbenzene hydroxylation by <i>Aae</i> APO coupled with Flavin	35
Scheme 2.7	Cyclohexanecarboxylic acid hydroxylation by <i>Aae</i> APO coupled with Flavin	35
Scheme 2.8	The catalytic cycles of <i>Aae</i> APO reaction coupled with flavins	35
Scheme 3.1	Radical clock (Ingold's Model)	43
Scheme 3.2	The synthesis of bicycle[2.1.0]pentane	46
Scheme 3.3	Kinetic model of enzymatic reactions	48
Scheme 3.4	The synthesis of (<i>R</i>)-1-phenylethane [20]	53
Scheme 4.1	The generation of <i>Aae</i> APO-I and its reaction with substrates	62
Scheme 4.2	Proposed mechanism of <i>Aae</i> APO-I formation assisted by the deprotonated glutamate in the active site.	66
Scheme 5.1	Reversible oxygen atom transfer between ferric <i>Aae</i> APO and HOBr or HOCl (k_{for}), and <i>Aae</i> APO-I with halide ions (k_{rev})	77
Scheme 5.2	Phenol red conversion to bromophenol blue upon the addition of HOBr	79
Scheme 5.3	Nernst half-reactions for HOX and $^{+}\text{PorFe}^{\text{IV}}=\text{O}$	83
Scheme 5.4	Relationship between three different redox couples	85
Scheme 6.1	Reaction cycle for <i>Aae</i> APO-II generation and reduction with substrates	93

Scheme 6.2	The equilibrium between protonated <i>Aae</i> APO-II and deprotonated <i>Aae</i> APO-II	97
Scheme 6.3	The generation of <i>Aae</i> APO-II and its reaction with substrates	101
Scheme 6.4	Possible formation pathways for desaturation products catalyzed by <i>Aae</i> APO	105
Scheme 6.5	Proposed mechanism of phenolic oxidation activated by <i>Aae</i> APO-II.	107

Chapter 1

Hydrocarbon Oxygenation by Heme-Thiolate Enzymes



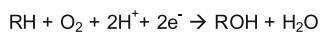
Abstract The heme-thiolate enzymes such as cytochrome P450 (CYP), chloroperoxidase (CPO), P450_{BS_P} and recently discovered peroxygenase, *AaeAPO*, catalyze a variety of crucial oxidative reactions. Among them, the activation of inert hydrocarbons via C–H bond hydroxylation plays an important role in biology. These reactions are involved in the biosynthesis of steroids, the degradation of xenobiotics, the metabolism of drugs and so on. Understanding the mechanisms of these reactions provides us guidelines for the design of new catalysts and the application of biocatalysts to chemical synthesis and drug development. In this chapter, we review the discovery and function of several important heme-thiolate enzymes. Next, the characterization of intermediates in the catalytic cycle during the oxidative reactions is addressed. Finally, applications of the knowledge obtained from these mechanistic investigations on the design of new enzymatic catalysts are discussed.

1.1 Introduction

Selectively and efficiently converting inert carbon hydrogen bonds to oxygen-containing functional groups under mild conditions is a difficult class of transformations that has attracted considerable attention for several decades [1, 2]. Nature has designed various metalloenzymes to perform these transformations [3–5]. Alpha-ketoglutarate and iron(II)-dependent dioxygenases catalyze various reactions and have significant roles in biology [6, 7]. For example, ten-eleven translocation 1-3 (TET 1-3) enzymes have been discovered to convert 5-methylcytosine to 5-hydroxymethylcytosine, thus changing the DNA methylation pattern and regulating gene expression [8]. The alkane hydroxylase (AlkB) from *Pseudomonas putida* GPo1 hydroxylates propane and butane to support cell growth [9, 10]. Di-iron and copper-containing methane monooxygenases from methanotrophic bacteria are able to activate the inert C–H bond of methane (BDE 104 kcal/mol) as the carbon energy source [11, 12]. Peptidylglycine monooxygenases, mononuclear copper-containing enzymes, activate C-terminal glycine-extend peptides to their α -hydroxylated products [13–15]. Heme enzymes with a cysteine sulfur as the axial ligand also have the capability of activating hydrocarbons. Cytochrome P450 monooxygenases are a family of enzymes that incorporate an oxygen atom into various biomolecules [16–18]. It has been proposed that the cysteine plays a crucial role in driving the chemistry in several ways. From a mechanistic point of view, sulfur ligation of the heme iron promotes the heterolytic cleavage of the O–O bond to form the ferryl (Fe=O) species in the so-called compound I [19]. The electron donating properties of the thiolate ligand also make the ferryl oxygen more basic, facilitating the C–H hydrogen atom abstraction at a lower potential than would otherwise be possible [20]. In this chapter, we first summarize the nature of several heme-thiolate enzymes that have the ability to oxidize hydrocarbons. Then we will summarize both their functions and reaction mechanisms.

1.1.1 Cytochrome P450S (CYPs)

Cytochrome P450 proteins (CYP) are monooxygenases that utilize oxygen (O₂) as the oxidant and NAD(P)H as an electron source, performing two-electron oxidation including alkane hydroxylation, olefin epoxidation, alkane desaturation, heteroatom oxidation and so on (Scheme 1.1). The cytochrome P450 family has been found in bacteria, fungi, plants, insects and mammals. Their physiological functions include the biosynthesis of steroids, lipids and many other signaling molecules. They are



Scheme 1.1 Alkane hydroxylation reactions catalyzed by CYPs

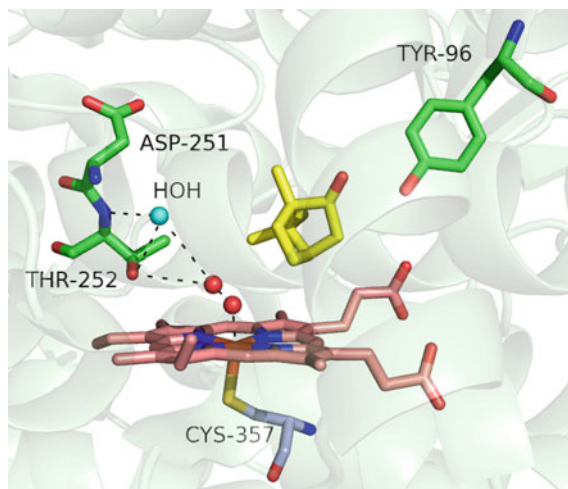


Fig. 1.1 The active site structure of cytochrome P450cam (also called CYP101) from the gram-negative soil bacterium *Pseudomonas putida* (PDB 1DZ8) [22]. The cyan sphere is water molecule. The red spheres are oxygen atoms

also responsible for the degradation of xenobiotics and the metabolism of drugs [21]. For example, CYP3A4 metabolizes over 50 % of all drugs currently on the market. Because of their important roles, cytochrome P450s have been the interests for biological, chemical and pharmacological research for a long time. The name of P450 derives from the fact that these proteins were first discovered in particulate cell fractions and displayed an unusual 450 nm absorption in the visible spectrum upon reduction in the presence of carbon monoxide. This absorbance is now understood to result from the Cys-S-Fe^{II}-CO ligation of the heme.

The crystal structures of many cytochrome P450s have been characterized [22] (Fig. 1.1). Unlike peroxidases and catalases, there are no obvious acid and base residues close to the heme iron where the oxygen molecule is bound. The hydroxyl group of a highly conserved threonine in the substrate and O₂ binding pocket has been proposed to play an important role in proton delivery and initiation of the catalytic cycle [24]. There is also a network of other hydrophilic side chains and water molecules to deliver protons in the active site [23]. A proposed mechanism of P450-I formation is shown in Fig. 1.2.

1.1.2 Chloroperoxidase (CPO)

CPO from *Caldariomyces fumigo* was first discovered by Clutterbuck and coworkers in 1940 and was found to mediate the chlorination of β -ketoacidic acid [25]. The isolated enzyme was found to be highly glycosylated with a molecular

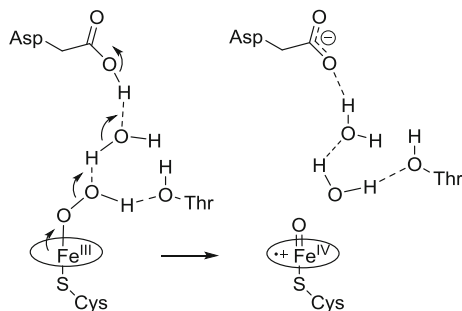
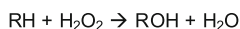


Fig. 1.2 The proposed mechanism of P450 compound I formation assisted by threonine, aspartic acid and the water network [23]

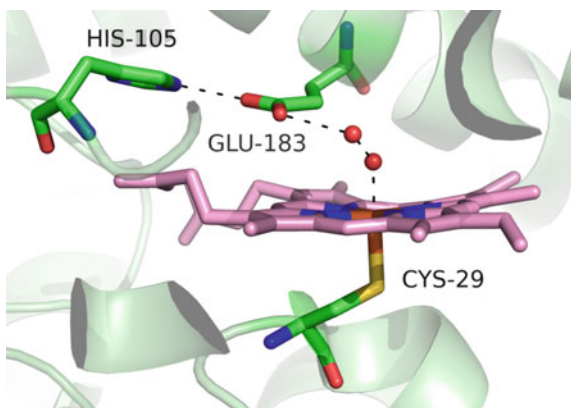


Scheme 1.2 Alkane hydroxylation reactions catalyzed by CPO

weight of about 42 kDa [26]. Unlike cytochrome P450s, chloroperoxidase utilizes peroxides as the terminal oxidants (Scheme 1.2). Besides the one-electron oxidations catalyzed by most of the peroxidases and halogenation reactions, CPO is also able to catalyze two-electron oxidations, such as oxygen atom transfer reactions, although the efficiency is much lower than CYPs [27]. For example, CPO catalyzes C–H hydroxylation at benzylic position while CYPs are able to catalyze aliphatic hydroxylation with stronger C–H bonds (~ 101 kcal/mol). Because of its good solubility, easy handling and catalytic versatility, CPO has become a good model for the study of P450 reaction mechanisms [28]. It has also been utilized for synthetic and biocatalytic applications.

The active site of CPO includes a glutamic acid and a histidine as the acidic and basic catalytic residues [31] (Fig. 1.3). Glu183 has been proposed to facilitate

Fig. 1.3 The active site structure of chloroperoxidase (also called CPO) from the fungus *Caldariomyces fumago* (PDB 2J5M) [29]



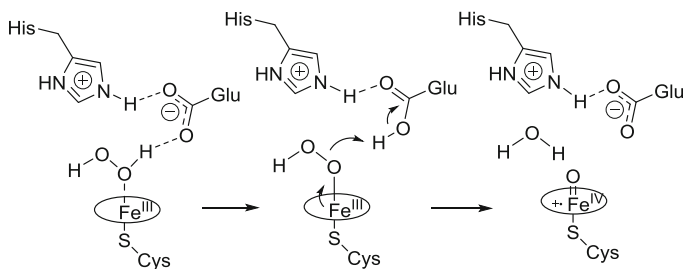


Fig. 1.4 Proposed mechanism of CPO compound I formation assisted by glutamic acid and histidine in the active site [30]

compound I formation via O–O bond cleavage of a hydroperoxoiron(III) precursor ($\text{Fe}^{\text{III}}\text{--O--OH}$, so-called compound 0) by supplying a proton during O–O bond scission to form water and compound I. A mechanistic scheme is shown in Fig. 1.4. Upon replacement of Glu183 the chlorination activity of CPO is reduced [32]. Also, the highest activity of CPO is achieved at acid pH. This is possibly due to the higher potential of compound I at lower pH.

1.1.3 $P450_{\text{SP}\alpha}$ and $P450_{\text{BS}\beta}$

Cytochrome $P450_{\text{SP}\alpha}$ (CYP152B1) from *Sphingomonas paucimobilis* and $P450_{\text{BS}\beta}$ (CYP152A1) from *Bacillus subtilis* are CYPs classified as H_2O_2 -dependent enzymes [33, 34]. It has been shown that $P450_{\text{SP}\alpha}$ and $P450_{\text{BS}\beta}$ catalyze fatty acid hydroxylation with high selectivity. Further, with the use of carboxylate group of the fatty acid, $P450_{\text{SP}\alpha}$ and $P450_{\text{BS}\beta}$ have been demonstrated to catalyze H_2O_2 dependent monooxygenation of styrene and ethylbenzene. Although crystal structures of substrate-free forms showed their lack of general acid-base residues in the active site, crystal structure of a heptanoic acid bound form of $P450_{\text{BS}\beta}$ showed an interaction between Arg242 and the carboxylate group of heptanoic acid [35] (Fig. 1.5). This investigation demonstrates the importance of glutamate and the important role of salt bridge between Arg242 and carboxylate group. A proposed schematic representation of the mechanism is shown in Fig. 1.6.

1.1.4 Aromatic Peroxygenase (*AaeAPO*)

A new heme-thiolate peroxygenase, *AaeAPO*, from the filamentous fungus *Agrocybe aegerita* was discovered recently [36, 37]. The isolated *AaeAPO* has a molecular weight of about 45 kDa. It is a highly glycosylated protein with about 30 % sequence similarity to CPO (Fig. 1.8) and no homology to CYPs. The ferrous

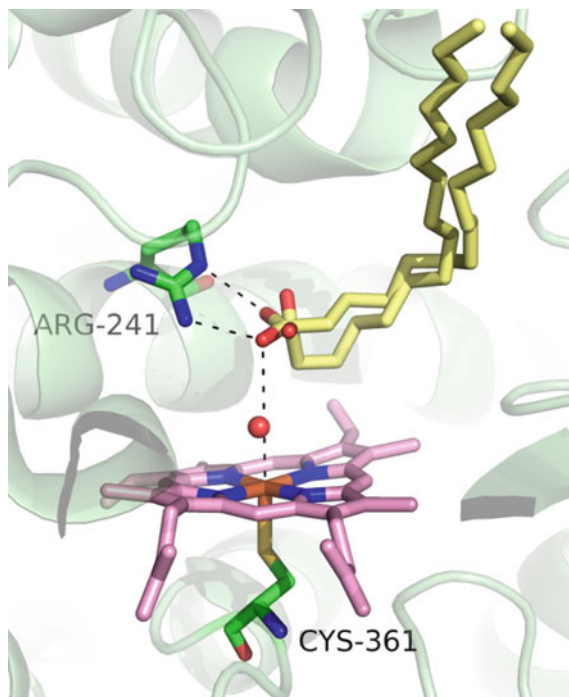


Fig. 1.5 The active site structure of P450_{BSβ} from gram-positive *Bacillus subtilis* (PDB 1IZO) [35]

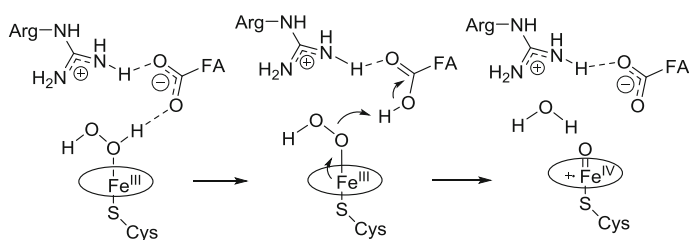


Fig. 1.6 The proposed schematic representation of P450_{BSβ} compound I formation mechanism

form of *AaeAPO* bound with CO also has an absorption peak at 445 nm, closely resembling typical CYPs (Fig. 1.7). APOs have been shown to catalyze various kinds of reactions including hydrocarbon hydroxylation [38]. Unlike CYPs however, and similar to CPO, *AaeAPO* utilizes peroxides as the sole oxidants. Apparently, hydrogen peroxide is a preferred co-substrate. Accordingly, *AaeAPO* has been considered to be a hybrid of monooxygenases/peroxidases or *peroxygenases*. Cytochrome P450 enzymes have had limited use for industrial and

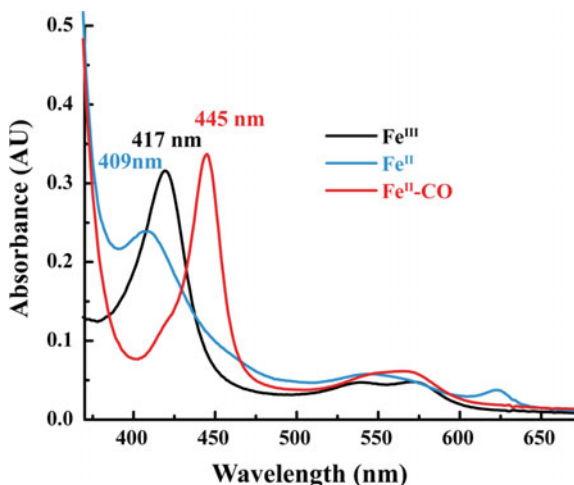


Fig. 1.7 *AaeAPO* UV-vis spectra under different conditions. *Black* trace is ferric *AaeAPO* at pH 7.0. *Blue* trace is ferrous *AaeAPO* reduced by $\text{Na}_2\text{S}_2\text{O}_4$ at pH 7.0. *Red* trace is reduced *AaeAPO* bound with CO (experimental in Chap. 7)

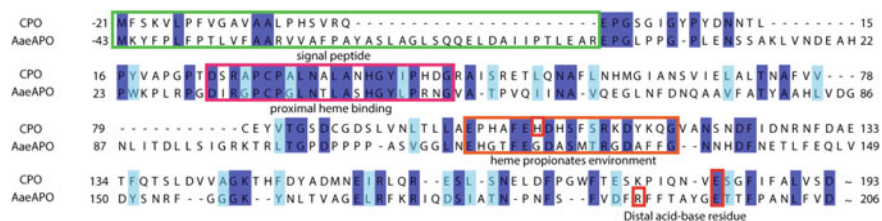
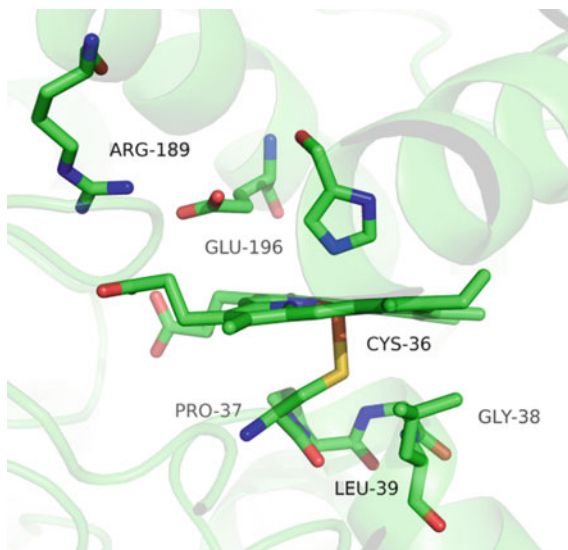


Fig. 1.8 N-terminal sequence alignment of *AaeAPO* with CPO. Identical residues are highlighted in *blue*. Chemically similar residues are colored in *light blue*. The access number of *AaeAPO* protein sequence is B9W4V6

biocatalytic applications because of their general lack of stability, expensive cofactor requirements and limited solvent tolerance. By contrast, as the extracellular protein, *AaeAPO*, has been found to be extremely stable and robust. It uses readily available and cheap H_2O_2 as the oxidant and can be used in wide pH conditions and organic solvents as well. Considering these significant advantages, detailed mechanistic investigations on *AaeAPO* have been carried out recently.

A preliminary crystal structure of *AaeAPO* has been reported [39] (Fig. 1.9). The structure has confirmed that *AaeAPO* is a heme-thiolate protein with acid-base residues of glutamic acid and arginine in the active site. Comparing the acid-base residues and the two-electron oxidation activity of *AaeAPO* with CPO, P450_{SP α} and P450_{BS β} , suggests an important role of the Arg-Glu salt bridge diad in the initiation of the catalytic cycle. The positively charged arginine side group might make

Fig. 1.9 The preliminary active site structure of *Aae*APO from fungus *Agrocybe aegerita* [39]. *Aae*APO crystal structure is preliminary data from Dr. Klaus Piontek. Figures are reproduced with permission from Prof. Martin Hofrichter



glutamate more acidic, assisting compound I formation. Compound I of *Aae*APO has been directly observed during the oxidative reaction catalytic cycle, kinetically characterized and compared with other heme enzymes [40]. Figure 1.10 showed a proposed mechanism on the *Aae*APO compound I formation assisted with glutamic acid and arginine. The reactive ferryl species ($\text{Fe}=\text{O}$) is able to cleave strong C–H bonds so that *Aae*APO has great potential to be a robust biocatalyst with board range of synthetic applications.

*Aae*APO has recently been classified as an “unspecific peroxygenase” in the E.C. nomenclature (E.C.1.11.2.1). The APO family contains other members such as *Cra*APO from Ink cap mushroom *Coprinellus radians* and *Mro*APO from Pinwheel mushroom *Maramius rotula* (unknown sequence). Along with the well characterized CPO from *Caldariomyces fumago*, they are all heme-thiolate proteins

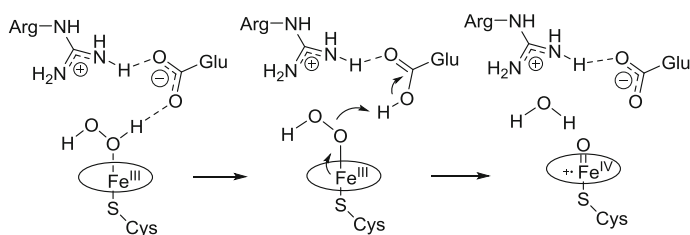


Fig. 1.10 The proposed schematic representation of *Aae*APO compound I formation mechanism

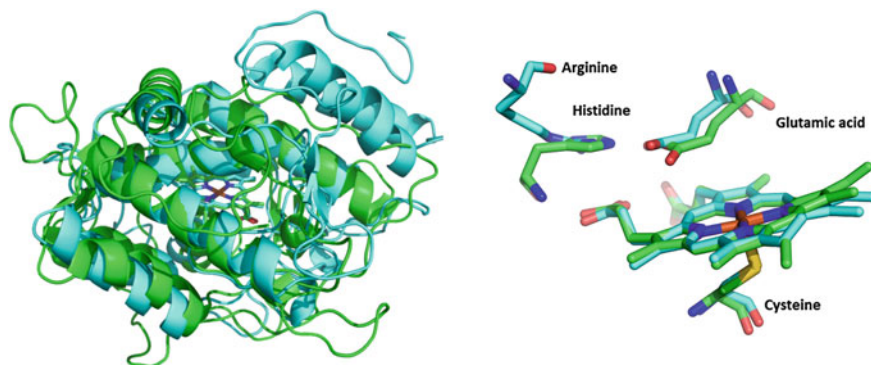


Fig. 1.11 The alignment of CPO structure (*green*) with *AaeAPO* structure (*cyan*) [39]. *Left figure* is the alignment of two tertiary structures. *Right figure* is the alignment of active sites

belonging to the heme-thiolate peroxxygenase/peroxidase super-family. Figure 1.12 shows a simplified phylogenetic tree of this super-family [36]. It is also interesting, as shown in Fig. 1.11, that the tertiary structures and the acid site structures of CPO and *AaeAPO* resemble each other. They are close related and have conserved structure near the heme.

1.2 Mechanistic Investigations of Intermediates in the Catalytic Cycle

The understanding of the catalytic cycle of heme-thiolate enzymes comes from the direct observation of the intermediates by a variety spectroscopic techniques [41]. Some other indirect methods, such as mechanistically diagnostic substrates, radical clocks [17] and KIEs [42] can also be used to study the step of C–H bond cleavage and the radical formation. Figure 1.13 shows the consensus mechanism of P450 catalyzed hydrocarbon hydroxylation reactions [43]. After the ferric enzyme binds with the substrate, the resting, six-coordinate ferric heme switches to five coordinated state by loss of a water ligand and a iron *d*-orbital spin state change from low-spin, $S = 1/2$, state (one unpaired electron) to a high-spin state with five unpaired electrons. After the formation of the enzyme-substrate adduct, this high-spin, five coordinate heme iron(III) is reduced to the ferrous, iron(II) state by a reductase and NAD(P)H. The ferrous P450 can bind molecular oxygen and becomes a ferrous cytochrome P450-dioxygen complex, sometimes considered to be a ferric-superoxo species. A second reduction and oxygen protonation produces compound 0 ($\text{Fe}^{\text{III}}\text{-OOH}$). Peroxidase and peroxxygenase compounds 0 are generated directly from the reaction between ferric enzymes with peroxides, the so-called peroxide shunt pathway. The protonation of the hydroxyl oxygen in this complex results in the O–O bond heterolytic cleavage to form $\text{Fe}^{\text{IV}}\text{-oxo}$ porphyrin radical

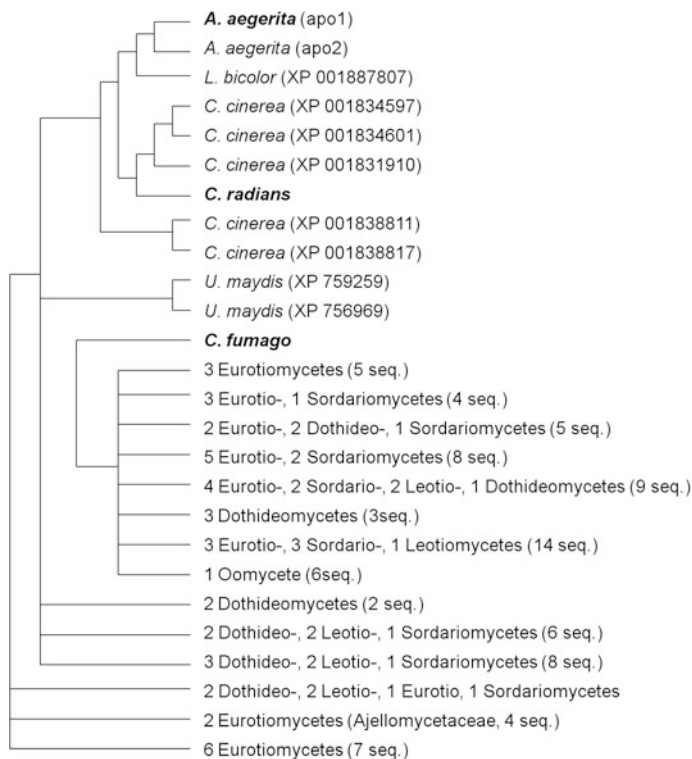


Fig. 1.12 A simplified phylogenetic tree of the heme/thiolate superfamily. Three characterized heme-thiolate proteins are in bold [36]

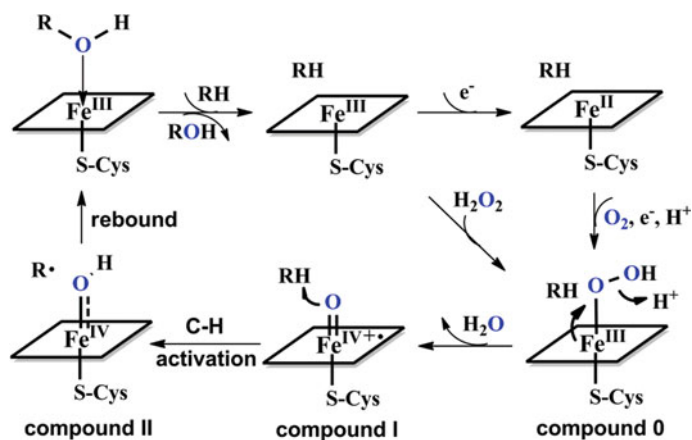


Fig. 1.13 Catalytic cycle of heme-thiolate enzyme catalyzed hydroxylation reactions

cation (compound I) and water. During the C–H abstraction step, compound I is reduced to compound II. Then, in the so-called rebound step, the iron-bound hydroxyl group captures the incipient carbon radical, resulting in the hydroxylated product and ferric enzyme. Last, the product is released from the active site and completes the cycle.

Detailed knowledge of the structural and electronic features of the intermediates are very important for a thorough understanding of the mechanism of heme-thiolate enzyme catalysts. So far, many intermediates have been detected and characterized in the catalytic cycle of porphyrin model complexes, *Aae*APO, CPO and CYP enzymes by various biophysical experimental methods [41, 44, 45]. Some text books introducing physical methods used in the field of bioinorganic chemistry are referenced here [46, 47]. Among these methods, UV-vis absorption spectroscopy is a sensitive method for intermediate detection due to the strong and very characteristic absorbances of the heme. The combination of fast, stopped-flow techniques with optical spectroscopy makes kinetic study of these intermediates possible [48]. Electron paramagnetic resonance (EPR) is a method to characterize paramagnetic centers of metals if there is an odd number of electron spins, such as the electronic spin states of ferric iron (Fe^{III}), hyperfine interactions with other nuclei, the zero-field splitting and so on [49, 50]. Mössbauer spectroscopy is a probe of the electronic structure of the iron center. It provides information such as the oxidation state of iron center, the spin state, the molecular geometry and so on [51]. Raman spectroscopy is another tool to characterize the interaction between metal and ligands. It provides information on the bond vibration modes [52]. In particular, resonance Raman spectroscopy provides bond vibrational information specifically in the vicinity of the heme. X-ray absorption fine structure (EXAFS) is a useful tool used to explore the structural information of the complexes [53]. It can provide information such as the distance between the metal-ligand, the number of ligated atoms and also the geometry. EXAFS is particularly useful if a protein crystal structure is not available. Redox properties of the metal can also be determined. There are many other bioinorganic tools for the study of metalloenzymes, such as NMR [54], MCD [55], X-ray diffraction [56], ENDOR [57], mass spectrometry [58], electrochemistry [59] and so on. Further, theoretical approaches, such as QM/MM calculations, have shown to be very informative on the structure, reactivity and selectivity characterization and provide a complementary tool to aid experiments [60, 61]. Usually, many different tools support each other, thus providing a complete characterization. A summary of important data which has been obtained for several intermediates in the catalytic cycle is presented here.

1.2.1 Compound 0

Cytochrome P450 iron-hydroperoxo complexes, also called compound 0, have been produced via either a direct reaction of the ferric enzyme with H_2O_2 or reduction of dioxygen bound to the ferrous enzyme followed by protonation [45]. Compound 0

of HRP, CPO and P450 have been characterized by UV/vis, EPR, ENDOR, X-ray absorption, Raman spectroscopy and QM/MM calculations before [62–64]. One of the obvious observations of P450 compound 0 formation is the ~ 30 nm red shift of Soret band [65]. From the electrical and structural characterization of P450 compound 0, it is clear that compound 0 has end-on coordination geometry [62]. From a crystal structure at 1.75 Å resolution and quantum chemical calculations, CPO compound 0 was determined to be ferric low-spin doublet ground state, with a Fe–O bond length of 1.8 Å and O–O bond length of 1.5 Å [29]. From the study of compound 0, we are able to understand how nature uses the cheap and accessible dioxygen as the oxidant.

1.2.2 Compound I

Heterolytic cleavage of the O–O bond in compound 0 results in an iron(IV)-oxo porphyrin radical cation species (compound I) [44]. The first evidence for a P450-I was provided by Egawa et al. [66]. It was generated from the reaction with *m*CPBA. A broad and weak band at 690 nm observed in the visible spectrum is characteristic of an iron(IV)-oxo porphyrin radical cation. Recently, a complete observation of a P450 compound I of CYP119 from the thermophilic archaeobacterium *Sulfolobus acidocaldarius* has been achieved using stopped-flow spectroscopy and freeze-quench techniques [67]. Substrate kinetics, EPR and Mössbauer spectroscopies were all well characterized. The kinetic data is consistent with the high reactivity of compound I toward hydrocarbons. For example, the second-order rate constant for lauric acid is 10^7 . Structural profiling of CPO-I indicated that the Fe=O bond length is short, 1.65 Å, determined by EXAFS [68], and confirmed by the high frequency ν (Fe–O) of 790 cm^{-1} in resonance Raman spectra [69]. This short Fe–O bond distance is indicative of the multiple bonding in the ferryl unit. An isotopic solvent H/D exchange experiment was recently done to show intermediate states during hydroxylation catalyzed by P450s. With the use of D_2 -camphor in H_2O , C5-OH_{exo} signal detected by ^1H ENDOR spectroscopy reappeared during annealing to 230 K [70]. All of these results provide convincing evidence that compound I is the reactive species responsible for C–H bond cleavage in hydrocarbon hydroxylation reactions.

1.2.3 Compound II

The one electron reduction of compound I that occurs during hydrogen atom abstraction forms another intermediate species called compound II. This is an important intermediate for the rebound step and sometimes called the rebound intermediate. Some spectroscopic studies of P450-II, CPO-II and related metalloporphyrin complexes are available [71–73]. The π -bonding orbitals of the porphyrin

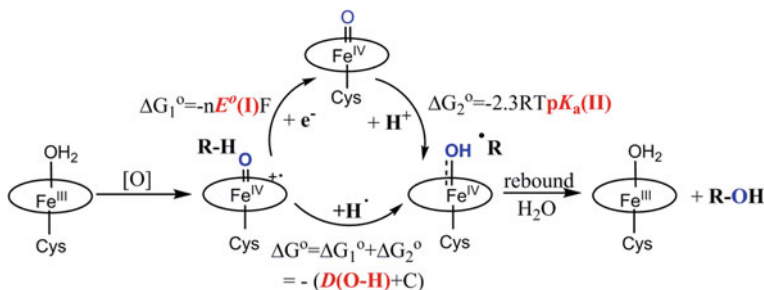


Fig. 1.14 Thermodynamic relationships between intermediates in the catalytic cycle of heme-thiolate enzymes

ring of compound II are fully occupied, resulting in a less powerful oxidant than compound I. Some studies suggested a two-electron oxidation catalyzed by compound II [74]. Attempts to generate P450-II were also achieved recently by cyro reduction of P450-I or the reaction between ferric enzyme with peroxyxynitrite [75].

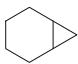
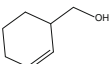

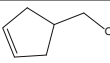
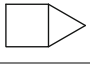
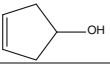

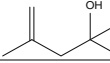

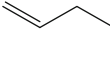
Besides the kinetic and electronic features of compound II, EXAFS data determined that CPO-II has a longer than expected Fe–O bond length of 1.82 Å [73]. This value was in good agreement with a density functional calculation of a highly unusual thiolate-ligated Fe(IV)–OH heme unit (1.81 Å). Resonance Raman spectra of CPO-II also detected the Fe(IV)–OD and Fe(IV)–¹⁸OH isotopic shift [76]. All of these results indicate that CPO-II is protonated at physiological pH. The study of P450-II is important because the capability of P450-I for hydrocarbon C–H activation depends on both the pK_a of P450-II and the one electron redox potential of P450-I *E*^o(I) (Eq. 1.1) [77]. Figure 1.14 is a Borwell thermodynamic cycle showed the relationship between three intermediates during the catalytic cycle based on expanded Hess’s law. It also explained how Eq. 1.1 was obtained. *D*(O–H) is the strength of the FeO–H bond that is forming, while *D*(C–H) is the strength of the substrate C–H bond that is breaking. This activation process has been called a proton coupled electron transfer (PCET) since the proton of the scissile C–H bond ends up on the basic ferryl oxygen while the electron reduces the porphyrin radical cation of compound I. As you can see, the basic nature of P450-II increases the driving force which is $\Delta G = D(\text{C-H}) - D(\text{O-H})$ for hydrocarbon abstraction.

$$D(\text{O} - \text{H}) = nFE^\circ(\text{I}) + 2.3RTpK_a(\text{II}) + 57 \pm 2 \quad (1.1)$$

1.2.4 Diagnostic Radical Clocks

Besides the direct characterization of reaction intermediates, indirect methods can also reveal the mechanism of the reaction cycle [78]. Diagnostic substrates are compounds that reveal the presence of particular substrate intermediates, radicals or

Table 1.1 Radical clocks used in heme-enzyme studies

Radical clocks	Radical rearranged products	Rearrangement rates	Enzymes	Radical lifetime (ps)	References
		2.0×10^8	P450 _{cam} CYP2B1 <i>Aae</i> APO	52 16 9.4	[81] [38]
		2.9×10^7	P450 _{cam} CYP153A6	252 74	[82]
		2.1×10^9	Liver microsomes	50	[84]
		2.0×10^9	CYP2E1	120	[85]
		3.0×10^{11}	CYP2B4	1–500	[86]

cations, by the nature of the rearranged products that are observed. Radical clocks are compounds that reveal the life-times of substrate radical intermediates produced by C–H bond abstraction. Those radicals can either recombine to form unrearranged products or undergo rearrangement to another radical that result in distinct rearranged products. If the rate constants of the rearrangements are known and one assumes that the radical behavior in the enzyme active site is similar to that in solution, the radical life time and the rebound rates can be calculated. The hydrocarbon norcarane was first used as a mechanistically diagnostic substrate in the characterization of radical intermediates produced by reactive oxo-manganese(V) porphyrin model compounds [79]. The first radical clocks used in the study of P450 mechanism is bicyclo[2.1.0]pentane, showing significant amounts of radical rearranged products [80]. The rebound rate was calculated as $1.4 \times 10^{10} \text{ s}^{-1}$. Later, a series of different radical clocks were used [17]. Some of them can differentiate a radical pathway from a cation pathway, such as norcarane [81, 82]. The study with radical clocks proved the presence of a substrate radical, although some radical clocks suggest extremely fast rebound rates [83]. Table 1.1 is a summary of radical clocks have been used in heme-enzyme studies. Average radical lifetimes in the range of 10–100 ps mean that the radical lives long enough to tumble and rearrange in the active site but not long enough to freely diffuse from the active site.

1.2.5 Kinetic Isotope Effects

The hydrogen kinetic isotope effect (KIE) is another indirect method to study the C–H abstraction step [42]. Large intrinsic isotope effects are associated with hydrogen abstraction. For example, kinetic characterization of CYP119-I generated

by reaction with *m*CPBA showed extraordinarily fast pseudo-first-order rate constants, in the range of $10^6 \text{ M}^{-1}\text{s}^{-1}$. The KIE for hexanoic acid was 12.5 [67]. For *Aae*APO, intramolecular KIE of 16.0 was determined with *n*-hexane-1,1,1,2,2,3,3-*d*₇ for 2-hexanol under turnover conditions [38]. These large KIEs are indicative of a hydrogen abstraction with a symmetrical transition state structure. However, isotope effects can be masked if the C–H bond breaking step is not the rate-determining step, such as when binding and positioning of the substrate is partially rate-limiting. For example, the KIE for *o*-xylene with one methyl group deuterated is 9 but for *p*-xylene, the KIE is 6. For 4,4'-dimethylbiphenyl the KIE is almost masked completely, possibly because the two methyl groups are separated further, by a distance of 11 Å and the reorganization of the substrate is slow with respect to the rate of C–H scission [87]. This kind of kinetic masking of isotope effects is sometimes discussed in terms of commitment to catalysis [88]. The investigation on intrinsic KIE and intramolecular KIEs provide important information on the understanding the C–H abstraction step and also the substrate dynamics in the active site.

1.3 Application on the Design of New Biocatalysts with Protein Engineering

Regio- and stereospecific oxidation of non-functionalized hydrocarbons has continued to be a challenge in the field of synthetic chemistry, which has received considerable attention recently [89]. The knowledge obtained from investigations on the mechanism of heme-thiolate enzymes can be used to guide the design of new catalysts.

Protein engineering is a powerful tool for biocatalysts. In order to overcome intrinsic limitations of the application of many wild type CYPs, such as low solubility, low activity and lack of selectivity, proteins are engineered to be more robust catalysts both by site-directed mutagenesis and evolutionary approaches [90, 91]. One of the advantages of rational approaches is the relatively small variant library. This is based on the information obtained from crystal structures and mechanistic studies. Some active site volumes of proteins can be engineered to become bigger in order to increase the binding affinity of large substrate molecules. For example, cytochrome P450cam has been redesigned to be able to catalyze the regioselective aromatic hydroxylation of diphenylmethane by using a Y96A variant [92]. On the other hand, some active site volumes were down-sized with more bulky active site residues in order to fit small alkanes. For example, the F87W/Y96F/T101L/V247L variant of P450cam is able to oxidize *n*-butane with a high turnover rate of $755 \text{ nmol}(\text{nmolP450cam})^{-1}(\text{min})^{-1}$ [93]. Further, some variants have the capability to oxidize terminal alkanes [94].

However, rational redesign is not always possible because many protein crystal structures are not available. In this situation, evolutionary protein engineering plays

an important role as a complementary tool [95]. This approach creates a library of randomly mutated genes, then engineered proteins are screened for the desired property. This process is a mimic of the Darwinian evolution. The advantage of this method is that information about the protein structure is not necessary. With this strategy, some engineered proteins are found to be highly efficient in hydrocarbon activation. For example, evolutionary variants of P450_{BM3} were generated with multiple rounds. High activity was shown towards gaseous alkanes and ultimately on ethane with BDE of 101 kcal/mol [96].

1.4 Conclusions

Heme-thiolate enzymes, CYPs, CPO and now *Aae*APO, have attracted considerable attention due to their ability to mediate hydrocarbon oxygenation. Thus, these heme proteins join a select cohort of iron- and copper-containing proteins, such as methane monooxygenases and the environmentally ubiquitous non-heme diiron alkane hydroxylase AlkB that have this ability. In order to understand the reaction mechanisms of C–H oxygenation, a combination of spectroscopic techniques has been employed that have provided an opportunity to obtain electronic and structural properties of various reactive intermediates that perform the difficult chemistry. The primary Fe=O oxidant, compound I, and the radical rebound mechanism have been proven by many ways in these systems. It therefore guides us in designing new and better biocatalysts.

References

1. Crabtree, R.H.: Alkane C-H activation and functionalization with homogeneous transition metal catalysts: a century of progress—a new millennium in prospect. *J. Chem. Soc. Dalton* 2437–2450 (2001)
2. Dick, A.R., Sanford, M.S.: Transition metal catalyzed oxidative functionalization of carbon-hydrogen bonds. *Tetrahedron* **62**, 2439–2463 (2006)
3. Austin, R.N., Groves, J.T.: Alkane-oxidizing metalloenzymes in the carbon cycle. *Metallomics* **3**, 775–787 (2011)
4. Groves, J.T.: High-valent iron in chemical and biological oxidations. *J. Inorg. Biochem.* **100**, 434–447 (2006)
5. Lewis, J.C., Coelho, P.S., Arnold, F.H.: Enzymatic functionalization of carbon-hydrogen bonds. *Chem. Soc. Rev.* **40**, 2003–2021 (2011)
6. Hausinger, R.P.: Fe(II)/ α -ketoglutarate-dependent hydroxylases and related enzymes. *Crit. Rev. Biochem. Mol.* **39**, 21–68 (2004)
7. Krebs, C., Fujimori, D.G., Walsh, C.T., Bollinger Jr, J.M.: Non-heme Fe(IV)-oxo intermediates. *Acc. Chem. Res.* **40**, 484–492 (2007)
8. Tahiliani, M., Koh, K.P., Shen, Y., Pastor, W.A., Bandukwala, H., Brudno, Y., Agarwal, S., Iyer, L.M., Liu, D.R., Aravind, L., Rao, A.: Conversion of 5-methylcytosine to 5-hydroxymethylcytosine in mammalian DNA by MLL partner TET1. *Science* **324**, 930–935 (2009)

9. Koch, D.J., Chen, M.M., Van Beilen, J.B., Arnold, F.H.: In vivo evolution of butane oxidation by terminal alkane hydroxylases AlkB and CYP153A6. *Appl. Environ. Microbiol.* **75**, 337–344 (2009)
10. Smith, C.A., Hyman, M.R.: Oxidation of methyl tert-butyl ether by alkane hydroxylase in dicyclopropylketone-induced and n-octane-grown *Pseudomonas putida* GPo1. *Appl. Environ. Microbiol.* **70**, 4544–4550 (2004)
11. Lipscomb, J.D.: Biochemistry of the soluble methane monooxygenase. *Annu. Rev. Microbiol.* **48**, 371–399 (1994)
12. Lieberman, R.L., Rosenzweig, A.C.: Crystal structure of a membrane-bound metalloenzyme that catalyses the biological oxidation of methane. *Nature* **434**, 177–182 (2005)
13. Hatcher, L.Q., Karlin, K.D.: Oxidant types in copper-dioxygen chemistry: the ligand coordination defines the Cu-O₂ structure and subsequent reactivity. *J. Biol. Inorg. Chem.* **9**, 669–683 (2004)
14. Klinman, J.P.: The copper-enzyme family of dopamine β-monooxygenase and peptidylglycine α-hydroxylating monooxygenase: resolving the chemical pathway for substrate hydroxylation. *J. Biol. Chem.* **281**, 3013–3016 (2006)
15. Prigge, S.T., Mains, R.E., Eipper, B.A., Amzel, L.M.: New insights into copper monooxygenases and peptide amidation: structure, mechanism and function. *Cell. Mol. Life Sci.* **57**, 1236–1259 (2000)
16. Groves, J.T.: In: Ortiz de Montellano, P.R. (ed.) *Cytochrome P450: Structure, Mechanism and Biochemistry*, 3rd edn. pp. 1–44. Kluwer Academic/Plenum, New York (2004)
17. Ortiz de Montellano, P.R.: Hydrocarbon hydroxylation by cytochrome P450 enzymes. *Chem. Rev.* **110**, 932–948 (2010)
18. Omura, T.: Heme-thiolate proteins. *Biochem. Biophys. Res. Co.* **338**, 404–409 (2005)
19. Sono, M., Roach, M.P., Coulter, E.D., Dawson, J.H.: Heme-containing oxygenases. *Chem. Rev.* **96**, 2841–2887 (1996)
20. Green, M.T.: C-H bond activation in heme proteins: the role of thiolate ligation in cytochrome P450. *Curr. Opin. Chem. Biol.* **13**, 84–88 (2009)
21. Hsu, M.H., Savas, Ü., Griffin, K.J., Johnson, E.F.: Human cytochrome P450 family 4 enzymes: Function, genetic variation and regulation. *Drug Metab. Rev.* **39**, 515–538 (2007)
22. Schlichting, I., Berendzen, J., Chu, K., Stock, A.M., Maves, S.A., Benson, D.E., Sweet, B.M., Ringe, D., Petsko, G.A., Sligar, S.G.: The catalytic pathway of cytochrome P450cam at atomic resolution. *Science* **287**, 1615–1622 (2000)
23. Aikens, J., Sligar, S.G.: Kinetic solvent isotope effects during oxygen activation by cytochrome P-450cam. *J. Am. Chem. Soc.* **116**, 1143–1144 (1994)
24. Imai, M., Shimada, H., Watanabe, Y., Matsuhima-Hibiya, Y., Makino, R., Koga, H., Horiuchi, T., Ishimura, Y.: Uncoupling of the cytochrome P-450cam monooxygenase reaction by a single mutation, threonine-252 to alanine or valine: a possible role of the hydroxy amino acid in oxygen activation. *Proc. Natl. Acad. Sci. USA* **86**, 7823–7827 (1989)
25. Clutterbuck, P.W., Mukhopadhyay, S.L., Oxford, A.E., Raistrick, H.: Studies in the biochemistry of micro-organisms 65. (A) A survey of chlorine metabolism by moulds (B) Caldariomycin, C₅H₈O₂Cl₂, a metabolic product of *Caldariomyces fumago* woronichin. *Biochem. J.* **34**, 664–677 (1940)
26. Morris, D.R., Hager, L.P.: Chloroperoxidase. I. Isolation and properties of the crystalline glycoprotein. *J. Biol. Chem.* **241**, 1763–1768 (1966)
27. Zaks, A., Dodds, D.R.: Chloroperoxidase-catalyzed asymmetric oxidations-substrate-specificity and mechanistic study. *J. Am. Chem. Soc.* **117**, 10419–10424 (1995)
28. Dawson, J.H., Sono, M.: Cytochrome P-450 and chloroperoxidase: thiolate-ligated heme enzymes. Spectroscopic determination of their active site structures and mechanistic implications of thiolate ligation. *Chem. Rev.* **87**, 1255–1276 (1987)
29. Kühnel, K., Derat, E., Turner, J., Shaik, S., Schlichting, I.: Structure and quantum chemical characterization of chloroperoxidase compound 0, a common reaction intermediate of diverse heme enzymes. *Proc. Natl. Acad. Sci. USA* **104**, 99–104 (2007)

30. Sundaramoorthy, M., Turner, J., Poulos, T.L.: Stereochemistry of the chloroperoxidase active site: crystallographic and molecular-modeling studies. *Chem. Biol.* **5**, 461–473 (1998)
31. Sundaramoorthy, M., Turner, J., Poulos, T.L.: The crystal structure of chloroperoxidase: a heme peroxidase-cytochrome P450 functional hybrid. *Structure* **3**, 1367–1377 (1995)
32. Yi, X., Conesa, A., Punt, P.J., Hager, L.P.: Examining the role of glutamic acid 183 in chloroperoxidase catalysis. *J. Biol. Chem.* **278**, 13855–13859 (2003)
33. Fujishiro, T., Shoji, O., Nagano, S., Sugimoto, H., Shiro, Y., Watanabe, Y.: Crystal structure of H₂O₂-dependent cytochrome P450(SP alpha) with its bound fatty acid substrate insight into the regioselective hydroxylation of fatty acids at the alpha position. *J. Biol. Chem.* **286**, 29941–29950 (2011)
34. Shoji, O., Fujishiro, T., Nakajima, H., Kim, M., Nagano, S., Shiro, Y., Watanabe, Y.: Hydrogen peroxide dependent monooxygenations by tricking the substrate recognition of cytochrome P450(BS beta). *Angew. Chem. Int. Ed.* **46**, 3656–3659 (2007)
35. Lee, D.S., Yamada, A., Sugimoto, H., Matsunaga, I., Ogura, H., Ichihara, K., Adachi, S., Park, S.Y., Shiro, Y.: Substrate recognition and molecular mechanism of fatty acid hydroxylation by cytochrome P450 from *Bacillus subtilis*: crystallographic, spectroscopic, and mutational studies. *J. Biol. Chem.* **278**, 9761–9767 (2003)
36. Hofrichter, M., Ullrich, R., Pecyna, M.J., Liers, C., Lundell, T.: New and classic families of secreted fungal heme peroxidases. *Appl. Microbiol. Biotechnol.* **87**, 871–897 (2010)
37. Ullrich, R., Nuske, J., Scheibner, K., Spantzel, J., Hofrichter, M.: Novel haloperoxidase from the agaric basidiomycete *Agrocybe aegerita* oxidizes aryl alcohols and aldehydes. *Appl. Environ. Microbiol.* **70**, 4575–4581 (2004)
38. Peter, S., Kinne, M., Wang, X., Ullrich, R., Kayser, G., Groves, J.T., Hofrichter, M.: Selective hydroxylation of alkanes by an extracellular fungal peroxxygenase. *FEBS J.* **278**, 3667–3675 (2011)
39. Piontek, K., Ullrich, R., Liers, C., Diederichs, K., Plattner, D.A., Hofrichter, M.: Crystallization of a 45 kDa peroxxygenase/peroxidase from the mushroom *Agrocybe aegerita* and structure determination by SAD utilizing only the haem iron. *Acta Crystallogr. F* **66**, 693–698 (2010)
40. Wang, X., Peter, S., Kinne, M., Hofrichter, M., Groves, J.T.: Detection and kinetic characterization of a highly reactive heme-thiolate peroxxygenase compound I. *J. Am. Chem. Soc.* **134**, 12897–12900 (2012)
41. Luthra, A., Denisov, I.G., Sligar, S.G.: Spectroscopic features of cytochrome P450 reaction intermediates. *Arch. Biochem. Biophys.* **507**, 26–35 (2011)
42. Nelson, S.D., Trager, W.F.: The use of deuterium isotope effects to probe the active site properties, mechanism of cytochrome P450-catalyzed reactions, and mechanisms of metabolically dependent toxicity. *Drug Metab. Dispos.* **31**, 1481–1498 (2003)
43. Groves, J.T.: The bioinorganic chemistry of iron in oxygenases and supramolecular assemblies. *Proc. Natl. Acad. Sci. USA* **100**, 3569–3574 (2003)
44. Jung, C.: The mystery of cytochrome P450 Compound I: a mini-review dedicated to Klaus Ruckpaul. *BBA-proteins proteom* **1814**, 46–57 (2011)
45. Sligar, S.G., Makris, T.M., Denisov, I.G.: Thirty years of microbial P450 monooxygenase research: peroxo-heme intermediates: the central bus station in heme oxygenase catalysis. *Biochem. Biophys. Res. Co.* **338**, 346–354 (2005)
46. Que, L.J.: *Physical methods in bioinorganic chemistry*, 1st edn. University Science Books (2000)
47. Solomon, E.I.; Hodgson, K.O.: *Spectroscopic methods in bioinorganic chemistry*. American Chemical Society (1998)
48. Johnson, K.A.: Transient-state kinetic analysis of enzyme reaction pathways. *Enzymes* **XX**, 1–61 (1992)
49. Carrington, A., McLachlan, A.D.: *Introduction to magnetic resonance*. Harper and Row, New York (1967)
50. Pilbrow, J.R.: *Transition ion electron paramagnetic resonance*. Oxford University Press, Oxford (1991)

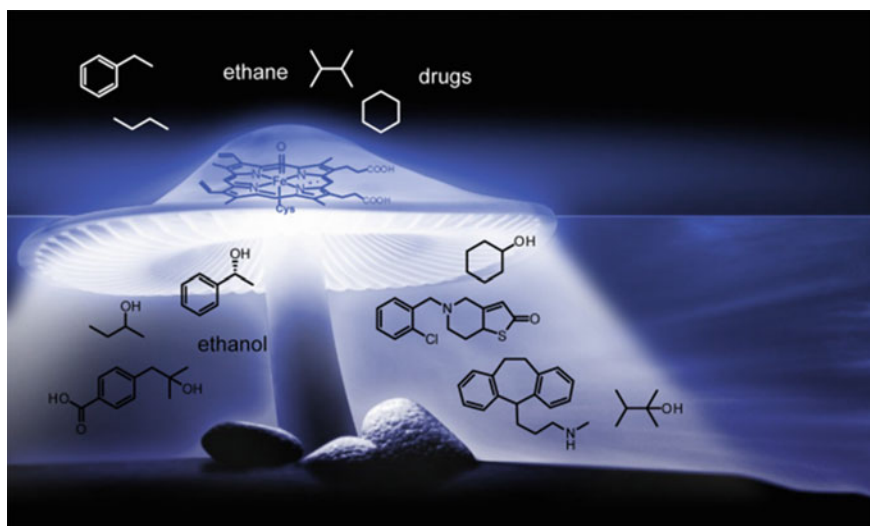
51. Güttlich, P., Bill, E., Trautwein, A.X.: Mössbauer spectroscopy and transition metal chemistry. Fundamentals and applications. Springer, Berlin (2011)
52. Spiro, T.G.: Biological applications of raman spectroscopy, vol. 2. Wiley, Canada (1988)
53. DeBeer, S.: X-ray absorption spectroscopy. In: Ribbe, M.W. (ed.) Nitrogen fixation: methods and protocols, vol. 766, pp. 165–176 (2011)
54. Iggo, J.A.: NMR spectroscopy in inorganic chemistry. Oxford University Press, Oxford (2000)
55. Stephens, P.J.: Theory of magnetic circular dichroism. *J. Chem. Phys.* **52**, 3489–3516 (1970)
56. Drenth, J.: Principles of protein X-ray crystallography, 3rd edn. Springer, Berlin (2006)
57. Schweiger, A., Jeschke, G.: Principles of pulse electron paramagnetic resonance. Oxford (2001)
58. Hoffmann, E.D., Stroobant, V.: Mass spectrometry: principles and applications. Wiley, New York (2007)
59. Bard, A.J.: Electrochemical methods: fundamental and applications, 2nd edn. Wiley, New York (2000)
60. Shaik, S., Cohen, S., Wang, Y., Chen, H., Kumar, D., Thiel, W.: P450 enzymes: their structure, reactivity, and selectivity-modeled by QM/MM calculations. *Chem. Rev.* **110**, 949–1017 (2010)
61. Neese, F.: Prediction of molecular properties and molecular spectroscopy with density functional theory: from fundamental theory to exchange-coupling. *Coordin. Chem. Rev.* **253**, 526–563 (2009)
62. Davydov, R., Makris, T.M., Kofman, V., Werst, D.E., Sligar, S.G., Hoffman, B.M.: Hydroxylation of camphor by-reduced oxy-cytochrome P450cam: mechanistic implications of EPR and ENDOR studies of catalytic intermediates in native and mutant enzymes. *J. Am. Chem. Soc.* **123**, 1403–1415 (2001)
63. Denisov, I.G., Makris, T.M., Sligar, S.G.: Formation and decay of hydroperoxo-ferric heme complex in horseradish peroxidase studied by cryoradiolysis. *J. Biol. Chem.* **277**, 42706–42710 (2002)
64. Denisov, I.G., Dawson, J.H., Hager, L.P., Sligar, S.G.: The ferric-hydroperoxo complex of chloroperoxidase. *Biochem. Biophys. Res. Co.* **363**, 954–958 (2007)
65. Denisov, I.G., Makris, T.M., Sligar, S.G.: Cryotrapped reaction intermediates of cytochrome P450 studied by radiolytic reduction with phosphorus-32. *J. Biol. Chem.* **276**, 11648–11652 (2001)
66. Egawa, T., Shimada, H., Ishimura, Y.: Evidence for compound I formation in the reaction of cytochrome-P450cam with M-chloroperbenzoic acid. *Biochem. Biophys. Res. Co.* **201**, 1464–1469 (1994)
67. Rittle, J., Green, M.T.: Cytochrome P450 compound I: capture, characterization, and C-H bond activation kinetics. *Science* **330**, 933–937 (2010)
68. Stone, K.L., Behan, R.K., Green, M.T.: X-ray absorption spectroscopy of chloroperoxidase compound I: Insight into the reactive intermediate of P450 chemistry. *Proc. Natl. Acad. Sci. USA* **102**, 16563–16565 (2005)
69. Egawa, T., Miki, H., Ogura, T., Makino, R., Ishimura, Y., Kitagawa, T.: Observation of the Fe (IV)=O stretching Raman band for a thiolate-ligated heme protein. Compound I of chloroperoxidase. *FEBS Lett.* **305**, 206–208 (1992)
70. Davydov, R., Dawson, J.H., Perera, R., Hoffman, B.M.: The use of deuterated camphor as a substrate in 1H ENDOR studies of hydroxylation by cryoreduced oxy P450cam provides new evidence of the involvement of compound I. *Biochemistry* **52**, 667–671 (2013)
71. Groves, J.T., Gross, Z., Stern, M.K.: Preparation and reactivity of oxoiron(IV) porphyrins. *Inorg. Chem.* **33**, 5065–5072 (1994)
72. Behan, R.K., Hoffart, L.M., Stone, K.L., Krebs, C., Green, M.T.: Evidence for basic ferryls in cytochromes P450. *J. Am. Chem. Soc.* **128**, 11471–11474 (2006)
73. Green, M.T., Dawson, J.H., Gray, H.B.: Oxoiron(IV) in chloroperoxidase compound II is basic: implications for P450 chemistry. *Science* **304**, 1653–1656 (2004)

74. Nam, W., Park, S.E., Lim, I.K., Lim, M.H., Hong, J., Kim, J.: First direct evidence for stereospecific olefin epoxidation and alkane hydroxylation by an oxoiron(IV) porphyrin complex. *J. Am. Chem. Soc.* **125**, 14674–14675 (2003)
75. Newcomb, M., Halgrimson, J.A., Horner, J.H., Wasinger, E.C., Chen, L.X., Sligar, S.G.: X-ray absorption spectroscopic characterization of a cytochrome P450 compound II derivative. *Proc. Natl. Acad. Sci. USA* **105**, 8179–8184 (2008)
76. Stone, K.L., Behan, R.K., Green, M.T.: Resonance Raman spectroscopy of chloroperoxidase compound II provides direct evidence for the existence of an iron(IV)-hydroxide. *Proc. Natl. Acad. Sci. USA* **103**, 12307–12310 (2006)
77. Mayer, J.M.: Hydrogen atom abstraction by metal-oxo complexes: understanding the analogy with organic radical reactions. *Acc. Chem. Res.* **31**, 441–450 (1998)
78. Griller, D., Ingold, K.U.: Free-radical clocks. *Acc. Chem. Res.* **13**, 317–323 (1980)
79. Groves, J.T., Kruper, W.J., Haushalter, R.C.: Hydrocarbon oxidations with oxometalporphyrinates: isolation and reactions of a (porphinato)manganese(V) complex. *J. Am. Chem. Soc.* **102**, 6375–6377 (1980)
80. Ortiz de Montellano, P.R., Stearns, R.A.: Timing of the radical recombination step in cytochrome-P-450 catalysis with ring-strained probes. *J. Am. Chem. Soc.* **109**, 3415–3420 (1987)
81. Auclair, K., Hu, Z.B., Little, D.M., Ortiz de Montellano, P.R., Groves, J.T.: Revisiting the mechanism of P450 enzymes with the radical clocks norcarane and spiro[2,5]octane. *J. Am. Chem. Soc.* **124**, 6020–6027 (2002)
82. Austin, R.N., Deng, D.Y., Jiang, Y.Y., Luddy, K., van Beilen, J.B., Ortiz de Montellano, P.R., Groves, J.T.: The diagnostic substrate bicyclohexane reveals a radical mechanism for bacterial cytochrome P450 in whole cells. *Angew. Chem. Int. Ed.* **45**, 8192–8194 (2006)
83. Newcomb, M., Toy, P.H.: Hypersensitive radical probes and the mechanisms of cytochrome P450-catalyzed hydroxylation reactions. *Acc. Chem. Res.* **33**, 449–455 (2000)
84. Bowry, V.W., Ingold, K.U.: A radical clock investigation of microsomal cytochrome P-450 hydroxylation of hydrocarbons. Rate of oxygen rebound. *J. Am. Chem. Soc.* **113**, 5699–5707 (1991)
85. Cooper, H.L.R., Groves, J.T.: Molecular probes of the mechanism of cytochrome P450. Oxygen traps a substrate radical intermediate. *Arch. Biochem. Biophys.* **507**, 111–118 (2011)
86. Toy, P.H., Newcomb, M., Hollenberg, P.F.: Hypersensitive mechanistic probe studies of cytochrome P450-catalyzed hydroxylation reactions. Implications for the cationic pathway. *J. Am. Chem. Soc.* **120**, 7719–7729 (1998)
87. Iyer, K.R., Jones, J.P., Darbyshire, J.F., Trager, W.F.: Intramolecular isotope effects for benzylic hydroxylation of isomeric xylenes and 4,4'-dimethylbiphenyl by cytochrome P450: relationship between distance of methyl groups and masking of the intrinsic isotope effect. *Biochemistry* **36**, 7136–7143 (1997)
88. Cleland, W.W.: Use of isotope effects to elucidate enzyme mechanisms. *CRC Cr. Rev. Biochem. Mol.* **13**, 385–428 (1982)
89. Bordeaux, M., Galameau, A., Drone, J.: Catalytic, mild, and selective oxyfunctionalization of linear alkanes: current challenges. *Angew. Chem. Int. Ed.* **51**, 10712–10723 (2012)
90. O'Reilly, E., Köhler, V., Flitsch, S.L., Turner, N.J.: Cytochromes P450 as useful biocatalysts: addressing the limitations. *Chem. Commun.* **47**, 2490–2501 (2011)
91. Jung, S.T., Lauchli, R., Arnold, F.H.: Cytochrome P450: taming a wild type enzyme. *Curr. Opin. Biotech.* **22**, 809–817 (2011)
92. Fowler, S.M., England, P.A., Westlake, A.C.G., Rouch, D.R., Nickerson, D.P., Blunt, C., Braybrook, D., West, S., Wong, L.L., Flitsch, S.L.: Cytochrome P-450 cam monooxygenase can be redesigned to catalyse the regioselective aromatic hydroxylation of diphenylmethane. *J. Chem. Soc. Chem. Comm.* 2761–2762 (1994)
93. Bell, S.G., Orton, E., Boyd, H., Stevenson, J.A., Riddle, A., Campbell, S., Wong, L.L.: Engineering cytochrome P450cam into an alkane hydroxylase. *Dalton T.* **11**, 2133–2140 (2003)

94. Meinhold, P., Peters, M.W., Hartwick, A., Hernandez, A.R., Arnold, F.H.: Engineering cytochrome P450BM3 for terminal alkane hydroxylation. *Adv. Synth. Catal.* **348**, 763–772 (2006)
95. Romero, P.A., Arnold, F.H.: Exploring protein fitness landscapes by directed evolution. *Nat. Rev. Mol. Cell Biol.* **10**, 866–876 (2009)
96. Meinhold, P., Peters, M.W., Chen, M.M.Y., Takahashi, K., Arnold, F.H.: Direct conversion of ethane to ethanol by engineered cytochrome P450 BM3. *Chem. Biol. Chem.* **6**, 1765–1768 (2005)

Chapter 2

Efficient and Selective Alkane Hydroxylation Reactions Catalyzed by the Fungal Peroxygenase *AaeAPO*



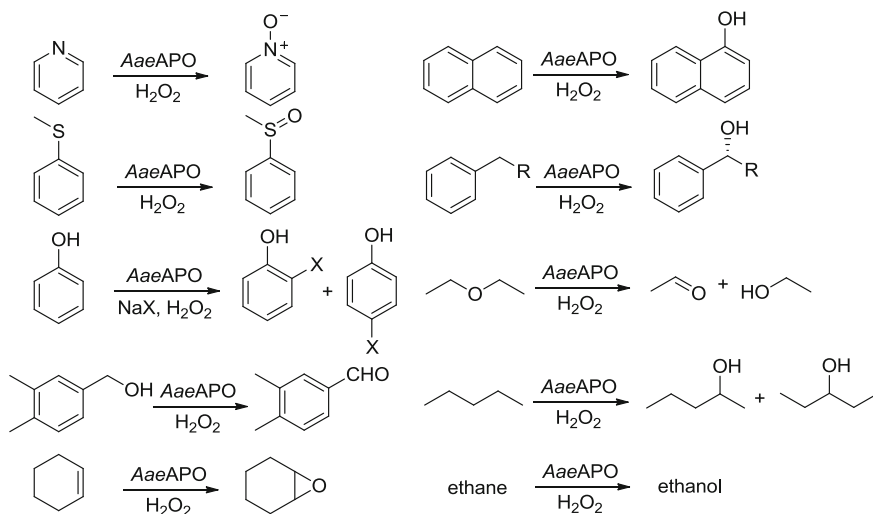
Abstract In this chapter, we report *AaeAPO* catalyzed alkane hydroxylations with H_2O_2 as the sole oxidant. High selectivity for alcohols, high efficiency of H_2O_2 utilization, high regioselectivity and stereospecificity were observed. The scope of the alkane substrates includes linear, branched and cyclic hydrocarbons, further expanding to gaseous ethane, propane and neopentane. Metabolites of several drug molecules were also analyzed and compared with P450s metabolites. Combining with coenzymes or cofactors, *AaeAPO* can also utilize the environmentally desirable oxidant O_2 to perform C–H oxidation. All these various reactions suggest that *AaeAPO* has potential practical application as an industrial biocatalyst.

2.1 Introduction

The fungal peroxygenase *Aae*APO has become a promising biocatalyst in biotechnological applications. It has a proximal cysteine ligating to the heme iron, the same as chloroperoxidase (CPO) and cytochrome P450s. It also fills the gap between peroxidases and monooxygenases, catalyzing various kinds of reactions [1], such as nitrogen oxidation, sulfoxidation, halogenations [2], olefin epoxidation, ether cleavage [3], aromatic [4], benzylic [5] and alkyl [6] hydroxylation by using peroxide as oxidants (Scheme 2.1). More importantly, *Aae*APO catalyzes reactions with high efficiency and selectivity, making them have more potential industrial applications such as producing pharmaceutical drugs, use as antimicrobial agents or detergents and so on.

Since *Aae*APO is a highly glycosylated, extracellular enzyme, it has high stability with wide tolerant temperature range and even tolerates in organic solvents [6]. For example, its stability has been tested in different nonpolar organic solvents over time. Data showed that the peroxygenase maintained at least 50 % of its activity after 30 min of incubation in all solvents tested and almost no loss of activity after 2 h of incubation in acetone/water mixture (60 % v/v) (Table 2.1). There are numerous advantages to use an enzyme in organic or organic-water mixed solvents system [7, 8]. For example, the possibility of carrying out new reactions that are impossible in water because of kinetic, thermodynamic or solubility restrictions. It might also prevent side reactions caused by the high concentration of water molecules. So, this high stability of *Aae*APO in organic solvents broadens its technological utility.

The C–H bonds strength of alkanes are quite strong, for example 99 kcal/mol for C–H bonds in cyclohexane. Sometimes, alkanes are even ideal solvents for very



Scheme 2.1 Different types of reactions catalyzed by *Aae*APO

Table 2.1 Stability of peroxygenase *AaeAPO* in different organic solvents

Solvent	Relative enzyme activity (%)		
	30 min	60 min	120 min
Acetone ^a	98.5 ± 5.6	101.4 ± 2.8	108.5 ± 1.4
HMN ^b	102.7 ± 9.2	106.7 ± 13.1	99.9 ± 9.4
<i>n</i> -Hexane	96.4 ± 2.8	101.4 ± 4.7	99.6 ± 13.5
Tetra ^b	87.6 ± 0.3	54.4 ± 0.5	65.5 ± 0.1
Tridecane	105.7 ± 23.6	86.1 ± 11.8	55.3 ± 18.5
2,3-DMB	85.8 ± 13.6	76.6 ± 5.1	32.8 ± 17.7
DCM ^b	51.9 ± 0.2	43.0 ± 0.2	–

Experiments were performed by Dr. Sebastian Peter and data were from Ref. [6]

^a(60 %); *HMN* Heptamethylnonane, *DMB* Dimethylbutane, *DCM* Dichloromethane

^bAlthough the enzyme was still active after aqueous extraction, the conversion of *n*-hexane in this solvent was not efficient

reactive oxidation catalysts. So they are difficult to activate. The functionalization of inert C–H bonds has been a challenge in the field of organic chemistry for a long time. Biomimetic transition-metal complexes are designed as catalysts to hydroxylate alkanes, but these complexes support very few total turnovers. Nature has design several biological systems to perform this function. For example, methane monooxygenase (MMO) from *Methylococcus capsulatus* (Bath) can hydroxylate C–H bonds of methane as well as other alkanes to yield alcohols [9]. Alkane hydroxylase (AlkB) from *Pseudomonas putida* GPo1 hydroxylates propane and butane and supports cell growth [10, 11]. AlkB selectively oxidizes at the terminal carbon of *n*-alkanes to produce the 1-alkanols. Cytochrome P450s are also capable of hydroxylating alkanes, but most of the time the selectivity is not obvious. Most of the biological systems require cofactors, such as NADPH and partner enzymes, such as reductase, to transfer electrons. So, the discovery of a simple and high efficiency biocatalyst is quite desirable for the potential industrial applications.

2.2 Results and Discussion

2.2.1 Hydroxylation of Alkanes with High Efficiency and Selectivity

Peroxygenase *AaeAPO* was found to efficiently hydroxylate a variety of alkanes, including linear, branched and cyclic saturated hydrocarbons using H₂O₂ as the terminal oxidant [6] (Scheme 2.2). The alkane hydroxylation reaction catalyzed by *AaeAPO* showed both regioselectivity and stereoselectivity. For example, *AaeAPO* prefers tertiary and secondary carbons but not primary carbons. Most linear alkanes (C₂–C₁₆) hydroxylations happened at the 2-position and 3-position. Experiments with *n*-heptane and *n*-octane showed that the hydroxylation proceeded with

Scheme 2.2 Alkane hydroxylation catalyzed by *AaeAPO*

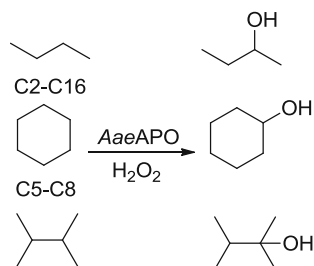


Table 2.2 Product distributions (% total alcohols) and % *ee* of selected products

Substrate	2-alcohol		3-alcohol		Ketones (%) ^b
	(%) ^a	<i>ee</i> %	(%) ^a	<i>ee</i> (%)	
Propane	100				Trace
<i>n</i> -Butane	100	(<i>S</i>) 30.8 ± 4.7			Trace
<i>n</i> -Pentane	34.1 ± 0.1	(<i>S</i>) 36.3 ± 4.7	65.9 ± 0.1		0.13 ± 0.18
<i>n</i> -Hexane	52.6 ± 0.7	(<i>R</i>) 62.5 ± 2.5	47.4 ± 0.7	(<i>R</i>) 79.5 ± 5.1	1.3 ± 0.1
<i>n</i> -Heptane	60.5 ± 0.1	(<i>R</i>) 62.2 ± 2.9	39.5 ± 0.1	(<i>R</i>) 99.9 ± 0.1	3.0 ± 0.2
<i>n</i> -Octane	55.0 ± 0.3	(<i>R</i>) 50.6 ± 1.5	45.0 ± 0.3	(<i>R</i>) 99.9 ± 0.1	1.1 ± 0.1

Experiments were performed by Dr. Sebastian Peter and data were from Ref. [6]

^aProduct distribution determined as ratio of a specific alcohol product in relation to the total amount of all alcohol products

^bProduct distribution for ketones was similar to that of alcohol product distribution. The numbers reported here are the total of all ketones (%) relative to total products (alcohols and ketones)

complete stereoselectivity for the (*R*)-enantiomer of the corresponding 3-alcohol. However, with short linear alkanes, such as *n*-butane and *n*-pentane, the major alcohol products were (*S*)-enantiomers (Table 2.2). Branched alkanes were oxidized regioselectively as well and cyclic alkanes (C₅–C₈) also yielded monohydroxylated products (Fig. 2.1). For example, 2,3-dimethylbutane was oxidized to 2,3-dimethylbutan-2-ol with 2,2,3,3-tetramethyloxirane as a minor product. Cyclohexane hydroxylation resulted cyclohexanol with only trace amounts of cyclohexanone as an over-oxidized product. However, multihydroxylated reaction products, such as diols, were not detected.

The high stereoselectivity of *AaeAPO* catalyzed linear alkane hydroxylation reactions are worthy of further discussion. It is interesting to compare the values obtained with those of engineered P450s [12], which were optimized for the selective oxidation of alkanes. In general, the *ee*-values of the (*R*)-enantiomers and (*S*)-enantiomers obtained are somewhat higher than those of engineered P450s; in particular, this applies to the *ee*-value of more than 99 % for the 3-alcohols obtained after the reaction of peroxigenase with *n*-heptane or *n*-octane.

Our results demonstrate that *AaeAPO* catalyzes the hydroxylation of diverse alkanes. This type of reaction suggests that *AaeAPO* may have a role in the

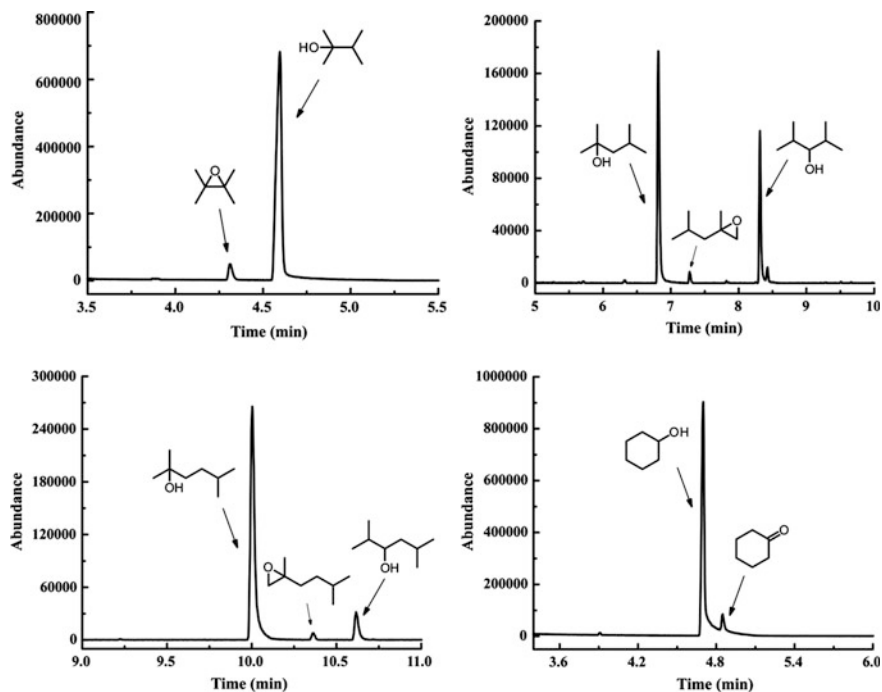
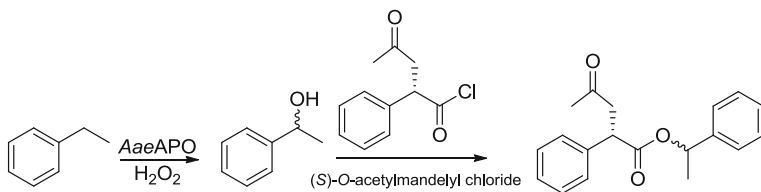


Fig. 2.1 GC/MS total ion chromatogram of alkane hydroxylation product mixtures catalyzed by *AaeAPO*

biodegradation of lignin or cutin fragments, or in the detoxification of aliphatic compounds that show fungicidal activity, such as terpenes and oxylipins in soils, plant litter, and wood [13].

2.2.2 Hydroxylation at Benzyl Position with a High Degree of Stereoselectivity

Enantiomeric analysis of the *R* and *S* stereoisomers of 1-phenylethanol was done by GC of the diastereomeric esters formed by the reaction of enzymatic mixture with (*S*)-*O*-acetylmandelyl chloride [14] (Scheme 2.3). Our result showed that the benzylic hydroxylation results in (*R*)-1-phenylethanol as the major product (Fig. 2.2). The highest *ee* could be 99 % [15]. The ability of producing pure *R*-isomer at the benzylic position is of high importance and has potential industrial application because they are important building blocks used in organic synthesis. The yield of (*R*)-1-phenylethanol per enzyme has been optimized in a fed-batch reactor, TTN of 43000 related to (*R*)-1-phenylethanol and a space-time yield of



Scheme 2.3 The determination of enantiomers

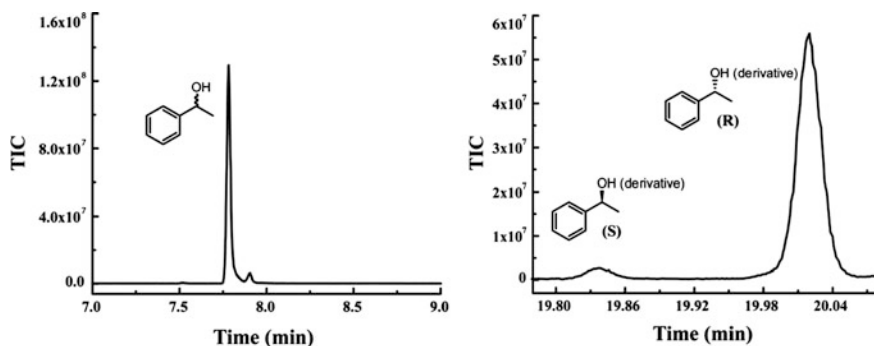


Fig. 2.2 Left GC trace of reaction mixture from the hydroxylation of ethylbenzene catalyzed by *AaeAPO*. Right GC trace of diastereomeric (*S*)-*O*-acetylmandelate esters of 1-phenylethanol mixtures

approximately $60 \text{ g L}^{-1} \text{ d}^{-1}$ [5]. It proves the application of *AaeAPO* in a process-oriented approach.

The range of acceptable substrates for *AaeAPO* is also wider than that of CPO. The benzylic oxidation of ethylbenzene catalyzed by CPO gave 2-phenethyl alcohol in the *R* configuration with *ee* of 97 %. The oxidation of propylbenzene resulted in *S*-1-phenyl-1-propanol in the *S* configuration, *ee* of 88 % [16]. However, *AaeAPO* oxidized propylbenzene producing the *R* isomer as well. Unlike CPO, cumene, tetralin and indane are all good substrates for *AaeAPO* [5].

The *ee* of benzylic hydroxylation by *AaeAPO* is also higher than some P450s. For example, P450cam hydroxylate ethylbenzene with *ee* of about 46 % [17]. Ethylbenzene hydroxylation by a newly discovered P450_{BSP} resulted the *ee* from 35 to 68 % with different carboxylic acids as decoy molecules [18].

2.2.3 Hydroxylation of Neopentane and Ethane

Methane (CH_4) is the simplest hydrocarbon and is the principal component of natural gas. It is abundant throughout the world. Methane is not used very efficiently because it is a combustible gas that requires impractical and expensive gas pipelines and liquefaction stations for transportation and handling. Lots of oil wells combust methane instead of storing it for future use. Methods of converting methane into more useful chemicals and fuels are challenging. Some costly and inefficient methods require high temperatures and pressures. A direct method for conversion of methane into methanol would be ideal because methanol is useful energy that is easy to handle. The oxidation of methane is difficult because the C–H bond strength in methane is as high as 104 kcal/mol.

The biological oxidation of methane is catalyzed by MMOs. But MMOs are complex enzymes and many of them are membrane proteins. There are many problems with using it as a biocatalyst for industrial application. P450s or engineered P450s have also been shown to accept methane. By using the enzyme P450 BM3 (CYP102A1) from *Bacillus megaterium* as the catalyst, a maximum TON of 2472 were achieved with perfluoro octanic acids as additives [19]. The additives are chemical inert to fill the binding pocket and reduce the freedom of small substrates. Another enzyme, P450153A6 has also shown the ability of methane oxidation by using iodossylbenzene as the oxidant [20]. These results confirmed that methane C–H bond can be activated by P450s. Engineered P450s have also shown the ability to oxidize ethane to ethanol [21]. We want to know about the ability of *Aae*APO for the oxidation of small gaseous molecules.

The reaction was set up with saturated neopentane or ethane in buffer under 1 atm pressure and at room temperature. The reaction mixtures were subjected to ^1H NMR analysis directly after the reactions were done. Then, neopentanol was extracted to organic solvent and can be analyzed by GC-MS. Figure 2.3 shows GC

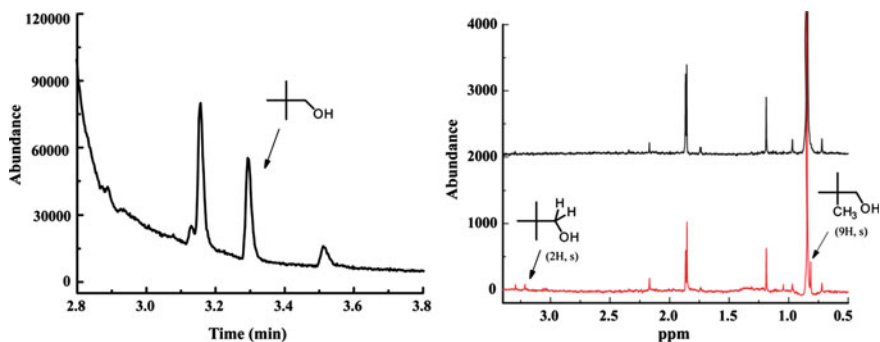
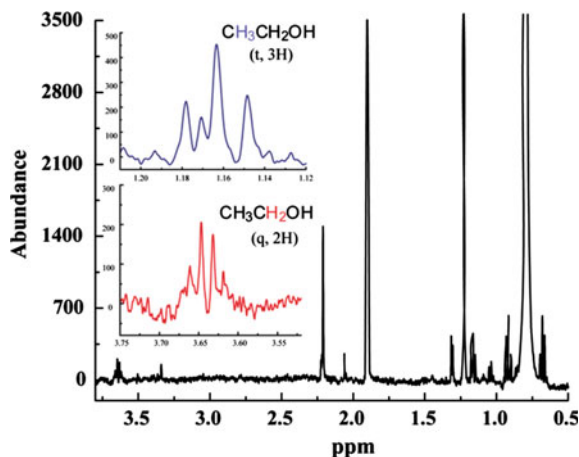


Fig. 2.3 Left GC trace of product mixture after the reaction of neopentane with H_2O_2 catalyzed by *Aae*APO. Right ^1H NMR of product mixture and compare it with control. There are new peaks corresponding to neopentanol. The total turnover was about 30. The final concentration of ethanol was 13 μM calculated from an internal standard which was added before doing NMR

Fig. 2.4 ^1H NMR of ethane oxidation catalyzed by *Aae*APO. New peaks are formed and corresponding to ethanol. The total turnover was about 10. The final concentration of ethanol was $6\ \mu\text{M}$ calculated from an internal standard which was added when doing NMR



trace and water suppressed ^1H NMR of mixtures after neopentane reactions. In the right figure, the arrows pointed to two new peaks corresponding to neopentanol (2H, s and 9H, s). No neopentanol was formed in the controls without adding *Aae*APO. The total turnover was about 30. In Fig. 2.4, the enlarged two panels show ethanol peaks (2H, q and 3H, t). No over-oxidized products were detected. The total turnover was about 10. Our results showed that without the help of additives, *Aae*APO is better than wild-type P450 BM3 for small alkanes oxidation. The result is competitive with some engineered P450s.

Methane oxidation was also carried out under the same conditions. But no detection of methanol was found. Maybe the TTN is so small that ^1H NMR is not sensitive enough for the detection of trace amount of products. But the successful conversion of ethane to ethanol is a good starting point. It is worth trying more reaction conditions on methane oxidation, such as the use of decoy molecules and run the reaction under high pressure.

2.2.4 Drug Metabolites

About one-third of the P450s within mammals are found in the liver and their major functions are involved in the degradation of xenobiotics. And it has been recognized that most of the pharmaceutical compounds are metabolized by P450s. So far the most intensively studied route of drug metabolism is the P450-catalysed oxidation reactions [23, 24]. Metabolite characterization has become one of the key drivers of the drug discovery process. Some of the drug metabolites kept active or even become more active. Some of the metabolites are toxic. So studying the metabolites of drugs helps the design of new drugs and makes important decisions on drug candidates.

Similar to P450s, *Aae*APO has showed powerful oxidization capability to selectivity functionalize inert C–H bonds to hydroxyl groups. So, here we expand

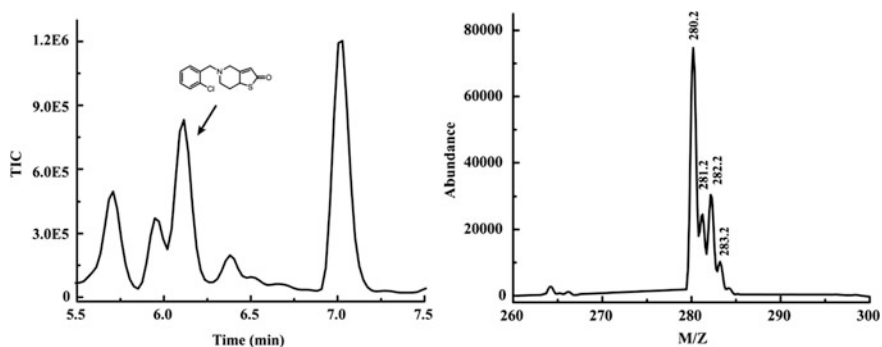
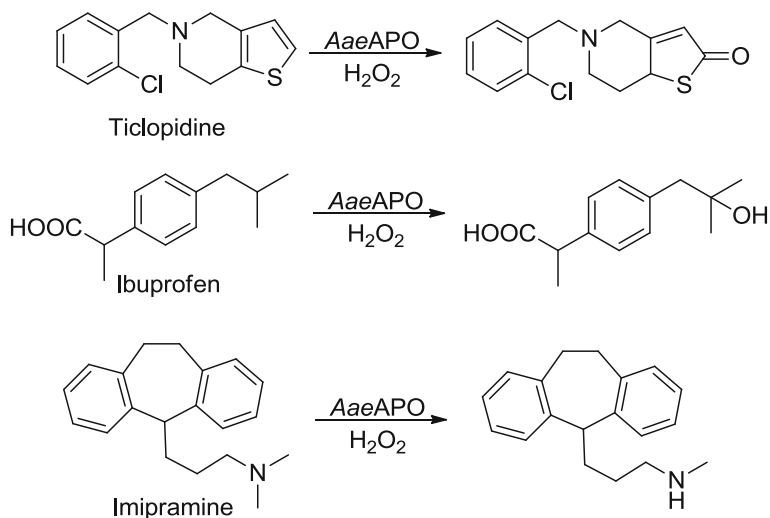


Fig. 2.5 HPLC trace and ESI-MS of ticlopidine metabolites

its substrates to pharmaceutical drugs and study the metabolites (Scheme 2.4). Our results suggest that *AaeAPO* could be a useful biocatalyst to prepare pharmacologically relevant drug metabolites and for the discovery of new commercial products including drugs.

Clopidogrel (Plavix) is a prodrug metabolized by cytochrome P450 to an active form that inhibits ADP-induced platelet aggregation. Before clopidogrel, its analog ticlopidine was used in patients. Early studies have showed that among all of metabolites of ticlopidine, 2-oxo-ticlopidine was the only metabolite that had anti-platelet activity in vivo [24]. Our HPLC-MS analysis showed that 40 % of the total metabolites by *AaeAPO* in vitro was 2-oxo-ticlopidine (Fig. 2.5). The retention



Scheme 2.4 Several examples of drug metabolites by *AaeAPO*

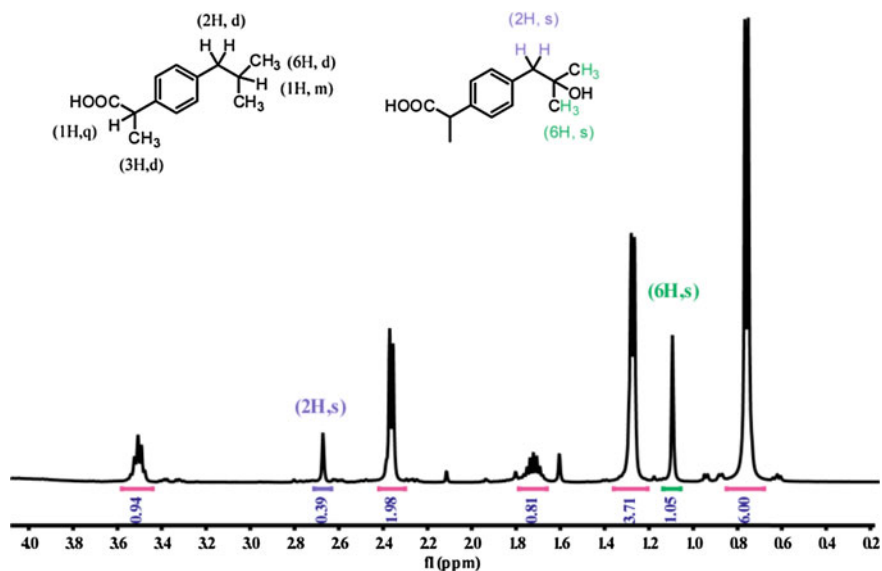


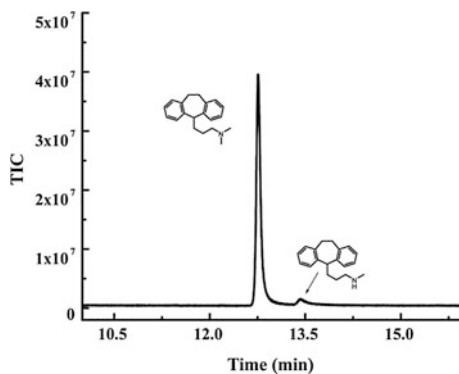
Fig. 2.6 Water suppressed ^1H NMR of ibuprofen metabolites

time and ESI-MS was confirmed by the authentic standard. So *Aae*APO might have the same function as CYP2C19 in the liver [25].

Ibuprofen is a drug to relieve pain, tenderness, swelling, and stiffness caused by osteoarthritis. Analyzed by ^1H NMR of the reaction mixture, the major metabolite of ibuprofen by *Aae*APO is 2-hydroxyibuprofen (80 % of total metabolites) (Fig. 2.6). Similar to CYPs, 2-hydroxyibuprofen is the major metabolite. Whereas 3-hydroxyibuprofen is almost exclusively produced by CYP2C9 [26].

Imipramine is an antidepressant medicine. The metabolite of imipramine by *Aae*APO is the demethylated product desipramine, the same as CYP1A2/2C19/3A4 [27]. With human liver microsomes in vitro, the major metabolites formed are desipramine and 2-hydroxyimipramine as well (Fig. 2.7).

Fig. 2.7 GC trace of the imipramine metabolites



2.2.5 Flavin Cofactors and Glucose Oxidase Coenzymes

2.2.5.1 Too Much H₂O₂ Can Kill the Activity of the Enzyme

High concentration of H₂O₂ could inactivate enzyme by oxidative degradation of the heme prosthetic group. The Michaelis-Menton profile of saturated veratryl alcohol or benzyl alcohol conversion catalyzed by *Aae*APO with different concentration of H₂O₂ showed that 2.5 mM of H₂O₂ decreased the formation rates dramatically (Fig. 2.8). Though portionwise addition of oxidants by the syringe pump can maintain the total H₂O₂ concentration at acceptable levels and it was shown to increase the total turnover number (TTN) of *Aae*APO. There are still contacts between highly concentrated H₂O₂ at the needle top with enzyme solution. The heterogeneous external addition speeds up the enzyme inactivation. So a method of generating H₂O₂ homogeneously by the reduction of O₂ is desirable.

2.2.5.2 Glucose Oxidase Coenzymes Catalytic Cycle

Glucose oxidase catalyzes the oxidation of glucose to produce H₂O₂ and gluconic acid. In the GOx-catalyzed redox reaction, its cofactor FAD works as the initial electron acceptor and is reduced to FADH₂. Then FADH₂ is oxidized by the final electron acceptor, molecular oxygen. O₂ is then reduced to hydrogen peroxide (H₂O₂) (Fig. 2.9). This enzymatic method solves the problem of generating H₂O₂ in situ. But in order to make a specific amount of product, equal amount of glucose has to be used. In the end, the reaction generates equal amount of gluconic acid as the by-product [16] (Scheme 2.5).

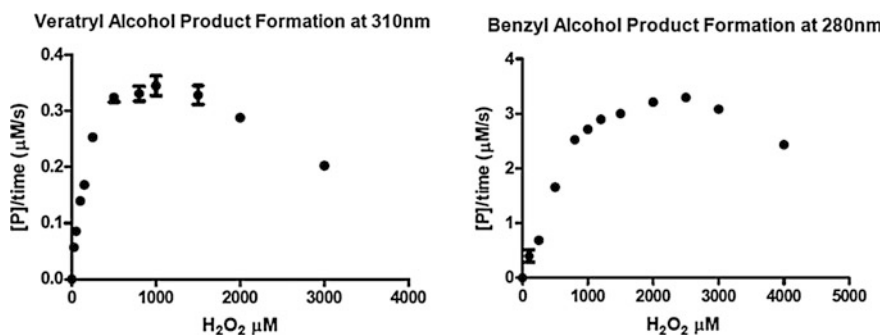


Fig. 2.8 The product formation rates change catalyzed by *Aae*APO with different concentration of H₂O₂

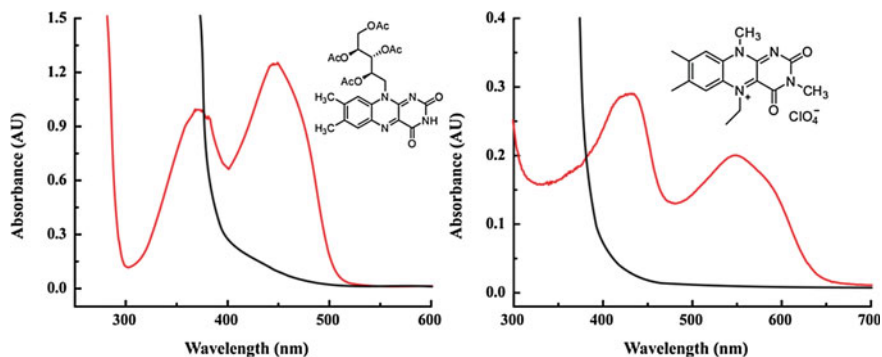
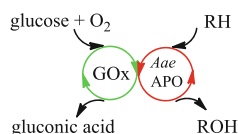


Fig. 2.9 The UV-vis spectrum of TARF and LumiFlEt at KP 50 mM pH 6. The red lines are oxidized forms and the black lines are reduced forms by excess DTT

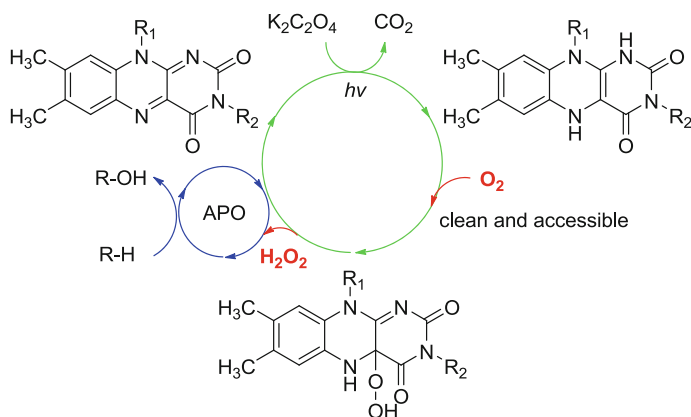


Scheme 2.5 The couple of *AaeAPO* and glucose oxidase catalytic cycles

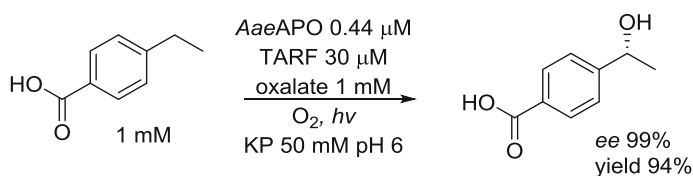
2.2.5.3 Flavin Cofactors Catalytic Cycle

Instead of using glucose oxidase as coenzyme, FAD or flavin moiety might serve the same function as the electron transport system in heme enzymes [28, 29]. A catalytic amount of flavin analogs were added into the system. Upon initiation by light, with the presence of electron sources such as EDTA or oxalate, flavin got reduced. The reduced $\text{Fl}_{\text{red}}\text{H}_2$ reacts with O_2 in the solution, produces H_2O_2 and regenerates the oxidative form of Fl_{ox} . When the flavin catalytic cycle is coupled with *AaeAPO* cycle, typical *AaeAPO* substrates are converted (Scheme 2.6). Control experiments without flavin, electron sources or under the dark results in no products formation. Without *AaeAPO*, there is also no products formation, flavin only catalyzed by itself. The region- and stereo-selectivity are the same as adding external oxidants. For example, when using ethylbenzoic acid as the substrate, almost 100 % conversion to (*R*)-1-phenylethanol was obtained (Scheme 2.7). The byproduct of the reaction using EDTA as the electron donors are formaldehyde and ethylene diamine. However, the byproduct of using oxalate is CO_2 which is a clean gas generated out of the reaction mixture (Scheme 2.8).

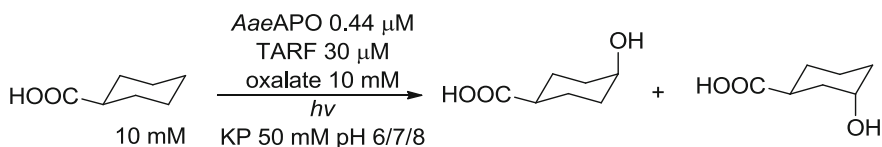
The percentage of conversion was confirmed by ^1H NMR (Fig. 2.10), the spectrum of products is distinct from the starting material. The triplet at 1.1 ppm is the methyl group of benzoic acid. The yield was calculated from the integration ratio between the new doublet at 1.36 ppm and the peak at 1.1 ppm. It turned out



Scheme 2.6 The catalytic cycles of *AaeAPO* reaction coupled with flavins



Scheme 2.7 Ethylbenzene hydroxylation by *AaeAPO* coupled with Flavin



Scheme 2.8 Cyclohexanecarboxylic acid hydroxylation by *AaeAPO* coupled with Flavin

the protein was still active when the reaction was stopped. We also optimized this clean photo-driven reaction by changing the concentration of flavin, using different flavins, different light sources, various reaction pHs and so on. The concentration of flavin concentration was optimized at 30 μ M. The TTN could not be improved with more concentrated flavin solution. N_2H_4 is also a good electron source. But the reaction did not work when EDTA and oxalate were replaced with N_2H_4 . The hydroxylation reaction at pH 6 was better than neutral and slightly basic conditions (Fig. 2.11) Four different flavins were tried (Table 2.3). The TARF gave the maximum yield. Lumiflavin and Phlumiflavin did not work well. This is possibly due to the positive charge on the catalysts.

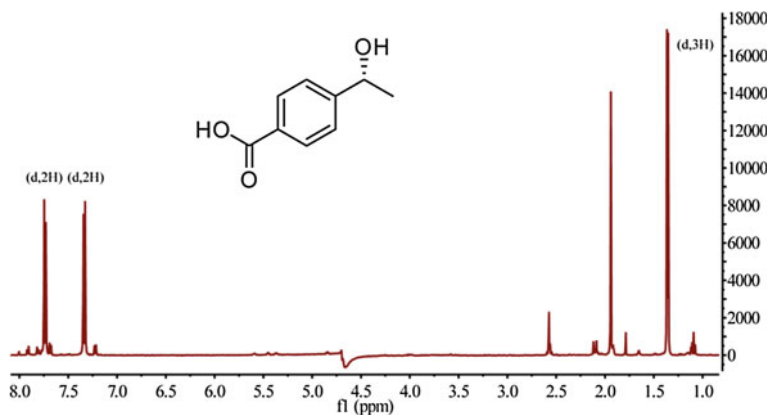


Fig. 2.10 Water suppressed ^1H NMR of ethylbenzoic acid hydroxylation products (94 % conversion)

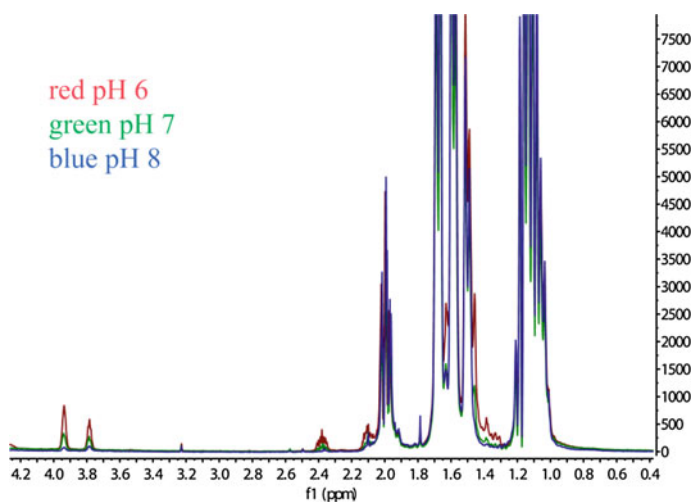
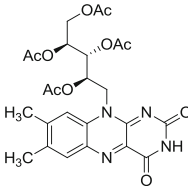
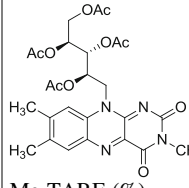
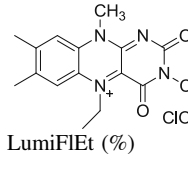
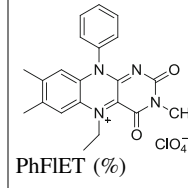


Fig. 2.11 Water suppressed ^1H NMR of cyclohexanecarboxylic acid hydroxylation product mixtures at pH 6, 7 or 8. The sharp two triplets at 3.78 and 3.95 ppm indicated that the hydroxylation happened on two axial sites

Like ethylbenzoic acid and cyclohexanecarboxylic acid, ethane and neopentane were also converted to their corresponding alcohol products with this new method. We are trying to carefully tune the active site of *Aae*APO by using different flavins in order to oxidize methane.

Table 2.3 Conversion of ethylbenzoic acid hydroxylation catalyzed by *Aae*APO and different flavins

 TARF (%)	 Me-TARF (%)	 LumiFIET (%)	 PhFIET (%)
45	36	4	0

2.3 Conclusions

In this chapter, we have demonstrated that *Aae*APO catalyzes the hydroxylation of diverse alkanes with high selectivity and efficiency. H_2O_2 was used as the sole friendly oxidant. But the flavin light-driven catalytic cycle coupled with *Aae*APO couple increases the stability of *Aae*APO and takes advantage of molecular oxygen as the green oxidant. The wide substrate scope and various kinds of reactions catalyzed by *Aae*APO prove its potential role as a good biocatalyst.

2.4 Experimental

Reagents: wild-type peroxygenase from *A. aegerita* (isoform II, pI 5.6, 46 kDa) was produced in bioreactors with a soybean-flour suspension as growth substrate, and purified as described previously [30]. The enzyme preparation was homogeneous by SDS/PAGE, and exhibited an $A_{418 \text{ nm}}/A_{280 \text{ nm}}$ ratio of 1.7. The specific activity of the peroxygenase was 59 U mg^{-1} , where 1 U represents the oxidation of 1 μmol of 3,4-dimethoxybenzyl alcohol to 3,4-dimethoxybenzaldehyde in 1 min at RT. All chemicals and glucose oxidase were of the best available purity from Aldrich. Different flavins were kindly provided by Dr. Erika Milczek. 2-oxo-ticlopidine authentic standard was kindly provided by Nick Boaz. (*S*)-*O*-acetylmandelyl chloride was made from thionyl chloride and (*S*)-*O*-acetylmandelic acid. D_2O was obtained from Cambridge Isotope Laboratories, Inc. Water used in all experiments was de-ionized (Millipore, Milli-Q). Buffers were prepared fresh daily using either citric acid/sodium citrate (pH 3–5), $\text{KH}_2\text{PO}_4/\text{K}_2\text{HPO}_4$ (pH 6–8).

Instruments: UV-vis spectral measurements were made with a Hewlett Packed 8453 diode array spectrophotometer at room temperature. GC-MS analysis were run using an Agilent 7890A GC coupled to a 5975 Inert MSD with a Rtx-5Sil MS column using the following temperature profile: $50 \text{ }^\circ\text{C}$ hold 2 min, $10 \text{ }^\circ\text{C min}^{-1}$ to $230 \text{ }^\circ\text{C}$. HPLC-MS analysis were done with HP 1100 A MS equipped with an auto-sampler. Separation was performed with a Luna C_{18} $50 \text{ mm} \times 4.6 \text{ mm}$ column

and gradient separation with acetonitrile and water. Water suppressed ^1H NMR and ^{13}C NMR spectra were recorded on a 500 MHz Bruker Avance II spectrometer.

Reaction conditions for alkane hydroxylation and drug metabolites: The reaction mixtures (0.20 ml, stirred at room temperature) contained 0.4 U of *Aae*APO, desired buffer pH (100 mM) and 2 μl of neat liquid alkanes or continuously bubbled with gaseous alkanes or 50 mM of drugs. The solution was mixed well by a stirred bar and then the reaction was started by syringe pumping 20 μl of 50 mM H_2O_2 with a rate of 1 $\mu\text{l}/\text{min}$. The mixture was extracted with ethyl acetate or DCM. The organic layers were combined, dried by Na_2SO_4 and then analyzed by GC/MS. Or when the reaction was done, the mixture was directly analyzed by HPLC/MS. Or when the reaction was done, several drops of D_2O were added into the solution then the mixture was subjected to water suppressed ^1H NMR and ^{13}C NMR.

Diastereomeric derivatization of 1-phenylethanol: The dried and concentrated DCM solution of 1-phenylethanol from the enzyme reaction was kept on ice in a septum-sealed vial. Dry pyridine (2 μL) was added, followed by excess amount of (S)-*O*-propionylmandelyl chloride (100 mM solution in DCM). The solution was stirred and allowed to stand at room temperature for at least 1 h. Sufficient reaction time was always used to ensure quantitative conversion of alcohol to ester. The resulting solution went through a short silicone gel column and then the solution was directly analyzed by GC-MS.

Coenzyme and cofactor reaction condition: A typical flavin light-driven reaction was performed by well mixing *Aae*APO (1U) with flavin (100 μM), EDTA or oxalate (10 mM) and substrates (10 mM) in a buffered solution. The open vial was placed in front of a lamp and illuminated for 30 min under aerobic conditions. If a closed vial was used, its cap was connected with a balloon filling with pure oxygen.

References

1. Hofrichter, M., Ullrich, R.: Heme-thiolate haloperoxidases: versatile biocatalysts with biotechnological and environmental significance. *Appl. Microbiol. Biotechnol.* **71**, 276–288 (2006)
2. Ullrich, R., Hofrichter, M.: The haloperoxidase of the agaric fungus *Agrocybe aegerita* hydroxylates toluene and naphthalene. *FEBS Lett.* **579**, 6247–6250 (2005)
3. Kinne, M., Poraj-Kobielska, M., Ralph, S.A., Ullrich, R., Hofrichter, M., Hammel, K.E.: Oxidative cleavage of diverse ethers by an extracellular fungal peroxygenase. *J. Biol. Chem.* **284**, 29343–29349 (2009)
4. Kinne, M., Zeisig, C., Ullrich, R., Kayser, G., Hammel, K.E., Hofrichter, M.: Stepwise oxygenations of toluene and 4-nitrotoluene by a fungal peroxygenase. *Biochem. Biophys. Res. Co.* **397**, 18–21 (2010)
5. Kluge, M., Ullrich, R., Scheibner, K., Hofrichter, M.: Stereoselective benzylic hydroxylation of alkylbenzenes and epoxidation of styrene derivatives catalyzed by the peroxygenase of *Agrocybe aegerita*. *Green Chem.* **14**, 440–446 (2012)

6. Peter, S., Kinne, M., Wang, X., Ullrich, R., Kayser, G., Groves, J.T., Hofrichter, M.: Selective hydroxylation of alkanes by an extracellular fungal peroxxygenase. *FEBS J.* **278**, 3667–3675 (2011)
7. Natarajan, K.R.: Biocatalysis in organic solvents. *J. Chem. Educ.* **68**, 13–16 (1991)
8. Klibanov, A.M.: Improving enzymes by using them in organic solvents. *Nature* **409**, 241–246 (2001)
9. Colby, J., Stirling, D.I., Dalton, H.: The soluble methane mono oxygenase of *Methylococcus capsulatus* (Bath). Its ability to oxygenate n alkanes, n alkenes, ethers, and alicyclic, aromatic and heterocyclic compounds. *Biochem. J.* **165**, 395–402 (1977)
10. Johnson, E.L., Hyman, M.R.: Propane and n-butane oxidation by *Pseudomonas putida* GPo1. *Appl. Environ. Microbiol.* **72**, 950–952 (2006)
11. Koch, D.J., Chen, M.M., Van Beilen, J.B., Arnold, F.H.: In vivo evolution of butane oxidation by terminal alkane hydroxylases AlkB and CYP153A6. *Appl. Environ. Microbiol.* **75**, 337–344 (2009)
12. Peters, M.W., Meinhold, P., Glieder, A., Arnold, F.H.: Regio- and enantioselective alkane hydroxylation with engineered cytochromes P450 BM-3. *J. Am. Chem. Soc.* **125**, 13442–13450 (2003)
13. Leonowicz, A., Matuszewska, A., Luterek, J., Ziegenhagen, D., Wojtaś-Wasilewska, M., Cho, N.S., Hofrichter, M., Rogalski, J.: Biodegradation of lignin by white rot fungi. *Fungal Genet. Biol.* **27**, 175–185 (1999)
14. White, R.E., Miller, J.P., Favreau, L.V., Bhattacharyya, A.: Stereochemical dynamics of aliphatic hydroxylation by cytochrome P-450. *J. Am. Chem. Soc.* **108**, 6024–6031 (1986)
15. Kluge, M., Ullrich, R., Scheibner, K., Hofrichter, M.: Stereoselective benzylic hydroxylation of alkylbenzenes and epoxidation of styrene derivatives catalyzed by the peroxxygenase of *Agrocybe aegerita*. *Green Chem.* **14**, 440–446 (2012)
16. Zaks, A., Dodds, D.R.: Chloroperoxidase-catalyzed asymmetric oxidations: substrate-specificity and mechanistic study. *J. Am. Chem. Soc.* **117**, 10419–10424 (1995)
17. Filipovic, D., Paulsen, M.D., Loida, P.J., Sligar, S.G., Ornstein, R.L.: Ethylbenzene hydroxylation by cytochrome P450cam. *Biochem. Biophys. Res. Co.* **189**, 488–495 (1992)
18. Shoji, O., Fujishiro, T., Nakajima, H., Kim, M., Nagano, S., Shiro, Y., Watanabe, Y.: Hydrogen peroxide dependent monooxygenations by tricking the substrate recognition of cytochrome P450(BS beta). *Angew. Chem. Int. Ed.* **46**, 3656–3659 (2007)
19. Zilly, F.E., Acevedo, J.P., Augustyniak, W., Deege, A., Reetz, M.T.: Tuning a P450 enzyme for methane oxidation. *Angew. Chem. Int. Ed.* **50**, 2720–2724 (2011)
20. Chen, M.M., Coelho, P.S., Arnold, F.H.: Utilizing terminal oxidants to achieve P450-catalyzed oxidation of methane. *Adv. Synth. Catal.* **354**, 964–968 (2012)
21. Meinhold, P., Peters, M.W., Chen, M.M.Y., Takahashi, K., Arnold, F.H.: Direct conversion of ethane to ethanol by engineered cytochrome P450 BM3. *Chem. Biol. Chem.* **6**, 1765–1768 (2005)
22. Xu, F., Bell, S.G., Lednik, J., Insley, A., Rao, Z., Wong, L.L.: The heme monooxygenase cytochrome P450cam can be engineered to oxidize ethane to ethanol. *Angew. Chem. Int. Ed.* **44**, 4029–4032 (2005)
23. Kawakami, N., Shoji, O., Watanabe, Y.: Direct hydroxylation of primary carbons in small alkanes by wild-type cytochrome P450BM3 containing perfluorocarboxylic acids as decoy molecules. *Chem. Sci.* (2013)
24. Fraire, Picard: C.: Ticlopidine hydrochloride: relationship between dose, kinetics, plasma concentration and effect on platelet function. *Thromb. Res.* **30**, 119–128 (1983)
25. Holmes, M.V., Perel, P., Shah, T., Hingorani, A.D., Casas, J.P.: CYP2C19 genotype, clopidogrel metabolism, platelet function, and cardiovascular events: a systematic review and meta-analysis. *JAMA-J. Am. Med. Assoc.* **306**, 2704–2714 (2011)
26. Hamman, M.A., Thompson, G.A., Hall, S.D.: Regioselective and stereoselective metabolism of ibuprofen by human cytochrome P450 2C. *Biochem. Pharmacol.* **54**, 33–41 (1997)

27. Bull, S., Catalani, P., Garle, M., Coecke, S., Clothier, R.: Imipramine for cytochrome P450 activity determination: a multiple-species metabolic probe. *Toxicol. In Vitro* **13**, 537–541 (1999)
28. Perez, D.I., Grau, M.M., Arends, I.W.C.E., Hollmann, F.: Visible light-driven and chloroperoxidase-catalyzed oxygenation reactions. *Chem. Comm.* 6848–6850 (2009)
29. Churakova, E., Kluge, M., Ullrich, R., Arends, I., Hofrichter, M., Hollmann, F.: Specific photobiocatalytic oxyfunctionalization reactions. *Angew. Chem. Int. Ed.* **50**, 10716–10719 (2011)
30. Ullrich, R., Nuske, J., Scheibner, K., Spantzel, J., Hofrichter, M.: Novel haloperoxidase from the agaric basidiomycete *Agrocybe aegerita* oxidizes aryl alcohols and aldehydes. *Appl. Environ. Microbiol.* **70**, 4575–4581 (2004)

Chapter 3

Hydrocarbon Hydroxylations Catalyzed by *Aae*APO: Evidence of Radical Intermediates and Kinetic Isotope Effects



Abstract Recently, a new heme-thiolate peroxygenase enzyme from the fungus *Agrocybe aegerita*, was identified and found to be capable of catalyzing hydrocarbon hydroxylation by using H_2O_2 as co-substrate with high efficiency and selectivity. It not only shows potential for practical biocatalytic application but also might provide some inspiration for designing biomimetic catalysts. In order to investigate the reaction mechanism, several radical clocks were used in this chapter. Products indicative of radical intermediates were all detected during the oxidation of norcarane, bicycle[2.1.0]pentane and 1,1,2,2-tetremethylcyclopropane with lifetimes ranging from 3.0 to 132 ps. At the same time, a large intramolecular deuterium isotope effect was measured with the hydroxylation of 1,1,1,2,2,3,3- d_7 -n-hexane and methyl partially deuterated toluenes. Taken together, a mechanism involving hydrogen atom abstraction and rebound is suggested. More interestingly, small intramolecular KIEs probed by (*R*)-1-ethylbenzene were also observed. We thought these suppressions were caused by steric hindrance in the active site of enzyme. These isotope masking effects can give us some information about the dynamics of substrates and map the active site environment of enzyme.

3.1 Introduction

The consensus mechanism, hydrogen atom abstraction followed by a rebound mechanism, for hydroxylation reactions catalyzed by cytochrome P450 enzymes was first proposed in 1978 by Groves. It is based on the observation that the cytochrome P450-catalyzed hydroxylation of 2,3,5,6-tetradeuterated norbornane results in a partial inversion of stereochemistry at the carbon, indicating a carbon radical in the reaction mechanism [1]. As shown in Fig. 3.1, the catalytic cycle is initiated by substrate binding with resting enzyme and displacement of the water molecules in the active site. It also causes the spin-state change of iron center and conformational change of the enzyme. The ferric enzyme is reduced to its ferrous form with electron supplies from NAD(P)H and reductases. Ferrous iron binds a dioxygen, followed by further reduction and protonation, resulting in a Fe^{III} -hydroperoxo intermediate, also named compound 0. The heterolytic cleavage of the O–O bond in compound 0 gives the active species Fe^{IV} -porphyrin radical cation intermediate, compound I. After the step of C–H activation, compound II is formed by a one electron reduction of the porphyrin ring. The iron-bound hydroxyl group finally rebounds back to the substrate carbon radical to complete the catalytic cycle and release the product.

Some indirect methods have been used to probe the presence of a carbon-radical intermediate in the catalytic cycle and study the C–H bond cleavage step in the context of cytochrome P450 studies. For example, by using different radical clocks, this mechanism would render radical rearranged products [2, 3]. If the C–H bond cleavage is the rate determining step, this hydrogen atom abstraction mechanism would be subject to a large kinetic isotope effect [4]. Here, in this chapter, we want to use radical clocks and KIE probes to study the mechanism of *Aae*APO catalyzed alkane hydroxylation reactions.

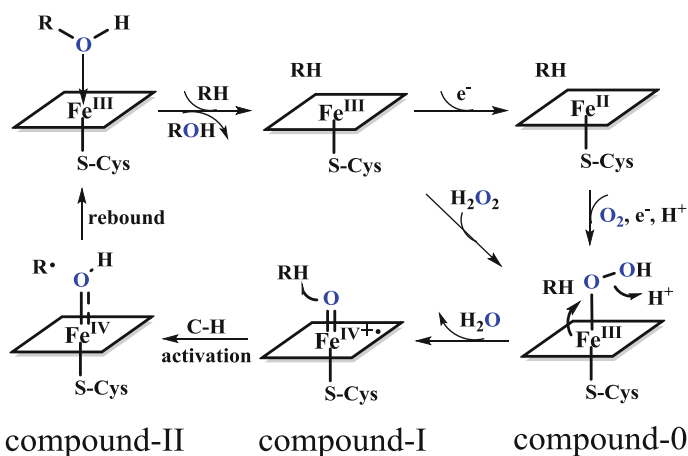


Fig. 3.1 Mechanism for the cytochrome P450 reaction cycle and peroxide shunt pathway

3.2 Results and Discussion

3.2.1 Radical Clocks

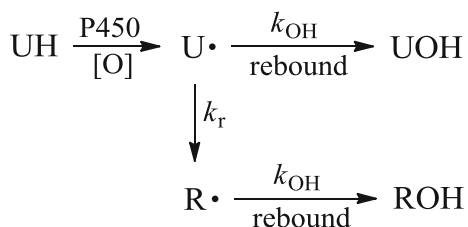
The rebound mechanism can be studied with radical clocks [3, 5]. When a radical clock (UH) is converted to a radical by hydrogen abstraction, it can collapse to an unrearranged product (UOH) or can undergo a rearrangement to a different product (ROH). From the known rearrangement rate, it is possible to estimate the radical lifetime (τ) and rebound rate (k_{OH}) as shown in Scheme 3.1 and calculated according to Eq. 3.1 [2]. The first radical clock substrates used in the P450 area is bicycle[2.1.0]pentane by Ortiz de Montellano and Stearns [6]. This study suggested a lifetime of 70 ps for the radical. Many other radical clocks substrates with different rearranged rates were also used for the study of P450s mechanism later. Some radical clocks, such as norcarane [7], can also differentiate a radical pathway from a cation pathway.

$$\tau = \frac{1}{k_{OH}} = \frac{ROH}{UOH \bullet k_r} \quad (3.1)$$

We examined the behavior of several radical clocks, such as norcarane, bicycle [2.1.0]pentane and TMCP, as diagnostic substrates with *Aae*APO. We detected rearranged alcohol products, measured radical life time, thus pointing to the mechanism involving hydrogen abstraction and OH rebound.

3.2.1.1 Bicycloheptane

To verify whether a substrate radical is formed, we studied the oxidation of norcarane (bicyclo[4.1.0]heptane), a radical clock substrate that has often been used to evaluate the reaction mechanism of P450s and other alkane-oxidizing enzymes [8–10]. The GC/MS profile of the *Aae*APO catalyzed hydroxylation of norcarane shows that diverse reaction products were formed [11] (Fig. 3.3). The reactions yielded exo-2-norcaranol as the major product, smaller amounts of endo-2-norcaranol, and exo-norcaranol and endo-3-norcaranol; they also yielded a product expected to be



Scheme 3.1 Radical clock (Ingold's Model)

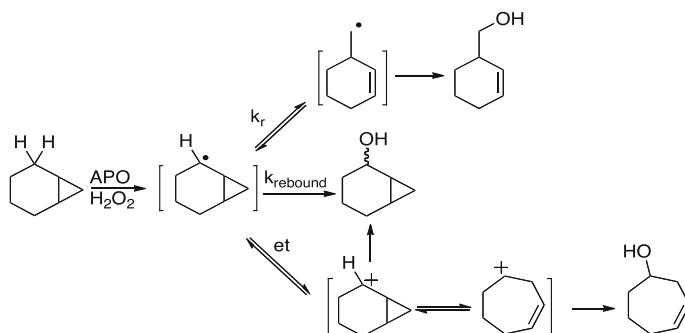
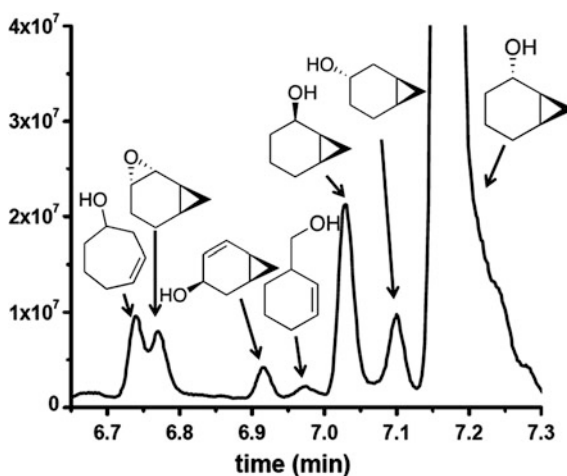


Fig. 3.2 Rearrangement pathways and products resulting from formation of a radical or a cation intermediate upon oxidation of norcarane

Fig. 3.3 GC/MS total ion current chromatogram in the region of the alcohols produced from the hydroxylation of norcarane by *Aae*APO. In addition, traces of desaturation products and an epoxide were detected



derived from the cationic intermediate 3-cyclohepten-1-ol, and the radical rearrangement product 4-(hydroxymethyl)-cyclohexane, which have all previously been described for P450s [7].

On the basis of the ratio of the rearranged radical reaction product cyclohex-2-enyl methanol and norcaranol, we calculated a radical lifetime of 9.4 ps and an oxygen rebound rate of $1.06 \times 10^{11} \text{ s}^{-1}$, which is six-fold to 20-fold faster than the values observed for functional similar P450s ($0.62 \sim 2 \times 10^{10} \text{ s}^{-1}$) [7, 12]. Interestingly, the major product of peroxygenase catalysis was exo-2-norcaranol. Its amount was about 25-fold higher than that of endo-2-norcaranol, which is different from what is seen with P450s [7]. Moreover, 3-cyclohepten-1-ol is also observed and its amount is more than that of radical rearranged product. Its formation was attributed to a competing electron transfer oxidation of the incipient radical (Fig. 3.2).

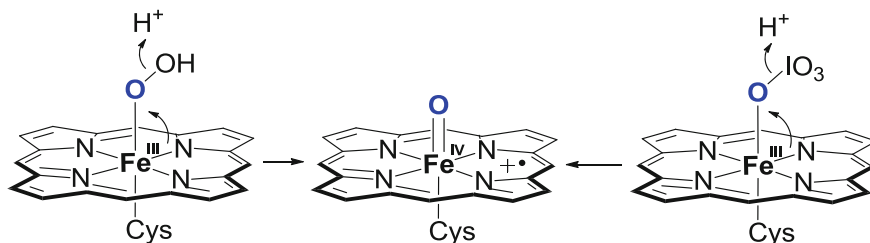


Fig. 3.4 Compound I formation from H_2O_2 and NaClO_4

Besides H_2O_2 , with other oxidants such as PAC, TBHP, NaClO_4 and *m*CPBA, the radical rearranged product was also detected and the mixture of products are the same ratio as Fig. 3.3. This result suggests that the same reactive species (compound I) was formed by different oxygen sources and the hydrogen abstractor is compound I (Fig. 3.4).

3.2.1.2 Bicyclo[2.1.0]Pentane

Hydrogen abstraction of bicyclo[2.1.0]pentane gives a radical that could rearrange to a monocyclic radical. The rearrangement rate is $2.1 \times 10^9 \text{ s}^{-1}$ [6]. We also made this radical clock. (Scheme 3.2) The GC-MS of products mixture showed the major product was the unrearranged endo-2-hydroxybicyclo[2.1.0]pentane. And a significant amount of ring opened product 3-cyclopenten-1-ol was detected (Fig. 3.6). From the ratio, the radical life time of 132 ps was calculated. This number is longer than that obtained from norcarane. Possibly it is caused by the fact that bicycle [2.1.0]pentane could not differentiate a radical intermediate from a cation intermediate (Fig. 3.5). This can also be explained by the competition between cage escape and geminate recombination. Smaller substrates are more mobile than bigger ones in the active site of the enzymes [13].

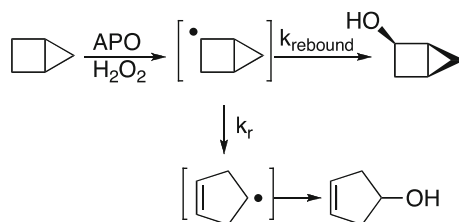
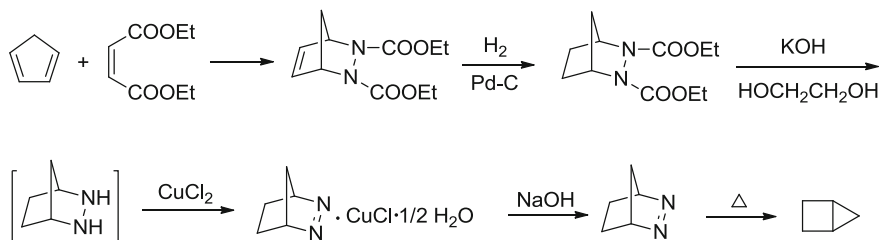
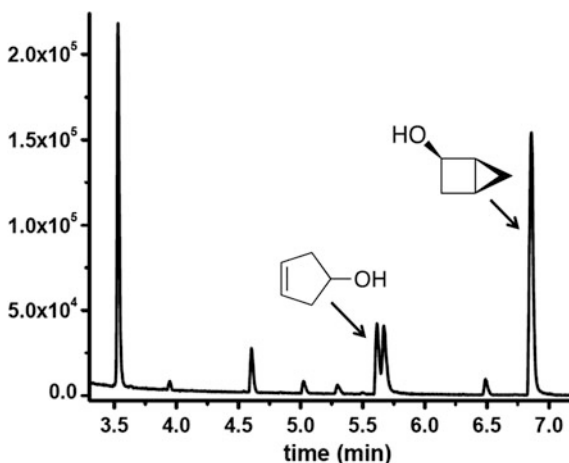


Fig. 3.5 Rearrangement pathways and products resulting from the oxidation of bicycle[2.1.0] pentane



Scheme 3.2 The synthesis of bicyclo[2.1.0]pentane

Fig. 3.6 GC/MS of the oxidation of bicyclo[2.1.0]pentane by *Aae*APO



3.2.1.3 TMCP

Alkylsubstituted cyclopropane rings, such as 1,1,2,2-tetramethylcyclopropane (TMCP), were also used in the radical clock study [12] (Fig. 3.8). The major hydroxylation product was the unrearranged primary alcohol. Some small amounts of rearranged tertiary alcohol were also detected. The oxygen trapped radical intermediate, diacetone alcohol, was also observed. But its amount was much smaller than several P450s we examined before [12]. Another interesting thing about TMCP oxidation by *Aae*APO is the desaturation products.

The desaturation products accounts for about 30 % of total turnover. This might come from the second hydrogen abstraction on the carbon adjacent to the carbon radical center. Or it might be caused by the electron transfer to form a cationic carbon and followed by proton transfer (Fig. 3.7). The olefins are easily further epoxidated. Previous TMCP results with three P450s (CYP2E1, CYP3A4 and rat CYP2B1) show no desaturation products [12]. Maybe the relative orientation of TMCP in the active site promotes desaturation. Or maybe the active species compound II of *Aae*APO promotes electron transfer. Recently, catalysis with mixed

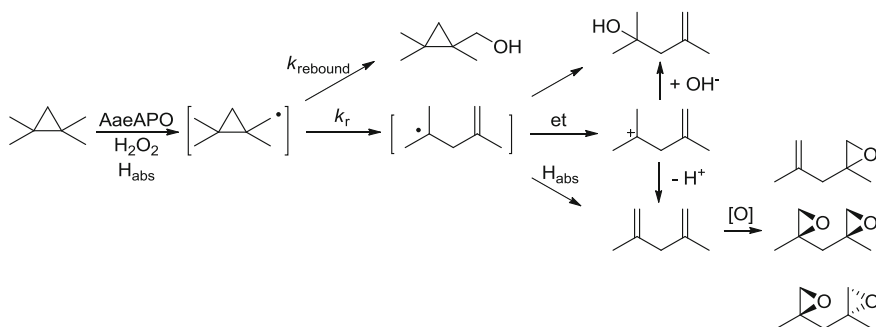
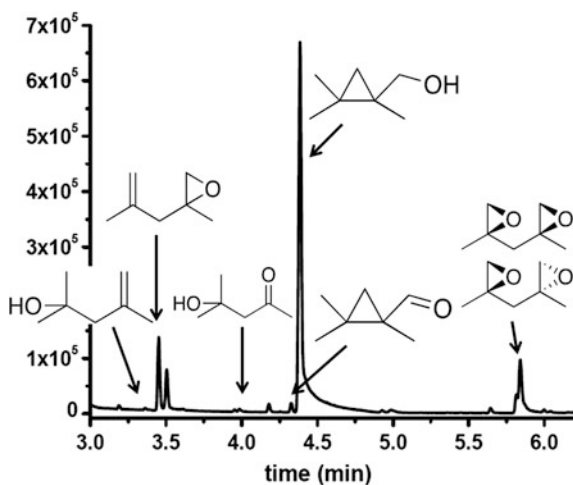


Fig. 3.7 Rearrangement pathways and products resulting from the oxidation of TMCP

Fig. 3.8 GC/MS of the oxidation of TMCP by *AaeAPO*



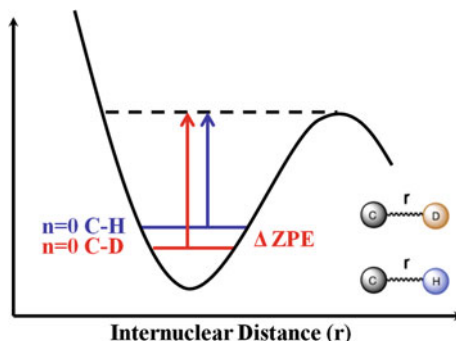
hydroxylation/desaturation activity has been designed. By understanding the reason of large amount of desaturation products formed by *AaeAPO*, we might be inspired to design new catalysis.

The rearrange rate of TMCP is $2 \times 10^9 \text{ s}^{-1}$. The radical life time is 3 ps and rebound rate is $3.3 \times 10^{11} \text{ s}^{-1}$, similar to the numbers obtained from norcarane oxidation [11]. These values also closely match the reported value for P450 catalyzed hydroxylation reactions reported by Ingold et al. [14].

3.2.2 Kinetic Isotope Effect (KIE)

$$\frac{k_H}{k_D} = e^{\frac{-AZPE}{kT}} = e^{\frac{hc(v_H - v_D)}{2kT}} \quad (3.2)$$

Fig. 3.9 The simplest model of kinetic isotope effect



Measuring kinetic isotope effects ($k_{\text{H}}/k_{\text{D}}$) is another way to unravel the C–H bond cleavage step and to define the mechanism of alkane hydroxylation catalyzed by enzymes [15]. Figure 3.9 is the simplest model illustrating the origin of kinetic isotope effect. When a hydrogen atom is replaced by a deuterium atom, this heavier atom leads to a lower vibration frequency. From quantum mechanical point of view, it causes a lower zero point energy (ZPE). Thus, more energy has to be supplied to break the bond. A higher activation energy is needed for bond cleavage, which in turn lowers the measured rate. Theoretically, KIE can be calculated according to Eq. 3.2. Its theoretical limit is 9 at 37 °C, without tunneling effects. Ideally, the primary intrinsic isotope effect is related to the nature of the transition state involving the bond cleavage.

However, most of the enzymatically mediated reactions have $\text{KIE}_{(\text{obs})}$ different from intrinsic KIEs. Besides the step of the catalytic reaction, there are also substrates binding and products release steps (Scheme 3.3). Considering this complicated situation, intramolecular KIE measurement has advantages since the active species attacks one of the two symmetrically equivalent sites, one deuterated and the other protonated, within the same molecule. Therefore, if the molecule reorients freely in the active site of the enzyme, the intramolecular $\text{KIE}_{(\text{obs})}$ should be close to the intrinsic KIE.

In this chapter, several intramolecular isotope labeling probes are used to define the hydrogen atom abstraction step by *Aae*APO. With *n*-hexane-1,1,1,2,2,3,3-*d*₇ and methyl group stepwise deuterated toluenes, large KIEs were obtained. The rate of C–H bond interchange in methyl groups must be faster than the rate of bond cleavage, so the KIE reflects the intrinsic KIE. Our large KIEs are consistent with the abstraction-recombination mechanism for aliphatic hydroxylation. On the other hand, single methyl-deuterated xylenes and chirally labeled ethylbenzenes resulted in some masking effects. This is related to the limited dynamics of substrates in the



Scheme 3.3 Kinetic model of enzymatic reactions

active site. The relative small KIE on the hydroxylation of weaker C–H bond of ethylbenzene also suggests the transition state is earlier than those with stronger C–H bonds.

3.2.2.1 *N*-Hexane-1,1,1,2,2,3,3- D_7

The symmetrical *n*-hexane-1,1,1,2,2,3,3- d_7 was used to determine whether alkane hydroxylation by *Aae*APO exhibits an intramolecular kinetic isotope effect [11]. Both sites 2 and 3 were hydroxylated catalyzed by *Aae*APO upon oxidation with H_2O_2 . The MS of each peak showed a high percentage of 2-hexanol- d_7 and 3-hexanol- d_7 over 2-hexanol- d_6 and 3-hexanol- d_6 (Fig. 3.10). The observed intramolecular isotope effects, $KIE_{(obs)}$ were 16.0 ± 1.0 for 2-hexanol and 8.9 ± 0.9 for 3-hexanol. These large values strongly indicate a hydrogen abstraction mechanism with the formation of a radical intermediate in the reaction cycle of *Aae*APO.

3.2.2.2 Methyl Group Stepwise Deuterated Toluenes

We used methyl group stepwise deuterated toluenes as probes. Since C–H bonds of methyl group rotate fast, the observed KIEs should be close to the intrinsic ones. Table 3.1 shows the analyzed results from GC-MS data. First, comparison of the alcohol/cresol ratios for $PhCH_3$ vs $PhCD_3$ indicated a very large net isotope effect of 20.5 for benzylic hydroxylation. Second, the extensive deuterium retention (92.4

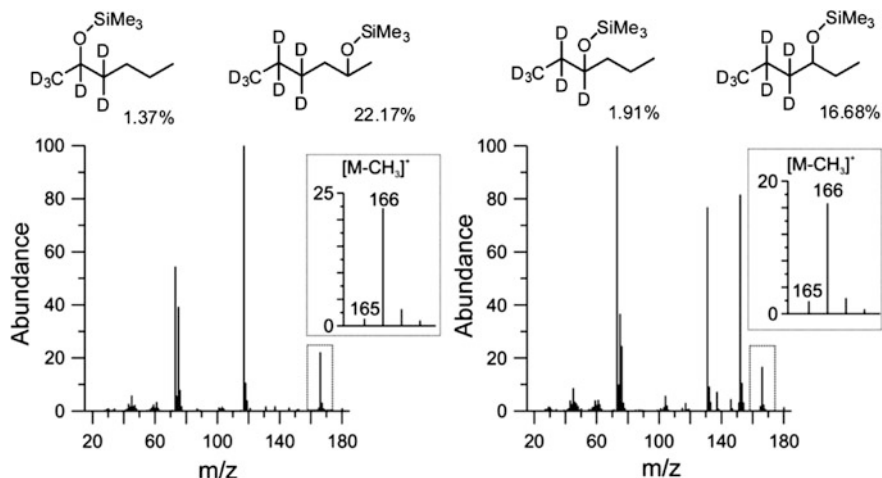


Fig. 3.10 Preferential hydroxylation products of 2-hexanol- d_7 and 3-hexanol- d_7 in *n*-hexane-1,1,1,2,2,3,3- d_7 by *Aae*APO. Mass spectra of trimethylsilylether derivatives resulted the KIE of the reactions (experiments were performed by Sebastian Peter and data were from Ref. [11])

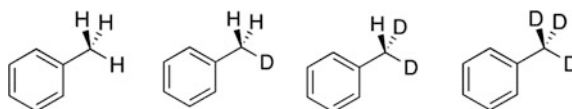
Table 3.1 Hydroxylation products of methyl stepwise deuterated toluenes

Probes	Benzyl alcohol (%)		<i>o</i> -cresol (%)	<i>p</i> -cresol (%)	<i>o</i> -cresol/ <i>p</i> -cresol	Cresols/benzyl alcohol
	H abs	D abs				
Toluene	34.4		53.9	11.7	4.6	1.9
Toluene- α - d_1	21.9		66.6	11.6	5.7	3.6
	92.4	7.63				
Toluene- α,α - d_2	13.2		71.2	15.7	4.5	6.6
	80.4	19.6				
Toluene- α,α,α - d_3	2.5		79.7	17.9	4.5	39.0

Table 3.2 Derived isotope effects for *Aae*APO hydroxylation of deuterated toluenes

Primary KIEs		Secondary KIEs	
$P_1 = \frac{k_{HH}^{HH}}{k_{HD}^{HH}}$	8.3	$S_1 = \frac{k_{HH}^{HH}}{k_{HD}^{HD}}$	1.37
$P_2 = \frac{k_{HD}^{HD}}{k_{DD}^{HD}}$	8.5	$S_2 = \frac{k_{HD}^{HD}}{k_{DD}^{DD}}$	1.02
$P_3 = \frac{k_{DD}^{DD}}{k_{DD}^{DD}}$	14.7	$S_3 = \frac{k_{DD}^{DD}}{k_{DD}^{DD}}$	1.39
–	–	$S_4 = \frac{k_{DD}^{DD}}{k_{DD}^{DD}}$	1.75

and 80.4 %) in the benzyl alcohols from PhCH₂D and PhCHD₂ suggests there is a large intrinsic isotope effect. Finally, we can also calculate primary KIEs_(obs) and secondary KIEs_(obs) as shown in Table 3.2 [16]. All these values are consistent with a hydrogen atom abstraction process.



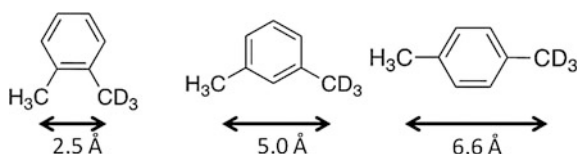
3.2.2.3 Single Methyl Group Deuterated Xylenes

Not only can intramolecular isotope effect experiments provide mechanistic information, they can also provide useful information about the dynamics of substrates and the active site environment of enzymes. This takes advantage of the isotope effect suppression, masking effect of intrinsic KIEs. If there is a full expression of the isotope effect, it means the probe can reorient rapidly within the active site. However, if there is some masking isotope effect, the rate of interchange between labeled and unlabeled groups is slowed. This suggests that the repositioning of the molecules is restricted. It may be caused by steric hindrance in the active site. In our study, we used *o*-xylene- α - d_3 , *m*-xylene- α - d_3 and *p*-xylene- α - d_3 . They are all symmetrical compounds with one methyl group labeled and the other unlabeled. The

Table 3.3 Intramolecular KIE_(obs) on selective deuterated substrates for *Aae*APO and P450s

Probes	<i>Aae</i> APO	CYP2B1 [18]	CYP4B1 [18]	CYP2E1 [19]	CYP2A6 [19]
<i>o</i> -xylene- <i>d</i> ₃	6.8 ± 0.3	8.82 ± 0.05	9.72 ± 0.02	9.03 ± 0.42	11.5 ± 0.28
<i>m</i> -xylene- <i>d</i> ₃	5.7 ± 0.3	–	–	6.65 ± 0.29	7.21 ± 0.43
<i>p</i> -xylene- <i>d</i> ₃	5.4 ± 0.7	6.96 ± 0.05	6.81 ± 0.03	6.04 ± 0.26	5.53 ± 0.19

distances between two methyl groups increase from *o*-xylenes (2.5 Å), *m*-xylenes (5.0 Å) to *p*-xylenes (6.6 Å) [17]. Table below shows the data and comparison of KIE_(obs) between *Aae*APO and some P450s.



As shown in Table 3.3, larger isotope effects were also observed for *o*-xylene. This is the same as some P450s [18, 19]. This results can be explained by the short distance of two methyl groups. The interchange of the two methyl groups in *o*-xylene is more rapidly than that of *p*-xylene. Comparing and contrasting the set of KIEs generated by using *Aae*APO to the sets of data generated by P450s, we found that there are some isotope masking effects for all probes. Overall, this set of data suggests that the active site of *Aae*APO is smaller and more constricted than some P450s.

3.2.2.4 Stereo-Deuterated Ethylbenzene

An extreme isotope masking effect was observed when using (*S*)- and (*R*)-PhCHDCH₃ (Scheme 3.4) as probe substrates. Figure 3.11 is the stereochemical courses of phenylethane-1-*d*₁ hydroxylation by *Aae*APO. We found that *Aae*APO abstracted the pro-*R* hydrogen preferentially. The selectivity of *Aae*APO is much higher than some P450s with this substrate [20]. KIE_(obs) for the *S* site was 4.2 and for the *R* site it was only 1.2. Ethyl group rotation and whole molecule flip-flop are two dynamics for ethylbenzene in the active site. We proposed that these two dynamics are restricted possibly due to some steric hindrance or some weak interactions between probes and protein residues (Fig. 3.12). It is known that the active site of *Aae*APO has many phenylalanine residues. They might hold aromatic substrates tightly or in some specific orientation. So the iron-oxo of *Aae*APO can only access one side of the proton instead of the other side. Another explanation of the small isotope effect is that the transition state of the rate determining step is early. So the active species, the compound I intermediate, doesn't differentiate C–H from C–D. Its oxidant strength is high enough to activate strong C–H bonds. The

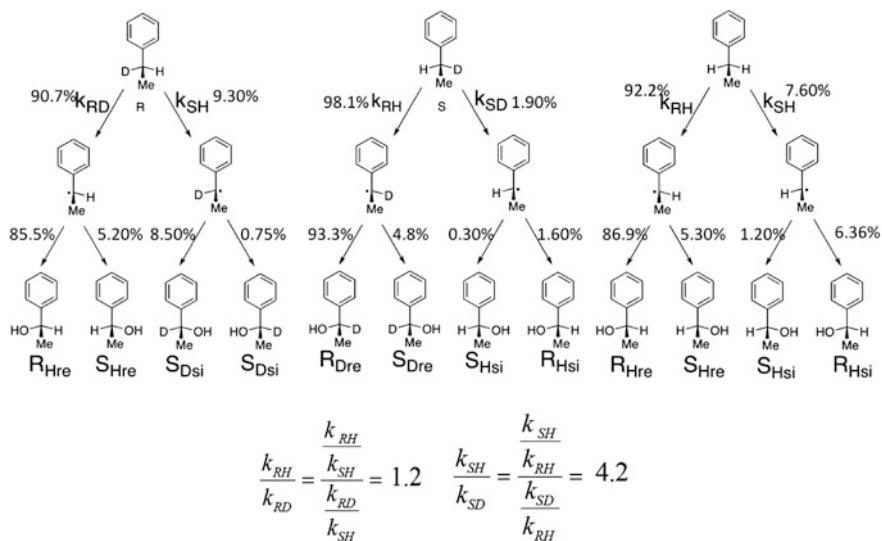


Fig. 3.11 Stereochemical courses of phenylethane-1- d_1 hydroxylation and the calculation of KIEs for *R* and *S* sites separately

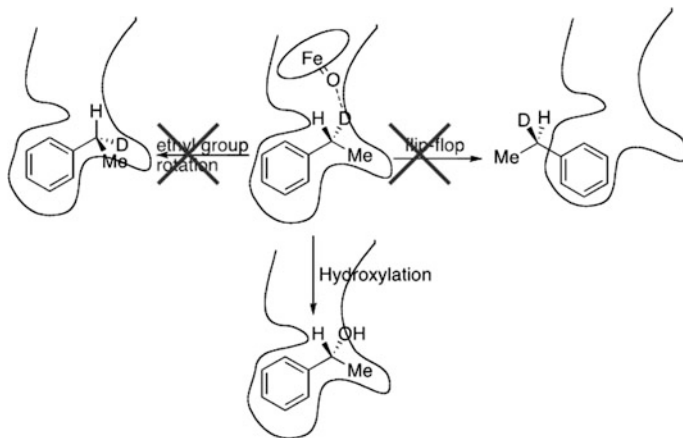
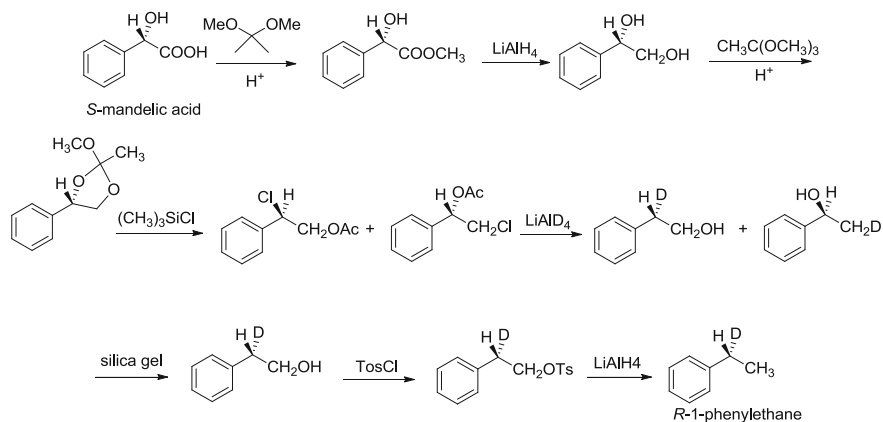


Fig. 3.12 The steric restriction in the active site of *AaeAPO*

Pro-*S* KIE is 4.2 which is larger than Pro-*R* and smaller than normal KIEs, so the ethylbenzene masking effects are considered to be the combination of the two factors.



Scheme 3.4 The synthesis of (*R*)-1-phenylethane [20]

3.3 Conclusions

Several radical clocks and isotopic labeling probes were used to investigate the *Aae*APO hydrocarbon hydroxylation reaction mechanism. The oxidation of radical clocks involves an amount of radical rearranged alcohol products, suggesting the hydrogen abstraction and rebound step. Different oxidants resulting in the same oxidation products of norcarane indicate that the real hydrogen abstractor is generated from the enzyme, the compound I. With the use of site-directly isotopic labeling substrates, large KIEs were obtained from the fast rotating methyl group of toluenes, showing the intrinsic isotope effect. However, the oxidation of some other probes, such as (*R*)-PhCHDCH₃, prefers pro-*R* site hydroxylation. This implies that the orientation of ethyl group in ethylbenzene is restricted in *Aae*APO active site.

3.4 Experimental

Reagents: Unless otherwise mentioned, all the reagents were from Sigma-Aldrich. All the chemicals were used without further purification. 98 atom % D α,α -*d*₂-benzyl bromide was purchased from CDN Isotopes and used without further purification. 99 atom % D *p*-xylene- α,α,α -*d*₃ was purchased from CDN Isotopes and went through a short basic alumina column before use.

3.4.1 Synthesis of Substrates and Authentic Samples

Toluene- α - d_1 : Benzyl chloride (3 g, 23.6 mmol) was added dropwise to a stirred suspension of 98 atom % D LiAlD₄ (1.3 g, 30 mmol) in 25 ml of tetralyme in a 100 ml three-necked flask at 0 °C. After reacting at 40 °C for 2 h, the product was carefully distilled from the reaction mixture and redistilled from bulb to bulb. It went through a short basic alumina column before use. The resulting toluene- α - d_1 is >99 % pure by GC-MS and ¹HNMR.

Toluene- α , α - d_2 : Benzyl bromide- α , α - d_2 (5 g, 29 mmol) was added dropwise to a stirred suspension of LiAlH₄ (1.1 g, 29 mmol) in 25 mL of tetralyme in a 100 mL three-necked flask at 0 °C. After reacting at 40 °C for 2 h, product was carefully distilled from the reaction mixture and redistilled from bulb to bulb. It went through a short basic alumina column before use. The resulting toluene- α , α - d_2 was >99 % pure by GC-MS and ¹HNMR.

Benzyl alcohol- α - d_1 : Benzaldehyde (6.0 g, 56.6 mmol) was added dropwise to a stirred suspension of 98 atom % D LiAlD₄ (2.4 g, 56.6 mmol) in 40 ml of anhydrous THF in a 100-mL three-necked flask at 0 °C. After being stirred for 2 h at room temperature the reaction was worked up by successive addition of 1.2 ml of H₂O, 1.2 ml of 15 % NaOH, and 3.6 ml of H₂O. The liquid phase was decanted from the granular residue, the THF removed on a rotary evaporator, and the residue chromatographed over silica gel, yielding 5.4 g of product. The resulting benzyl alcohol- α - d_1 was >99 % pure by GC-MS and ¹HNMR.

***o*-xylene- α , α , α - d_3 :** *o*-methyl-toluate (25 g, 0.15 mol) was added dropwise to a stirred suspension of 98 atom % D LiAlD₄ (5 g, 0.12 mol) in 300 ml anhydrous diethyl ether at 0 °C. The reaction was stirred at room temperature overnight under N₂ atmosphere. After cooling, the reaction the hydrolyzed with saturated NH₄Cl solution and acidified with concentrated HCl. The mixture was further extracted with ether. The combined organic layer was washed with saturated NaHCO₃ solution and saturated NaCl solution. It was dried with anhydrous Na₂SO₄ and concentrated to give 21 g of *o*-methylbenzyl alcohol. The resulting alcohol (7 g, 56 mmol) dissolved in ether was added to NaH (9 g of 60 % NaH in mineral oil, 225 mmol) ether suspension and refluxed overnight. It was then cooled down to -40 °C. TsCl (10.8 g, 56 mmol) was added. The reaction was kept at -40 °C for 3 h then 4 °C two more hours. After which, NaH was filtered. The ethereal solution was cooled at -78 °C. At low temperature, white *o*-methylbenzyl tosylate was precipitated out. 5 g of *o*-methylbenzyl tosylate was added to a stirred suspension of 98 atom % D LiAlD₄ (0.8 g) in 20 ml of anhydrous ether at 0 °C. After stirring at room temperature overnight, acidic workup and distillation from bulb to bulb gives 300 μ l *o*-xylene- α , α , α - d_3 . It went through basic alumina before use. The resulting *o*-xylene- α , α , α - d_3 was >99 % pure by GC-MS and ¹HNMR.

***m*-xylene- α , α , α - d_3 :** This compound was synthesized from *m*-methyl-toluate similar to the method described above. It went through basic alumina before use. The resulting *m*-xylene- α , α , α - d_3 was >99 % pure by GC-MS and ¹HNMR.

(R)-ethylbenzene- α - d_1 and (S)-ethylbenzene- α - d_1 : The synthetic scheme developed by Elsenbaumer and Mosher was followed [21], starting from chirally pure mandelic acid. *D*-(-)-mandelic acid yields (S)-ethylbenzene- α - d_1 , while *L*-(+)-mandelic acid yields (R)-ethylbenzene- α - d_1 . The resulting products were >99 % pure by GC-MS and ^1H NMR.

Norcarane: norcarane was prepared by using the Simmons-Smith reaction as previously described [22]. Authentic standards of the product norcaranols [22, 23] and the rearranged products cyclohept-3-enol [24] and cyclohex-2-enyl methanol [25] were prepared according to published procedures.

Bicyclo[2.1.0]pentane: This compound was prepared as described in the literature [26] by condensation of cyclopentadiene with diethyl azodicarboxylate, reduction of the resulting adduct over palladium/charcoal, hydrolytic removal of the two carboxy groups, oxidation over cuprous chloride, and pyrolysis.

Preparation of the Enzymes: Wild-type peroxygenase from *A. aegerita* (isoform II, pI 5.6, 46 kDa) was produced in bioreactors with a soybean-flour suspension as growth substrate, and purified as described previously [27]. The enzyme preparation was homogeneous by SDS/PAGE, and exhibited an $A_{418 \text{ nm}}/A_{280 \text{ nm}}$ ratio of 1.7. The specific activity of the peroxygenase was 59 U/mg, where 1 U represents the oxidation of 1 μmol of 3,4-dimethoxybenzyl alcohol to 3,4-dimethoxybenzaldehyde in 1 min at RT.

Reaction condition of AaeAPO catalyzed oxidation of different substrates: 2 μl of substrates and 4 μl of purified peroxygenase (440 U/ml) was added into 200 μl of potassium phosphate buffer (50 mM, pH 7.0). The reactions were started by the addition 500 μl of 1 mM H_2O_2 , stirred at room temperature for 5 min, and stopped by adding 200 μl of CH_2Cl_2 . The reaction mixtures were extracted by vigorous shaking. CH_2Cl_2 layer was separated from aqueous layer by centrifugation. The bottom CH_2Cl_2 layer was then collected and dried over anhydrous sodium sulfate before analyzed by GC-MS.

GC-MS Analysis: Most of the GC-MS analyses were performed on an Agilent GC-MS (7890A) with a HP-5 ms cross-linked 5 % PH ME siloxane capillary column (250 μm in diameter by 30 m length, 0.25 μm film thickness, Agilent Technologies J&W, Santa Clara, California, USA) using two GC-MS thermal gradient methods: method 1 started at 30 $^\circ\text{C}$, holding for 6 min, ramping to 230 $^\circ\text{C}$ at 10 $^\circ\text{C}/\text{min}$ and method 2 started at 50 $^\circ\text{C}$, holding for 2 min, ramping to 230 $^\circ\text{C}$ at 10 $^\circ\text{C}/\text{min}$. Retention times and mass spectra were compared to those of authentic oxidation products. The radical lifetime and rebound rate were calculated as described previously. In order to measure intramolecular KIEs, 200 μl product extractions were dried over sodium sulfate 15 min and then derivatized to their trimethylsilyl ethers by incubation with 2 μl of MSTFA 15 min at 60 $^\circ\text{C}$. KIEs were calculated by dividing the integration of the respective fragment ion of $[\text{M}-15]^+$ for the various deuterated states of products. Primary and Secondary KIEs were measured based on previous method.

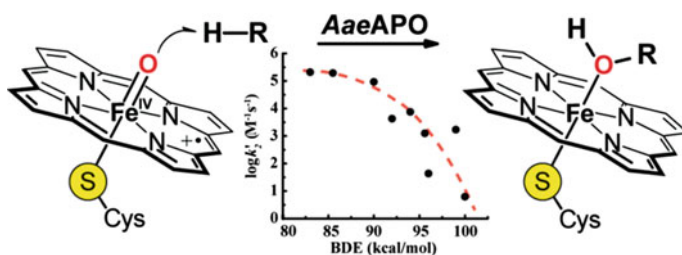
References

1. Groves, J.T., Mcclusky, G.A., White, R.E., Coon, M.J.: Aliphatic hydroxylation by highly purified liver microsomal cytochrome-P-450—evidence for a carbon radical intermediate. *Biochem. Biophys. Res. Co.* **81**, 154–160 (1978)
2. Griller, D., Ingold, K.U.: Free-Radical clocks. *Acc. Chem. Res.* **13**, 317–323 (1980)
3. Ortiz de Montellano, P.R.: Hydrocarbon hydroxylation by cytochrome P450 enzymes. *Chem. Rev.* **110**, 932–948 (2010)
4. Johnson, K.A.: Transient-state kinetic analysis of enzyme reaction pathways. In: *The Enzymes*, vol. XX, pp. 1–61 (1992)
5. Newcomb, M., Toy, P.H.: Hypersensitive radical probes and the mechanisms of cytochrome P450-catalyzed hydroxylation reactions. *Acc. Chem. Res.* **33**, 449–455 (2000)
6. Demontellano, P.R.O., Stearns, R.A.: Timing of the radical recombination step in cytochrome-P-450 catalysis with ring-strained probes. *J. Am. Chem. Soc.* **109**, 3415–3420 (1987)
7. Auclair, K., Hu, Z.B., Little, D.M., de Montellano, P.R.O., Groves, J.T.: Revisiting the mechanism of P450 enzymes with the radical clocks norcarane and spiro[2,5]octane. *J. Am. Chem. Soc.* **124**, 6020–6027 (2002)
8. Newcomb, M., Shen, R., Lu, Y., Coon, M.J., Hollenberg, P.F., Kopp, D.A., Lippard, S.J.: Evaluation of norcarane as a probe for radicals in cytochrome P450—and soluble methane monooxygenase-catalyzed hydroxylation reactions. *J. Am. Chem. Soc.* **124**, 6879–6886 (2002)
9. Bertrand, E., Sakai, R., Rozhkova-Novosad, E., Moe, L., Fox, B.G., Groves, J.T., Austin, R. N.: Reaction mechanisms of non-heme diiron hydroxylases characterized in whole cells. *J. Inorg. Biochem.* **99**, 1998–2006 (2005)
10. Chakrabarty, S., Austin, R.N., Deng, D., Groves, J.T., Lipscomb, J.D.: Radical intermediates in monooxygenase reactions of Rieske dioxygenases. *J. Am. Chem. Soc.* **129**, 3514–3515 (2007)
11. Peter, S., Kinne, M., Wang, X., Ullrich, R., Kayser, G., Groves, J.T., Hofrichter, M.: Selective hydroxylation of alkanes by an extracellular fungal peroxxygenase. *FEBS J.* **278**, 3667–3675 (2011)
12. Cooper, H.L.R., Groves, J.T.: Molecular probes of the mechanism of cytochrome P450. Oxygen traps a substrate radical intermediate. *Arch. Biochem. Biophys.* **507**, 111–118 (2011)
13. Austin, R.N., Luddy, K., Erickson, K., Pender-Cudlip, M., Bertrand, E., Deng, D., Buzdygon, R.S., Van Beilen, J.B., Groves, J.T.: Cage escape competes with geminate recombination during alkane hydroxylation by the diiron oxygenase AlkB. *Angew. Chem. Int. Ed.* **47**, 5232–5234 (2008)
14. Bowry, V.W., Ingold, K.U.: A radical clock investigation of microsomal cytochrome P-450 hydroxylation of hydrocarbons. Rate of oxygen rebound. *J. Am. Chem. Soc.* **113**, 5699–5707 (1991)
15. Nelson, S.D., Trager, W.F.: The use of deuterium isotope effects to probe the active site properties, mechanism of cytochrome P450-catalyzed reactions, and mechanisms of metabolically dependent toxicity. *Drug Metab. Dispos.* **31**, 1481–1498 (2003)
16. Hanzlik, R.P., Ling, K.H.J.: Active site dynamics of toluene hydroxylation by cytochrome P-450. *J. Org. Chem.* **55**, 3992–3997 (1990)
17. Audergon, C., Iyer, K.R., Jones, J.P., Darbyshire, J.F., Trager, W.F.: Experimental and theoretical study of the effect of active-site constrained substrate motion on the magnitude of the observed intramolecular isotope effect for the P450 101 catalyzed benzylic hydroxylation of isomeric xylenes and 4,4'-dimethylbiphenyl. *J. Am. Chem. Soc.* **121**, 41–47 (1999)
18. Henne, K.R., Fisher, M.B., Iyer, K.R., Lang, D.H., Trager, W.F., Rettie, A.E.: Active site characteristics of CYP4B1 probed with aromatic ligands. *Biochemistry* **40**, 8597–8605 (2001)
19. Harrelson, J.P., Henne, K.R., Alonso, D.O.V., Nelson, S.D.: A comparison of substrate dynamics in human CYP2E1 and CYP2A6. *Biochem. Biophys. Res. Co.* **352**, 843–849 (2007)

20. White, R.E., Miller, J.P., Favreau, L.V., Bhattacharyya, A.: Stereochemical dynamics of aliphatic hydroxylation by cytochrome P-450. *J. Am. Chem. Soc.* **108**, 6024–6031 (1986)
21. Elsenbaumer, R.L., Mosher, H.S.: Enantiomerically pure (R)-(+)-2-phenylethanol-2-d and -1,1,2-d₃, and (S)-(-)-1-phenylethane-1-d, -1,2,-d₂, -1,2,2-d₃, and -1,2,2,2-d₄. *J. Org. Chem.* **44**, 600–604 (1979)
22. Legoff, E.: Cyclopropanes from an easily prepared, highly active zinc-copper couple, dibromomethane, and olefins. *J. Org. Chem.* **29**, 2048–2050 (1964)
23. Lambert, J.B., Marko, D.E.: Factors influencing conformational preferences in cyclohexenes. *J. Am. Chem. Soc.* **107**, 7978–7982 (1985)
24. Åkermark, B., Hansson, S., Rein, T., Vgberg, J., Heumann, A., Bäckvall, J.E.: Palladium-catalyzed allylic acetoxylation: an exploratory study of the influence of added acids. *J. Orgaomet. Chem.* **369**, 433–444 (1989)
25. Snider, B.B., Rodini, D.J.: Diaklyluminum chloride catalyzed ene reactions of aldehydes. *Synth. Ipsenol. Tetrahedron Lett.* **21**, 1815–1818 (1980)
26. Gassman, P.G., Mansfield, K.T.: *Org. Synth.* **49**, 1 (1969)
27. Ullrich, R., Nuske, J., Scheibner, K., Spantzel, J., Hofrichter, M.: Novel haloperoxidase from the agaric basidiomycete *Agrocybe aegerita* oxidizes aryl alcohols and aldehydes. *Appl. Environ. Microb.* **70**, 4575–4581 (2004)

Chapter 4

Detection and Kinetic Characterization of a Highly Reactive Heme-Thiolate Peroxygenase AaeAPO Compound I



Abstract The extracellular heme-thiolate peroxxygenase from *Agrocybe aegerita* (*AaeAPO*) has been shown to hydroxylate alkanes and numerous other substrates using hydrogen peroxide as the terminal oxidant. In this chapter, we describe the kinetics of formation and decomposition of *AaeAPO* compound I upon its reaction with *mCPBA*. The UV-vis spectral features of *AaeAPO*-I (361, 694 nm) are similar to those of chloroperoxidase-I and the recently-described cytochrome P450-I. The second-order rate constant for *AaeAPO*-I formation was $1.0 (\pm 0.4) \times 10^7 \text{ M}^{-1} \text{ s}^{-1}$ at pH 5.0, 4 °C. The relatively slow decomposition rate, $1.4 (\pm 0.03) \text{ s}^{-1}$, allowed the measurement of its reactivity toward a panel of substrates. The observed rate constants, k_2' , spanned five orders of magnitude and correlated linearly with bond dissociation enthalpies of strong C-H bond substrates with a $\log k_2'$ versus BDE slope of ~ 0.4 . However, the hydroxylation rate was insensitive to C-H BDE below 90 kcal/mol, similar to the behavior of the *t*-butoxy radical. The shape and slope of the Brønsted-Evans-Polanyi plot indicate a symmetrical transition state for the stronger C-H bonds and suggest entropy control of the rate in an early transition state for weaker C-H bonds. The *AaeAPO*-II Fe^{IV}O-H BDE was estimated to be ~ 103 kcal/mol. All results support the formation of a highly reactive *AaeAPO* oxoiron (IV) porphyrin radical cation intermediate that is the active oxygen species in these hydroxylation reactions.

4.1 Results and Discussion

The fungal peroxxygenase *AaeAPO* (EC 1.11.2.1) from *Agrocybe aegerita* is a new and highly active heme-thiolate protein [1]. *AaeAPO* is a hybrid of cytochrome P450s and chloroperoxidase because it functions as a monooxygenase, similar to cytochrome P450s catalyzing a wide range of oxidations including alkane and aromatic hydroxylations, alkene epoxidations, halogenations and ether cleavage reactions [2–4]. It has also been shown to produce human metabolites efficiently from drugs [5]. However, it has no significant sequence homology to P450s and utilizes H_2O_2 as the terminal oxidant. *AaeAPO* shares a 30 % similarity with chloroperoxidase (CPO) [6]. The active site of *AaeAPO* contains a glutamic acid and an arginine near the distal side of the heme, rather than the highly conserved threonine found within P450s [7]. The corresponding residues for CPO are glutamate and histidine [8, 9]. Another new heme-thiolate hydroxylase, P450_{BSP}, lacks the active site glutamate but apparently supplements that with a carboxylate provided by its fatty acid substrate [10, 11]. Aside from this similarity and obvious analogs in the substrate reaction profile, little is known about the mechanism of oxygen transfer catalyzed by *AaeAPO* or the nature of any reactive intermediates in its catalytic cycle.

4.1.1 Kinetic Characterization of *AaeAPO* Binding with Substrates

As we already discovered in previous chapters, *AaeAPO* catalyzes alkane hydroxylation reactions with high efficiency and selectivity, giving only trace amounts of over-oxidation products. This might be caused by the special design of the substrate binding pocket. The crystal structure showed that stacked phenylalanines residues form a hydrophobic tunnel connecting the enzyme surface and the active site (Fig. 4.1). Here, we want to characterize the substrate binding events. The results we obtained here might provide important information for the understanding of overall reaction kinetics as both substrate binding and releasing are key steps.

The spectrum of resting *AaeAPO* displays an intense Soret band at 417 nm and two Q bands at 538 and 571 nm as shown as the black trace in Fig. 4.4. The position of the Soret band indicates that resting ferric *AaeAPO* is low-spin. The binding of substrate displaces the water molecule as the sixth ligand to the heme iron and we observed obvious and diagnostic changes in the UV-vis spectrum of ferric *AaeAPO* upon substrate binding as shown in Fig. 4.2. This change indicates a low-spin to high-spin inter-conversion, typical of cytochrome P450 enzymes [12].

The UV-vis difference spectra showed two types of the heme Soret band changes upon substrate binding. They are referred to as type I and type II shifts [12]. As shown in Fig. 4.2, benzyl alcohol, veratryl alcohol and cyclohexylcarboxylic acid

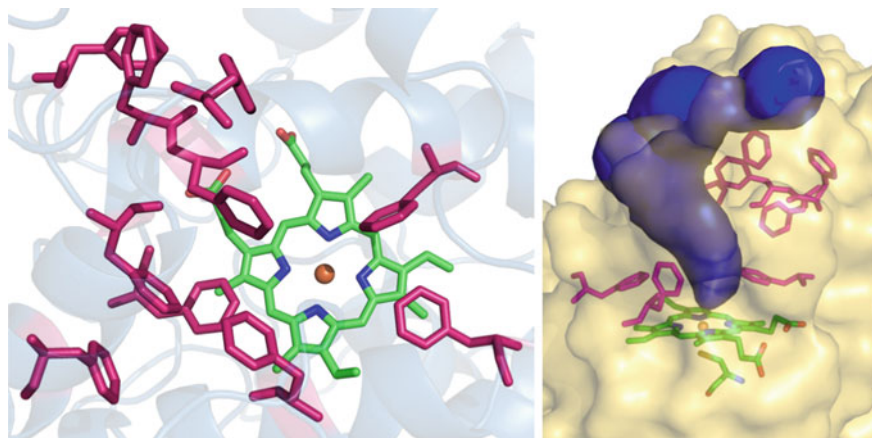
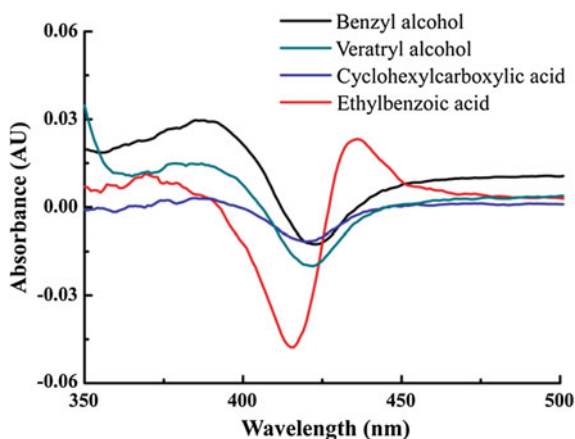


Fig. 4.1 *Left top view*, the crystal structure of *AaeAPO* showing stacked phenylalanine residues above the heme binding pocket. *Right side view*, crystal structure of *AaeAPO* showing the substrate entering channel which is surrounded by phenylalanine residues

Fig. 4.2 Type I and type II changes of *AaeAPO* UV-vis difference spectra upon substrate binding



resulted in type I shifts. The UV-vis difference spectra showed peaks at 390 nm and troughs at 420 nm. However, ethylbenzoic acid gave a type II shift, which is possibly caused by direct coordination of ligand to the heme iron center. Its UV-vis difference spectrum has characteristic shifts at 415 and 433 nm.

These diagnostic peaks are useful information for the study of substrate binding kinetics. As shown in Fig. 4.3a, when solutions of ethylbenzoic acid at different concentrations were mixed with resting ferric *AaeAPO* by using a rapid stopped-flow mixing unit, the UV-vis spectra showed increased absorptions at 433 nm. The kinetics of the binding process was characterized by fitting the initial velocity changes versus substrate concentration (Figure 4.3b). p-Ethylbenzoic acid

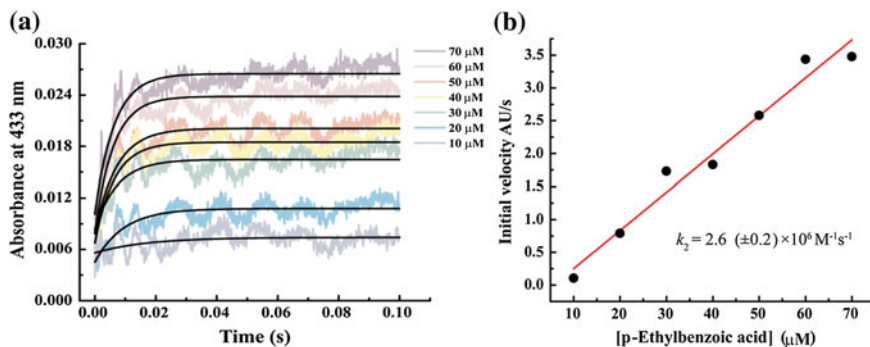
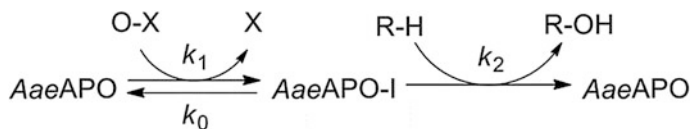


Fig. 4.3 **a** Absorbance changes of *AaeAPO* at 433 nm upon binding with different concentration of *p*-ethylbenzoic acid at pH 5.0. **b** Plot the initial velocities of ethylbenzoic acid binding with substrate concentration gave a second order rate constant of $2.6 \times 10^6 \text{ M}^{-1} \text{ s}^{-1}$. The final concentration of resting *AaeAPO* is 2 μM . A similar rate constant was obtained by fitting with single exponential decay and pseudo first order kinetics

binding with resting *AaeAPO* is a very fast process as the calculated second order rate constant is $2.6 \times 10^6 \text{ M}^{-1} \text{ s}^{-1}$. We suggest that the phenylalanine residues have a special interaction with hydrophobic substrates and might assist the binding. As we did not observe much over-oxidation ketone products, we think this is caused by the hydrophobicity of the binding pocket. Alcohol products are able to be released quickly enough without a chance of over-oxidation.

4.1.2 Detection and Generation of *AaeAPO-I*

We generate and characterize the spectra of *AaeAPO* compound I, formed by the reaction of ferric *AaeAPO* with *m*-chloroperoxybenzoic acid (*m*CPBA) (k_1) as shown in Scheme 4.1 and Fig. 4.4. Reaction of the ferric enzyme with two equivalents of *m*CPBA at 4 °C, using rapid-mixing, stopped-flow techniques, generated a short-lived intermediate that displayed a new band at 361 nm and a distinct absorbance at 694 nm. This spectral transient appeared within 30 ms of mixing. The Soret band of the remaining ferric enzyme decreased dramatically during this time.



Scheme 4.1 The generation of *AaeAPO-I* and its reaction with substrates

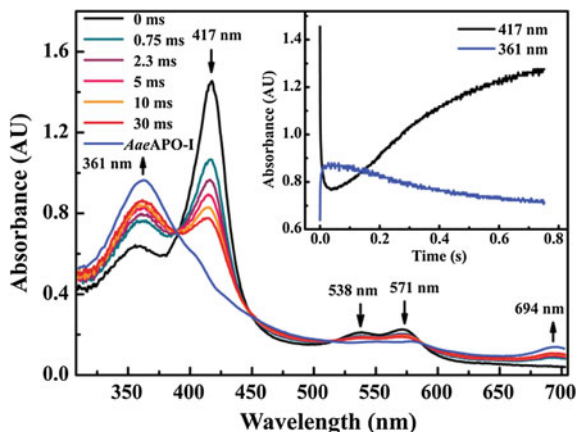


Fig. 4.4 UV-vis transients observed upon 1:1 mixing of $13 \mu\text{M}$ of ferric enzyme with $25 \mu\text{M}$ of *mCPBA* at pH 5.0, 4°C . Maximum yield of *AaeAPO-I* reached 70 % at 30 ms

The observation of a clear set of multiple isosbestic points (390, 448, 516 and 586 nm) indicated that only two major species were present during this transformation. SVD analysis is linear algebraic method to determine the number of significant species that are involved in the reaction [13]. In Eq. 4.1, D is the stopped-flow generated data matrix [$w \times t$] composing w wavelengths and t absorptions at different time points. The eigenvalues obtained from the diagonalization of D is the square of the singular values. The number of non-zero singular values represents the number of species in the reaction. Matrix D can also be written as 4.2. U is the [$w \times n$] matrix containing n eigenvectors. It gives the abstract spectra. S is the [$n \times n$] matrix. V is a [$n \times t$] matrix representing the concentration files. Only two significant non-zero singular values were obtained after SVD analysis. Figure 4.5 shows the abstract spectra obtained from the SVD

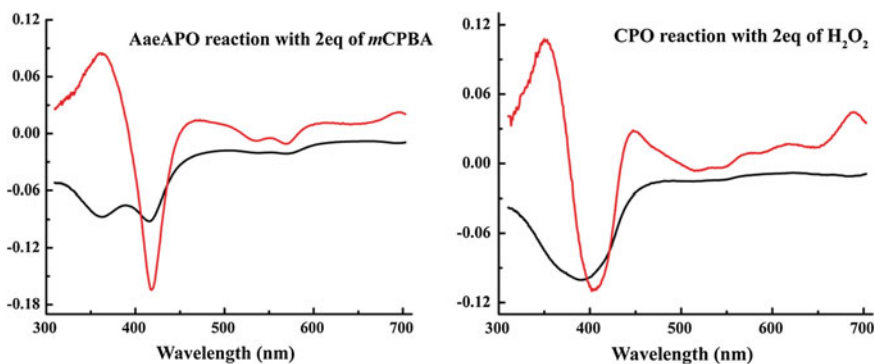


Fig. 4.5 Abstract spectra of SVD analysis on the stopped-flow data sets of *AaeAPO* reaction with 2 eq of *mCPBA* and *CPO* reaction with 2 eq of H_2O_2 , both at pH 5.0

analysis on the time dependent data sets of *Aae*APO reaction with 2 eq of *m*CPBA and CPO reaction with 2 eq of H_2O_2 . The difference of the black traces from *Aae*APO and CPO reactions reflects that resting enzymes have different spin states. However, both shapes and the position of bands of red traces are similar, for the second significant species in the reactions.

$$Z = D^T D \quad (4.1)$$

$$D = USV^T \quad (4.2)$$

By examination of the UV-vis spectrum of the new intermediate, the weak, blue-shifted Soret band and the absorbance at 694 nm strongly suggest the presence of a porphyrin radical cation species and the intermediate suggests the presence of *Aae*APO compound I. In Eq. 4.3, a projection operator P is created from abstract vectors. The target testing method can be applied to determine if a target species is involved in the reaction, Eq. 4.4 [13]. Here, X represents the CPO-I UV-vis spectrum, as the target vector. Target testing return results Y , as shown in Fig. 4.6, indicate that a CPO-I like intermediate is involved in the reaction between *Aae*APO with *m*CPBA. In other words, the newly generated intermediate during the *Aae*APO reaction with *m*CPBA is the *Aae*APO-I intermediate and it has a similar UV-vis spectrum to CPO-I.

$$P = UU^T \quad (4.3)$$

$$Y = PX \quad (4.4)$$

Finally, the spectrum of *Aae*APO-I, which was obtained by globally fitting the data as shown the blue trace, recapitulates those of P450 [14–17] and CPO [18, 19].

Fig. 4.6 Target testing of *Aae*APO reaction with CPO-I

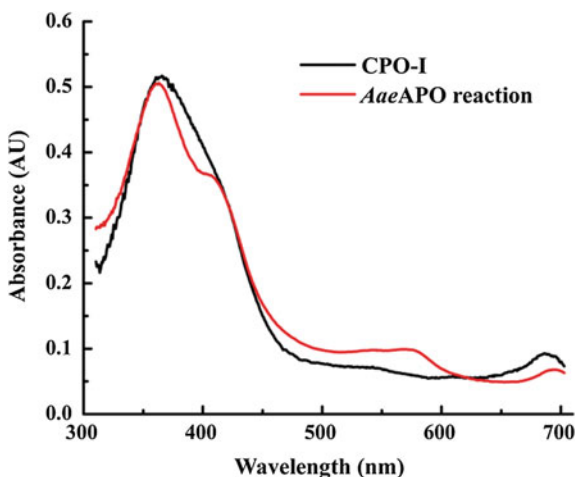
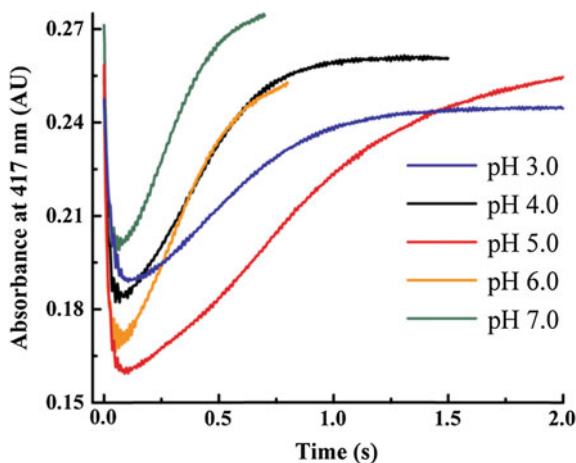


Table 4.1 The observed *Aae*APO compound I formation and spontaneous decay rate constants

pH	k_1 ($M^{-1} s^{-1}$)	k_0 (s^{-1})
3.0	$3.4 (\pm 0.1) \times 10^6$	$2.5 (\pm 0.03)$
4.0	$5.3 (\pm 0.1) \times 10^6$	$3.9 (\pm 0.04)$
5.0	$1.0 (\pm 0.4) \times 10^7$	$1.4 (\pm 0.03)$
6.0	$1.1 (\pm 0.5) \times 10^7$	$3.1 (\pm 0.03)$
7.0	$9.1 (\pm 0.7) \times 10^6$	$4.1 (\pm 0.04)$

Fig. 4.7 Absorbance traces at 417 nm upon mixing of ferric enzyme with 2 eq of *m*CPBA over a range of pHs

The deconvolution indicated that *Aae*APO-I had been formed in 70 % yield. Accordingly, no spectral subtractions were necessary in these analyses.

The extent of *Aae*APO-I formation and the rate of its subsequent decay were found to be optimal at pH 5.0 (Table 4.1 and Fig. 4.7). Second-order rate constants for the reaction of *Aae*APO with *m*CPBA were obtained by monitoring the conversion of ferric protein at 417 nm and plotting the single exponential decay of ferric enzyme against a range of *m*CPBA concentrations (Fig. 4.8). Full diode array spectra confirmed that the porphyrin radical cation absorbances at 361 and 694 nm grew in and decayed with the same kinetics. The maximal rate constant observed was $1.1 (\pm 0.5) \times 10^7 M^{-1} s^{-1}$ at pH 6.0, which is consistent with a reaction of *Aae*APO with the protonated form of *m*CPBA (pK_a 7.6) [16]. It is interesting that the formation rate decreased significantly from pH 5.0 to pH 3.0. *Aae*APO is known to have an active site glutamate close to the heme center [6, 20], which could play a role in the formation of *Aae*APO-I by hydrogen peroxide, apparently its natural co-substrate. Thus, *m*CPBA would initially replace a distal water ligand in resting *Aae*APO with proton transfer to the neighboring glutamate to form an unseen peroxo-adduct, similar to peroxidase compound 0. Subsequently, O-O bond heterolysis and formation of *Aae*APO-I would be assisted by proton transfer from the active site glutamate to the product, *m*CBA, as outlined in Scheme 4.2. This role for

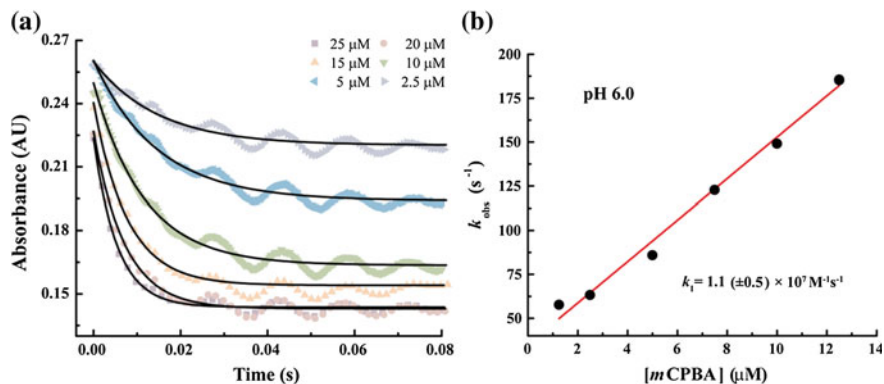
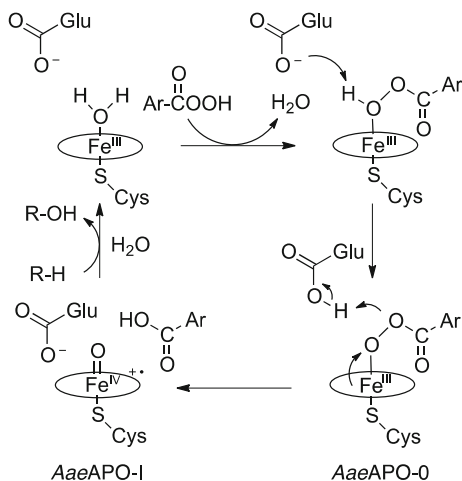


Fig. 4.8 **a** The Absorbance at 417 nm upon mixing ferric *Aae*APO with different concentration of *m*CPBA at pH 6.0. **b** Single exponential decay of ferric enzyme as a function of *m*CPBA concentration. The second order rate constant of *Aae*APO-I formation gave similar result if one uses initial velocity fitting

Scheme 4.2 Proposed mechanism of *Aae*APO-I formation assisted by the deprotonated glutamate in the active site



the distal glutamate is similar to that proposed for the substrate carboxylate group in fatty acid hydroxylation by cytochrome P450_{BSP} [10, 11] and P450_{SPα} [21].

The rate of *Aae*APO-I decay followed first-order kinetics and could be fitted directly from the data in Fig. 4.7. This spontaneous reduction of *Aae*APO-I was slowest at pH 5.0, $k_1 = 1.4 (\pm 0.03) \text{ s}^{-1}$. The decay rate is faster than that of CPO-I (0.5 s⁻¹ at pH 4.7, 25 °C) [22], but slower than that of CYP119-I (9 s⁻¹, pH 7.0, 4 °C) [14, 16]. While the mechanism of spontaneous decay of compound I is unknown, more than 90 % ferric protein was recovered in the process.

4.1.3 Kinetic Characterization of *Aae*APO-I Towards a Series of Alkanes

As we have recently reported, *Aae*APO has a high selectivity for the hydroxylation of saturated hydrocarbons [4, 23], similar to P450 enzymes but in distinct contrast with chloroperoxidase [14, 24, 25]. The persistence of *Aae*APO-I over nearly a second at pH 5.0 allowed us to measure its reactivity toward a panel of typical aliphatic substrates over a wide range of C-H bond BDE (83–100 kcal/mol). In each case we determined the identity of the products and product ratios under catalytic conditions by comparing NMR and GC-MS data with those of authentic samples. For example, slow addition of 20 mM H₂O₂ or peroxyacid to a solution containing 0.22 μM *Aae*APO and 10 mM *p*-ethylbenzoic acid produced (*R*)-4-(1-hydroxyethyl) benzoic acid in high conversion and 99 % *ee* (Fig. 4.9) [23]. Subsequent oxidation of the benzylic alcohol product occurred only after all of the *p*-ethylbenzoic acid had been consumed. Remarkably, *Aae*APO was found to hydroxylate a methyl C-H bond in dimethyl butyric acid and even neopentane (BDE ~ 100 kcal/mol) to produce the corresponding primary alcohols.

We used double mixing, stopped-flow techniques to monitor the kinetics of the *Aae*APO-I reaction with various substrates [14, 26]. Figure 4.10a shows a typical kinetic experiment. At pH 5.0, 4 °C, the first mixing generated *Aae*APO-I within an aging time of 20 ms. Then, solutions with varying concentrations of each substrate were mixed with *Aae*APO-I in the second push. The observed decay rates (k_{obs}) were obtained by fitting the return of the ferric enzyme. Plots of k_{obs} against substrate concentration gave linear relationships as shown in Fig. 4.10a inset and Fig. 4.10b. Lastly, apparent per-hydrogen second-order rate constants, k_2' , for the reaction of *Aae*APO-I with each substrate were obtained from the observed slopes

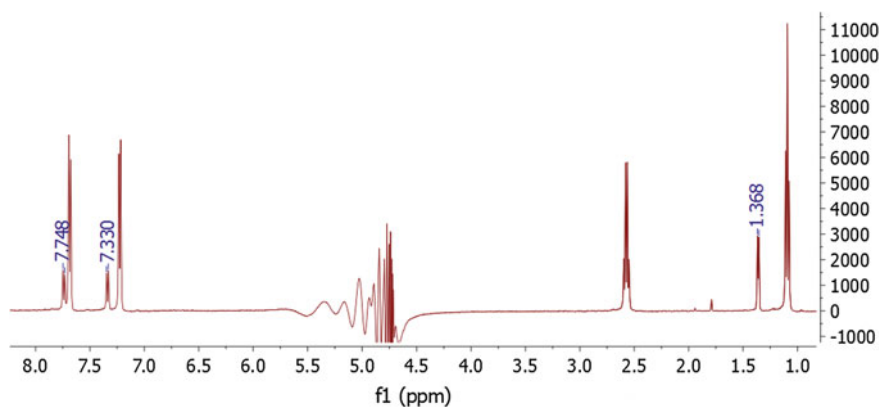


Fig. 4.9 Water suppressed ¹H NMR of the reaction mixture of oxidation of *p*-ethylbenzoic acid by 0.22 μM of *Aae*APO and H₂O₂. Labeled resonances correspond to the product (*R*)-4-(1-hydroxyethyl) benzoic acid at 7.748 ppm (2H, dd), 7.330 ppm (2H, dd) and 1.368 ppm (3H, d). The benzylic proton resonance was obscured by the suppressed water peak

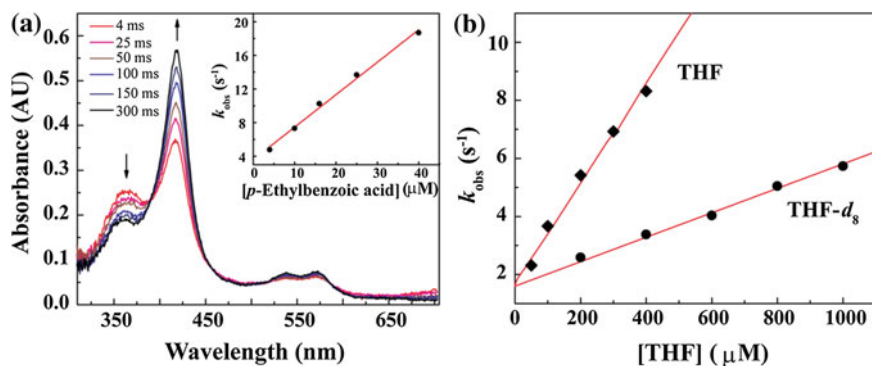


Fig. 4.10 **a** UV-vis spectra obtained during the reaction of 10 μM *AaeAPO-I* with 16 μM *p*-ethylbenzoic acid at pH 5.0, 4 $^{\circ}\text{C}$. Inset: Observed first-order decay rates versus *p*-ethylbenzoic acid concentration. The apparent second-order rate constant, k_2 , was obtained from the slope. **b** Observed first-order decay rates versus concentrations of THF or THF- d_8 . A KIE of 4.3 for THF and THF- d_8 was determined from the ratio of the slopes

in the usual manner. As shown in Fig. 4.10b, a kinetic hydrogen isotope effect ($k_{\text{H}}/k_{\text{D}} = 4.3$) could also be measured from the ratio of k_2 obtained for THF and THF- d_8 as substrates. Table 4.2 lists the rate constants, k_2 , k_2' , for each of the substrates under study.

It is of interest to compare the reactivity of *AaeAPO-I* observed here to those of CYP119 compound I, recently reported by Rittle and Green [14], CPO compound I reported by Newcomb et al. [25] and the reactive model oxoiron(IV) porphyrin radical cation species, $[\text{O} = \text{Fe}^{\text{IV}}\text{-4-TMPyP}]^+$, we have recently described [26]. Further, it is instructive to consider these comparisons in light of insights derived from computational approaches [27–29]. The rate constant observed for benzylic C-H hydroxylation of ethylbenzoic acid by *AaeAPO-I* is 125-fold faster than that observed for our model compound I ferryl porphyrin at 10 $^{\circ}\text{C}$ and 250 times faster than those of CPO-I with similar substrates at 22 $^{\circ}\text{C}$. For CYP119-I, rate constants of $10^3\text{--}10^7 \text{ M}^{-1} \text{ s}^{-1}$ have been reported for unactivated methylene groups of fatty acids [14]. The slower of these rates, which are for hexanoic and octanoic acid, are similar to those observed here for *AaeAPO-I*, while the fastest rate constant for CYP119-I was for lauric acid, a tight-binding substrate, and may be an irreversible binding event.

We note that even the fastest C-H hydroxylation reactions found here for *AaeAPO-I* are still more than an order of magnitude slower than the rate of oxidation of the ferric protein by *mCPBA*. Similarly, the low-spin to high-spin transition upon substrate binding was found to be very fast ($>2 \times 10^6 \text{ M}^{-1} \text{ s}^{-1}$) (Fig. 4.3). Thus, the rate of substrate access to the active site is significantly faster than the rate of reaction and, accordingly, the observed rates are likely to be measures of the intrinsic C-H reactivity toward *AaeAPO-I*. Consistent with this expectation, the preliminary X-ray structure of *AaeAPO* shows a shallow, hydrophobic substrate-binding cavity flanked by several phenylalanine residues [20]

Table 4.2 Summary of all substrates, equivalent C-H bonds, BDE, k_2 , k_2' and $\log k_2'$

Number	Substrates	Equivalent C-H bonds*	BDE (kcal/mol)	k_2 ($M^{-1} s^{-1}$)	$k_2'^{**}$ ($M^{-1} s^{-1}$)	$\log k_2'$ ($M^{-1} s^{-1}$)
1	<i>p</i> -Isopropylbenzoic acid	1	83	2.0 (± 0.09) $\times 10^5$	2.0×10^5	5.3
2	<i>p</i> -Ethylbenzoic acid	2	85.5	3.9 (± 0.2) $\times 10^5$	1.9×10^5	5.3
3	<i>p</i> -Toluic acid	3	90	2.8 (± 0.2) $\times 10^5$	9.3×10^4	5.0
4	THF	4	92	1.7 (± 0.05) $\times 10^4$	4.3×10^3	3.6
4'	THF- <i>d</i> ₈	4	–	4.0 (± 0.1) $\times 10^3$	–	–
5	Cycloheptane Carboxylic acid	4	94	3.0 (± 0.1) $\times 10^4$	7.5×10^3	3.9
6	Cyclopentane Carboxylic acid	8	95.6	1.0 (± 0.1) $\times 10^4$	1.3×10^3	3.1
7	Cyclohexane Carboxylic acid	6	99	1.0 (± 0.2) $\times 10^4$	1.7×10^3	3.2
8	1,4-Dioxane	8	96	3.5 (± 0.02) $\times 10^2$	4.4×10^1	1.6
9	3,3-Dimethylbutyric acid	9	100	6.0 (± 0.05) $\times 10^1$	6.7	0.8

*The numbers of equivalent C-H bonds were based on the numbers of sites being hydroxylated

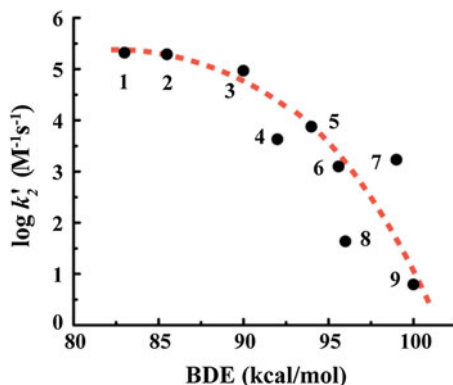
**Second-order rate constants k_2' were adjusted based on the number of equivalent C-H bonds in the substrates

(Fig. 4.1). Further evidence for fast, reversible substrate binding is the observation of the *intermolecular* isotope effect (k_H/k_D) of 4.3 for THF and THF-*d*₈.

A plot of second-order rate constants for C-H hydroxylation by *Aae*APO-I for all substrates versus BDE of the scissile C-H bond revealed a very distinct, *non-linear* correlation (Fig. 4.11). Notably, there was almost no change in k_2' for the substrates with C-H BDE less than 90 kcal/mol. By contrast, the slope of $\log k_2'$ versus BDE above 90 kcal/mole was ~ 0.4 . Based on the Brønsted-Evans-Polanyi (BEP) relationship: $\log(k_H) = \alpha \Delta H^{\circ} + C$, where ΔH° is related to the C-H BDE and α is a measure of transition state location. An α of 0.4 for the stronger C-H bonds indicates that these hydrocarbon hydroxylations mediated by *Aae*APO-I have a nearly symmetrical [FeO—H—C] transition state. We recently reported a linear BEP relationship for a model compound I with a series of C-H substrates [26]. The observed $\log k$ versus BDE plot was rather flat ($\alpha = 0.28$) in that case, intermediate between the high and low values observed for *Aae*APO-I (Fig. 4.11).

As can be seen in Fig. 4.11, the two ether substrates, THF (point 4) and dioxane (point 8), were found to be significantly less reactive than predicted by their C-H BDE (92 and 96 kcal/mol, respectively). We ascribe this deviation to the more hydrophilic nature of these substrates and a polar effect [27–29] due to the

Fig. 4.11 Plot of $\log k_2'$ versus substrate C-H BDE



neighboring oxygen. Competitive KIEs were also carried out under turnover conditions between dioxane and dioxane- d_8 , affording a KIE of 12, consistent with the stronger C-H bond and, accordingly, a more symmetrical transition state $[\text{Fe}-\text{O}-\text{H}-\text{C}]^\ddagger$. Cyclohexane carboxylic acid (point 7), by contrast, was found to be ~ 30 fold more reactive than predicted by the trend line. This anomaly, which has also been observed for six-membered rings with synthetic oxometalloporphyrins [30], may be attributed to eclipsing strain relief in the chair-like transition state for hydrogen abstraction for that substrate [31]. The competitive KIE for cyclohexane and cyclohexane- d_{12} was found to be 3.

The insensitivity of the reaction rate to the strength of the C-H bond in the region of BDE below 90 kcal/mol is worth further comment. Nearly identical behavior, including the change of slope near 90 kcal/mol, has been reported by Tanko et al. for hydrogen abstraction from a variety of substrates by the *t*-butoxy radical, which has been suggested to be a model of P450 reactivity [32, 33]. Since the fastest rates observed for *Aae*APO-I are slower than substrate exchange at the active site and certainly much slower than the diffusion limit, neither of these effects are likely explanations of the insensitivity of the rate to BDE. However, as with the *t*-butoxy radical, an early transition state for weaker C-H bonds and the anticipated small activation enthalpy, suggest that the hydroxylation of these weaker C-H bonds by *Aae*APO-I may be in the regime of entropy control in which $T\Delta S^\ddagger > \Delta H^\ddagger$ [33]. In such a case, the *Aae*APO-I intermediate is so reactive that rates of hydrogen abstraction are governed more by factors such as accessibility, orientation and trajectory toward the highly ordered substrate-like transition state.

For the model system we estimated the intermediate compound-II $\text{Fe}^{\text{IV}}\text{O}-\text{H}$ BDE to be ~ 100 kcal/mol. The reaction of *Aae*APO-I with ethylbenzoic acid is much faster than that of our model system. Mapping the results for *Aae*APO-I with ethylbenzoic acid and toluic acid onto the plot correlating $\log k_{(\text{H})}$ with O-H bond strength [35], we found that the rate constants were only slightly slower than those of *t*-butoxy radical (*t*-BuO-H BDE 105 kcal/mol [33]). Accordingly, we estimate

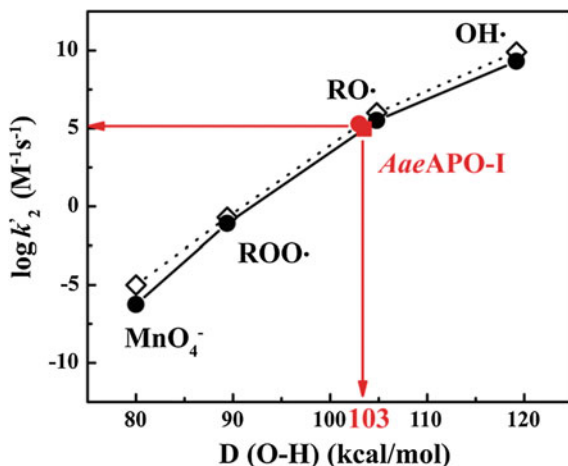


Fig. 4.12 Rate constants for the hydrogen abstraction by MnO_4^- , $\text{ROO}\cdot$, $\text{RO}\cdot$ and $\text{HO}\cdot$ versus the strength of the O-H bonds formed for toluene (solid circles) and *p*-ethylbenzene (open diamonds [34, 35]). Plotting rate constants for hydrogen abstraction by *AaeAPO-I* with *p*-toluic acid and *p*-ethylbenzoic acid on the curves gives an $\text{Fe}^{\text{IV}}\text{O-H}$ bond strength of about 103 kcal/mol

that the $\text{Fe}^{\text{IV}}\text{O-H}$ BDE for *AaeAPO-II* to be ~ 103 kcal/mol (Fig. 4.12), larger than the value of 98 kcal/mol that has been estimated for the $\text{Fe}^{\text{IV}}\text{O-H}$ BDE of CPO compound II [36].

4.2 Conclusions

In summary, our study of *AaeAPO* supports the formation of a highly reactive *AaeAPO* oxoiron(IV) porphyrin radical cation intermediate. Reaction kinetics for *AaeAPO-I* with a variety of substrates have revealed an informative correlation between the C-H BDE and the observed bimolecular rate constants. The large estimated $\text{Fe}^{\text{IV}}\text{O-H}$ BDE of 103 kcal/mol for *AaeAPO-II* is significant with regard to its relationship to the $\text{p}K_{\text{a}}$ of *AaeAPO-II* and the one-electron reduction potential of *AaeAPO-I*.

4.3 Experimental

Materials wild-type extracellular aromatic peroxygenase of *A. aegerita* (isoform II, pI 5.6, 46 kDa) was produced in stirred-tank bioreactors with a soybean-flour suspension as growth substrate, and purified as described previously [37, 38]. The enzyme preparation was homogeneous by SDS/PAGE, and exhibited an

$A_{418 \text{ nm}}/A_{280 \text{ nm}}$ ratio of 1.7. The specific activity of the peroxygenase was 59 U/mg, where 1 U represents the oxidation of 1 μmol of 3,4-dimethoxybenzyl alcohol to 3,4-dimethoxybenzaldehyde in 1 min at room temperature. *m*CPBA (3-chloroperoxybenzoic acid) was obtained from Aldrich and purified by stirring in 100 mM pH 7.4 phosphate buffer for 1 h followed by filtering and washing thoroughly with water. *p*-Isopropylbenzoic acid, *p*-ethylbenzoic acid, *p*-toluic acid, THF, THF-*d*₈, cycloheptanecarboxylic acid, cyclopentanecarboxylic acid, cyclohexanecarboxylic acid, 1,4-dioxane, 3,3-dimethylbutyric acid were obtained from Aldrich and purified by recrystallization or distillation under vacuum. D₂O was obtained from Cambridge Isotope Laboratories, Inc. Water used in all experiments was de-ionized (Millipore, Milli-Q). Buffer solutions were prepared by mixing sodium citrate and citric acid in water and adjusted with NaOH. Phosphate-citrate buffer was prepared by mixing 0.2 M dibasic potassium phosphate with 0.1 M citric acid and the pH was adjusted with KOH.

Instrumentation UV-vis spectral measurements were made with a Hewlett Packed 8453 diode array spectrophotometer at room temperature. Stopped-flow experiments were performed with a Hi-Tech SF-61 DX2 double mixing instrument with a 1 cm path length equipped with an ISOTEMP 3013 D thermostat bath. NMR spectra were recorded on a 500 MHz Bruker Avance II spectrometer. GC-MS analyses were run using an Agilent 7890A GC coupled to a 5975 Inert MSD with a Rtx-5Sil MS column.

Reaction kinetics kinetic data were collected at 4 °C in 100 mM buffer, citrate buffer for pH 5.0 and phosphate-citrate buffer for pH 3.0–7.0. Each experiment was repeated two or three times. Concentrations presented are the final concentrations after mixing. Kinetic data for substrate hydroxylation were obtained in double-mixing mode using either diode array detection or single wavelength mode at 417 nm. Values of k_1 were obtained by the fitting of initial rates with a series of *m*CPBA concentrations. Values of k_{obs} were processed by fitting the kinetic profile to a single exponential equation using Kinetic Studio from Hi-Tech. Values of k_2 were obtained from the slope of a k_{obs} versus the [substrate] plot. SVD and global analyses were analyzed by ReactLab™ Kinetics from Jplus Consulting. Target testing was analyzed by using Matlab.

References

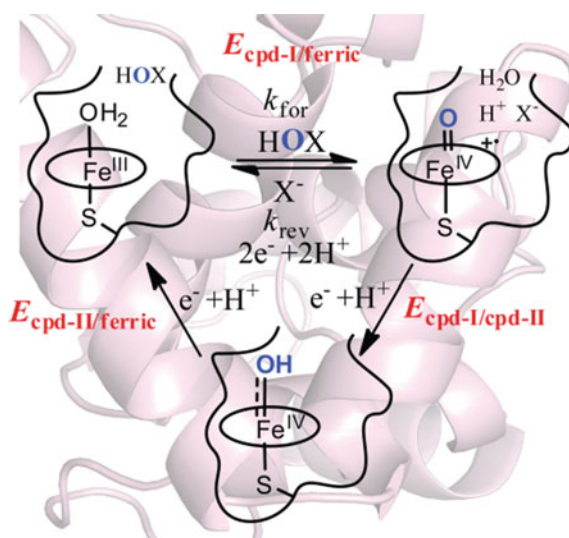
1. Hofrichter, M., Ullrich, R., Pecyna, M.J., Liers, C., Lundell, T.: New and classic families of secreted fungal heme peroxidases. *Appl. Microbiol. Biotechnol.* **87**, 871–897 (2010)
2. Fang, Z., Breslow, R.: A thiolate ligand on a cytochrome P-450 mimic permits the use of simple environmentally benign oxidants for biomimetic steroid hydroxylation in water. *Bioorg. Med. Chem. Lett.* **15**, 5463–5466 (2005)
3. Kinne, M., Poraj-Kobielska, M., Ralph, S.A., Ullrich, R., Hofrichter, M., Hammel, K.E.: Oxidative cleavage of diverse ethers by an extracellular fungal peroxygenase. *J. Biol. Chem.* **284**, 29343–29349 (2009)

- Peter, S., Kinne, M., Wang, X., Ullrich, R., Kayser, G., Groves, J.T., Hofrichter, M.: Selective hydroxylation of alkanes by an extracellular fungal peroxxygenase. *FEBS J.* **278**, 3667–3675 (2011)
- Poraj-Kobielska, M., Kinne, M., Ullrich, R., Scheibner, K., Kayser, G., Hammel, K.E., Hofrichter, M.: Preparation of human drug metabolites using fungal peroxxygenases. *Biochem. Pharmacol.* **82**, 789–796 (2011)
- Pecyna, M.J., Ullrich, R., Bittner, B., Clemens, A., Scheibner, K., Schubert, R., Hofrichter, M.: Molecular characterization of aromatic peroxxygenase from *Agrocybe aegerita*. *Appl. Microbiol. Biotechnol.* **84**, 885–897 (2009)
- Schlichting, I., Berendzen, J., Chu, K., Stock, A.M., Maves, S.A., Benson, D.E., Sweet, B.M., Ringe, D., Petsko, G.A., Sligar, S.G.: The catalytic pathway of cytochrome P450cam at atomic resolution. *Science* **287**, 1615–1622 (2000)
- Sundaramoorthy, M., Terner, J., Poulos, T.L.: The crystal structure of chloroperoxidase: a heme peroxidase-cytochrome P450 functional hybrid. *Structure* **3**, 1367–1377 (1995)
- Sundaramoorthy, M., Terner, J., Poulos, T.L.: Stereochemistry of the chloroperoxidase active site: crystallographic and molecular-modeling studies. *Chem. Biol.* **5**, 461–473 (1998)
- Lee, D.S., Yamada, A., Sugimoto, H., Matsunaga, I., Ogura, H., Ichihara, K., Adachi, S., Park, S.Y., Shiro, Y.: Substrate recognition and molecular mechanism of fatty acid hydroxylation by cytochrome P450 from *Bacillus subtilis*—Crystallographic, spectroscopic, and mutational studies. *J. Biol. Chem.* **278**, 9761–9767 (2003)
- Shoji, O., Fujishiro, T., Nakajima, H., Kim, M., Nagano, S., Shiro, Y., Watanabe, Y.: Hydrogen peroxide dependent monooxygenations by tricking the substrate recognition of cytochrome P450 (BS beta). *Angew. Chem. Int. Ed.* **46**, 3656–3659 (2007)
- Isin, E.M., Guengerich, F.P.: Substrate binding to cytochromes P450. *Anal. Bioanal. Chem.* **392**, 1019–1030 (2008)
- Rittle, J., Younker, J.M., Green, M.T.: Cytochrome P450: the active oxidant and its spectrum. *Inorg. Chem.* **49**, 3610–3617 (2010)
- Rittle, J., Green, M.T.: Cytochrome P450 compound I: capture, characterization, and C-H bond activation kinetics. *Science* **330**, 933–937 (2010)
- Egawa, T., Shimada, H., Ishimura, Y.: Evidence for compound I formation in the reaction of cytochrome-P450cam with *m*-Chloroperbenzoic acid. *Biochem. Biophys. Res. Commun.* **201**, 1464–1469 (1994)
- Kellner, D.G., Hung, S.C., Weiss, K.E., Sligar, S.G.: Kinetic characterization of compound I formation in the thermostable cytochrome P450 CYP119. *J. Biol. Chem.* **277**, 9641–9644 (2002)
- Spolitak, T., Dawson, J.H., Ballou, D.P.: Reaction of ferric cytochrome P450cam with peracids: kinetic characterization of intermediates on the reaction pathway. *J. Biol. Chem.* **280**, 20300–20309 (2005)
- Egawa, T., Proshlyakov, D.A., Miki, H., Makino, R., Ogura, T., Kitagawa, T., Ishimura, Y.: Effects of a thiolate axial ligand on the $\pi \rightarrow \pi^*$ electronic states of oxoferryl porphyrins: a study of the optical and resonance Raman spectra of compounds I and II of chloroperoxidase. *J. Biol. Inorg. Chem.* **6**, 46–54 (2001)
- Palcic, M.M., Rutter, R., Araiso, T., Hager, L.P., Dunford, H.B.: Spectrum of chloroperoxidase compound I. *Biochem. Biophys. Res. Commun.* **94**, 1123–1127 (1980)
- Piontek, K., Ullrich, R., Liers, C., Diederichs, K., Plattner, D.A., Hofrichter, M.: Crystallization of a 45 kDa peroxxygenase/peroxidase from the mushroom *Agrocybe aegerita* and structure determination by SAD utilizing only the haem iron. *Acta Crystallogr. Sect. F* **66**, 693–698 (2010)
- Fujishiro, T., Shoji, O., Nagano, S., Sugimoto, H., Shiro, Y., Watanabe, Y.: Crystal structure of H(2)O(2)-dependent Cytochrome P450 (SP alpha) with its bound fatty acid substrate insight into the regioselective hydroxylation of fatty acids at the alpha position. *J. Biol. Chem.* **286**, 29941–29950 (2011)

22. Araiso, T., Rutter, R., Palcic, M.M., Hager, L.P., Dunford, H.B.: Kinetic-analysis of compound-I formation and the catalytic activity of chloroperoxidase. *Can. J. Biochem.* **59**, 233–236 (1981)
23. Kluge, M., Ullrich, R., Scheibner, K., Hofrichter, M.: Stereoselective benzylic hydroxylation of alkylbenzenes and epoxidation of styrene derivatives catalyzed by the peroxxygenase of *Agrocybe aegerita*. *Green Chem.* **14**, 440–446 (2012)
24. Zaks, A., Dodds, D.R.: Chloroperoxidase-catalyzed asymmetric oxidations—substrate-specificity and mechanistic study. *J. Am. Chem. Soc.* **117**, 10419–10424 (1995)
25. Zhang, R., Nagraj, N., Lansakara, D.S.P., Hager, L.P., Newcomb, M.: Kinetics of two-electron oxidations by the Compound I derivative of chloroperoxidase, a model for cytochrome P450 oxidants. *Org. Lett.* **8**, 2731–2734 (2006)
26. Bell, S.R., Groves, J.T.: A highly reactive P450 model Compound I. *J. Am. Chem. Soc.* **131**, 9640–9641 (2009)
27. Shaik, S., Lai, W.Z., Chen, H., Wang, Y.: The valence bond way: reactivity patterns of cytochrome P450 enzymes and synthetic analogs. *Acc. Chem. Res.* **43**, 1154–1165 (2010)
28. Shaik, S., Cohen, S., Wang, Y., Chen, H., Kumar, D., Thiel, W.: P450 enzymes: their structure, reactivity, and selectivity-modeled by QM/MM calculations. *Chem. Rev.* **110**, 949–1017 (2010)
29. Shaik, S., Kumar, D., de Visser, S.P.: A valence bond modeling of trends in hydrogen abstraction barriers and transition states of hydroxylation reactions catalyzed by cytochrome P450 enzymes (vol. 130, p. 10128, 2008). *J. Am. Chem. Soc.* **130**, 14016 (2008)
30. Liu, W., Groves, J.T.: Manganese porphyrins catalyze selective C-H bond halogenations. *J. Am. Chem. Soc.* **132**, 12847–12849 (2010)
31. Chen, K., Eschenmoser, A., Baran, P.S.: Strain release in C-H bond activation? *Angew. Chem. Int. Ed.* **48**, 9705–9708 (2009)
32. Tanko, J.M., Friedline, R., Suleman, N.K., Castagnoli, N.: Tert-butoxyl as a model for radicals in biological systems: caveat emptor. *J. Am. Chem. Soc.* **123**, 5808–5809 (2001)
33. Finn, M., Friedline, R., Suleman, N.K., Wohl, C.J., Tanko, J.M.: Chemistry of the t-butoxyl radical: evidence that most hydrogen abstractions from carbon are entropy-controlled. *J. Am. Chem. Soc.* **126**, 7578–7584 (2004)
34. Gardner, K.A., Kuehnert, L.L., Mayer, J.M.: Hydrogen atom abstraction by permanganate: oxidations of arylalkanes in organic solvents. *Inorg. Chem.* **36**, 2069–2078 (1997)
35. Mayer, J.M.: Hydrogen atom abstraction by metal-oxo complexes: understanding the analogy with organic radical reactions. *Acc. Chem. Res.* **31**, 441–450 (1998)
36. Green, M.T., Dawson, J.H., Gray, H.B.: Oxoiron (IV) in chloroperoxidase compound II is basic: implications for P450 chemistry. *Science* **304**, 1653–1656 (2004)
37. Ullrich, R., Nuske, J., Scheibner, K., Spantzel, J., Hofrichter, M.: Novel haloperoxidase from the agaric basidiomycete *Agrocybe aegerita* oxidizes aryl alcohols and aldehydes. *Appl. Environ. Microbiol.* **70**, 4575–4581 (2004)
38. Ullrich, R., Liers, C., Schimpke, S., Hofrichter, M.: Purification of homogeneous forms of fungal peroxxygenase. *Biotechnol. J.* **4**, 1619–1626 (2009)

Chapter 5

Driving Force for Oxygen Atom Transfer by Heme-Thiolate Enzymes



Abstract The heme-thiolate peroxygenase *AaeAPO* from *Agroclybe aegerita* is an important biocatalyst and P450 analog. We have found that *AaeAPO* compound I can be formed via oxidation of the ferric protein with HOBr and HOCl. The rate constant for the formation of *AaeAPO*-I induced by HOBr at pH 5.0, 4 °C was $7.1 \times 10 \text{ M}^{-1}\text{s}^{-1}$. *AaeAPO*-I reacts with bromide and chloride ions to regenerate the resting ferric protein. Similar measurements were made for chloroperoxidase (CPO). The rate constant for the reaction of *AaeAPO*-I with bromide ion at pH 5.0, 4 °C was $2.6 \times 10^5 \text{ M}^{-1}\text{s}^{-1}$. By measuring the rates of the forward and reverse reactions over a wide range of pH, Nernst plots of the driving force for oxygen atom transfer from *AaeAPO*-I and CPO-I can be constructed. It is found that CPO-I and *AaeAPO*-I have a two-electron redox potential similar to that of HOBr and about 200 mV less than that of HOCl. Interestingly, CPO-I and *AaeAPO*-I are both much more oxidizing than HRP compound I. The results are informative with regard to the reactivity of these proteins toward C–H bonds.

5.1 Results and Discussion

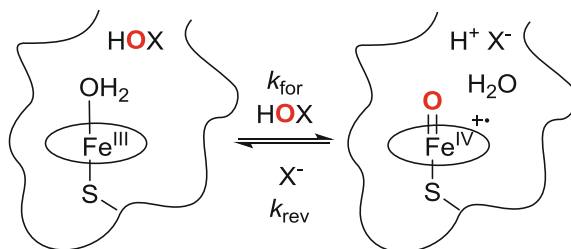
The heme-thiolate peroxygenase from *Agrocybe aegerita* (*AaeAPO*, EC 1.11.2.1) is a versatile biocatalyst and cytochrome P450 analog that catalyzes a variety of oxygenation reactions with high efficiency and selectivity [1–3]. Our recent kinetic characterization of *AaeAPO*-catalyzed reactions has shown that *AaeAPO* compound I is an oxo-Fe^{IV} porphyrin radical cation [4]. The reactivity of *AaeAPO*-I toward a panel of substrates showed very fast C–H hydroxylation rates, similar to those of cytochrome P450 (CYP119-I) [5], and much faster than chloroperoxidase compound I (CPO-I) [6]. Mechanistic probes have revealed a large hydrogen isotope effect for aliphatic C–H hydroxylation and rearranged products from the hydroxylation of norcarane [2]. There is, however, very little information available regarding the thermodynamic properties of such highly reactive oxo-iron species for any heme-thiolate proteins.

For hydrogen abstraction reactions, the redox potential of the oxidant is correlated with the rates of C–H activation [7–17]. Yet these values are often not readily accessible, especially for highly reactive oxidants. We have developed a method to measure redox potentials for oxometalloporphyrin model compounds that takes advantage of the rapid, reversible oxygen atom transfer between oxo-metal complexes and halide ions [18]. By using rapid-mixing stopped-flow spectroscopy, rate constants of both forward and reverse reactions are measured. Thus, the driving force of the unknown oxo-transfer redox couple ($M^{n+2}=O/M^n$) is obtained from the equilibrium constants for the reaction and the known potentials of the HOX/X[−] couples. Using this method, the oxo-transfer driving force for several heme-enzyme model complexes have been measured, such as oxo-Mn^VTDMIMP [18–21] and [oxo-Fe^{IV}-4-TMPyP]⁺ [22].

Here, we describe measurements of the driving force for oxygen atom transfer by the heme-thiolate proteins *AaeAPO* and CPO. We have found that oxo-transfer between *AaeAPO*-I and chloride or bromide ions is fast *and reversible* (Scheme 5.1). The redox potential of the couple *AaeAPO*-I/ferric-*AaeAPO* has been obtained over a wide pH range from the rate constants of the forward and reverse reactions. Thus, the highly reactive *AaeAPO*-I can be placed on an absolute energy scale and compared with those of CPO and HRP for the first time.

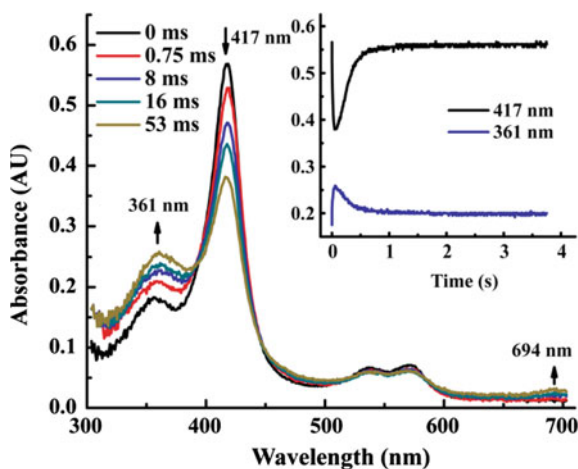
5.1.1 Kinetic Characterization of Compound I Generation by Hypohalous Acids

AaeAPO-I was generated by the stoichiometric reaction of Fe^{III}-*AaeAPO* with HOCl or HOBr and characterized by rapid mixing, stopped-flow spectroscopy. The UV/Vis spectral features of *AaeAPO*-I generated with these hypohalous acids (Fig. 5.1) are the same as those we recently reported for peroxyacid oxidations [4]. The Soret band of the ferric enzyme at 417 nm diminished over the first 50 ms after



Scheme 5.1 Reversible oxygen atom transfer between ferric *AaeAPO* and HOBr or HOCl (k_{for}), and *AaeAPO*-I with halide ions (k_{rev})

Fig. 5.1 UV/vis spectra observed upon 1:1 mixing of 5 μM *AaeAPO* with 15 μM NaOBr at pH 5.0, 4 $^{\circ}\text{C}$. *Inset* Time courses of data obtained at 417 nm (ferric *AaeAPO*) and 361 nm (*AaeAPO*-I)



mixing while new absorbances characteristic of the formation of an oxo-Fe^{IV} porphyrin radical cation appeared at 361 and 694 nm. *AaeAPO*-I subsequently decayed in a second, slower phase. SVD analysis of these transient spectra indicated that only two species were present in significant amounts during this transformation.

The *AaeAPO*-I formation rate was directly measured by monitoring the conversion of the ferric enzyme to oxo-Fe^{IV} radical cation (Fig. 5.2). Binding of HOX to the heme iron is a rapid step and heterolytic FeO-X bond cleavage is rate-limiting [4]. Plotting the initial absorbance change at 417 nm against the HOX concentration afforded a linear relationship with no evidence of saturation. Second-order rate constants were obtained from the slopes (Fig. 5.3). For example, the rate constant for the formation of *AaeAPO*-I induced by HOBr at pH 5.0, 4 $^{\circ}\text{C}$ was $7.1 \times 10^5 \text{ M}^{-1}\text{s}^{-1}$.

The oxidation of *AaeAPO* with HOCl or HOBr was examined over a range of pH as shown in Table 5.1. At pH 3.0, HOCl was used because HOBr is not stable at this pH. The slightly milder oxidant, HOBr, was used to generate *AaeAPO*-I from

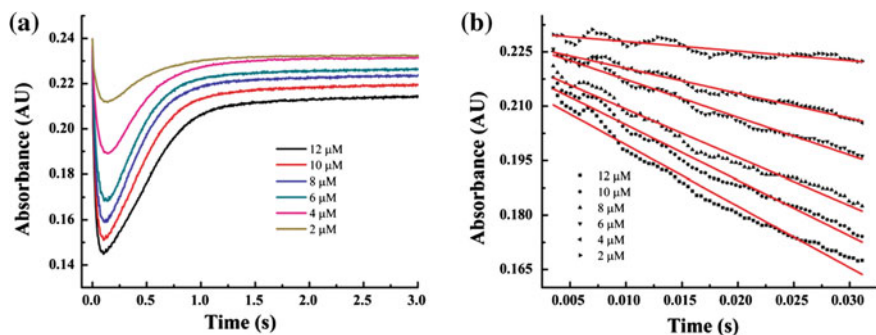


Fig. 5.2 **a** UV-vis absorbance change at 417 nm upon *AaeAPO* mixing with different concentration of HOBr at pH 5.0 and 4 °C, monitored by single wavelength stopped-flow instruments. **b** Initial velocity fitting of the absorbance changes versus time with the use of different concentration of HOBr

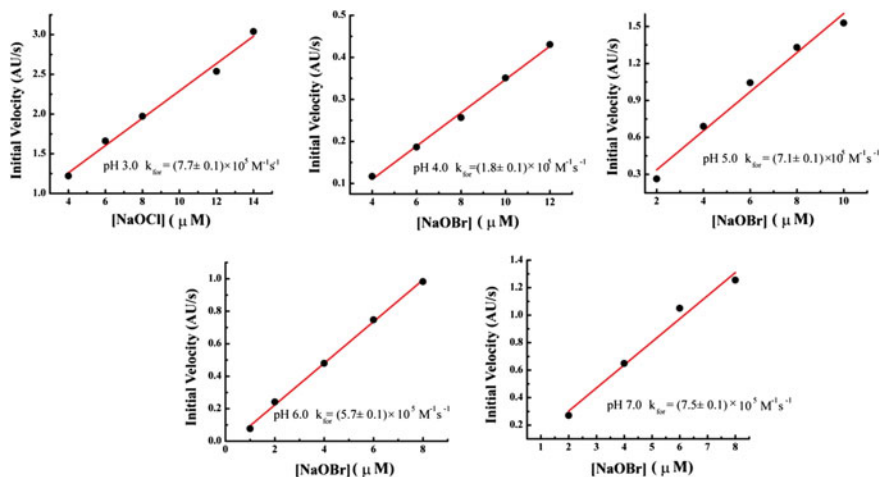


Fig. 5.3 Initial velocity of ferric *AaeAPO* oxidation as a function of [NaOX] for the reaction between 2 μM *AaeAPO* with NaOX, pH 3–7

Table 5.1 Data for oxygen atom transfer between halide ions and *AaeAPO*-I at different pHs

pH	k_{for}	k_{rev}	K_{equi}	$E'_{(\text{cpd-I}/\text{ferric})}$ ^a (V versus NHE)
3.0	7.7×10^5	1.0×10^2	7680	1.32 ^b
4.0	1.8×10^5	4.3×10^5	0.4	1.25
5.0	7.1×10^5	2.6×10^5	2.8	1.19
6.0	5.7×10^5	1.9×10^5	3.0	1.17
7.0	7.5×10^5	5.1×10^4	15	1.12

^aBased on the HOBr/Br⁻ couple at 4 °C except as noted [25]

^bBased on the HOCl/Cl⁻ couple at 4 °C [25]

Table 5.2 Kinetic and thermodynamic data, k_{for} , k_{rev} , K_{equi} and $E'_{(\text{cpd-I}/\text{ferric})}$, for oxygen atom transfer between halide ions and CPO-I at different pHs

pH	k_{for}	k_{rev}	K_{equi}	$E'_{(\text{cpd-I}/\text{ferric})}$ ^a (V versus NHE)
4.0	1.1×10^6	5.0×10^5	2.28	1.22
5.0	2.3×10^6	6.7×10^4	34.8	1.16
6.0	1.6×10^6	1.5×10^3	1067	1.10
7.0	1.6×10^6	7.4×10^2	2176	1.06

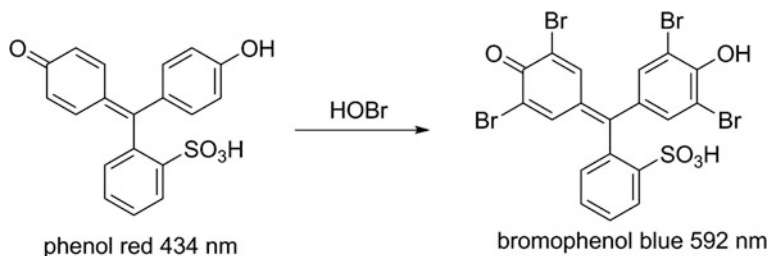
Typical errors for the rate data are $\sim 1\%$ or less

^aBased on the HOBr/Br⁻ couple at 4 °C except as noted [25]

pH 4.0–7.0 in good yields. We also measured the rates of CPO-I formation by the same method (Table 5.2). At pH 5.0, 4 °C, the second-order rate constant for CPO-I formation was $2.3 \times 10^6 \text{ M}^{-1}\text{s}^{-1}$, which is three-fold faster than that of *AaeAPO*. Although *AaeAPO* and CPO share $\sim 30\%$ sequence similarity, their active site environments, especially the acid-base residues, differ and CPO has a less accessible active site [23, 24].

5.1.2 Kinetic Characterization of Compound I Reaction with Halide Ions

AaeAPO-I has been shown to have extraordinarily large rate constants for hydroxylation of even very strong C–H bonds [4]. We have found that *AaeAPO*-I is also highly reactive toward halide ions. The formation of HOBr for the reaction of bromide ion with *AaeAPO*-I was detected conveniently with the diagnostic indicator, phenol red [26, 27]. The rapid tetra-bromination of phenol red was monitored by the characteristic red shift from 434 to 592 nm as shown in Scheme 5.2 and Fig. 5.4. The oxygenation of bromide by CPO-I was found to be much slower than that of *AaeAPO*-I at the same pH (Fig. 5.5). The reaction of chloride ion with *AaeAPO*-I to afford hypochlorous acid was also found to occur with high efficiency but only under acidic conditions.



Scheme 5.2 Phenol red conversion to bromophenol blue upon the addition of HOBr

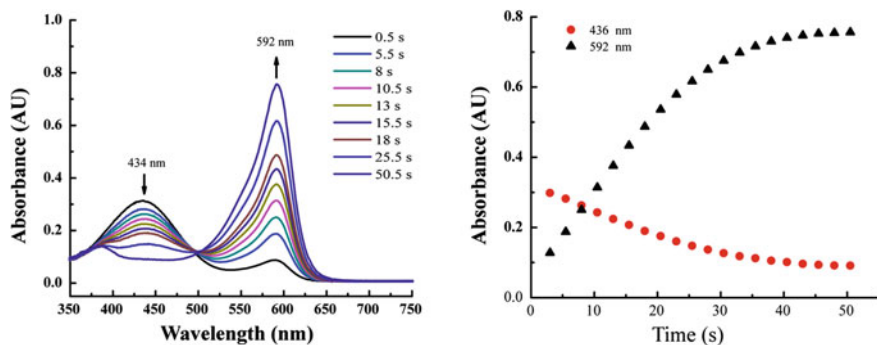


Fig. 5.4 UV/Vis spectral changes observed for the bromination of phenol red ($\lambda_{\text{max}} = 434$ nm to form bromophenol blue ($\lambda_{\text{max}} \geq 592$ nm) by 1 mM of H_2O_2 , 10 mM NaBr and 20 nM of *AaeAPO* at pH 5.0, RT

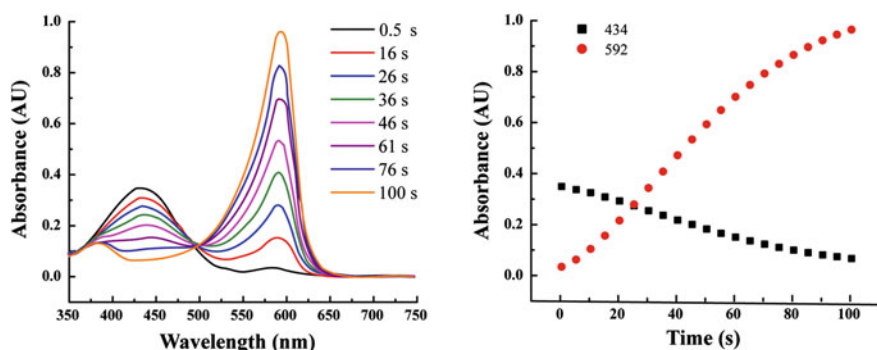


Fig. 5.5 UV/Vis spectral changes observed for the bromination of phenol red ($\lambda_{\text{max}} = 434$ nm) to bromophenol blue ($\lambda_{\text{max}} = 592$ nm) by 1 mM of H_2O_2 , 10 mM NaBr and 20 nM of CPO at pH 5.0, RT

The kinetic behavior of halide ion oxygenation by *AaeAPO*-I was then investigated by double-mixing, stopped-flow spectroscopy. At each selected pH, *AaeAPO*-I was formed in the first push by mixing ferric enzyme with 3 eq of NaOBr or NaOCl. NaBr or NaCl solution was added in the second push after the peak amount of compound I had been achieved (~ 50 ms). Time-resolved, diode array spectra clearly showed the transformation of compound I back to the resting ferric state. Kinetic profiles were obtained by monitoring the return of the Soret band of ferric *AaeAPO* at 417 nm Fig. 5.6 or ferric CPO at 399 nm and fitted to a single exponential equation. The observed pseudo-first order rate constants (k_{obs}) were found to vary linearly with [NaBr] or [NaCl] (Fig. 5.7). The apparent second-order rate constants (k_{rev}) were calculated from the slopes and are summarized in Tables 5.1 and 5.2. The pH dependence of $\log k_{\text{rev}}$ is plotted in Fig. 5.8. A slope of -1.0 was obtained over the pH range studied for CPO, suggesting that a

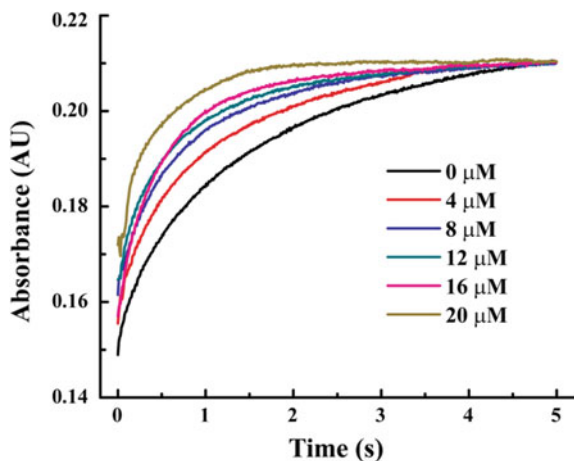


Fig. 5.6 The decay of *AaeAPO-I* monitored at 417 nm upon its reaction with different concentration of Br^- at pH 6.0

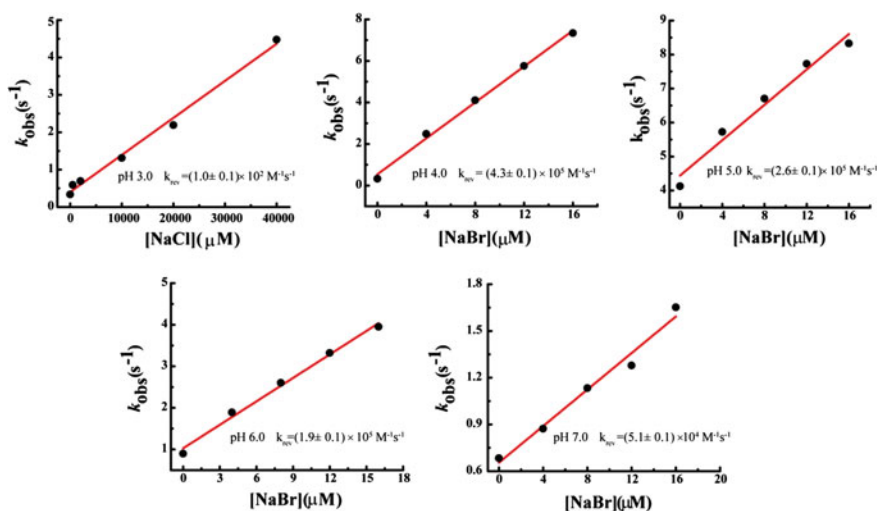
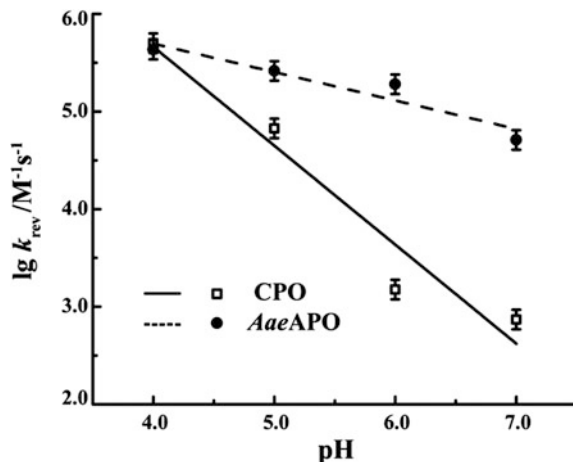


Fig. 5.7 Pseudo-first order rate constants, k_{obs} , as a function of $[\text{NaX}]$ for the reaction between *AaeAPO-I* with halide ions at different pHs

single proton is involved in the reaction. However, for *AaeAPO*, the $\log k_{\text{rev}}/\text{pH}$ slope is only -0.3 , suggesting that a protonation may not occur in the rate-determining step.

Fig. 5.8 Plots of $\log k_{\text{rev}}$ as a function of pH for oxo-transfer from *Aae*APO-I and CPO-I to bromide ion



5.1.3 Determination the Redox Potential of Compound I and the Nernst Plots

Taking advantage of this reversible and kinetically well-behaved oxygen atom transfer reaction (Scheme 5.1), we determined a set of equilibrium constants, K_{equi} , from the ratios of the measured forward and reverse rate constants (Eq. 5.1). As can be seen in Table 5.1, K_{equi} increased at higher pH. Since the redox potentials for the couples HOBr/Br^- (4 °C, $E_{(\text{HOBr}/\text{Br}^-)}^\circ = 1.344 \text{ V}$) and HOCl/Cl^- (4 °C, $E_{(\text{HOCl}/\text{Cl}^-)}^\circ = 1.51 \text{ V}$) are known [28], the corresponding oxygen atom transfer driving force for *Aae*APO-I could be calculated at each pH and 4 °C as shown in Eqs. (5.2), (5.3) and (5.4) ($n = 2$).

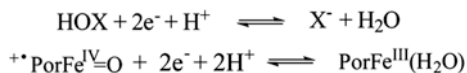
$$K_{\text{equi}} = \frac{k_{\text{for}}}{k_{\text{rev}}} \quad (5.1)$$

$$\Delta E' = \frac{2.303RT}{nF} \lg K_{\text{equi}} \quad (5.2)$$

$$E'_{\text{HOX}/\text{X}^-} = E_{\text{HOX}/\text{X}^-}^\circ - \frac{2.303RT}{2F} \text{pH} \quad (5.3)$$

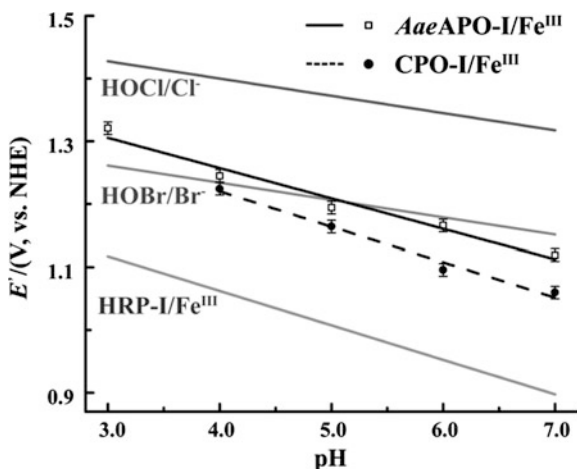
$$E'_{\text{cpd-I}/\text{Fe}^{\text{III}}} = E'_{\text{HOX}/\text{X}^-} - 0.0275 \lg K_{\text{equi}} \quad (5.4)$$

The derived compound I/ferric enzyme redox potentials for *Aae*APO and CPO are summarized in Tables 5.1 and 5.2 and plotted in Fig. 5.9. Fitting those points from pH 3.0 to 7.0 gave linear relationships with a slope of 0.048 for *Aae*APO and 0.056 for CPO, close to the theoretical value of 0.055 for the Nernst equation at



Scheme 5.3 Nernst half-reactions for HOX and $^{+2}\text{PorFe}^{\text{IV}}=\text{O}$

Fig. 5.9 Calculated redox potentials $E'_{(\text{cpd-I}/\text{ferric})}$ as a function of pH for *AaeAPO-I/Fe*^{III} (open squares) and *CPO-I/Fe*^{III} (closed circles) at 4 °C. Nernst equations for *HRP-I/Fe*^{III} [32], *HOBr/Br*⁻ and *HOCl/Cl*⁻ are plotted in gray for comparison



4 °C. This similarity supports a Nernst half-reaction involving two electrons and two protons as shown in Scheme 5.3.

As can be seen in Fig. 5.9, the driving force for oxygen atom transfer for *AaeAPO-I* and *CPO-I* are similar to that of *HOBr* and about 200 mV less than that of *HOCl*. *AaeAPO-I* and *CPO-I* are both significantly more oxidizing than *HRP-I*, while *AaeAPO-I* has slightly larger redox potentials than those of *CPO-I* over the entire pH range. Thus, the ordering of the redox potentials parallels the reactivity of these heme proteins: *CPO-I* reacts slowly with even weak C–H bonds [6, 29], while *HRP-I* is barely able to oxidize C–H bonds at all. By contrast, *AaeAPO-I* is highly reactive toward even very strong C–H bonds such as the methyl group of neopentane with a C–H BDE of 100 kcal mol⁻¹ [4]. Similar halide oxidation data for cytochrome P450 is not available. However, by comparing the hydroxylation kinetics of *AaeAPO* and *CYP119* with similar aliphatic substrates [5, 30, 31], the redox properties of *P450-I* and *AaeAPO-I* appear to lie on a similar scale.

What factors contribute to the significantly higher driving force for ferryl oxygen atom transfer by *AaeAPO-I* and *CPO-I* reported here as compared to that of *HRP-I*? The axial ligand for *AaeAPO* and *CPO* are both cysteine thiolate anions, while for *HRP*, it is a neutral, histidine nitrogen. According to the Nernst half reaction (Scheme 5.3), the driving force for the conversion of $^{+2}\text{PorFe}^{\text{IV}}=\text{O}$ to $\text{PorFe}^{\text{III}}$ via oxygen atom transfer has two contributions—the electron affinity and the *proton affinity* of the ferryl species. Although DFT calculations have indicated that the frontier orbitals of a heme-histidine compound I are at lower energy than the

corresponding orbitals in heme-thiolate compound I [33, 34], the strong proton affinity of a thiolate bound compound I may provide a large driving force resulting in a higher net redox potentials and more reactive oxidants [17, 35–38]. The intrinsic basicity of the ferryl oxygen in Cys–S–Fe^{IV}=O (compound II) in heme-thiolate enzymes has been established [39]. Since Cys–S–Fe^{III}–OH₂ is the resting state, Cys–S–Fe^{III}–OH is also basic, thus contributing further to the two-electron, two-proton oxo-transfer redox couples determined here.

5.1.4 Implication of Compound I Redox Properties on C–H Activation

The *one-electron* redox potential of *Aae*APO-I, [$E^\circ(\text{I})$], is a particularly important thermodynamic value because it is related to the bond strength [$D(\text{O–H})$] and the pK_a , [$pK_a(\text{II})$] of Fe^{IV}O–H in *Aae*APO-II (Eq. 5.5) [7, 8]. For cases in which $E^\circ(\text{I})$ and $pK_a(\text{II})$ cannot be measured independently, Eq. 5.6 can be derived [40]. Since both $E^\circ(\text{I})$ and $pK_a(\text{II})$ have not been measured independently for any heme-enzyme, the two-electron, two-proton redox potential of *Aae*APO-I measured here may be a good first approximation of $E^\circ(\text{I})$. $E'_{(\text{HRP-I}/\text{HRP-II})}$ and $E'_{(\text{HRP-II}/\text{Ferric})}$ for HRP have been measured and were found to be similar (~ 0.95 V at pH 6.0) [32, 41]. However, this result might be due to the fact that HRP-II is not basic and exists in the Fe^{IV}=O form in the functional pH range. The situation is different if we consider that *Aae*APO compound II is protonated [39].

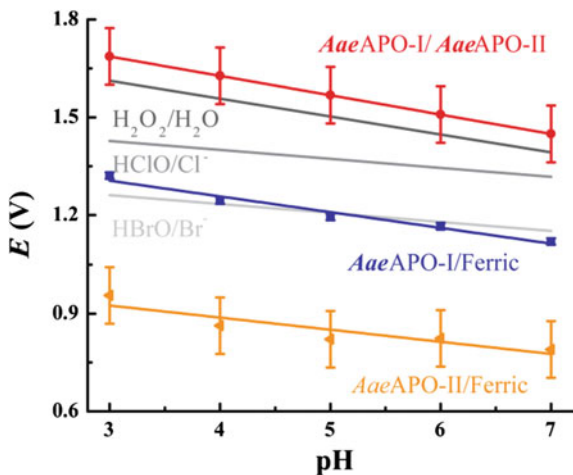
$$D(\text{O–H}) = nFE^\circ(\text{I}) + 2.3RTpK_a(\text{II}) + 57 \pm 2 \quad (5.5)$$

$$D(\text{O–H}) = nFE'_{\text{cpd-I}/\text{cpd-II}} + 2.3RTpH + 57 \pm 2 \quad (5.6)$$

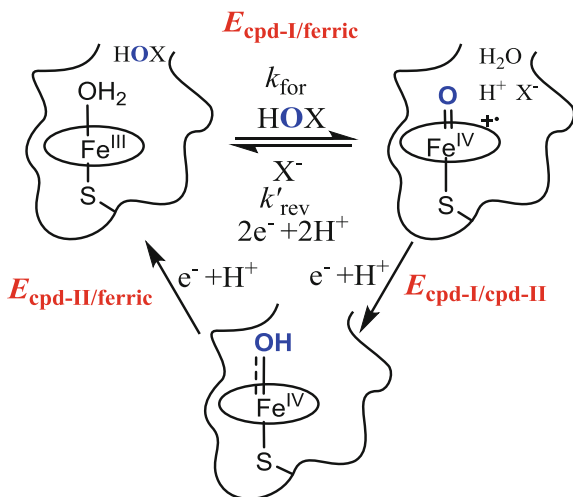
$$2E'_{\text{cpd-I}/\text{Fe}^{\text{III}}} = E'_{\text{cpd-I}/\text{cpd-II}} + E'_{\text{cpd-II}/\text{Fe}^{\text{III}}} \quad (5.7)$$

Based on our estimation that *Aae*APO-II has a $D(\text{O–H})$ of about 100 kcal/mol [4, 42], and two electron two proton redox potentials of ferric *Aae*APO/*Aae*APO-I measured at different pHs from the equilibrium reactions with halide ions, then, we can derive redox properties of the other two important redox couples: ferric *Aae*APO/*Aae*APO-II and *Aae*APO-I/*Aae*APO-II. Nernst plots for all these different redox couples are shown in Fig. 5.10. For example, the one-electron redox potential $E'_{(\text{cpd-I}/\text{cp-II})}$, would be 1.4 V versus NHE at pH 7.0, significantly higher than the two-electron $E'_{(\text{cpd-I}/\text{ferric})}$ potential of 1.1 V. Accordingly, from Eq. 5.7 and Scheme 5.4, the reduction potential of *Aae*APO-II ($E'_{(\text{cpd-II}/\text{ferric})}$) can be estimated to be ~ 0.8 V. This unsymmetrical partitioning of the two redox steps may be an important factor in facilitating homolytic C–H bond scission by heme-thiolate proteins.

Fig. 5.10 Nernst plots for three different intermediate couples: ferric *AaeAPO*/ *AaeAPO*-I, *AaeAPO*-I/ *AaeAPO*-II and ferric *AaeAPO*/*AaeAPO*-II. The error bar is the ± 2 from Eq. (5.5)

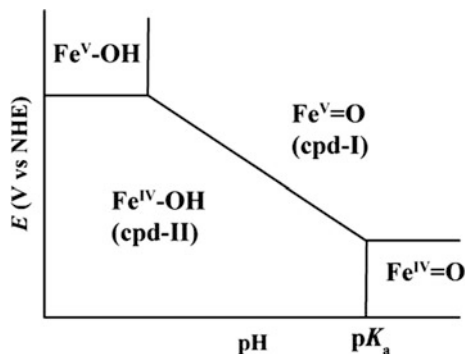


Scheme 5.4 Relationship between three different redox couples



We can derive Eq. (5.8) as below if we know the pK_a of *AaeAPO*-II. $E(I)$ is the one electron redox potential of compound I. $E_{\text{cpd-I/cpd-II}}$ is the one electron one proton redox potential (PCET process). If compound II has a very basic pK_a , the latter term is positive. Then, the PCET process results a higher potential than the one electron transfer potential. The relationship between compound I, compound II and deprotonated compound II can be plotted as shown in Fig. 5.5, a stability (Pourbaix) diagram for *AaeAPO* intermediates ($n = 1$).

Fig. 5.11 The stability (Pourbaix) diagram for *Aae*APO high-valent iron intermediates



$$E_{\text{cpd-I/cpd-II}} = E(I) + \frac{2.303RT}{nF} (pK_a - \text{pH}) \quad (5.8)$$

5.2 Conclusions

The results show that chloride and bromide ions are readily oxidized by *Aae*APO-I to the corresponding hypohalous acid. The reversibility of this oxo-transfer reaction provides a rare opportunity to place ferryl oxo-transfers by the highly reactive heme-thiolate *Aae*APO-I and that of CPO-I on an absolute energy scale. With an estimated BDE for $\text{Fe}^{\text{IV}}\text{O-H}$ in *Aae*APO-II we are able to obtain redox potentials of three redox couples interconnecting the resting ferric protein with its two oxidized forms, $^+\text{Por-Fe}^{\text{IV}}\text{=O}$ and $\text{Fe}^{\text{IV}}\text{O-H}$. In next chapter, more investigations another important rebound intermediate, *Aae*APO-II, and its pK_a value will be evaluated.

5.3 Experimental

Reagents: Wild-type extracellular peroxxygenase of *A. aegerita* (isoform II, pI 5.6, 46 kDa) was produced in bioreactors with a soybean-flour suspension as the growth substrate and purified as described previously [43]. The enzyme preparation was homogeneous by SDS/PAGE, and exhibited an $A_{418\text{nm}}/A_{280\text{nm}}$ ratio of 1.7. The specific activity of the peroxxygenase was 59 U mg^{-1} , where 1 U represents the oxidation of 1 μmol of 3,4-dimethoxybenzyl alcohol to 3,4-dimethoxybenzaldehyde in 1 min at room temperature. Chloroperoxidase was purchased from Bio-Research Products, Inc. with RZ of $A_{400\text{nm}}/A_{280\text{nm}} > 1.3$, 1.296 U mg^{-1} , where 1 U represents the amount of CPO catalyzing the formation of 1 μmol of dichlorodimedone from monochlorodimedone in 1 min at 25 °C, pH 2.75, 0.02 M KCl, 2 mM H_2O_2 . All chemicals were of the best available purity from

Aldrich. Sodium hypochlorite solution was standardized spectrophotometrically ($\epsilon_{292\text{nm}} = 350 \text{ M}^{-1}\text{cm}^{-1}$). Sodium hypobromite solution was freshly prepared by mixing sodium hypochlorite with sodium bromide under slightly basic conditions. A 5 % excess of sodium bromide was used to ensure full conversion [19]. The final concentration of sodium hypobromite solution was determined spectrophotometrically ($\epsilon_{329\text{nm}} = 332 \text{ M}^{-1}\text{cm}^{-1}$). Buffers were freshly prepared daily using either citric acid/sodium citrate (pH 3–5) or $\text{KH}_2\text{PO}_4/\text{K}_2\text{HPO}_4$ (pH 6 and 7).

Instruments: UV/Vis spectral measurements were performed on a Hewlett-Packard 8453 diode-array spectrophotometer at RT. Stopped-flow experiments were carried out on a Hi-Tech SF-61 DX2 double-mixing instrument with a 1 cm path length equipped with an ISOTEMP 3013 D thermostat bath. Bromination of phenol red was detected by UV/Vis spectroscopy [19].

Bromination assay: At a chosen pH, 2 μl of 10 μM APO or CPO was added to a reaction mixture containing 20 μM of phenol red (sodium salt), 1 mM H_2O_2 and 10 mM NaBr. The disappearance of phenol red was monitored at 434 nm and the formation of phenol blue was monitored at 592 nm.

Kinetic characterization: The oxidation of ferric enzyme with NaOBr or NaOCl was performed by stopped-flow spectroscopy with the single-mixing mode under the diode-array or single wavelength mode. The first syringe was filled with enzyme in a 100 mM buffer at a chosen pH. The second syringe was filled with the oxidant in slightly basic water solution. Equal volumes of the two reactants were mixed quickly. The halide ion oxidation reactions were performed using the double-mixing mode. Native enzyme was mixed with an equal volume of oxidants (NaOCl or NaOBr) in the first push. After an aging time (optimized for each pH), the sodium halide solution was added in the second push. All concentrations reported are the final concentrations. All the experiments were carried out at 4 °C. The data were analyzed using Kinetic Studio from Hi-Tech.

References

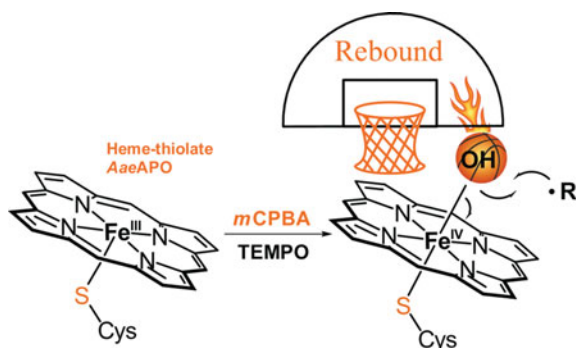
1. Hofrichter, M., Ullrich, R., Pecyna, M.J., Liers, C., Lundell, T.: New and classic families of secreted fungal heme peroxidases. *Appl. Microbiol. Biotechnol.* **87**, 871–897 (2010)
2. Peter, S., Kinne, M., Wang, X., Ullrich, R., Kayser, G., Groves, J.T., Hofrichter, M.: Selective hydroxylation of alkanes by an extracellular fungal peroxxygenase. *FEBS J.* **278**, 3667–3675 (2011)
3. Ullrich, R., Hofrichter, M.: The haloperoxidase of the agaric fungus *Agrocybe aegerita* hydroxylates toluene and naphthalene. *FEBS Lett.* **579**, 6247–6250 (2005)
4. Wang, X., Peter, S., Kinne, M., Hofrichter, M., Groves, J.T.: Detection and kinetic characterization of a highly reactive heme-thiolate peroxxygenase compound I. *J. Am. Chem. Soc.* **134**, 12897–12900 (2012)
5. Rittle, J., Green, M.T.: Cytochrome P450 compound i: capture, characterization, and C-H bond activation kinetics. *Science* **330**, 933–937 (2010)
6. Zhang, R., Nagraj, N., Lansakara, D.S.P., Hager, L.P., Newcomb, M.: Kinetics of two-electron oxidations by the compound I derivative of chloroperoxidase, a model for cytochrome P450 oxidants. *Org. Lett.* **8**, 2731–2734 (2006)

7. Mayer, J.M.: Hydrogen atom abstraction by metal-oxo complexes: understanding the analogy with organic radical reactions. *Acc. Chem. Res.* **31**, 441–450 (1998)
8. Bordwell, F.G., Cheng, J.P., Ji, G.Z., Satish, A.V., Zhang, X.: Bond dissociation energies in DMSO related to the gas phase. *J. Am. Chem. Soc.* **113**, 9790–9795 (1991)
9. Concepcion, J.J., Jurss, J.W., Brennaman, M.K., Hoertz, P.G., Patrocínio, A.O.T., Iha, N.Y. M., Templeton, J.L., Meyer, T.J.: Making oxygen with ruthenium complexes. *Acc. Chem. Res.* **42**, 1954–1965 (2009)
10. Meyer, T.J., Huynh, M.H.V., Thorp, H.H.: The possible role of proton-coupled electron transfer (PCET) in water oxidation by photosystem II. *Angew. Chem. Int. Ed.* **46**, 5284–5304 (2007)
11. Mayer, J.M.: Proton-coupled electron transfer: a reaction chemist's view. *Annu. Rev. Phys. Chem.* **55**, 363–390 (2004)
12. Cukier, R.I., Nocera, D.G.: Proton-coupled electron transfer. *Annu. Rev. Phys. Chem.* **49**, 337–369 (1998)
13. Borovik, A.S.: Role of metal-oxo complexes in the cleavage of C-H bonds. *Chem. Soc. Rev.* **40**, 1870–1874 (2011)
14. Warren, J.J., Tronic, T.A., Mayer, J.M.: Thermochemistry of proton-coupled electron transfer reagents and its implications. *Chem. Rev.* **110**, 6961–7001 (2010)
15. Gunay, A., Theopold, K.H.: C-H bond activations by metal oxo compounds. *Chem. Rev.* **110**, 1060–1081 (2010)
16. Waidmann, C.R., Miller, A.J.M., Ng, C.W.A., Scheuermann, M.L., Porter, T.R., Tronic, T.A., Mayer, J.M.: Using combinations of oxidants and bases as PCET reactants: thermochemical and practical considerations. *Energy Environ. Sci.* **5**, 7771–7780 (2012)
17. Lai, W.Z., Li, C.S., Chen, H., Shaik, S.: Hydrogen-abstraction reactivity patterns from A to Y: the valence bond way. *Angew. Chem. Int. Ed.* **51**, 5556–5578 (2012)
18. Jin, N., Bourassa, J.L., Tizio, S.C., Groves, J.T.: Rapid, reversible oxygen atom transfer between an oxomanganese(V) porphyrin and bromide: a haloperoxidase mimic with enzymatic rates. *Angew. Chem.* **112**, 4007–4009 (2000); *Angew. Chem. Int. Ed.* **39**, 3849–3851 (2000)
19. Lahaye, D., Groves, J.T.: Modeling the haloperoxidases: reversible oxygen atom transfer between bromide ion and an oxo-Mn(V) porphyrin. *J. Inorg. Biochem.* **101**, 1786–1797 (2007)
20. Umile, T.P., Wang, D., Groves, J.T.: Dissection of the mechanism of manganese porphyrin-catalyzed chlorine dioxide generation. *Inorg. Chem.* **50**, 10353–10362 (2011)
21. Umile, T.P., Groves, J.T.: Catalytic generation of chlorine dioxide from chlorite using a water-soluble manganese porphyrin. *Angew. Chem. Int. Ed.* **50**, 695–698 (2011)
22. Bell, S.R.: Modeling heme monooxygenases with water-soluble iron porphyrins. PhD, Princeton University (2010)
23. Pecyna, M.J., Ullrich, R., Bittner, B., Clemens, A., Scheibner, K., Schubert, R., Hofrichter, M.: Molecular characterization of aromatic peroxxygenase from *Agroclybe aegerita*. *Appl. Microbiol. Biotechnol.* **84**, 885–897 (2009)
24. Sundaramoorthy, M., Termer, J., Poulos, T.L.: Stereochemistry of the chloroperoxidase active site: crystallographic and molecular-modeling studies. *Chem. Biol.* **5**, 461–473 (1998)
25. Bard, A.J., Parsons, R., Jordan, J.: Standard potentials in aqueous solution. Marcel Dekker Inc., New York (1985)
26. Walker, J.V., Morey, M., Carlsson, H., Davidson, A., Stucky, G.D., Butler, A.: Peroxidative halogenation catalyzed by transition-metal-ion-grafted mesoporous silicate materials [2]. *J. Am. Chem. Soc.* **119**, 6921–6922 (1997)
27. Totaro, R.M., Williams, P.A.M., Apella, M.C., Blesa, M.A., Baran, E.J.: Bromination of phenol red mediated by vanadium(v) peroxo complexes at pH 6.5. *J. Chem. Soc. Dalton Trans.* 4403–4406 (2000)
28. Holm, R.H., Donahue, J.P.: A thermodynamic scale for oxygen atom transfer reactions. *Polyhedron* **12**, 57–589 (1993)

29. Zaks, A., Dodds, D.R.: Chloroperoxidase-catalyzed asymmetric oxidations: substrate-specificity and mechanistic study. *J. Am. Chem. Soc.* **117**, 10419–10424 (1995)
30. Su, Z., Horner, J.H., Newcomb, M.: Rates of fatty acid oxidations by P450 compound I are pH dependent. *ChemBioChem* **13**, 2061–2064 (2012)
31. Davydov, R., Dawson, J.H., Perera, R., Hoffman, B.M.: The use of deuterated camphor as a substrate in H-1 ENDOR studies of hydroxylation by cryoreduced Oxy P450cam provides new evidence of the involvement of compound I. *Biochemistry* **52**, 667–671 (2013)
32. Farhangrazi, Z.S., Fossett, M.E., Powers, L.S., Ellis Jr, W.R.: Variable-temperature spectroelectrochemical study of horseradish peroxidase. *Biochemistry* **34**, 2866–2871 (1995)
33. Kumar, D., De Visser, S.P., Sharma, P.K., Derat, E., Shaik, S.: The intrinsic axial ligand effect on propene oxidation by horseradish peroxidase versus cytochrome P450 enzymes. *J. Biol. Inorg. Chem.* **10**, 181–189 (2005)
34. Kumar, D., Sastry, G.N., de Visser, S.P.: Axial ligand effect on the rate constant of aromatic hydroxylation by Iron(IV)-oxo complexes mimicking cytochrome P450 enzymes. *J. Phys. Chem. B* **116**, 718–730 (2012)
35. Dey, A., Jiang, Y., Ortiz de Montellano, P.R., Hodgson, K.O., Hedman, B., Solomon, E.I.: S K-edge XAS and DFT calculations on cytochrome P450: covalent and ionic contributions to the cysteine-Fe bond and their contribution to reactivity. *J. Am. Chem. Soc.* **131**, 7869–7878 (2009)
36. Takahashi, A., Yamaki, D., Ikemura, K., Kurahashi, T., Ogura, T., Hada, M., Fujii, H.: Effect of the axial ligand on the reactivity of the Oxoiron(IV) porphyrin pi-cation radical complex: higher stabilization of the product state relative to the reactant state. *Inorg. Chem.* **51**, 7296–7305 (2012)
37. Hughes, T.F., Friesner, R.A.: Development of accurate DFT methods for computing redox potentials of transition metal complexes: results for model complexes and application to cytochrome P450. *J. Chem. Theory Comput.* **8**, 442–459 (2012)
38. Isobe, H., Yamaguchi, K., Okumura, M., Shimada, J.: Role of perferryl-oxo oxidant in alkane hydroxylation catalyzed by cytochrome P450: a hybrid density functional study. *J. Phys. Chem. B* **116**, 4713–4730 (2012)
39. Green, M.T., Dawson, J.H., Gray, H.B.: Oxoiron(IV) in chloroperoxidase compound II is basic: implications for P450 chemistry. *Science* **304**, 1653–1656 (2004)
40. Wang, D., Zhang, M., Buhlmann, P., Que, L.: Redox potential and C–H bond cleaving properties of a nonheme Fe-IV=O complex in aqueous solution. *J. Am. Chem. Soc.* **132**, 7638–7644 (2010)
41. Hayashi, Y., Yamazaki, I.: Oxidation-reduction potentials of compound-I-compound-II and compound-II-ferric couples of horseradish peroxidases A2 and C. *J. Biol. Chem.* **254**, 9101–9106 (1979)
42. Bell, S.R., Groves, J.T.: A highly reactive P450 model compound I. *J. Am. Chem. Soc.* **131**, 9640–9641 (2009)
43. Ullrich, R., Nuske, J., Scheibner, K., Spantzel, J., Hofrichter, M.: Novel haloperoxidase from the agaric basidiomycete *Agrocybe aegerita* oxidizes aryl alcohols and aldehydes. *Appl. Environ. Microbiol.* **70**, 4575–4581 (2004)

Chapter 6

Detection and Characterization of Heme-Thiolate Compound II from *Aae*APO Peroxygenase



Abstract A kinetic and spectroscopic characterization of the unusual, high-valent Cys–Fe^{IV}–OH intermediate (compound II) from *Aae*APO, the heme-thiolate peroxxygenase from *Agrocybe aegerita*, is described. *Aae*APO-II was generated by the reaction of ferric enzyme with *m*CPBA in the presence of nitroxides and detected with the use of fast-mixing UV-vis stopped-flow spectroscopy. The nitroxides served as a selective reductant of *Aae*APO-I, reacting only slowly with *Aae*APO-II. *Aae*APO-II displayed a characteristic split Soret UV-vis spectrum (370 and 428 nm). Rapid-mixing, pH-jump spectrophotometry revealed a basic pK_a of 10 for the Fe^{IV}–O–H of *Aae*APO-II, indicating that *Aae*APO-II is protonated under typical turnover conditions. Kinetic characterization showed that *Aae*APO-II is unusually reactive toward a panel of benzylic C–H and phenolic substrates, with second-order rate constants in the range of 10 – 10^7 M⁻¹ s⁻¹. Our results demonstrate the important role of the axial cysteine ligand in increasing the proton affinity of the Fe-oxo, *Aae*APO compound I, thus providing driving force of C–H bonds oxygenation.

6.1 Introduction

Nature has evolved varied and remarkably efficient strategies for the selective oxygenation of even the most unreactive C–H bonds in hydrocarbons and other small molecules. Copper-containing methane monooxygenases (MMO), non-heme, diiron hydroxylases such as soluble MMO, and the alkane ω -hydroxylases, AlkB, allow microorganisms to grow on petroleum and natural gas as their sole sources of carbon [1, 2]. The widely distributed heme-thiolate monooxygenases, cytochromes P450 (CYP), serve similar roles in archaea and numerous bacteria, including human pathogens such as *Mycobacterium tuberculosis* [3–5]. These processes are environmentally significant, particularly after oil spills such as the Deepwater Horizon event in 2010. P450 enzymes also comprise the primary pathways for oxidative steroid and prostaglandin biosynthesis as well as phase I drug metabolism [6].

Cytochrome P450 has been called the Rosetta Stone of iron enzymes [5]. Decades of research have created a rich tapestry that has intertwined structural, spectroscopic, mechanistic, computational, genetic, metabolic and chemical modeling approaches toward a deep understanding of such an important oxygenation system [7–10]. The central paradigm of P450 oxygen activation is now recognized to involve the formation ferryl, $\text{Fe}^{\text{IV}}=\text{O}$, intermediates. Oxoiron(IV) porphyrin cation radicals (compound I) [11–13] and oxoiron(IV) porphyrins (compound II) [14] have been observed in cytochrome P450 as well as peroxidases, chloroperoxidase (CPO), and in a variety of model systems [15–19].

Aromatic peroxygenases (APO), sometimes referred to as unspecific peroxygenases (UPO) (EC 1.11.2.1), are a newly discovered and very large superfamily of heme-thiolate proteins from fungal sources [20]. These proteins are unrelated to cytochrome P450 according to their amino acid sequences and are only distantly related to CPO, with about 30 % sequence similarity and a similar tertiary structure [21, 22]. In sharp contrast to CPO, however, APO proteins have shown high activity toward aliphatic and aromatic hydrocarbons and other organic substrates [23, 24]. These APO proteins are highly stable, heavily glycosylated, extracellular proteins that apparently serve to mobilize food sources for the growing organisms through oxidative degradation. As such they are proving to be efficient biocatalysts. Numerous drug compounds are efficiently oxidized to products that are often the same as those from mammalian CYPs [25]. These properties have also afforded a rare opportunity to study C–H bond hydroxylations in a heme protein that is not a P450, but which may function in an analogous way.

We have recently shown that the APO from *Agrocybe aegerita* (*AaeAPO*) forms an oxoiron(IV) porphyrin radical cation (*AaeAPO*-I) that can be detected by UV-vis spectroscopy [26]. This intermediate was shown to be competent to hydroxylate even strong C–H bonds at very fast rates. Further, *AaeAPO*-I reacts with chloride and bromide ions rapidly and reversibly, allowing a direct determination of the thermodynamics of oxygen transfer by *AaeAPO*-I ($E' = 1.1$ V at pH 7) [27]. Here, we report a novel method of generating *AaeAPO*-II directly from *AaeAPO*-I at different pHs. By fitting the titration curve, we are able to determine the ferryl–O–H

pK_a of 10. Also, with the well distinct spectrum discovered, series of kinetic studies were carried out towards various alkanes and phenols. This is the first time that a highly reactive enzymatic heme-thiolate compound II has been kinetically characterized.

6.2 Results and Discussion

6.2.1 Direct Reductive Generation of AaeAPO-II from AaeAPO-I with Nitroxyl Radicals

AaeAPO-II is the key intermediate in the reaction pathway for C–H hydroxylation. Since *AaeAPO-I* can be generated in good yield via *mCPBA* oxidation of the resting ferric protein [26], we sought a method to produce *AaeAPO-II* via a one-electron reduction. We considered several nitroxyl radicals as substrates to reduce *AaeAPO-I* to *AaeAPO-II* (Scheme 6.1). The one-electron oxidation of nitroxyl radicals is known to produce oxo-ammonium species and the one-electron oxidation potentials of nitroxides are in the range of 0.8–1 V [28]. As shown in Fig. 6.1, the oxidation potentials of 3-carboxy-PROXYL and 4-carboxy-TEMPO are about 0.9 V versus NHE, which are higher than our estimate for the *AaeAPO-II*/ferric *AaeAPO* couple, which is ~ 0.8 V versus NHE at pH 7 [27]. Accordingly, we anticipated that these nitroxides might be able to reduce *AaeAPO-I*

Scheme 6.1 Reaction cycle for *AaeAPO-II* generation and reduction with substrates

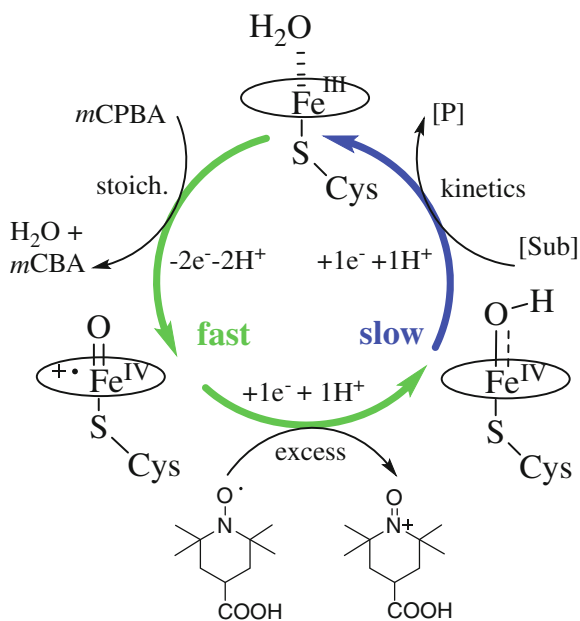
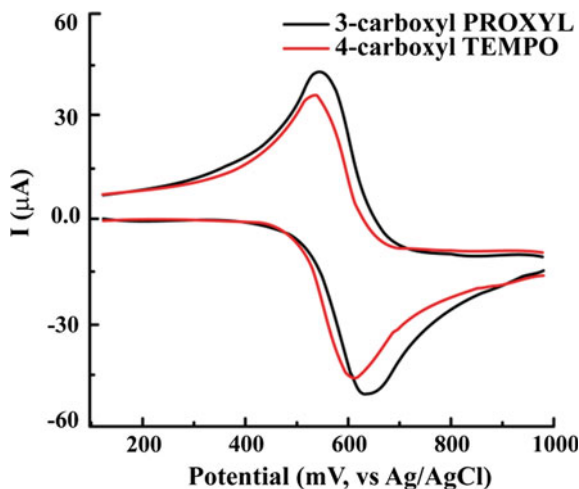


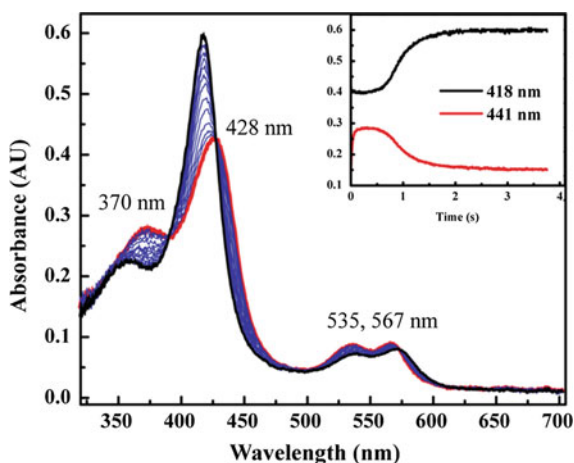
Fig. 6.1 Cyclic voltammograms of 3-carboxyl PROXYL and 4-Carboxy TEMPO at pH 7.0 100 mM KP buffer at 4 °C. E° is 593 mV for 3-carboxyl PROXYL and 572 mV for 4-carboxy TEMPO versus Ag/AgCl



readily, but might be incapable of reducing *Aae*APO-II efficiently, allowing it to accumulate. Furthermore, since cyclohexane carboxylic acid was found to be an excellent substrate for *Aae*APO [26], the similar molecular templates of TEMPO and PROXYL suggested that they would fit the relatively small active site of *Aae*APO. Lastly, in order to make the nitroxides sufficiently soluble in aqueous solution, TEMPO and PROXYL are modified with carboxylic groups.

With the use of fast-mixing UV-vis stopped-flow spectroscopy, single mixing and diode-array mode, reaction of ferric *Aae*APO (10 μ M) with *m*CPBA (50 μ M) and excess PROXYL (10 mM), a distinct UV-vis spectrum characteristic of a heme-thiolate compound II was obtained as shown in Fig. 6.2. The spectrum of *Aae*APO-II has split Soret bands at 370 and 428 nm. Two Q bands centered at 535 and 567 nm and both of them slightly blue shifted from those Q-bands of ferric

Fig. 6.2 UV-vis transients observed upon 1:1 mixing of 10 μ M of ferric enzyme with 50 μ M of *m*CPBA and 10 mM of 3-carboxy PROXYL (blanked) at pH 7.0, 4 °C. The *insert* shows the formation and decay kinetics under these conditions



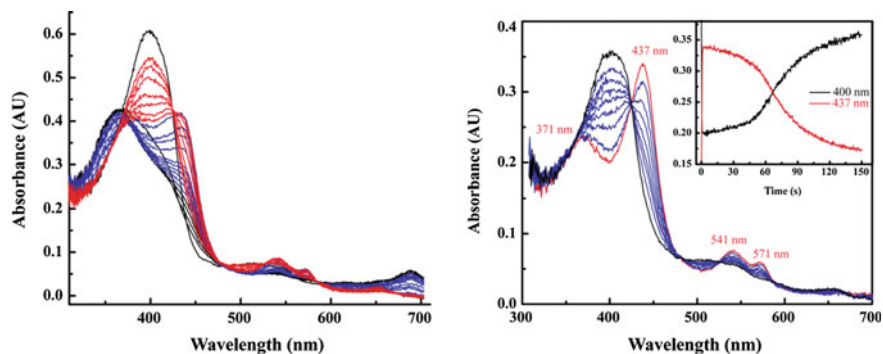


Fig. 6.3 *Left* 10 μM CPO mixed with a solution containing 20 μM of *mCPBA* and 0.5 mM of 3-carboxy PROXYL at pH 6.0. *Right* 4 μM CPO mixed with a solution containing 10 μM of *mCPBA* and 10 mM of 3-carboxy PROXYL at pH 6.0

state. Under these conditions, the accumulation of *AaeAPO-I* was not apparent, indicating that the reductive conversion of *AaeAPO-I* to *AaeAPO-II* is fast and efficient. The kinetic traces showed that *AaeAPO-II* reached its maximal amount after 0.2 s, persisted for about 0.5 s, and then decayed back to the ferric state. The accumulation of *AaeAPO-II* was optimized at pH 7.0. Two control experiments were done. Mixing the ferric enzyme with *mCPBA* without nitroxides, generated only *AaeAPO-I* and mixing the resting enzyme with nitroxides without *mCPBA* produced no spectral changes. These controls indicate that *AaeAPO-II* is generated by directly reductive conversion from *AaeAPO-I*.

In order to confirm that 4-carboxy-TEMPO or 3-carboxy PROXYL directly reduced *AaeAPO-I* to *AaeAPO-II*, we also performed the same reaction with the well-studied enzyme CPO, and compared the intermediate generated by our new method with those generated by other methods. When 4 μM CPO was mixed with 2 eq of *mCPBA* and 10 mM of 3-carboxy-PROXYL, CPO-II can be detected (371, 438, 541 and 571 nm), as shown in Fig. 6.3, and its spectrum is the same as those generated by other methods [17].

6.2.2 Determination of the Ferryl-OH pK_a in *AaeAPO-II*

Because *AaeAPO* is a highly robust, extracellular protein, its UV-vis spectra could be obtained over a wide range of pH. Under basic conditions, when the pH was above the pK_a of $\text{Fe}^{\text{IV}}\text{-OH}$, the proton is dissociated (Scheme 6.2), which leads to the change of its UV-vis spectrum. The pH effect on *AaeAPO-II* was examined with a pH-jump experiment using a double-mixing stopped-flow technique. *AaeAPO-II* was produced in the first push with *mCPBA* in the presence of 3-carboxy-PROXYL as described above using 25 mM NaP buffer at pH 7.0. After a 200 ms aging time, *AaeAPO-II* was mixed 1:1 with a 200 mM buffer solution with a pH in the range of

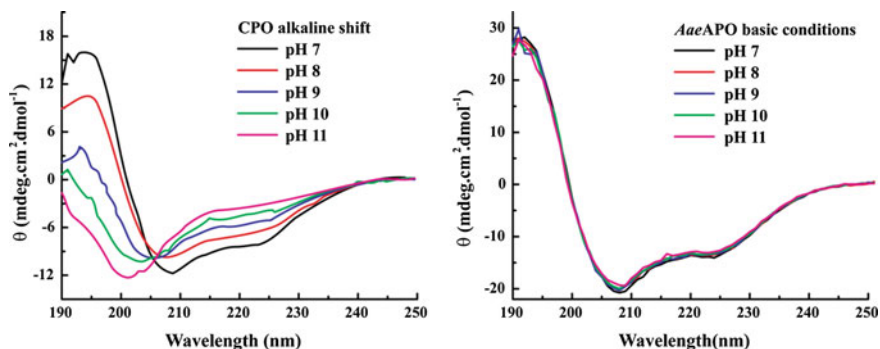
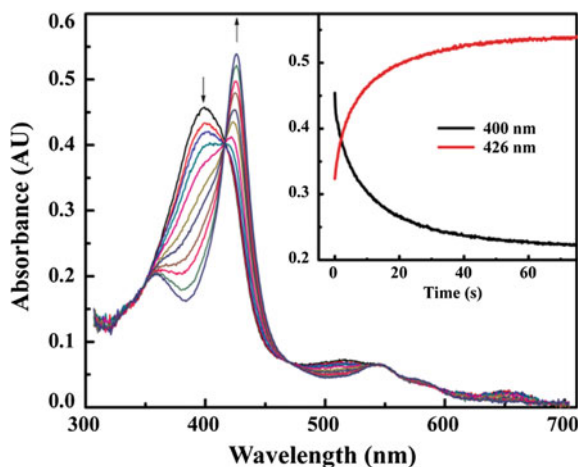
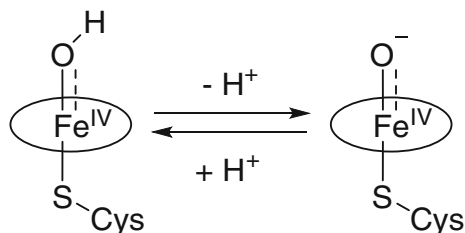


Fig. 6.4 *Left* Far-UV CD spectra of wt CPO at different pHs. *Right* Far-UV CD spectra of wt *AaeAPO* at different pHs. CD spectra were the average of three parallel experiments and taken with a 1 mm pathway cuvette, 3.1 μM of CPO and 2.1 μM of *AaeAPO* at 4 $^{\circ}\text{C}$

Fig. 6.5 UV-vis spectral change of 10 μM of ferric CPO in 10 mM pH 7 buffer upon mixing with a pH 9 200 mM strong buffered solution by stopped-flow single mixing experiments



7.0–12. More basic conditions were not used for these pH-jump experiments because ferric *AaeAPO* was found to be unstable above pH 12. As shown in Fig. 6.6 right, when ferric *AaeAPO* was mixed with buffer at pH 13, the heme started decomposition. There were no changes of ferric *AaeAPO* UV-vis spectra when pH < 13 (Fig. 6.6 left). We also did not observe far-UV CD spectral changes for ferric *AaeAPO*, as shown in Fig. 6.4 right, indicating that the secondary structure of ferric *AaeAPO* has not changed appreciably. However, unlike *AaeAPO*, far-UV CD spectra of CPO showed a dramatic changes when pH was raised from 7 to 11, as shown in Fig. 6.4 left, suggesting significant conformational changes under basic conditions. This observation is consistent with the alkaline shift observed by UV-vis stopped-flow spectroscopy when titrating ferric CPO in strong buffered solution at pH > 8, as shown in Fig. 6.5 [29].



Scheme 6.2 The equilibrium between protonated *AaeAPO-II* and deprotonated *AaeAPO-II*

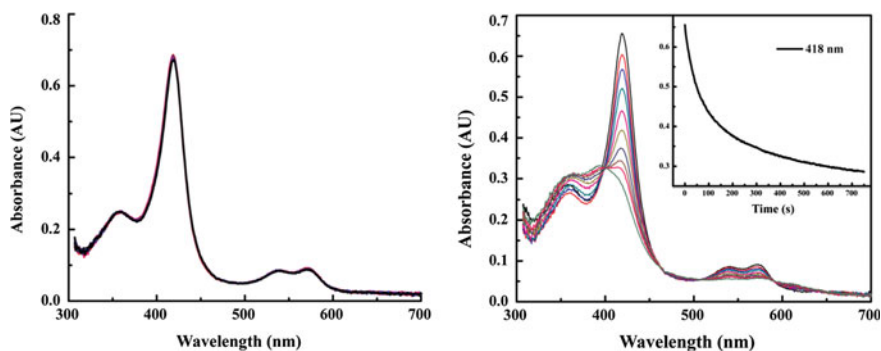


Fig. 6.6 *Left* *AaeAPO* has no UV-vis spectral change at pH 12 after 150 s mixing. *Right* The heme of ferric resting *AaeAPO* begins to bleach away at pH 13. The spectral changes were obtained by mixing ferric enzyme in 10 mM NaP buffer at pH 7.0 with 200 mM strong buffered solution at pH 13 by using UV-vis stopped-flow spectroscopy

Combining and plotting all *AaeAPO-II* spectra obtained via pH-jump to various pHs, we observed a spectral shift as shown in Fig. 6.7. The ratios of the split Soret bands (428 nm/370 nm) become smaller and both of the Q bands were slightly red shifted. More importantly, only one set of multiple isosbestic points were observed. All *AaeAPO-II* spectra have split Soret bands, suggesting the cysteine is always ligated to the heme iron. Since we have shown that *AaeAPO* does not appreciably change conformation in this pH range, and showed no heme bleaching under working conditions, we assign this spectral change to the deprotonation of Fe(IV)–O–H of *AaeAPO-II* at high pHs. The Fe^{IV} bound hydroxyl group was converted to an oxo group as shown in Scheme 6.2. Titration curves were obtained by plotting absorbance versus pHs as shown in Fig. 6.8. pK_a of 10 was determined for the hydroxyl group in *AaeAPO-II* by fitting the absorbance at 455 and 569 nm versus pHs.

The spectral kinetics of *AaeAPO-II*, characterized by monitoring the absorbance changes at 441 nm, followed a single exponential decay. It is turned out that the decay of *AaeAPO-II* is a pH depended process. The rates (k_0) become faster under

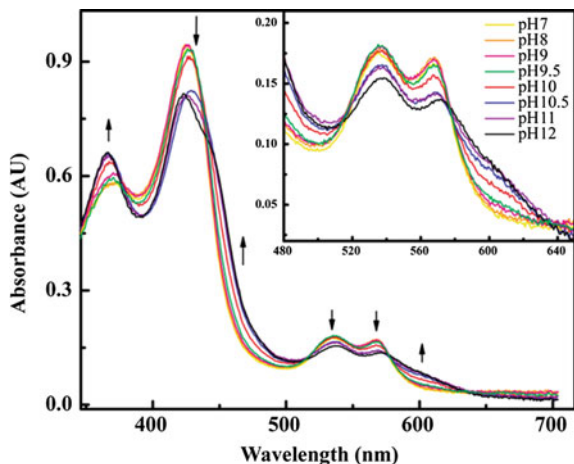
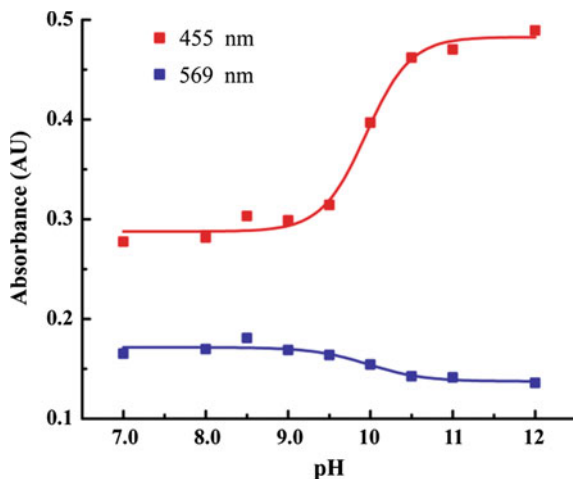


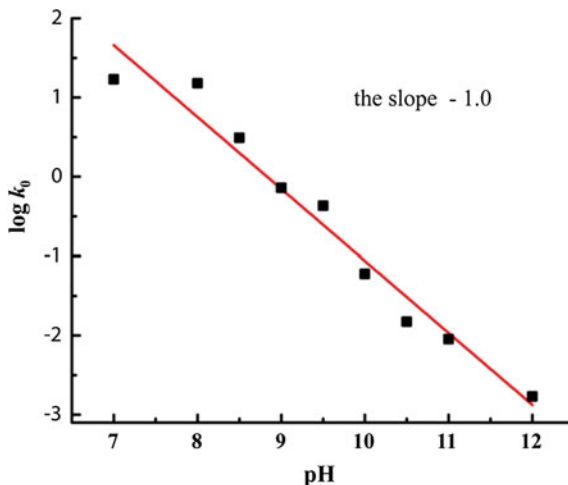
Fig. 6.7 UV-vis spectra of *AaeAPO-II* at different pHs were obtained by using double mixing stopped-flow instrument. During the first mixing, *AaeAPO-II* was generated with its highest yield after 50 ms age time by mixing 45 μM ferric *AaeAPO* in 10 mM NaP buffer at pH 7.0 with 500 μM *mCPBA* and 10 mM PROXYL radical in 50 mM NaP buffer at pH 7.0. The second mixing was a pH jump experiment. *AaeAPO-II* spectra at various pHs were generated by mixing the low buffered *AaeAPO-II* with 200 mM strong buffered solution at different pHs. At pH 7, 8 and 12 NaP buffers were used. At pH 8 and 9, Tris buffers were used. At pH 9.5, 10, 10.5 and 11, $\text{NaHCO}_3/\text{Na}_2\text{CO}_3$ buffers were used

Fig. 6.8 pH titration curves for *AaeAPO-II*. pK_a of 10.0 was obtained for the hydroxyl group in *AaeAPO-II* by fitting the absorbance at 455 and 569 nm versus pHs



low pH conditions. And a slope of -1 was obtained from the correlation of the $\log k_0$ with pH as shown in Fig. 6.9, which is consistent with the fact that the conversion from *AaeAPO-II* to ferric state is a proton coupled electron transfer process,

Fig. 6.9 A linear correlation between $\log k_0$ and pH was obtained with a slope of -1 . The kinetics was obtained by fitting the absorbance at 441 nm during the decay of *Aae*APO-II

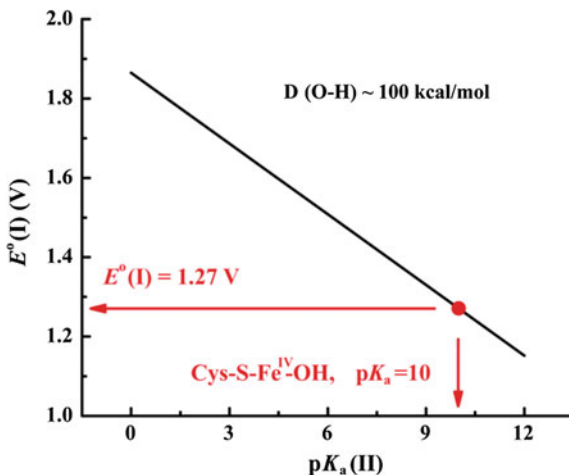


(Cys-Fe(IV)-OH \geq Cys-Fe(III)-OH₂), the higher concentration of proton in solution, the faster the conversion.

The basic pK_a might be caused by the electron donating property of the sulfur in cysteine as the axial ligand. Negative charged sulfur makes compound I have more proton affinity. So far only heme-thiolate compound II species have been discovered to have basic pK_a . Green and coworkers reported that chloroperoxidase compound II is basic at physiological conditions [16, 30]. They showed, with the use of X-ray absorption spectroscopy, that the Fe-O bond length in CPO-II is 1.82 Å, agreeing closely with the calculated value of 1.81 Å on protonated ferryl (Fe^{IV}-OH). Another study of CPO-II, from the same group, using resonance Raman spectroscopy, revealed a unique isotope [18] O-²H band at $\nu_{\text{Fe-O}} = 565 \text{ cm}^{-1}$. CPO-II is estimated to have a $pK_a \geq 8.2$ based on the fact that CPO-II has the same UV-vis spectrum from pH 3 to pH 7 [16]. HRP-II, on the other hand, has a neutral histidine ligated to the heme. Its compound II is in the ferryl-oxo form at physiological condition [16]. Resonance Raman measurements, X-ray absorption and crystallographic results suggest its ferryl $pK_a \leq 3.5$ [8, 31]. Similarly, both ferryl forms of cytochrome c peroxidase and myoglobin have $pK_a \leq 4$, according to a Badger's rule analysis of available data [31]. This $pK_a = 10$ for *Aae*APO-II is the first measured value for heme-thiolate protein. The basic pK_a suggests *Aae*APO-II is in the ferryl hydroxide form at physiological conditions. This is important because our result proves that compound II serves as the rebound intermediate in the C-H catalytic cycle. It is the Fe^{IV}-bound hydroxyl group that rebounds to the carbon radical, resulting in the alcohol products.

The basic pK_a of compound II, $pK_a(\text{II})$, also has important implications in C-H activation chemistry. It provides driving force for hydrogen atom abstraction by compound I. As shown in Eq. 6.1, $pK_a(\text{II})$ and the one electron redox potential of compound I, $E^\circ(\text{I})$, are in a close relationship with the newly formed O-H bond dissociate energy $D(\text{O-H})$ of compound II [32]. The strength of newly formed

Fig. 6.10 The relationship of ferryl pK_a and one electron redox potential of compound I according to Eq. 6.1

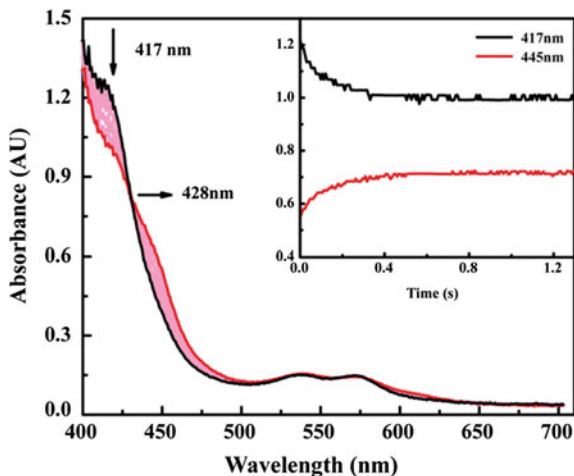


O–H bond is related to the strength of C–H bond broken. Both $pK_a(II)$ and $E^\circ(I)$ are important terms describing the C–H bond activation capability of the active species in hydroxylation reaction catalyzed by heme enzymes. With the same $E^\circ(I)$, a higher ferryl pK_a makes the $D(O-H)$ stronger. So the hydrogen atom abstraction by Fe-oxo becomes more favored ($\Delta G = D(C-H) - D(O-H)$). Also, thinking about these terms' relationship in another way, with the same $D(O-H)$, a high ferryl pK_a could lower the $E^\circ(I)$. It makes C–H bond activation happen with a reasonable redox potential, without raising the oxidative potential too high to damage the protein. If pK_a plays no role, the $E^\circ(I)$ is more than 1.8 V (Fig. 6.10). Based on our measured $pK_a(II)$ and $D(O-H) \sim 100$ kcal/mol, we are able to estimate the $E^\circ(I)$ of ~ 1.27 . Considering both of these factors, the basic pK_a in heme-thiolate protein plays a really important role in activating C–H bonds and protecting the protein scaffold.

$$D(O-H) = nFE^\circ(I) + 2.3RTpK_a(II) + 57 \pm 2 \quad (6.1)$$

Attempts to generate P450-II have been achieved by an alternative method which is mixing the native enzyme with excess peroxynitrite [33, 34]. Reported by Newcomb and coworkers, P450-II prepared by this method gives an iron-oxo bond length of 1.82 Å. But considering the fact that one of the decomposition products of peroxynitrite at neutral pH is nitrite and the result that P450-II and $Fe^{III}-NO$ have similar UV-vis spectra, P450-II generated by this way leaves open the possibility of nitrosyl complex [35]. It is interesting that the intermediate generated by mixing ferric *Aae*APO with excess peroxynitrite in basic solution showed similar isosbestic point at 428 nm as shown in Fig. 6.11. But Q bands of this new species do not have blue shifts as those of *Aae*APO-II. So, the new intermediate generated by the peroxynitrite reaction is possibly not ferryl–OH or ferryl-oxo complexes, on the other hand, it might be a nitrosyl complex which has been characterized before [35].

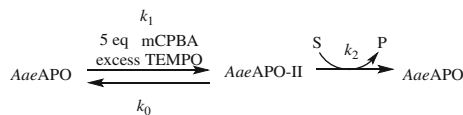
Fig. 6.11 20 μM ferric *Aae*APO mixed with a basic solution of 1 mM of peroxyxynitrite at pH 5.0



6.2.3 Kinetic Characterization of *Aae*APO-II Towards Alkanes and Phenols

The accumulation and slow decay of *Aae*APO-II at pH 7.0 made it possible to investigate its reactions with a panel of substrates. High reactivity was observed both for phenols and substrates with relatively weak, benzylic C–H bonds. Data was collected for a double-mixing, stopped-flow experiment wherein *Aae*APO-II was prepared in the first push with *m*CPBA/carboxyTEMPO as described above. Various concentrations of substrate were then added in the second push. The observed *Aae*APO-II decay rates (k_{obs}) were obtained by fitting the disappearance *Aae*APO-II at 441 nm. Plots of k_{obs} versus substrate concentrations gave linear relationships. And the second order rate constants were calculated from the slopes (Scheme 6.3).

*Aae*APO-II kinetics towards ascorbate which is a reducing reagent was characterized. As shown in Fig. 6.12 left, the disappearing of absorbance at 441 nm is an indication of the decay of *Aae*APO-II and its kinetics followed an exponential course. The pseudo-first-order rate constants for the reaction have a linear relationship with the concentration of ascorbate as shown in Fig. 6.12 right, which is characteristic of a second-order reaction. k_2 was determined from the slope to be $3.3 \times 10^4 \text{ s}^{-1} \text{ M}^{-1}$ at pH 7.0. This rate was measured to be $70 \text{ s}^{-1} \text{ M}^{-1}$ for CPO-II at



Scheme 6.3 The generation of *Aae*APO-II and its reaction with substrates

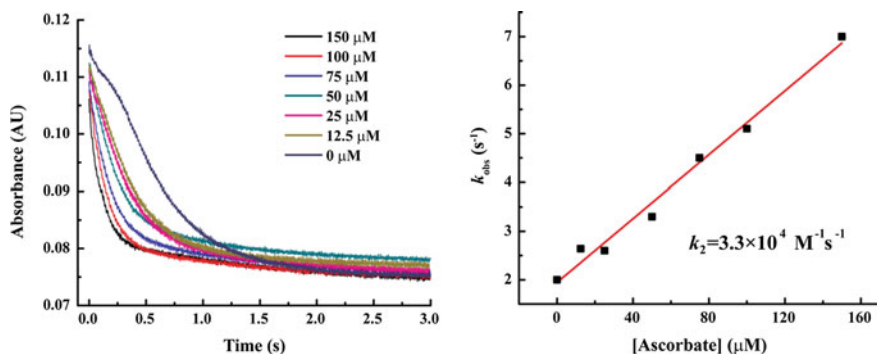


Fig. 6.12 *Left* time traces of the disappearing of *AaeAPO*-II (2.5 μM) at 441 nm reacting with different concentration of ascorbate solutions at pH 7.0, 4 °C. *Right* the plot of observed rate constants k_{obs} versus [ascorbate] resulted in a linear correlation and a second order rate constant was determined from the slope

Table 6.1 Summary of alkane substrates, equivalent C–H bonds, BDE, k_2 , k_2' and $\log k_2'$

Substrates	Equivalent C–H bonds	BDE (kcal/mol)	k_2 (M ⁻¹ s ⁻¹)	k_2' (per H) (M ⁻¹ s ⁻¹)	$\log k_2'$ (M ⁻¹ s ⁻¹)
Xanthene	2	75.5	54,000	27,000	4.4
Fluorene-4-carboxylic acid	2	80	3890	1945	3.3
<i>p</i> -isopropylbenzoic acid	1	83	150	150	2.2
<i>p</i> -ethylbenzoic acid	2	85.6	13.6	6.8	0.8

pH 5.0 and about $5 \text{ s}^{-1} \text{ M}^{-1}$ at pH 7.0 according to a published value [36]. So *AaeAPO* appears to be a better peroxidase than CPO.

Then, the reactivity of *AaeAPO*-II toward a panel of typical substrates over a wide range of C–H bond BDE (75–90 kcal/mol) were measured. The results are summarized in Table 6.1. Figure 6.13 showed an example, which is the kinetic characterization of *AaeAPO*-II reacting with different concentrations of xanthene solutions.

Apparent per-hydrogen second order rate constants, k_2' , was corrected based on the number of equivalent protons in the benzylic C–H substrates. First, it is interesting to compare the reactivity of *AaeAPO*-II with those of *AaeAPO*-I measured before. As shown in Fig. 6.14, overall, the k_2' for *AaeAPO*-II are smaller than those of *AaeAPO*-I [26]. For example, the $\log k_2'$ of *AaeAPO*-II is 5 and 3.5 orders of magnitude smaller than those of *AaeAPO*-I with the same substrates, 4-ethylbenzoic acid and 4-isopropylbenzoic acid respectively. The observed differences in reactivity indicate that *AaeAPO*-II is a much poorer oxidant than *AaeAPO*-I, consistent with our estimation on the redox potentials of these

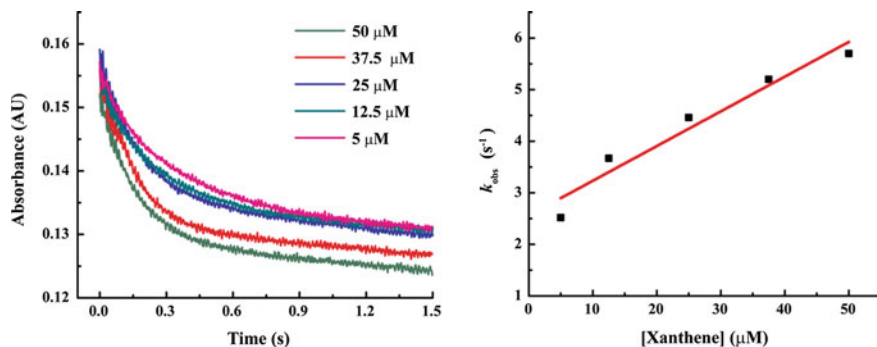
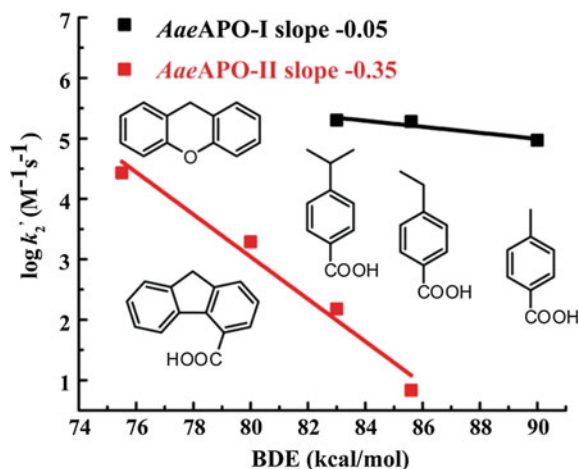


Fig. 6.13 Left time traces of the disappearing of *AaeAPO*-II (2.5 μM) at 441 nm reacting with different concentrations of xanthene at pH 7.0, 4 °C. Right correlation between observed rate constant k_{obs} versus [xanthene]

Fig. 6.14 Plot of $\log k_2'$ versus substrate C–H BDE for *AaeAPO*-II at pH 7.0 and *AaeAPO*-I at pH 5.0



intermediates, $E_{\text{cpdI}/\text{cpdII}} = 1.4$, $E_{\text{cpdII}/\text{ferric}} = 0.8$ at pH 7.0 [27]. The results also confirm that in a heme enzyme, the key intermediate activating C–H bonds is compound I and compound II serves as the rebound intermediate.

Compound II have been considered to be poor oxidants. The spectrum of P450-II are still obscure, no kinetic characterization on a reactive enzymatic heme-thiolate compound II has been reported so far towards different kinds of substrates. Limited kinetic studies were done with HRP-II [37, 38], CPO-II [36, 39] and metalloporphyrin complexes [19, 40–42]. HRP-II and CPO-II are known to be not reactive towards alkanes. CPO-II has only been reported to act as an oxidant of one-electron reducing reagents and reactive species, such as halophenols [39]. But it is also interesting to compare the reactivity of *AaeAPO*-II to some Fe^{IV}-oxo model complexes. For instance, an iron^{IV}-oxo porphyrin complex, (TPFPP)Fe^{IV}=O,

reported by Nam and coworkers, has been found to be able to catalyze alkane hydroxylation and olefin epoxidation with modest rate constants [40]. The rate constants for the reaction of xanthene and isopropylbenzoic acid with *Aae*APO-II are 200 and 1800 times faster than those for oxoFe^{IV}-4-TMPyP [43]. And the converted bimolecular rate constant for (TPFPP)Fe^{IV}=O reacting with triphenylmethane with a C–H BDE of 81 kcal/mol is only $\sim 0.85 \text{ M}^{-1}\text{s}^{-1}$ [40]. This rate is about three orders of magnitude lower than that of *Aae*APO-II reacting with 9H-fluorene-4-carboxylic acid which has C–H BDE of 80 kcal/mol. So our study is the first time showing that an enzymatic compound II was generated and demonstrated to have reactivity towards alkanes.

The correlation of $\log k_2'$ with the substrate C–H BDE showed a linear Brønsted–Evans–Polanyi relationship with a slope of -0.35 , much steeper than that of *Aae*APO-I, which is insensitive to the C–H BDE below 90 kcal/mol (Fig. 6.14). This slope is similar as *Aae*APO-I reacting with strong C–H bond substrates [26]. This suggests that *Aae*APO-II also has a nearly symmetrical transition state. Mapping the results for *Aae*APO-II with *p*-ethylbenzoic acid onto the plot correlating $\log k_{(\text{H})}$ with O–H bond strength, we estimate that the *Aae*APO Fe^{III}(H₂O) O–H BDE to be ~ 92 kcal/mol (Fig. 6.15). As we have noted, *Aae*APO Fe^{III}(OH) must also be basic since no spectral shift was observed up to pH 12 for the ferric enzyme. Thus, the fast reaction rates, and the large Fe^{III}(OH₂) BDE recapitulate situation for *Aae*APO-II.

Our result also provides evidence for one of the desaturation mechanisms related to the alkene formation from alkane catalyzed by heme enzymes (Scheme 6.4) [45].

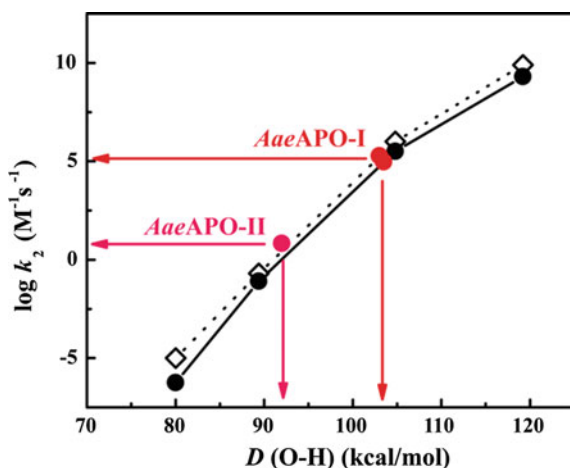
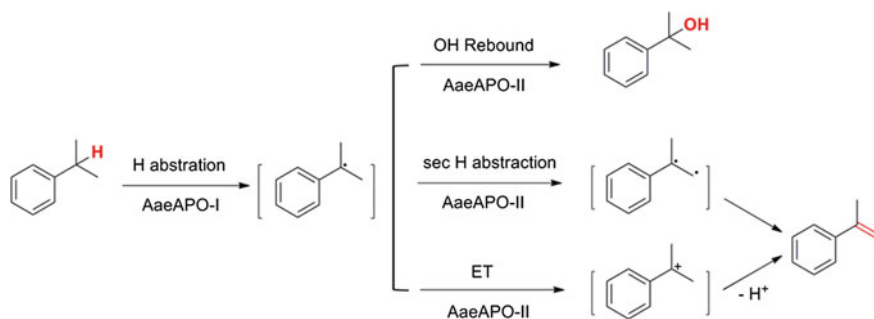


Fig. 6.15 Rate constants for the hydrogen abstraction by MnO_4^- , $\text{ROO}\cdot$, $\text{RO}\cdot$ and $\text{HO}\cdot$ versus the strength of the O–H bonds formed for toluene (solid circles) and *p*-ethylbenzene (open diamonds) [32, 44]. Plotting rate constants for hydrogen atom abstraction by *Aae*APO-I and *Aae*APO-II with *p*-toluic acid and *p*-ethylbenzoic acid on the curves gives an Fe^{IV}O–H bond strength of about 103 kcal/mol and Fe^{III}(H₂O) O–H bond strength of about 92 kcal/mol



Scheme 6.4 Possible formation pathways for desaturation products catalyzed by *AaeAPO*

It turned out that the minor products of alkane hydroxylation catalyzed by *AaeAPO* is desaturated alkene. For example, by using cumene as the substrate, about 15 % of the total products are α -methylstyrene and α -methylstyrene oxide. Our kinetics results suggest that the active *AaeAPO-II* has the capability to abstract hydrogen atom of weak C–H bond adjacent to the carbon-centered radical formed from the initial hydrogen atom abstraction by the highly reactive compound I.

Next, we expand our substrate scope to substituted phenolic compounds which are typical substrates for peroxidases. Proved by well-known mechanisms, the oxidation of phenols undertakes two consecutive one-electron steps [39]. Here, we characterized the reactivity of both *AaeAPO-I* and *AaeAPO-II* towards phenols. Data are summarized in Table 6.2. k_2 for *AaeAPO-I* were followed by the monitoring the peak at 361 nm. For *AaeAPO-II*, the wavelength at 441 nm was monitored as usual (Fig. 6.16). The kinetics were measured at pH 7.0 and all phenolic substrates chosen have $\text{p}K_a$ above 7.0 to make sure their unbound forms are all

Table 6.2 Summary of phenol substrates, sigma values, k_2 and $\log k_2$ for both *AaeAPO-I* and *AaeAPO-II*

Phenol substitutes	σ^+ [46]	<i>AaeAPO-II</i>		<i>AaeAPO-I</i>	
		pH 7		pH 7	
		k_2 ($\text{M}^{-1}\text{s}^{-1}$)	$\log k_2$ ($\text{M}^{-1}\text{s}^{-1}$)	k_2 ($\text{M}^{-1}\text{s}^{-1}$)	$\log k_2$ ($\text{M}^{-1}\text{s}^{-1}$)
4-Me	-0.26	7.7×10^7	7.9	4.8×10^7	7.7
4-Cl	0.04	6.4×10^7	7.8	4.7×10^7	7.7
H	0	5.4×10^7	7.7	3.1×10^7	7.5
4-CN	0.67	3.5×10^5	5.5	1.1×10^7	7.0
3-COOMe	0.37	7.5×10^6	6.9	2.1×10^7	7.3
3-CN	0.56	5.4×10^5	5.7	1.1×10^7	7.0
3-Me	-0.06	8.0×10^7	7.9	3.5×10^7	7.5
4-OCOMe	0.18	3.3×10^7	7.5	1.5×10^7	7.2
4-COOMe	0.49	4.2×10^6	6.6	2.4×10^7	7.4

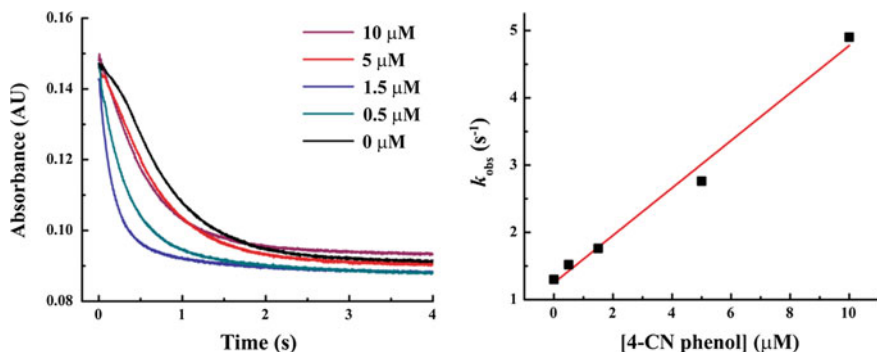
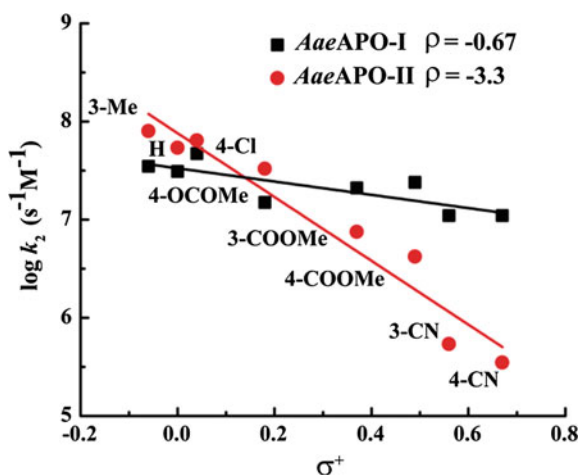


Fig. 6.16 *Left* time traces of the disappearing of *AaeAPO-II* (2.5 μM) at 441 nm reacting with different concentrations of 4-CN phenol at pH 7.0, 4 °C. *Right* observed rate constant k_{obs} at 441 nm versus [4-CN phenol] for its oxidation by *AaeAPO-II* at pH 7.0, 4 °C

Fig. 6.17 Plot of $\log k_2$ versus phenolic σ^+ for both *AaeAPO-I* ($R^2 = 0.6$) and *AaeAPO-II* ($R^2 = 0.93$) at pH 7.0

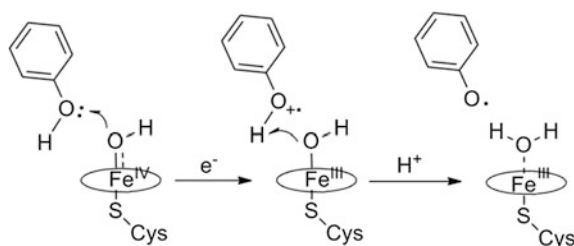


protonated. In general, the second order rate constants of *AaeAPO-I* are larger than those of *AaeAPO-II* with the same substrate.

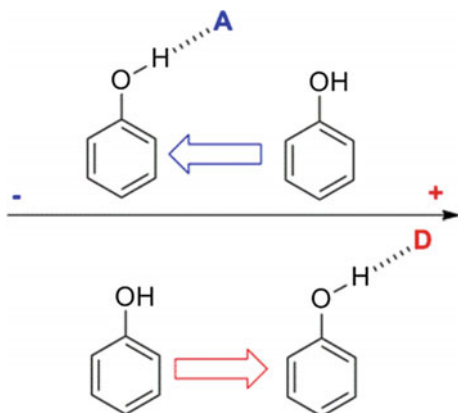
The observed rates of O–H bond scissions gave a good linear correlation with the Hammett σ^+ values for these substituted phenols [47]. Plots of $\log k_2$ versus σ^+ afforded ρ values of -0.67 and -3.3 for *AaeAPO-I* and *AaeAPO-II* respectively (Fig. 6.17). This large difference of ρ values is worth further discussion because it suggests that the degree of charge separation in transition states of the reaction is different for *AaeAPO-I* and *AaeAPO-II*. *AaeAPO-I* reacted very rapidly with the entire range of phenols with little sensitivity to either the O–H BDE or the Hammett σ^+ . The relatively small negative ρ value for *AaeAPO-I* agrees well with the mechanism of hydrogen atom abstraction [42, 48, 49] (Table 6.3). However, for *AaeAPO-II*, the negative large ρ value implies that *AaeAPO-II* is sensitive to the

Table 6.3 Previous data about phenol oxidation Hammett analysis, ρ values

Oxidants	ρ value
t BuO	-0.68 to -1.2
ROO	-0.3 to -1.5
$[\text{OFe}^{\text{IV}}\text{-4-TMPyP}]^+$	-0.1
$\text{OFe}^{\text{IV}}\text{-4-TMPyP}$	-0.6
$\text{OFe}^{\text{IV}}\text{-2-TMPyP}$	-1.1
$\text{Fe}(\text{CN})_6^{3-}$	-1.8
HRP-II	-2.7
HRP-I	Non-linear

**Scheme 6.5** Proposed mechanism of phenolic oxidation activated by *Aae*APO-II

electron deficiency on the oxygen and there is a large positive charge developed on the substrate in the transition state [50, 51]. It indicates that hydrogen abstraction by *Aae*APO-II might occur through an electrophilic mechanism (Scheme 6.5). The affinity of the second proton is not as easy at the first one by *Aae*APO-I. So the O-H bond cleavage by *Aae*APO-II possibly is initiated by transferring an electron from substrate, followed by spontaneously losing the proton (Fig. 6.18).

Fig. 6.18 Redox potential shift of phenols upon forming hydrogen bondings with surroundings

Although the measured redox potentials of phenols are similar as those of nitroxides in aqueous solution, they might be different in the protein active site because phenols might have hydrogen binds in the protein matrix. An H-bond acceptor can lower the potential of phenol a lot. Some literature shows a 0.8–1.5 V difference. That might explain the higher activity of phenol oxidations by *Aae*APO-II than those of nitroxides. Another reason might be due to the difference between PCET process and electron transfer process. For phenol oxidation, a proton is coupled to the electron transfer, so it might become much more efficient.

6.3 Conclusions

In conclusion, *Aae*APO-II was generated by using a new method from directly one electron reduction of *Aae*APO-I by nitroxides and monitored the use of fast mixing UV-vis stopped-flow spectroscopy. *Aae*APO-II spectra at basic conditions were recorded and a pK_a of 10 was able to determined from the titration curves. Kinetic characterization of *Aae*APO-II showed that it has reactivity toward C–H bond substrates, representing the first example of the C–H activation by an enzymatic compound II intermediate. The reactivity gap between *Aae*APO-II, CPO-II and HRP-II or some porphyrin Fe^{IV} -oxo complexes might arise from the difference of their heme distal ligands. Furthermore, the Hammett analysis on the phenol oxidation rates demonstrates that *Aae*APO-II is sensitive to electron deficiency and there might be a large positive charge development in the transition state of phenol oxidation catalyzed by *Aae*APO-II. Our intriguing results are helpful for the understanding on the rebound mechanism by heme-thiolate enzymes. It also sets the stage for the further investigation on this important intermediate and design new biocatalysts.

6.4 Experimental

Reagents: wild-type peroxygenase from *A. aegerita* (isoform II, pI 5.6, 46 kDa) was produced in bioreactors with a soybean-flour suspension as growth substrate, and purified as described previously [20]. The enzyme preparation was homogeneous by SDS-PAGE, and exhibited an $A_{418\text{ nm}}/A_{280\text{ nm}}$ ratio of 1.7. The specific activity of the peroxygenase was 59 U mg^{-1} , where 1 U represents the oxidation of 1 μmol of 3,4-dimethoxybenzyl alcohol to 3,4-dimethoxybenzaldehyde in 1 min at RT. Chloroperoxidase was purchased from Bio-Research Products, Inc. with RZ of $A_{400\text{ nm}}/A_{280\text{ nm}} > 1.3$, $1,296\text{ U mg}^{-1}$, where 1 unit represents the amount of CPO catalyzing the formation of 1 μmol of dichlorodimedone from monochlorodimedone in 1 min at 25 °C, pH 2.75, 0.02 M KCl, 2 mM H_2O_2 . All chemicals were of the best available purity from Aldrich. For chemicals with purity lower than 99 %, recrystallization were done with a proper solvent. 4-Acetoxyphenol was prepared by

reacting hydroquinone (4 g, 36 mmol) in pyridine (40 ml) with acetic anhydride (5.6 g, 55 mmol) under reflux overnight [52]. Pyridine was removed under vacuum and then product was further purified by column (EtOAc/hexane = 9:1). 4-Acetoxyphenol was obtained after recrystallization from ether.

Instruments: UV/Vis spectral measurements were performed on a Hewlett-Packard 8453 diode-array spectrophotometer at room temperature. Stopped-flow experiments were carried out on a Hi-Tech SF-61 DX2 double-mixing instrument with a 1 cm path length equipped with an ISOTEMP 3013 D thermostat bath. All concentrations reported are the final concentrations. All kinetics experiments were carried out at 4 °C. The data were analyzed using Kinetic Studio from Hi-Tech. CV was done with KP buffer 100 mM, Pt electrode, Ag/AgCl KCl 3 M as reference with a sweep rate of 0.1 V s⁻¹. $E^{\circ} = (E_{pc} + E_{pa})/2$. ¹HNMR spectra were recorded on a 500 MHz Bruker Avance II spectrometer. CD spectra were recorded using a circular dichroism spectrometer. The molar ellipticity, $[\theta]$ (mdeg cm² dmol⁻¹) is expressed. Cuvette with path length of 1 mm was used to measure far-UV (190–250 nm) CD spectra. GC-MS analyses were run using an Agilent 7890A GC coupled to a 5975 Inert MSD with a Rtx-5Sil MS column.

References

1. Austin, R.N., Groves, J.T.: Alkane-oxidizing metalloenzymes in the carbon cycle. *Metalomics* **3**, 775–787 (2011)
2. Lewis, J.C., Coelho, P.S., Arnold, F.H.: Enzymatic functionalization of carbon-hydrogen bonds. *Chem. Soc. Rev.* **40**, 2003–2021 (2011)
3. Groves, J.T.: High-valent iron in chemical and biological oxidations. *J. Inorg. Biochem.* **100**, 434–447 (2006)
4. Ortiz de Montellano, P.R.: Hydrocarbon hydroxylation by cytochrome P450 enzymes. *Chem. Rev.* **110**, 932–948 (2010)
5. Groves, J.T.: Models and Mechanisms of Cytochrome P-450 Action Chap. 1 in, 3e, pp. 1–44. Kluwer Academic/Plenum Publishers, New York (2004). In: Ortiz de Montellano, P.R. (ed.) *Cytochrome P450: Structure, Mechanism, and Biochemistry*, 3 edn, pp. 1–44. Kluwer Academic/Plenum, New York (2005)
6. Guengerich, F.P.: Cytochrome P450: what have we learned and what are the future issues? *Durg Metab. Rev.* **36**, 159–197 (2004)
7. Luthra, A., Denisov, I.G., Sligar, S.G.: Spectroscopic features of cytochrome P450 reaction intermediates. *Arch. Biochem. Biophys.* **507**, 26–35 (2011)
8. Green, M.T.: C{single bond}H bond activation in heme proteins: the role of thiolate ligation in cytochrome P450. *Curr. Op. Chem. Biol.* **13**, 84–88 (2009)
9. Hrycay, E.G., Bandiera, S.M.: The monooxygenase, peroxidase, and peroxygenase properties of cytochrome P450. *Arch. Biochem. Biophys.* **522**, 71–89 (2012)
10. Shaik, S., Lai, W., Chen, H., Wang, Y.: The valence bond way: reactivity patterns of cytochrome P450 enzymes and synthetic analogs. *Acc. Chem. Res.* **43**, 1154–1165 (2010)
11. Jung, C., Vries, S.D., Schünemann, V.: Spectroscopic characterization of cytochrome P450 Compound I. *Arch. Biochem. Biophys.* **507**, 44–55 (2011)
12. Jung, C.: The mystery of cytochrome P450 compound I: a mini-review dedicated to Klaus Ruckpaul. *BBA-Proteins Proteom.* **1814**, 46–57 (2011)

13. Rittle, J., Green, M.T.: Cytochrome P450 compound I: capture, characterization, and C-H bond activation kinetics. *Science* **330**, 933–937 (2010)
14. Behan, R.K., Hoffart, L.M., Stone, K.L., Krebs, C., Green, M.T.: Evidence for basic ferryls in cytochromes P450. *J. Am. Chem. Soc.* **128**, 11471–11474 (2006)
15. Stone, K.L., Behan, R.K., Green, M.T.: X-ray absorption spectroscopy of chloroperoxidase compound I: insight into the reactive intermediate of P450 chemistry. *Proc. Natl. Acad. Sci. U. S.A.* **102**, 16563–16565 (2005)
16. Green, M.T., Dawson, J.H., Gray, H.B.: Oxoiron(IV) in chloroperoxidase compound II is basic: implications for P450 chemistry. *Science* **304**, 1653–1656 (2004)
17. Egawa, T., Proshlyakov, D.A., Miki, H., Makino, R., Ogura, T., Kitagawa, T., Ishimura, Y.: Effects of a thiolate axial ligand on the $\pi \rightarrow \pi^*$ electronic states of oxoferryl porphyrins: a study of the optical and resonance Raman spectra of compounds I and II of chloroperoxidase. *J. Biol. Inorg. Chem.* **6**, 46–54 (2001)
18. Bell, S.R., Groves, J.T.: A highly reactive P450 model compound I. *J. Am. Chem. Soc.* **131**, 9640–9641 (2009)
19. Groves, J.T., Gross, Z., Stern, M.K.: Preparation and reactivity of oxoiron(IV) porphyrins. *Inorg. Chem.* **33**, 5065–5072 (1994)
20. Ullrich, R., Nüske, J., Scheibner, K., Spantzel, J., Hofrichter, M.: Novel haloperoxidase from the agaric basidiomycete *Agrocybe aegerita* oxidizes aryl alcohols and aldehydes. *Appl. Environ. Microb.* **70**, 4575–4581 (2004)
21. Piontek, K., Ullrich, R., Liers, C., Diederichs, K., Plattner, D.A., Hofrichter, M.: Crystallization of a 45 kDa peroxygenase/peroxidase from the mushroom *Agrocybe aegerita* and structure determination by SAD utilizing only the haem iron. *Acta Crystallogr. F* **66**, 693–698 (2010)
22. Pecyna, M.J., Ullrich, R., Bittner, B., Clemens, A., Scheibner, K., Schubert, R., Hofrichter, M.: Molecular characterization of aromatic peroxygenase from *Agrocybe aegerita*. *Appl. Microbiol. Biotech.* **84**, 885–897 (2009)
23. Peter, S., Kinne, M., Wang, X., Ullrich, R., Kayser, G., Groves, J.T., Hofrichter, M.: Selective hydroxylation of alkanes by an extracellular fungal peroxygenase. *FEBS J.* **278**, 3667–3675 (2011)
24. Hofrichter, M., Ullrich, R., Pecyna, M.J., Liers, C., Lundell, T.: New and classic families of secreted fungal heme peroxidases. *Appl. Microbiol. Biotechn.* **87**, 871–897 (2010)
25. Poraj-Kobielska, M., Kinne, M., Ullrich, R., Scheibner, K., Kayser, G., Hammel, K.E., Hofrichter, M.: Preparation of human drug metabolites using fungal peroxygenases. *Biochem. Pharmacol.* **82**, 789–796 (2011)
26. Wang, X., Peter, S., Kinne, M., Hofrichter, M., Groves, J.T.: Detection and kinetic characterization of a highly reactive heme-thiolate peroxygenase compound I. *J. Am. Chem. Soc.* **134**, 12897–12900 (2012)
27. Wang, X., Peter, S., Ullrich, R., Hofrichter, M., Groves, J.T.: Driving force for oxygen-atom transfer by heme-thiolate enzymes. *Angew. Chem. Int. Ed.* (2013)
28. Blinco, J.P., Hodgson, J.L., Morrow, B.J., Walker, J.R., Will, G.D., Coote, M.L., Bottle, S.E.: Experimental and theoretical studies of the redox potentials of cyclic nitroxides. *J. Org. Chem.* **73**, 6763–6771 (2008)
29. Lambeir, A.M., Dunford, H.B.: A kinetic and spectral study of the alkaline transitions of chloroperoxidase. *Arch. Biochem. Biophys.* **220**, 549–556 (1983)
30. Stone, K.L., Behan, R.K., Green, M.T.: Resonance Raman spectroscopy of chloroperoxidase compound II provides direct evidence for the existence of an iron(IV)-hydroxide. *Proc. Natl. Acad. Sci. U.S.A.* **103**, 12307–12310 (2006)
31. Green, M.T.: Application of Badger's rule to heme and non-heme iron-oxygen bonds: an examination of ferryl protonation states. *J. Am. Chem. Soc.* **128**, 1902–1906 (2006)
32. Mayer, J.M.: Hydrogen atom abstraction by metal-oxo complexes: understanding the analogy with organic radical reactions. *Acc. Chem. Res.* **31**, 441–450 (1998)

33. Newcomb, M., Halgrimson, J.A., Horner, J.H., Wasinger, E.C., Chen, L.X., Sligar, S.G.: X-ray absorption spectroscopic characterization of a cytochrome P450 compound II derivative. *Proc. Natl. Acad. Sci. U.S.A.* **105**, 8179–8184 (2008)
34. Yuan, X., Sheng, X., Horner, J.H., Bennett, B., Fung, L.W.M., Newcomb, M.: Low temperature photo-oxidation of chloroperoxidase compound II. *J. Inorg. Biochem.* **104**, 1156–1163 (2010)
35. Behan, R.K., Hoffart, L.M., Stone, K.L., Krebs, C., Green, M.T.: Reaction of cytochrome P450(BM3) and peroxyxynitrite yields nitrosyl complex. *J. Am. Chem. Soc.* **129**, 5855–5859 (2007)
36. Lambeir, A.M., Dunford, H.B., Pickard, M.A.: Kinetics of the oxidation of ascorbic acid, ferrocyanide and p-phenolsulfonic acid by chloroperoxidase compounds I and II. *Eur. J. Biochem.* **163**, 123–127 (1987)
37. Sakurada, J., Sekiguchi, R., Sato, K., Hosoya, T.: Kinetic and molecular orbital studies on the rate of oxidation of monosubstituted phenols and anilines by horseradish peroxidase compound II. *Biochemistry* **29**, 4093–4098 (1990)
38. Dunford, H.B., Adeniran, A.J.: Hammett ρ correlation for reactions of horseradish peroxidase compound II with phenols. *Arch. Biochem. Biophys.* **251**, 536–542 (1986)
39. Osborne, R.L., Coggins, M.K., Turner, J., Dawson, J.H.: *Caldariomyces fumago* chloroperoxidase catalyzes the oxidative dehalogenation of chlorophenols by a mechanism involving two one-electron steps. *J. Am. Chem. Soc.* **129**, 14838–14839 (2007)
40. Nam, W., Park, S.E., Lim, I.K., Lim, M.H., Hong, J., Kim, J.: First direct evidence for stereospecific olefin epoxidation and alkane hydroxylation by an oxoiron(IV) porphyrin complex. *J. Am. Chem. Soc.* **125**, 14674–14675 (2003)
41. Pan, Z., Newcomb, M.: Kinetics and mechanism of oxidation reactions of porphyrin-iron(IV)-oxo intermediates. *Inorg. Chem.* **46**, 6767–6774 (2007)
42. Colclough, N., Lindsay Smith, J.R.: A mechanistic study of the oxidation of phenols in aqueous solution by oxoiron(IV) tetra(N-methylpyridyl)porphyrins. A model for horseradish peroxidase compound II? *J. Chem. Soc. Perkin Trans.* **2**, 1139–1149 (1994)
43. Bell, S.R.: *Modelling Heme Monooxygenases with Water-Soluble Iron Porphyrins*. Princeton University (2010)
44. Gardner, K.A., Kuehnert, L.L., Mayer, J.M.: Hydrogen atom abstraction by permanganate: oxidations of arylalkanes in organic solvents. *Inorg. Chem.* **36**, 2069–2078 (1997)
45. Whitehouse, C.J.C., Bell, S.G., Wong, L.-L.: Desaturation of alkylbenzenes by cytochrome P450BM3 (CYP102A1). *Chem. Eur. J.* **14**, 10905–10908 (2008)
46. Dust, J.M., Arnold, D.R.: Substituent effects on benzyl radical ESR hyperfine coupling constants. The $\sigma\alpha$ scale based upon spin delocalization. *J. Am. Chem. Soc.* **105**, 1221–1227 (1983)
47. Krygowski, T.M., Stępień, B.T.: Sigma- and Pi-electron delocalization: focus on substituent effects. *Chem. Rev.* **105**, 3482–3512 (2005)
48. Das, P.K., Encinas, M.V., Steenken, S., Scaiano, J.C.: Reaction of tert-butoxy radicals with phenols. Comparison with the reactions of carbonyl triplets. *J. Am. Chem. Soc.* **103**, 4162–4166 (1981)
49. Howard, J.A., Ingold, K.U., Symonds, M.: Absolute rate constants for hydrocarbon oxidation 8. Reactions of cumylperoxy radicals. *Can. J. Chem.* **46**, 1017–000 (1968)
50. Nahor, G.S., Neta, P., Alfassi, Z.B.: Perfluorobutylperoxyl radical as an oxidant in various solvents. *J. Phys. Chem.* **95**, 4419–4422 (1991)
51. Powell, M.F., Wu, J.C., Bruce, T.C.: Ferricyanide oxidation of dihydropyridines and analogs. *J. Am. Chem. Soc.* **106**, 3850–3856 (1984)
52. Sapkota, K., Roh, E., Lee, E., Ha, E.M., Yang, J.H., Lee, E.S., Kwon, Y., Kim, Y., Na, Y.: Synthesis and anti-melanogenic activity of hydroxyphenyl benzyl ether analogues. *Bioorg. Med. Chem.* **19**, 2168–2175 (2011)

Chapter 7

Cloning and Expression of *Aae*APO from *Agrocybe aegerita* to *E. coli*, for Studies of Structure-Function Relationships by Site-Specific Mutagenesis



Abstract So far, much has been learned from the functional and mechanistic investigation on *Aae*APO. However, one of the major limitations of *Aae*APO investigation comes from the slow growth of *Agrocybe aegerita* and the low yield of protein production. Cloning *Aae*APO from its original host to *E. coli*, *Saccharomyces cerevisiae* or *Aspergillus niger* might be a way to produce the protein in large amounts within a short time and to perform mutations. In this chapter, we first address the successful purification of wild type *Aae*APO from *Agrocybe aegerita*. Next, results on the isolation of *apo* mRNA, RT-PCR obtaining the *apo* cDNA, cloning and expression *Aae*APO in *E. coli* will be reported. However, the recombinant protein from *E. coli* forms inclusion bodies thus has no activity. Last, several future experiments on protein reconstitution with heme and the expression of *Aae*APO in fungus strains will be discussed.

7.1 Results and Discussions

7.1.1 Purification of Wild Type *AaeAPO* from *Agrocybe aegerita*

The heme-thiolate enzyme *AaeAPO* in the wood and litter dwelling black poplar mushroom *A. aegerita* was identified very recently as a special peroxxygenase catalyzing two electron oxidations with H_2O_2 as the terminal oxidant [1]. They are highly stable and glycosylated. The typical culture of *A. aegerita* is in a bioreactor with soybean meal as liquid growth medium. It can be cultured in a flask on a shaker as well. In our lab, in a typical 1 L soybean meal and peptone liquid culture, the production of *AaeAPO* starts after about 1 month growth at room temperature. The oxidation activity of *AaeAPO* towards veratryl alcohol kept increasing as well as the pH of the medium (Fig. 7.1). When the pH reached about 9.0, the activity also reached its maximal, indicating the course of fermentation. However, the total activity is much less than cultures in a bioreactor. When the production of *AaeAPO* reached its maximal, we began to harvest the protein secreted in the cell culture medium.

The same purification procedure was followed as before [1]. After filtering the cells, the filtrate was frozen at $-20\text{ }^\circ\text{C}$. Polysaccharides were precipitated and filtered off. Then, the filtrate was concentrated by a stirred-cell ultra-filtration through a 10 kDa membrane and dialyzed against 10 mM NaP buffer at pH 6.6. Three steps of chromatography were used to purify the protein. The dialyzed medium was first subjected to a Sepharose Q FF column (20 cm length, 2 cm diameter) with 10 mM NaP buffer at pH 6.6. Fractions with activity were all

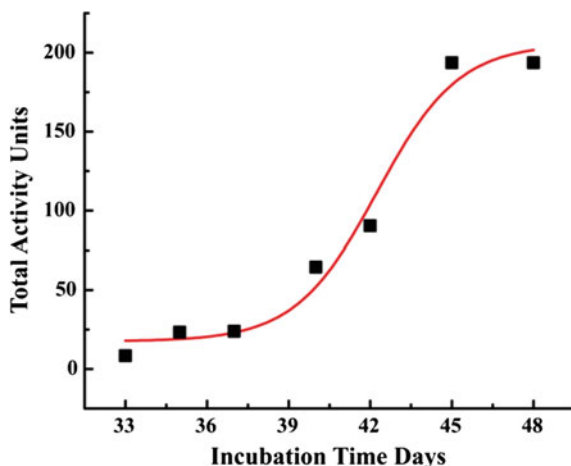
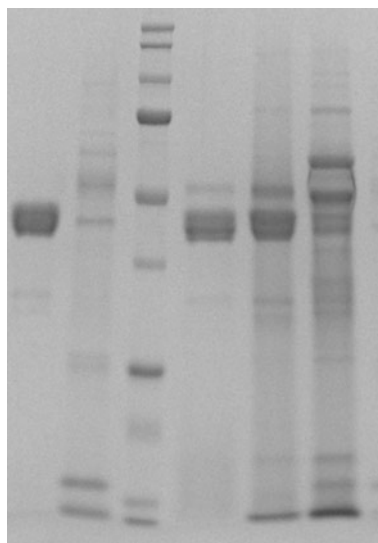


Fig. 7.1 The production of wild type *AaeAPO* over time in 1 L medium in a shaker. The activity was measured by determining the oxidation of veratryl alcohol into veratraldehyde with 1 mM of H_2O_2 at pH 7.0 and calculated as unit which is the micromoles of product formed per minute or micromoles of substrate converted per minute

Fig. 7.2 SDS-PAGE of purified *AaeAPO* from each step: from *left to right* the lanes are the purified protein by collaborators at Germany, the thawed medium after ultrafiltration, the protein marker, the protein after the third size exclusive column, the protein after the second Q Sepharose column and the protein after the first SP Sepharose separation



collected, combined and dialyzed against 10 mM acetate buffer at pH 4.0. The dialyze then ran through a Sepharose SP FF column (5 ml). Fractions with activity were collected, combined and concentrated. The final sample was separated with a Sephadex 75G column (20 cm length, 1 cm diameter). Fractions were analyzed by SDS-PAGE. Figure 7.2 is the result after each step of purification. The purified protein has a molecular weight of 46 kDa which is consistent with previous data. The final yield of *AaeAPO* is about 1 mg per liter with a R_z (420/280) of 0.8, about 10 % of total activity before purification. The yield is much lower than those cultured in a bioreactor with a moderate amount of 5–10 mg/L [2]. Figure 7.3 is an IEF gel of purified *AaeAPO* with two isoelectric points at about 4.4 and 4.9. The difference in PIs is possibly caused by different glycosylation percentages of the same protein. Then, the protein band on the SDS-PAGE gel at 46 kDa was cut and digested with trypsin for MS/MS analysis. The sequencing result indicates a match with wild type *AaeAPO* with a coverage of 64 % as shown in Fig. 7.4. UV-vis spectra of purified *AaeAPO* is shown in Fig. 7.5.

7.1.2 Construction Plasmids Containing apo Gene for the Over-Expression of *AaeAPO* in *E. coli*

Because of the limitation of slow growth and low yield of production, we are thinking of cloning *AaeAPO* in different organisms. The development of a heterologous expression system for *AaeAPO* could also provide a chance for studies on structure-function relationships with site-specific mutagenesis and protein engineering. A similar strategy has been done with CPO and many cytochrome

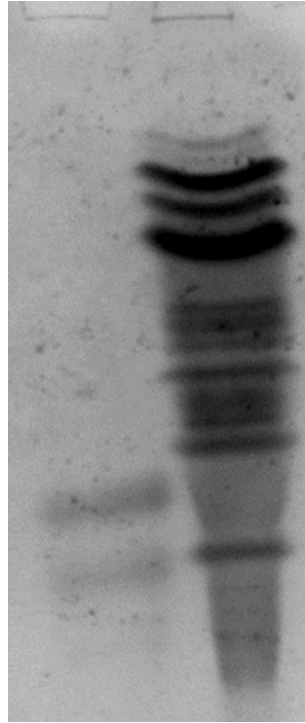


Fig. 7.3 IEF gel of purified *AaeAPO* in left lane with two pI at about 4.4 and 4.9

```

1 mkyfplfptl vfaarvvafp ayaslaglsq qeldaiiptl earepglppg
51 plenssaklv ndeahpwkpl rpgdirgpcp glntlashgy lprngvatpv
101 qiinavqegl nfdnqaavfa tyaaahlvdgn litdllsigr ktrltgpdpp
151 ppasvgglne hgtfegdasm trgdaffgn hdfnetlfeq lvdysnrfgg
201 gkynltvage lrfkriqdsi atnpnfsfvd frfftayget tfpanlfvdg
251 rrddgqldmd aarsffqfsr mpddffraps prsgtgvevv iqahpmqpgr
301 nvgkinsytv dptssdfstp clmyekfvni tvkslypnpt vqlrkalntn
351 ldfffqgvaa gctqvfpygr d
  
```

Fig. 7.4 Mascot search result of the sequence match between purified *AaeAPO* and *AaeAPO* in database with an accession number of B9W4V6. The signal peptide is colored in grey. The matched peptides are shown in red (color online)

P450 enzymes [3, 4]. Here, we first describe the construction of plasmids containing *apo* gene. Next, we report trials of *AaeAPO* expression in *E. coli*.

The sequence of *AaeAPO* has been identified [5]. It shows no homology to classic peroxidases, cytochrome P450s and only 30 % homology to CPO from *Caldariomyces fumago* [5]. The cDNA sequence of *apo* has also been identified. So we designed gene specific primers for *apo* cDNA with restriction sites at the ends for ligation (Fig. 7.6). *A. aegerita* is an eukaryotic organism, its gene contains

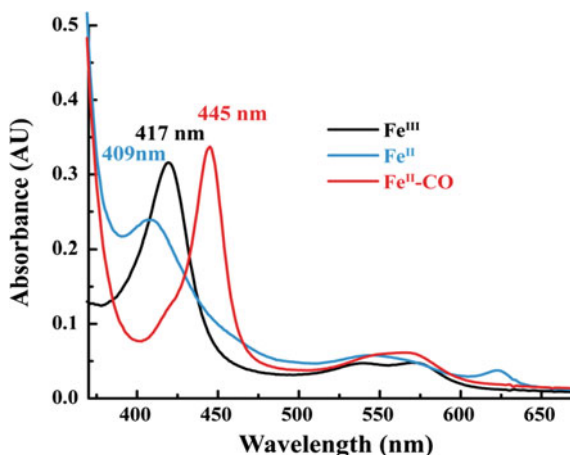


Fig. 7.5 UV-vis spectra *AaeAPO* under different conditions. *Black trace* is ferric *AaeAPO* at pH 7.0. *Blue trace* is ferrous *AaeAPO* reduced by $\text{Na}_2\text{S}_2\text{O}_4$ at pH 7.0. *Red trace* is reduced *AaeAPO* bound with CO (color online)

Forward: GGCGGAATTCACATGAAATATTTCCCC
 Reverse: GCGCGGATCCATCATTAAATCTCGCCCGTA

Fig. 7.6 Primers used for RT-PCR and ligation. *Purple* is *EcoRI*. *Green* is *BamHI*. *Red* is that start codon and the two *blue* codons are stop codons (color online)

introns. RNA splicing removes introns and joins exons. In order to obtain the *apo* cDNA, a reverse transcription from *apo* mRNA to cDNA is a necessary step. This is done by isolation of total mRNA, RT-PCR and amplified with specific primers. The ligation of *apo* cDNA with a pUC19 vector at the sites of *BamHI* and *EcoRI* was successful as shown in Fig. 7.7. Then, the resulting plasmid is used to construct *apo* expression plasmids.

A common vector for recombinant P450 expression in *E. coli* is pCWori. It contains two consecutive *tac* promoter cassettes upstream of a *Nde I* cloning site coincident with a ATG start codon. It also contains a strong *trpA* transcription terminator sequence, a phage M13 origin of DNA replication and *lacI^q* gene encoding the Lac repressor [4]. We designed primers with restriction enzyme sites of *Nde I* and *Xba I* and successfully ligate *apo* cDNA into this pCWori vector (Fig. 7.8). One important step that has to be done is to silence the *Nde I* site in the sequence of *apo* cDNA by site-specific mutagenesis of pUC19_apo. After the ligation, the *Nde I* site was recovered. Primers used for site-specific mutagenesis and ligation with pCWori are summarized in Table 7.1.

DH5 α is the common competent cell for pCWori vectors. Cells containing pCWori_apo plasmid were grown in TB broth and recombinant *AaeAPO* expression was attempted to express with IPTG initiation and δ -ALA (δ -aminolevulinic acid) supply. However, the cell pellets were not red, which indicated that holo-*AaeAPO* was not produced.

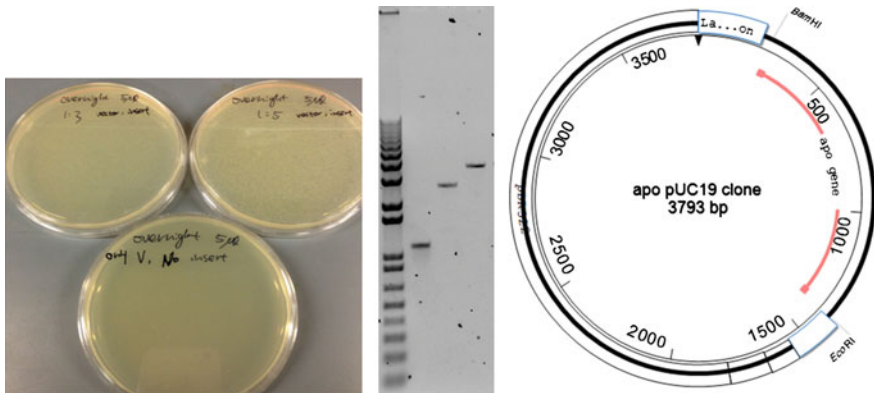


Fig. 7.7 The ligation of *apo* cDNA with double digested pUC19 vector. *Left* ligation experiment showed lots of colonies growing when inserts are provided but no colonies growing in the controls. *Middle* 2nd lane is *apo* cDNA, 3rd lane is empty pUC19 digested with *EcoRI*, 3rd lane is pUC19_*apo* digested with *EcoRI*. *Right* a map showing *apo* gene is inserted into pUC19

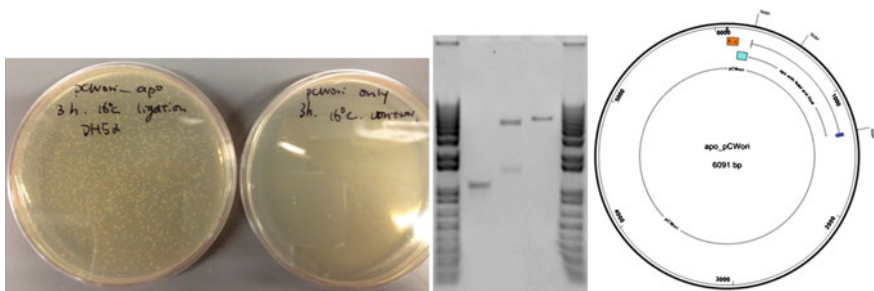


Fig. 7.8 The ligation of *apo* cDNA with double digested pCWori vector. *Left* ligation experiment showed lots of colonies growing when inserts are provided but no colonies in the controls. *Middle* 2nd lane is *apo* cDNA, 3rd lane is *Nde I* and *Xba I* double digested pCWori_CYP101, 3rd lane is pCWori_*apo* digested with both *Acc65 I*. *Right* a sequence map of the expression plasmid pCWori_*apo*

In order to make recombinant *AaeAPO* fold correctly, we thought to express the protein in *E. coli*'s periplasmic space which provides a more oxidative environment than that of the cytoplasmic space. By mimicking the fungal extra cellular environment, this strategy might assist the disulfide bond formation, thus helping the protein fold correctly and incorporating the heme. Signal peptides could be used to direct the protein expressing into the desired final locations [6]. Outer membrane protein A (OmpA) is a major outer membrane protein of *E. coli* [7]. Its signal peptide has been used to direct recombinant proteins to periplasmic space before [3]. So, we inserted the OmpA signal peptide before the *AaeAPO* peptide sequence in the new construct. The *apo* gene was also optimized to eliminate rare codons in order to increase the efficiency of translational performance. Finally, *Xho I* and *Nde I* restriction sites were used to ligate the optimized OmpA_*apo* into a pET21b vector.

Table 7.1 Primers used for pCWori and apo cDNA ligation

Primers	Forward primers	Reverse primers
Silence <i>Nde</i> I	CGCAGTCTTCGGCCACATTTGGCGGCCA	TGGGCCGCAAAATGTGGCGAATACTGCG
Recover <i>Nde</i> I	CGCAGTCTTCGGCCACATATGCGGCCA	TGGGCCGCATATGTGGCGAAAGACTGCG
<i>apo</i> cDNA amplification with <i>Nde</i> I and <i>Xba</i> I	GCGCCATATGAAAATATTTTCCCCCTGTTCCCA	GCGCTCTAGATCATTAAATCTCGCCCCGTATGGGAA

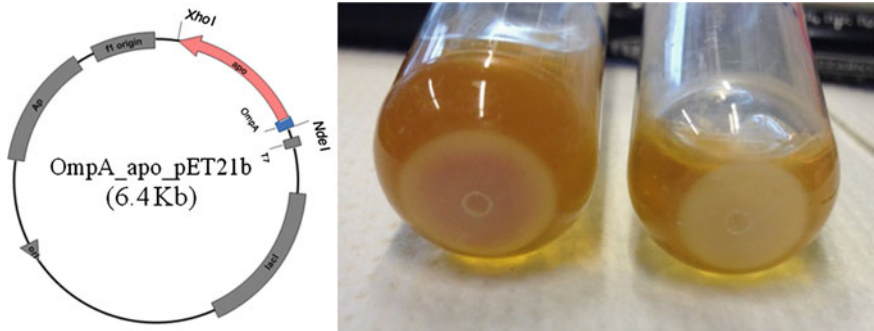
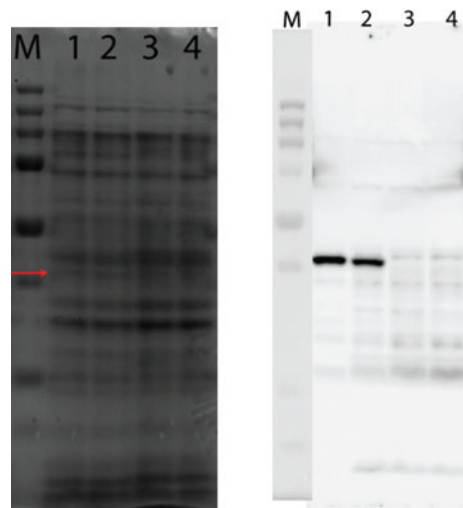


Fig. 7.9 *Left* the plasmid map of OmpA_apo_pET21b. *Right* BL21 (DE3) cell pellets transformed with OmpA_apo_pET21b and incubated at optimized conditions

Fig. 7.10 *Left* SDS-PAGE results of whole protein in cell lysis. *Right* Western blotting result of his-tag proteins in cell lysis. Lane 1 is 0.5 mM IPTG and 0.5 mM δ -ALA. Lane 2 is 0.5 mM IPTG. Lane 3 is 0.5 δ -ALA. Lane 4 is the control without adding any IPTG and δ -ALA



The new construct is shown in Fig. 7.9 left. This plasmid was then transformed into BL21 (DE3) competent cells. Several conditions were tried to express the proteins. After induction with 0.5 mM of IPTG, supplied with 0.5 mM of δ -ALA and incubation at 30 °C for 20 h, the cell pellets showed a light pink color. This promising result suggests that recombinant *AaeAPO* might be expressed under these conditions.

Cell lysis was then obtained by breaking the cells with SDS and sonication. Figure 7.10 left shows a SDS-PAGE of the protein mixture directly from cell lysis. Recombinant *AaeAPO* has a molecular weight \sim 37 kDa. Bands at \sim 37 kDa were also shown to be positive by western blotting analysis with his-tag antibody (Fig. 7.10 right). These bands were then cut for LC/MS/MS protein sequence. Results showed that only IPTG induction sample contained *AaeAPO*, but not the control. This result indicates that we are able to express *AaeAPO* in *E. coli*.

However, when we worked on the protein purification, we found that the recombinant *Aae*APO was not in the soluble form. Instead, inclusion bodies formed that had no catalytic activity.

The expression of recombinant *Aae*APO in *E. coli* still remains difficult, possibly because its wild type is a highly glycosylated protein (20 % of whole mass). It might be hard for the recombinant protein to fold in the active conformation without those post translational modifications [8]. The expression of CPO produced into the periplasmic space in *E. coli* was non-glycosylated in its apo-form. A high pressure-assisted reconstitution method was used to recover only a very limit amount of active holoenzymes [3]. Some eukaryotic expression systems with little glycosylation post-modifications were also tried for CPO expression but no active enzymes were produced by this method. Another filamentous fungal expression host, *Aspergillus niger*, was later used for successful expression of several fungal metalloproteins [9, 10]. Another study done by NOVOZYMES showed successful over-expression of recombinant APO from *Coprinopsis cinerea* in *Aspergillus oryzae* [11]. So, it is really promising that *Aspergillus niger* and *Aspergillus oryzae* might be useful heterologous hosts for the over-expression of *Aae*APO. The plasmid construction and expression is worth trying in the future. If that works, it could provide a powerful biocatalyst for industrial use and the mutated recombinant protein could be used for detailed mechanistic investigations and design better biocatalysts.

7.1.3 Comparison of Several Fungal Heme-Thiolate Enzymes

After the discovery of *Aae*APO from *Agrocybe aegerita* and *Cra*APO from *Coprinellus radians*, the third heme-thiolate peroxygenase *Mro*APO from *Marasmius rotula* was characterized. *Mro*APO is also the first fungal peroxygenase that can be produced in high yield [2]. Although cytochrome P450s, CPO, (*Aae*, *Cra* and *Mro*) APOs are all heme-thiolate enzymes, their physiological functions and reactivity differs. Cytochrome P450s use molecular oxygen as oxidants, need NAD(P)H as co-substrate and reductase as co-enzyme. CPO and APOs are all extracellular enzymes utilizing H₂O₂ as terminal oxidants. The halide oxidation and alkane hydroxylation catalyzed by CPO and APOs also show different efficiency and capability as the following orders [2].

Halide oxidation: *Cfu*CPO \gg *Aae*APO \approx *Cra*APO $>$ *Mro*APO

Alkane Hydroxylation: *Aae*APO $>$ *Cra*APO \approx *Mro*APO $>$ *Cfu*CPO

Reasons of the function differences include their sequence and structure differences. For example, their acid-base residues in the active sites are quite different. Most of cytochrome P450s have threonine as the conserved residue, its hydroxyl group has been proposed to assist in the catalytic function [12]. However, CPO and APOs possesses a polar environment distal to its heme prosthetic group and contains a

glutamic acid residue [5, 13]. Although the acidic residues are the same for CPO and APOs, the basic residues are different, histidine for CPO and arginine for *AaeAPO* respectively. Here, we compare the resting protein EPR spectra, the alkane hydroxylation activity and compound I stability of different fungal enzymes.

7.1.4 EPR Spectra of Resting Enzymes

AaeAPO and CPO share 30 % peptide sequence and have similar tertiary structures, as shown in Fig. 7.11 left. *AaeAPO* has no peptide homology and have different tertiary structures of P450cam, as shown in Fig. 7.11 right. Electron paramagnetic resonance (EPR) spectroscopy [14, 15] provides information about the identity of the paramagnetic center, the spin state, the magnitude of hyperfine interactions, zero-field splitting and so on. EPR spectrum of ferric *AaeAPO*, in Fig. 7.12 middle and right panels, showed that the iron is in the low-spin configuration, $S = 1/2$, with g -values $\sim [2.43, 2.25, 1.90]$. There is almost no high spin signals observed in resting substrate-free *AaeAPO*. This set of g -values is similar as P450s $\sim [2.45, 2.26, 1.91]$ [16] and another new peroxxygenase *MroAPO* [2.41, 2.25, 1.89]

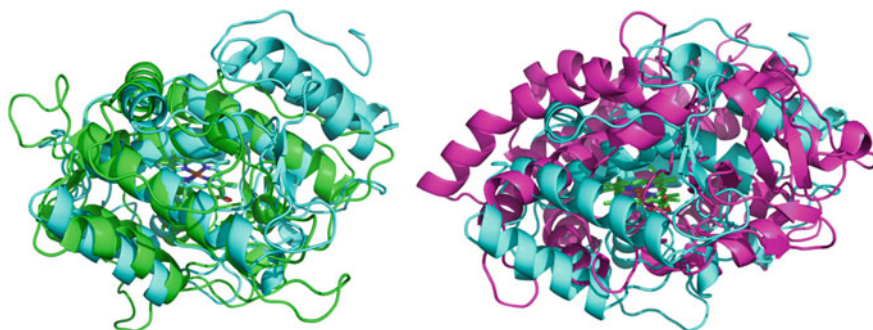


Fig. 7.11 Alignments the crystal structures of CPO (*green*, PDB 2J5M) with *AaeAPO* (*cyan*, unpublished data) and crystal structures of P450cam (*purple* 1DZ4) with *AaeAPO* (color online)

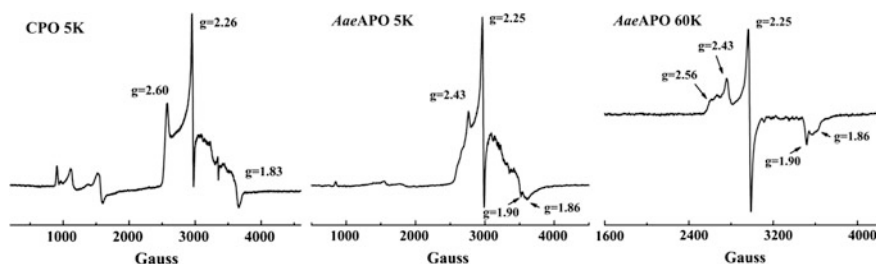


Fig. 7.12 X-band EPR spectra of resting CPO and *AaeAPO*

Fig. 7.13 X-band EPR spectrum of resting *Mro*APO

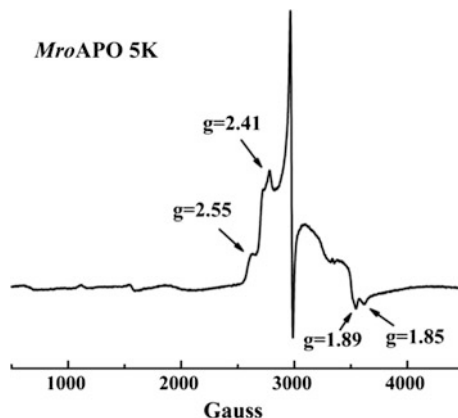


Table 7.2 Comparison of the proximal H-bonds to the cysteine sulfur in different heme-thiolate enzymes and g-values of ferric enzymes in EPR spectra

Proteins	1st residue and distance	2nd residue and distance	3rd residue and distance	g value (dominant)
CPO (2J5M)	Proline 3.6 Å	Alanine 3.4 Å	Leucine 3.5 Å	2.60, 2.26, 1.83 [17]
P450spa (3AWQ)	Proline 3.6 Å	Glycine 3.1 Å	Glutamic acid 4.0 Å	2.59, 2.25, 1.84 [18]
P450cam (1DZ4)	Leucine 3.5 Å	Glycine 3.3 Å	Glutamine 3.3 Å	2.45, 2.26, 1.91 [16]
<i>Aae</i> APO ^a	Proline, 3.6 Å	Glycine 3.3 Å	Leucine 3.3 Å	2.43, 2.25, 1.90
<i>Mro</i> APO	Unknown			2.41, 2.25, 1.89

^a*Aae*APO crystal structure is preliminary data from Dr. Piontek

(Fig. 7.13), but is different from CPO \sim [2.60, 2.26, 1.83] [17] (Fig. 7.1 left). Different sets of g-values of different ferric heme-thiolate enzymes are summarized in Table 7.2. Our result indicates that although *Aae*APO and CPO share sequence similarity, their electronic structures near the heme iron are different. Their iron centers have different rhombicity. Instead, electronic structure of *Aae*APO and *Mro*APO has been evolved to be similar as those of cytochrome P450 enzymes, possibly by subtle tuning of the H-bonds strength with cysteine sulfurs at their proximal pockets (Table 7.2). The new heme-thiolate peroxxygenase family fitting in the gap between chloroperoxidase and monooxygenases has been studied from both protein sequence and electronic structures points of view.

Another interesting finding is that when temperature increased from 5 to 60 K, the buried *Aae*APO LS signals decreased. This result indicates that there are different sets of heme iron, possibility caused by the different active site conformations or different networks of hydrogen bonds and H₂O molecule bindings at different

temperatures. *Aae*APO and CPO have shown to have different reactivity. The study of electronic properties of the heme iron by EPR at resting and active intermediate states is highly desirable. It may provide important information about the reaction mechanism and relationship between structure and function.

7.1.5 Alkane Hydroxylation Reactivity and Selectivity

*Mro*APO lacks the halogenation activity. Its alkane hydroxylation activity is also much less efficient than that of *Aae*APO. It can only slightly react with cyclohexane to produce cyclohexanol and cyclohexanone. It turned out that radical rearranged product (cyclohex-2-en-1-ylmethanol) was also detected in the radical clock (norcarane) experiments with *Mro*APO as shown in Fig. 7.14. The rebound rate was 2×10^7 and the radical life time was 60 ps which is about 5 times longer than that of *Aae*APO. The interesting thing about norcarane hydroxylation experiments is, opposite to *Aae*APO, *Mro*APO prefers producing endo-2-norcaranol, but the ratio of endo/exo < 11. *Aae*APO prefers exo-2-norcaranol, exo/endo > 60. We also tried different oxidants and pHs. The product distributions are the same for H₂O₂, PAC, TBHP, NaIO₄ and NaClO₂ at pH from 5.0 to 7.0.

7.1.6 Intermediate Generation and Stability

*Mro*APO compound I was detected with the use of excess peracetic acid by fast-mixing stopped-flow spectroscopy. As shown in Fig. 7.15 left, *Mro*APO-I is generated and persists for a while (~18 s) then it decayed back to its ferric state. The decay rate under optimized conditions was 0.7 s^{-1} . The stationary state is proposed to be the catalase-like reaction between *Mro*APO and PAC.

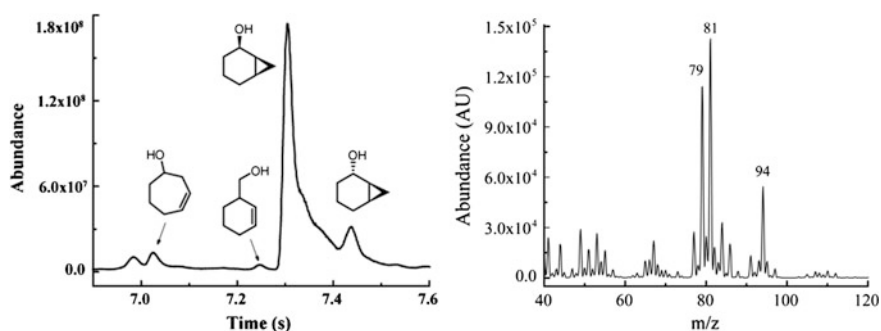


Fig. 7.14 Left GC/MS total ion trace in the region of the alcohols produced from the hydroxylation of norcarane by *Mro*APO. Right mass spectrum of the radical rearranged product cyclohex-2-en-1-ylmethanol

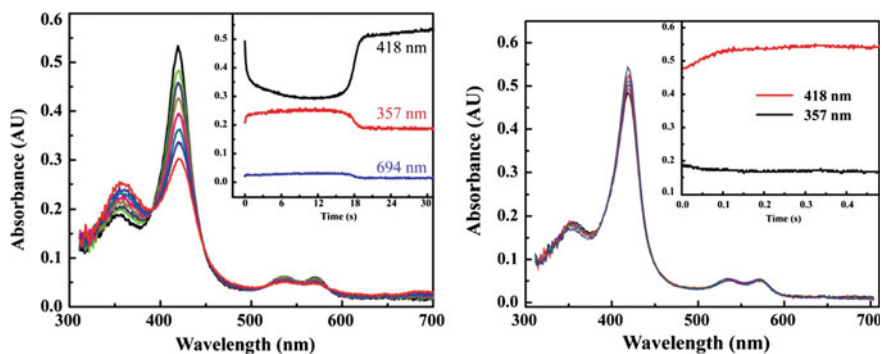


Fig. 7.15 *Left* the formation of *MroAPO-I* was detected by the fast-mixing stopped-flow spectroscopy at the optimized condition of 10 μM *MroAPO* mixing with 1 mM PAC at pH 7.0 at 4 $^{\circ}\text{C}$. *Right* similar and small amounts of *MroAPO-I* were detected with the use of stoichiometric amount of oxidants or using an excess amount of other oxidants including *mCPBA* and H_2O_2

$$d\text{CpdI}/dt = 0 = k_1[\text{APO}][\text{PAC}] - k_0[\text{CpdI}] - k_2[\text{CpdI}][\text{PAC}]$$

In terms of the compound I generation, *mCPBA* and H_2O_2 (stoichiometric to excess amounts) were worse than PAC, with much lower yields of the intermediate. As shown in Fig. 7.15 right, with the use of *mCPBA* and at pH 7, the decay rate is very fast, 12 s^{-1} . So the accumulation of *MroAPO* compound I was not obvious.

7.1.7 Site-Specific Mutagenesis for the Study of Structure-Function Relationships

Site-specific mutagenesis has proven to be a powerful tool in studying the structure-function relationships in P450s, CPO and other peroxidases [19]. The role of cysteine ligation to iron in P450s and CPO related to their catalytic properties has been revealed by using site-specific mutagenesis. For example, replacing the Cys to His in CPO resulted only 5 % of its original k_{cat} in term of chlorination and peroxidation. Catalase and epoxidation activities were also reduced to 30 % [13]. There are also studies showing that replacing Cys in P450cam with His resulted less or even no camphor hydroxylation activity any more [20, 21]. On the other hand, the activity of myoglobin increased fivefold by mutating His to Cys [22, 23]. The conclusion is that the axial ligand, cysteine, indeed plays a very important role in heme-thiolate enzyme catalysis. Furthermore, the function of different acid-base residues in the active sites of heme enzymes have also been studied and compared. For example, substitution of Glu183 in CPO with a His reduced 50 % of chlorination activity [13]. And replacement of Thr 252 in P450_{cam} to Ala or Val resulted an uncoupling monooxygenase reaction [12]. Not only investigation from the mechanistic views, the substrate specificity, reaction efficiency and stereochemistry can be also improved by adjusting the residues. For instance, some P450s have been

designed to activate small gaseous alkanes or terminal C–H bonds [24]. HRP have been rationally engineered to perform enantioselective sulfoxidation and epoxidation reactions [25]. Since efforts have been taken to express recombinant *Aae*APO in different systems, we want to do site-specific mutagenesis on *Aae*APO to study the roles of its important residues. We also want to mutate the substrate entering and releasing channels in order to change the substrate specificity and fine-tune the selectivity of products formation. Rational engineering or directly engineering strategies can be used with recombinant *Aae*APO to design better biocatalysts for a wider substrate scope and higher reaction efficiency.

7.2 Conclusions

In this chapter, we showed the production and purification of wild type *Aae*APO from *A. aegerita*. The strain grows slowly and we want to perform meaningful mutation studies, so we were trying to produce recombinant *Aae*APO in *E. coli*. Several constructs were tried. By using the OmpA signal peptide to direct protein expression in periplasmic space, we found that the cell pellets showed promising pink color. This indicates a heme protein production. However, recombinant *Aae*APO formed inclusion bodies and gave no catalytic activity. This might be caused by the lack of heavy glycosylation post translational modifications. In the future, the expression of recombinant *Aae*APO in yeast strain, *Saccharomyces cerevisiae*, and fungal strains such as *A. niger* or *Aspergillus oryzae* are worth trying. Also, with the discovery of the other fungal heme-thiolate peroxidases, for example *Mro*APO, their alkane hydroxylation activities, radical clock studies and intermediates characterization were performed and compared with CPO and *Aae*APO. These differences might be caused by the active site environments of different proteins. If recombinant *Aae*APO can be produced, we hope to use site-specific mutagenesis to investigate structure-function relationships, study the important roles of cysteine and several acid-base residues in the active sites. We also hope to perform protein engineering to design better biocatalysts, for example, to tune reaction specificities and improve the catalytic efficiency.

7.3 Experimental

Reagents: pCWori vector was kindly provided by Prof. Ortiz de Montellano. pUC19 vector was from New England Biolabs, Inc. (NEB). All restriction enzymes, T4 DNA ligase and alkaline phosphatase calf intestinal (CIP) were all bought from NEB. QuikChange Lighting Site-directed mutagenesis kit from Agilent Technologies was used. FastTrack[®] 2.0 kit from invitrogen was used for the isolation of mRNA. SuperScript[®] III One-Step RT-PCT System with Platinum[®] Taq DNA polymerase was used for cDNA synthesis and amplification. Platinum[®]

PCR superMix was used for all PCR reactions. QIAquick[®] Gel Extraction Kit was used for DNA purification after PCR. QIAprep[®] Miniprep was used for the purification of DNA from cell cultures. In-Gel Tryptic Digestion Kit from Thermo Scientific was used digestion for MS/MS analysis. Veratryl alcohol, 3 % H₂O₂ and peracetic acid were brought from Sigma-Aldrich. Bacto[™] Soytone, peptone from soybean meal, malt extract, yeast extract, LB and terrific broth modified were brought from Fishier Scientific. OmpA_apo_pET21b construct was optimized, synthesized and ligated by GenScript.

Instruments: UV-vis spectral measurements were made with a Hewlett Packed 8453 diode array spectrophotometer at room temperature. Stopped-flow experiments were performed with a Hi-Tech SF-61 DX2 double mixing instrument with a 1 cm path length. GC-MS analyses were run using an Agilent 7890A GC coupled to a 5975 inert MSD with a Rtx-5Sil MS column. The X-band ferric protein EPR spectra were taken with the Bruker EMXplus[™] spectrometer with a protein concentration of 150 μ M. Whole protein MS and digested peptide MS/MS were analysis by mass spectroscopy facility in Department of Molecular Biology at Princeton, DNA sequence identification were done by GENEWIZ and aligned with Seqman of Lasergene software package. Ultrafiltration is done with a stirred cell model 8400 from Millipore.

Organisms: *A. aegerita* TM A1 was from German collection of microorganisms and cell cultures-DSMZ, collection number DSM 22459. DH5 α competent cells were from NEB. 10XL Gold ultracompetent cells were from Agilent Technologies.

Cell cultures: *A. aegerita* TM A1 was maintained on malt extract agar slants and stored at 4 °C in the dark. One contents of the agar slant was homogenized by 0.5 ml of growth medium and the mycelia suspension was inoculated in 1 L liquid culture. The 1 L growth medium contains 30 g of soybean meal and 10 g of peptone. The flask was agitated in 4 L flask on a rotary shake 200 rpm at room temperature about 25 °C. One colony of *E. coli* containing pCWori_apo for reconstitute AaeAPO was first inoculated in 5 ml LB medium containing ampicillin (100 mg/L) and cultured overnight at 37 °C. 5 ml of the LB culture then was transferred to 1 L TB medium with ampicillin (100 mg/L) and allowed to growth at 37 °C until OD₆₀₀ reaching 0.3–0.5. At this point, IPTG (0.5 mM) and δ -ALA (0.5 mM) were added to the medium and agitate at 30 °C for 24 h.

Protein purification: wild type AaeAPO was purified according to published procedure with minor modification [1]. Wild type MroAPO was provided by our collaborators in Germany [2]. Recombinant AaeAPO from *E. coli* was produced by culturing competent cells with desired plasmids in LB broth or TB broth at optimized conditions. Generally, when the OD₆₀₀ of cell medium reaches 0.6, the protein production was induced by adding IPTG and δ -ALA. The concentrations of IPTG, δ -ALA, temperature and duration were various in order to optimize the condition. Cells were treated with detergent SDS. The whole lysis were then under sonication or heating to form a whole protein mixture. Then, protein contents were analyzed by SDS-PAGE and western blotting.

Enzyme activity assay and kinetic characterization: AaeAPO activity was measured at 310 nm by monitoring the oxidation of veratryl alcohol into

veratraldehyde ($\epsilon_{310} = 9.3 \text{ mM}^{-1} \text{ cm}^{-1}$) or the benzyl alcohol into benzaldehyde ($\epsilon_{280} = 1.4 \text{ mM}^{-1} \text{ cm}^{-1}$). Haloperoxidase activity was measured by monitoring the chlorination of MCD ($\epsilon_{290} = 20.1 \text{ mM}^{-1} \text{ cm}^{-1}$). Units definition is the micromoles of product formed per minute or micromoles of substrate converted per minute. Stopped-flow spectroscopy kinetic data were collected at 4 °C in 100 mM buffer, citrate buffer for pH 3.0–5.0 and phosphate for pH 6.0–8.0. Each experiment was repeated three times. Concentrations presented are the final concentrations after mixing.

Total mRNA isolation, apo cDNA synthesis: for mRNA isolation, protocol of FastTrack[®] 2.0 kit was followed. Because fungi have thick cell walls, for the total cell lysis collection, about 1 g of cells were harvested and ground with a mortar and pestle in liquid nitrogen. When the power was obtained, transfer the power in liquid nitrogen to a sterile 50 ml centrifuge tube. As soon as the liquid nitrogen evaporated, add 15 ml FastTrack[®] 2.0 Lysis Buffer with Proteinase K. Homogenization the power was done by using a Dounce homogenizer until no visible particle was obtained. The final concentration of total mRNA was measured by nanodrop at 260 nm. For apo cDNA synthesis, we followed the protocol of SuperScript[®] III one step RT-PCR system with Platinum[®] *Taq* DNA polymerase. Primers as shown in Fig. 7.3 were used for reverse transcription and amplification. The band on DNA gel at round 1200 bp was cut and sent for sequence.

pUC19_apo expression plasmid construction: both the resulting RT-PCR product and the empty pUC19 vectors were *Eco*RI/*Bam*HI digested and purified by either filtering through a column or gel purification. T4 DNA polymerase was used and the ligation was performed at 16 °C overnight with insert: vector molar ratio of 3:1 and 5:1. No insert religation was used as control. The resulting ligated samples were directed used for heat shock transformation.

pCWori_apo expression plasmid construction: site-specific mutagenesis protocol was followed to perform *Nde* I silence in pUC19_apo and recovery to pCWori_apo. Primers with *Nde* I and *Xba* I sites at the ends were used for PCR amplification. Both the PCR product and the empty pCWori vectors were *Nde* I/*Xba* I double digested and purified by either filtering through a column or gel purification. T4 DNA polymerase was used and the ligation was performed at 16 °C for 3 h with insert: vector molar ratio of 10:1. No insert religation was used as control. The resulting ligated samples were directed used for heat shock transformation.

References

1. Ullrich, R., Nuske, J., Scheibner, K., Spantzel, J., Hofrichter, M.: Novel haloperoxidase from the agaric basidiomycete *Agrocybe aegerita* oxidizes aryl alcohols and aldehydes. *Appl. Environ. Microb.* **70**, 4575–4581 (2004)
2. Grobe, G., Ullrich, R., Pecyna, M.J., Kapturska, D., Friedrich, S., Hofrichter, M., Scheibner, K.: High-yield production of aromatic peroxxygenase by the agaric fungus *Marasmius rotula*. *AMB Express* **1**, 31–42 (2011)

3. Zong, Q., Osmulski, P.A., Hager, L.P.: High-pressure-assisted reconstitution of recombinant chloroperoxidase. *Biochemistry* **34**, 12420–12425 (1995)
4. Barnes, H.J., Arlotto, M.P., Waterman, M.R.: Expression and enzymatic activity of recombinant cytochrome P450 17 α -hydroxylase in *Escherichia coli*. *Proc. Natl. Acad. Sci. U.S.A.* **88**, 5597–5601 (1991)
5. Pecyna, M.J., Ullrich, R., Bittner, B., Clemens, A., Scheibner, K., Schubert, R., Hofrichter, M.: Molecular characterization of aromatic peroxxygenase from *Agrocybe aegerita*. *Appl. Microbiol. Biot.* **84**, 885–897 (2009)
6. Sjöström, M., Wold, S., Wieslander, A., Rilfors, L.: Signal peptide amino acid sequences in *Escherichia coli* contain information related to final protein localization. A multivariate data analysis. *EMBO J.* **6**, 823–831 (1987)
7. Rao Movva, N., Nakamura, K., Inouye, M.: Amino acid sequence of the signal peptide of ompA protein, a major outer membrane protein of *Escherichia coli*. *J. Biol. Chem.* **255**, 27–29 (1980)
8. Roth, J., Zuber, C., Park, S., Jang, I., Lee, Y., Kysela, K.G., Le Fourn, V., Santimaria, R., Guhl, B., Cho, J.W.: Protein N-glycosylation, protein folding, and protein quality control. *Mol. Cells* **30**, 497–506 (2010)
9. Conesa, A., Van De Velde, F., Van Rantwijk, F., Sheldon, R.A., Van Den Hondel, C.A.M.J.J., Punt, P.J.: Expression of the *Caldariomyces fumago* chloroperoxidase in *Aspergillus niger* and characterization of the recombinant enzyme. *J. Biol. Chem.* **276**, 17635–17640 (2001)
10. Conesa, A., Van Den Hondel, C.A.M.J.J., Punt, P.J.: Studies on the production of fungal peroxidases in *Aspergillus niger*. *Appl. Environ. Microb.* **66**, 3016–3023 (2000)
11. Hofrichter, M.: Insights into catalysis, structure and phylogeny of fungal peroxxygenases. In: 18th International Conference on Cytochrome P450, Seattle, WA, USA (2013)
12. Imai, M., Shimada, H., Watanabe, Y., Matsuhima-Hibiya, Y., Makino, R., Koga, H., Horiuchi, T., Ishimura, Y.: Uncoupling of the cytochrome P-450cam monooxygenase reaction by a single mutation, threonine-252 to alanine or valine: a possible role of the hydroxy amino acid in oxygen activation. *Proc. Natl. Acad. Sci. U.S.A.* **86**, 7823–7827 (1989)
13. Yi, X., Conesa, A., Punt, P.J., Hager, L.P.: Examining the role of glutamic acid 183 in chloroperoxidase catalysis. *J. Biol. Chem.* **278**, 13855–13859 (2003)
14. Pilbrow, J.R.: Transition Ion Electron Paramagnetic Resonance. Oxford University Press, Oxford (1991)
15. Carrington, A., McLachlan, A.D.: Introduction to Magnetic Resonance. Harper and Row, New York (1967)
16. Lipscomb, J.D.: Electron paramagnetic resonance detectable states of cytochrome P-450cam. *Biochemistry* **19**, 3590–3599 (1980)
17. Hollenberg, P.F., Hager, L.P., Blumberg, W.E., Peisach, J.: An electron paramagnetic resonance study of the high and low spin forms of chloroperoxidase. *J. Biol. Chem.* **255**, 4801–4807 (1980)
18. Fujishiro, T., Shoji, O., Nagano, S., Sugimoto, H., Shiro, Y., Watanabe, Y.: Crystal structure of H₂O₂- dependent cytochrome P450 SP α with its bound fatty acid substrate: insight into the regioselective hydroxylation of fatty acids at the α position. *J. Biol. Chem.* **286**, 29941–29950 (2011)
19. Gillam, E.M.J.: Engineering cytochrome P450 enzymes. *Chem. Res. Toxicol.* **21**, 220–231 (2008)
20. Yoshioka, S., Takahashi, S., Hori, H., Ishimori, K., Morishima, I.: Proximal cysteine residue is essential for the enzymatic activities of cytochrome p450cam. *Eur. J. Biochem.* **268**, 252–259 (2001)
21. Auclair, K., Moëne-Loccoz, P., Ortiz de Montellano, P.R.: Roles of the proximal heme thiolate ligand in cytochrome P450cam. *J. Am. Chem. Soc.* **123**, 4877–4885 (2001)
22. Adachi, S.I., Nagano, S., Ishimori, K., Watanabe, Y., Morishima, I., Egawa, T., Kitagawa, T., Makino, R.: Roles of proximal ligand in heme proteins: replacement of proximal histidine of human myoglobin with cysteine and tyrosine by site-directed mutagenesis as models for P-450, chloroperoxidase, and catalase. *Biochemistry* **32**, 241–252 (1993)

23. Adachi, S.I., Nagano, S., Watanabe, Y., Ishimori, K., Morishima, I.: Alteration of human myoglobin proximal histidine to cysteine or tyrosine by site-directed mutagenesis: characterization and their catalytic activities. *Biochem. Biophys. Res. Commun.* **180**, 138–144 (1991)
24. Peters, M.W., Meinhold, P., Glieder, A., Arnold, F.H.: Regio- and enantioselective alkane hydroxylation with engineered cytochromes P450 BM-3. *J. Am. Chem. Soc.* **125**, 13442–13450 (2003)
25. Ozaki, S.I., Ortiz De Montellano, P.R.: Molecular engineering of horseradish peroxidase: thioether sulfoxidation and styrene epoxidation by Phe-41 leucine and threonine mutants. *J. Am. Chem. Soc.* **117**, 7056–7064 (1995)